BEST AVAILABLE IMAGES

Defective images within this document are accurate representations of the original documents submitted by the applicant.

Defects in the images may include (but are not limited to):

- BLACK BORDERS
- TEXT CUT OFF AT TOP, BOTTOM OR SIDES
- FADED TEXT
- ILLEGIBLE TEXT
- SKEWED/SLANTED IMAGES
- COLORED PHOTOS
- BLACK OR VERY BLACK AND WHITE DARK PHOTOS
- GRAY SCALE DOCUMENTS

IMAGES ARE BEST AVAILABLE COPY.

As rescanning documents *will not* correct images, please do not report the images to the Image Problem Mailbox.

Proc. Natl. Acad. Sci. USA
Vol. 93, pp. 1671–1676, February 1996
Genetics

Cyp1a2(−/−) null mutant mice develop normally but show deficient drug metabolism

(cytochrome P450/embryonic stem cells/arylamine carcinogenesis)

H.-C. LEONARD LIANG*, HUNG LI†, ROSS A. MCKINNON*, JOHN J. DUFFY‡, S. STEVEN POTTER†, ALVARO PUGA*, AND DANIEL W. NEBERT*§

*Department of Environmental Health, University of Cincinnati Medical Center, P.O. Box 670056, Cincinnati, OH 45267-0056; †Division of Basic Science Research, Children's Hospital Medical Center, University of Cincinnati, Cincinnati, OH 45229-2899; and ‡Department of Molecular Genetics, Biochemistry, and Microbiology, University of Cincinnati Medical Center, P.O. Box 650524, Cincinnati, OH 45267-0524

Communicated by I. C. Gunsalus, Gulf Breeze, FL, November 3, 1995

ABSTRACT **Cytochrome P450 1A2 (CYP1A2) is a predominantly hepatic enzyme known to be important in the metabolism of numerous foreign chemicals of pharmacologic, toxicologic, and carcinogenic significance. CYP1A2 substrates include aflatoxin B_1, acetaminophen, and a variety of environmental arylamines. To define better the developmental and metabolic functions of this enzyme, we developed a CYP1A2-deficient mouse line by homologous recombination in embryonic stem cells. Mice homozygous for the targeted *Cyp1a2* gene, designated *Cyp1a2*(−/−), are completely viable and fertile; histologic examination of 15-day embryos, newborn pups, and 3-week-old mice revealed no abnormalities. No CYP1A2 mRNA was detected by Northern blot analysis. Moreover, mRNA levels of *Cyp1a1*, the other gene in the same subfamily, appear unaffected by loss of the *Cyp1a2* gene. Because the muscle relaxant zoxazolamine is a known substrate for CYP1A2, we studied the *Cyp1a2*(−/−) genotype by using the zoxazolamine paralysis test: the *Cyp1a2*(−/−) mice exhibited dramatically lengthened paralysis times relative to the *Cyp1a2*(+/+) wild-type animals, and the *Cyp1a2*(+/−) heterozygotes showed an intermediate effect. Availability of a viable and fertile CYP1A2-deficient mouse line will provide a valuable tool for researchers wishing to define the precise role of CYP1A2 in numerous metabolic and pharmacokinetic processes.**

Cytochromes P450 represent the major class of phase I drug-metabolizing enzymes (1). Members of this enzyme superfamily are responsible for the metabolism of innumerable foreign chemicals. In addition, because of the metabolism of many endogenous compounds such as steroids, vitamin D_3, fatty acids, prostaglandins, and biogenic amines, cytochromes P450 are believed to be essential for such critical life functions as cell division, differentiation, apoptosis, homeostasis, and neuroendocrine functions (2–4).

As of October 1995, the P450 gene superfamily was composed of more than 480 genes classified into 74 families, 14 of which exist in all mammals (5). Both the murine and human *CYP1A* subfamilies comprise two genes, designated *Cyp1a1* and *Cyp1a2* in mouse, and *CYP1A1* and *CYP1A2* in humans (5, 6). In mice, the *Cyp1a* genes appear to be located within a 100-kb region on chromosome 9 (1, 7). The CYP1A enzymes are of particular interest due to their capacity for metabolizing numerous compounds relevant to the fields of pharmacology, toxicology, and carcinogenesis. In addition, both enzymes are induced by many foreign chemicals, including polycyclic aromatic hydrocarbons (e.g., benzo[*a*]pyrene) and 2,3,7,8-tetrachlorodibenzo-*p*-dioxin (1, 4). The induction process is regulated by the aromatic hydrocarbon receptor (AHR) (8, 9); the murine *Ahr* gene has been cloned (10, 11) and an *Ahr*(−/−) mouse line has recently been produced (12).

CYP1A2 is highly expressed in liver and is involved in the metabolism of many toxicologically significant compounds, including aflatoxin B_1, acetaminophen, and the food-derived heterocyclic amines (reviewed in ref. 13). In addition, most carcinogenic arylamines are known to be substrates for the human CYP1A2 enzyme (6, 14). To date, no endogenous substrate has been identified for the CYP1A2 enzyme, and there is little evidence for any physiologic role other than protection from chemical insult. On the basis of caffeine metabolism, two laboratories have suggested the presence of a human CYP1A2 genetic polymorphism, having a trimodal distribution of metabolizer phenotype (consistent with high/high, high/low, and low/low genotypes) in several populations (15, 16).

To define more clearly the involvement of the CYP1A2 enzyme in toxicity and carcinogenesis elicited by a variety of environmental chemicals, we have generated an embryonic stem (ES) cell-derived mouse line lacking a functional CYP1A2 enzyme. These null mutant mice exhibit normal development, viability, and fertility. The availability of this healthy *Cyp1a2*-deficient mouse line should provide an invaluable resource for researchers wishing to define the precise role of CYP1A2 in the metabolism of foreign, and perhaps endogenous, chemicals.¶

MATERIALS AND METHODS

Cloning of 129/SV *Cyp1a2* Genomic DNA. Using the mouse 1.5-kb 3′ *Cyp1a2*-specific cDNA probe (17), we isolated a 129/SV mouse genomic DNA clone isogenic to the ES cells used for recombination. DNA cloning and purification were performed as described (18). From the isolated clone, spanning 19 kb, we subcloned an 11-kb *Eco*RI fragment of the *Cyp1a2* gene into pBluescript II SK(+) (Stratagene). The wild-type *Eco*RI fragment includes exons 2–7 and the 3′ end of the *Cyp1a2* gene (Fig. 1 *Upper*).

Construction of *Cyp1a2* Gene-Targeting Vectors. The hypoxanthine phosphoribosyltransferase (*hprt*) gene-based vectors used for targeting the *Cyp1a2* gene were derived from the parent vector, pHPRT KO; this vector is derived from pBluescript II SK(+), contains a 2-kb *Kpn* I blunt-ended herpes simplex virus (HSV) thymidine kinase (*tk*) gene cassette, and features a 2.9-kb *Not* I–*Eco*RI blunt-ended *hprt* minigene cassette subcloned into the *Hin*dIII site (19). To generate the two vectors used for targeting, we subcloned a 0.4-kb *Hin*dIII–

The publication costs of this article were defrayed in part by page charge payment. This article must therefore be hereby marked "*advertisement*" in accordance with 18 U.S.C. §1734 solely to indicate this fact.

Abbreviations: ES cell, embryonic stem cell; GAPDH, glyceraldehyde-3-phosphate dehydrogenase.

§To whom reprint requests should be addressed.

¶This work was presented in abstract form at the Annual Meeting of the Society of Toxicology, March 5–9, 1995, Baltimore (43).

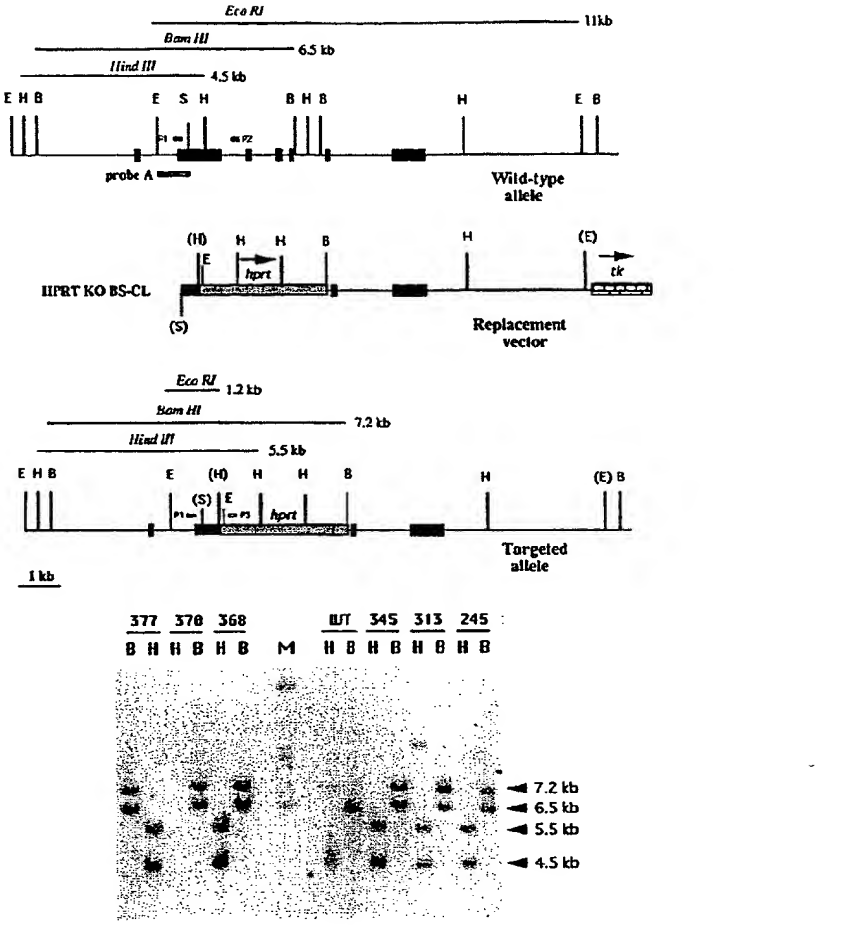

FIG. 1. Targeted modifications of the murine *Cyp1a2* gene. (*Upper*) The wild-type allele with all seven exons (solid boxes) and the targeted allele (containing the *hprt* gene) are shown. Probe A was used for genomic DNA analysis. E, *Eco*RI; H, *Hin*dIII; B, *Bam*HI; S, *Stu* I; sites in parentheses were lost during cloning/ligation. The predicted wild-type, and targeted allele, restriction fragment sizes for *Bam*HI and *Hin*dIII are shown. P1, P2, and P3 represent primers used for PCR analysis. (*Lower*) Diagnostic Southern blots for DNA from wild-type (WT) untargeted ES cells, plus DNA from six targeted ES cell lines designated 377, 370, 368, 345, 313, and 245. *Bam*HI (B) and *Hin*dIII (H) digests were hybridized with the flanking probe A. Heterozygote targeted lines contain the 7.2-kb *Bam*HI and the 5.5-kb *Hin*dIII fragments. M, molecular size markers.

Stu I fragment from exon 2 of the *Cyp1a2* gene into either the *Bam*HI site or the *Cla* I site of the pHPRT KO plasmid, generating products designated pHPRT KO BS and pHPRT KO CS, respectively. Subsequently, the *Cla* I site of the pHPRT KO BS plasmid and the *Bam*HI site of the pHPRT KO CS plasmid were used to subclone a 6.6-kb *Bam*HI–*Eco*RI fragment of the *Cyp1a2* gene. The resultant plasmids were designated pHPRT KO BS-CL and pHPRT KO CS-BL, respectively (Fig. 2*A*).

The targeting vector used in our earlier experiments was constructed from the multipurpose knockout vector pMJK KO, also derived from pBluescript II SK(+). pMJK KO possesses features similar to pHPRT KO, except that the *Hin*dIII site of pBluescript II SK(+) was used for subcloning a 1.6-kb *Xho* I–*Hin*dIII phophoglycerate kinase promoter–neomycin-resistance gene cassette instead of the *hprt* minigene cassette (20). The 0.4-kb *Hin*dIII–*Stu* I fragment of exon 2 of *Cyp1a2* (Fig. 1 *Upper*) was subcloned into the *Xho* I site of the pMJK KO plasmid. The *Bam*HI site of the pMJK KO plasmid was then used to subclone the 6.6-kb fragment. The resulting construct, designated pMJK KO XS-BL (Fig. 2*A Top*), contains 7.0 kb of target homology and produces a 2.2-kb deletion in the targeted locus. All three resulting plasmids were purified by the CsCl banding technique, linearized at the unique *Not* I site in the pBluescript II SK(+) backbone, and used for electroporation.

ES Cell Cultures. D3 ES cells (21) and E14tg2a ES cells, which are *hprt*$^-$ (22), were maintained at 37°C in a 5% CO_2 atmosphere on feeder layers of murine mitomycin C-treated embryonic fibroblasts in Dulbecco's modified Eagle's medium containing 15% heat-inactivated fetal bovine serum, 0.1 mM 2-mercaptoethanol, 1 mM sodium pyruvate, penicillin at 50 units/ml, streptomycin at 50 μg/ml, and leukemia inhibitory factor (LIF; GIBCO) at 1000 units/ml. The fibroblast feeder layer was prepared from 13- to 14-day-old mouse embryos and was grown in Dulbecco's modified Eagle's medium containing glucose at 4.5 mg/ml, penicillin at 50 units/ml, streptomycin at 50 μg/ml, and 1 mM L-glutamine, supplemented with 10% heat-inactivated fetal bovine serum. Confluent fibroblast monolayers were treated with mitomycin C at 10 μg/ml for 90 min at 37°C. The monolayers were then washed four times with phosphate-buffered saline prior to freezing or immediate use

A

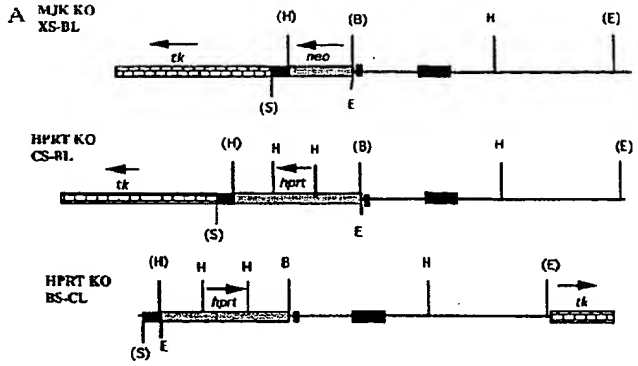

B

Construct	MJK KO XS-BL	HPRT KO CS-BL	HPRT KO BS-CL
ES cells	D3	E14	E14
Screened colonies	>800	200	380
Targeted lines	1	0	11
Chimera generated	13 males 9 females		12 males 1 females
Germline transmission	0		6

FIG. 2. Comparison of the three *Cyp1a2* gene-targeting constructs used in these experiments. (*A*) Diagram of the three constructs. The pMJK KO XS-BL vector carries the neomycin-resistance (*neo*) gene and the *Cyp1a2* gene fragment in opposite orientations. The pHPRT KO BS-CL vector carries the *hprt* gene in the same orientation as the *Cyp1a2* gene fragment, whereas the pHPRT KO CS-BL vector carries the *hprt* gene and the *Cyp1a2* gene fragment in opposite orientations. (*B*) Results of successfully targeted lines, generation of chimeric mice, and germline transmission.

as feeder layers (23). For electroporation, two confluent 100-mm dishes of ES cells were treated with trypsin and resuspended in 3 ml of phosphate-buffered saline (Ca^{2+}- and Mg^{2+}-free) containing *Not* I-digested targeting vector DNA at 20 μg/ml. Three 1-ml aliquots were electroporated at 900 V and 14 μF in a 0.4-cm-wide cuvette (Gene Zapper; IBI). The cells were then distributed onto 15-mm × 100-mm dishes containing mitomycin C-treated mouse embryo fibroblast feeder cells. Selection in hypoxanthine/aminopterin/thymidine (HAT) supplement (GIBCO/BRL) for E14 cells, or in G418 (150 μg/ml) for D3 cells, was initiated 24 h later. Further selection with 2 μM ganciclovir (Syntex, Palo Alto, CA) was begun at 48 hr following electroporation. Resistant ES colonies were selected 7 days after electroporation, treated with trypsin, and transferred to 24-well plates. After 2 or 3 days in culture, half the cells from each well were frozen, and the other half were transferred to gelatin-coated six-well plates. DNA was then prepared from each colony for PCR and/or Southern blot analysis, in order to identify putative homologous recombination events.

Selection of the Recombinant ES Cells. ES cells were lysed at 65°C for 10 min in 0.5 ml of buffer containing 0.2 M NaCl, 5 mM EDTA, 50 mM Tris·HCl (pH 7.5), 0.2% SDS, and proteinase K at 20 μg/ml. Genomic DNA was precipitated with potassium acetate and ethanol. The DNA was rinsed with 70% ethanol, then rinsed with 95% ethanol, air-dried, and resuspended in H_2O. Mouse tail DNA was prepared similarly, except that lysis buffer containing proteinase K at 15 μg/ml was used, and samples were incubated overnight at 65°C.

For Southern blotting, we digested DNA to completion with an excess of the restriction endonuclease *Eco*RI, *Bam*HI, or *Hin*dIII under reaction conditions recommended by the supplier (GIBCO/BRL). The digested DNA was fractionated through 0.8% agarose gels and transferred to Nytran Plus (Schleicher & Schuell) for further hybridization. Conditions for prehybridization and hybridization were as described (24). A 0.8-kb *Eco*RI–*Stu* I fragment was used as probe A (Fig. 1). Autoradiography was performed with Kodak XAR film and DuPont Lighting Plus intensifying screens.

For PCR screening of the HAT-resistant ES cell colonies, genomic DNA was added to a 20-μl PCR mixture containing 4 μl of 5× reaction buffer, 0.125 μg of each oligonucleotide primer (*Cyp1a2-5'*, CAGCCTGGGATGGAAATCAAGACA; *Cyp1a2-3'*, CGCTGCACACGGCACTCTGAGTAC; and *hprt* 3', AGCGCCTCCCCTACCCGGTAGAAT), 2.5 units of *Taq* DNA polymerase (GIBCO/BRL), and a mixture of dATP, dCTP, dGTP and dTTP nucleotides at a final concentration of 500 μM for each nucleotide. The 5× reaction buffer contained 250 μM NaCl, 750 μM $MgCl_2$, 100 mM Tris·HCl (pH 8.4), 7.5 mM $MgCl_2$, 0.05% gelatin, and 0.5% Triton X-100. Samples were overlaid with one drop of mineral oil. PCR was performed for 35 cycles of 94°C for 1 min, 62°C for 2 min, and 72°C for 3 min in a thermal cycler (Perkin–Elmer/Cetus). The generated PCR products were 1.2 and 0.9 kb for *Cyp1a2*(+) wild-type and *Cyp1a2*(−) mutant alleles, respectively (Fig. 1). For screening of G418-resistant colonies, the above conditions were used with the following primers: *neo*-3', ATGGCCGCTTTTCTGGATTCATCGACTTG; *Cyp1a2-5'*, GCGTTCTCCCAGTACATCTCCTTAGCCCCA; and *Cyp1a2-3'*, CTCACCTTGTTGAAGTCTTGGTAGTGCTCC.

Generation of the *Cyp1a2*(−/−) Mouse Line. Chimeric mice were generated by microinjection of targeted ES cells into embryos as described (24). Briefly, 10–15 targeted ES cells derived from the 129/Ola (slate, gray) mouse line were microinjected into the blastocoele cavity of C57BL/6J em-

bryos (nonagouti, black). Surviving blastocysts were transferred to pseudopregnant CD-1 females (albino, nonagouti) by uterine implantation. Identification of chimeric pups was determined by the presence of agouti or slate coat color at 10 days of age, depending on the origin of the ES cells. Chimeric males were bred to CF-1 females (nonagouti, white) or Swiss Black females (nonagouti, black). Germline transmission was determined by the presence of chinchilla-agouti and agouti coat colors in the offspring of the CF-1 and the Swiss Black females, respectively. Germline transmission was confirmed by both PCR and Southern blot analyses, as detailed above.

Northern Hybridization Analysis. Total RNA was isolated from the livers of 7- to 9-week-old mice by the acid guanidinium isothiocyanate extraction method (25). RNA was isolated 36 hr after treatment with a single intraperitoneal dose of either corn oil alone (25 ml/kg of body weight) or β-naphthoflavone (200 mg/kg) in corn oil. Total RNA (30 μg) was loaded onto 1% agarose/formaldehyde gels, transferred to nylon membranes (Nytran Plus; Schleicher & Schuell), and UV-crosslinked. Prehybridization and hybridization were performed in 10% dextran sulfate/1% SDS/6× standard saline citrate. Membranes were probed with a 1.5-kb 3′ fragment of CYP1A2 cDNA or a 1.2-kb 3′ fragment of CYP1A1 cDNA (17). The probe of a 780-bp *Pst* I–*Xba* I fragment of the glyceraldehyde-3-phosphate dehydrogenase (GAPDH) cDNA was used as an RNA-loading control. Hybridization was performed at 60°C, and the blots were washed at 60°C prior to autoradiography.

Zoxazolamine Paralysis Test. Four- to 6-week-old mice were given a single intraperitoneal dose of either β-naphthoflavone (200 mg/kg) in corn oil or corn oil alone. All animals received intraperitoneal zoxazolamine (300 mg/kg) in corn oil 36 hr later. Mice were then placed on their backs, and that time was recorded as time zero. The paralysis time was measured as that period of time until the animal had regained enough consciousness to right itself repeatedly (26).

Histology. Histologic specimens were prepared from 15-day embryos, newborn pups, and 3-week-old mice for analysis of any pathologic changes associated with the *Cyp1a2*-deficient genotype. The 15-day embryos and newborn pups were fixed whole in Bouin's fixative, whereas virtually all organs were dissected from 3-week-old mice and fixed in 10% formaldehyde. Paraffin-embedded sections (5 μm) were visualized by staining with hematoxylin and eosin.

RESULTS

Gene Targeting. Targeted disruption of the *Cyp1a2* gene was successfully achieved by insertion of the *hprt* gene in place of part of exon 2 and all of exons 3–5 (Fig. 1). Our design of the three gene-targeting vectors (Fig. 2*A*) was based on important structural features in the murine *Cyp1a2* gene, including a highly conserved cysteine-containing peptide in the N-terminus of the protein encoded by exon 2 and the so-called cytochrome P450 "conserved tridecapeptide" (27), encoded by exon 5 in the case of both of the *CYP1A* genes. Based on these structural details, homologous recombination constructs were designed in which the regions encoding the N-terminal cysteine-containing fragment and the conserved tridecapeptide would be replaced with either the *neo* or *hprt* positive selection markers. Targeted deletion of these essential gene components would be predicted to generate a null mutation.

Interestingly, pHPRT KO BS-CL (having the *hprt* promoter in the same orientation as the *Cyp1a2* gene) was the only successful construct of three used in our experiments (Fig. 2*B*). Whereas a high targeting frequency was achieved with pHPRT KO BS-CL in E14 ES cells, no homologous recombinant clones were generated from pHPRT KO CS-BL. In our earlier work using the *neo* gene in D3 ES cells, it is noteworthy that only a single homologous recombinant clone (of 800 screened) was obtained with the pMJK KO XS-BL construct, from which 13 chimeric males were produced, yet none of these was able to achieve germline transmission (Fig. 2*B*). The most widely accepted reason for the transmission of coat color but not the targeted gene is that a locus has been lost which allows colonization of the ES cells in the germline; this comes about through continued passage of ES cells both before and after targeting.

Homologous recombinant clones generated with the pHPRT KO BS-CL construct were confirmed by both genomic blotting and PCR analysis. Genomic blot analysis demonstrated that heterozygote clones were obtained, as indicated by the presence of extra 5.5-kb and 7.2-kb fragments upon digestion with *Hin*dIII and *Bam*HI, respectively (Fig. 1 *Lower*). PCR analysis of heterozygote clones showed the presence of a 0.9-kb band, corresponding to the mutant allele, in addition to the wild-type 1.2-kb band (Fig. 3). Two homologous recombinant clones generated with the pHPRT KO BS-CL construct were injected into the blastocoele cavity of C57BL/6J embryos; we subsequently generated 12 male chimeras, of which 6 gave germline transmission. Germline mice were derived from two independent ES clones, lines 368 and 377.

Viability and Fertility. The heterozygous *Cyp1a2*(+/−) mice displayed normal viability and fertility and were then used to generate homozygous mutants. Breeding of the heterozygotes produced offspring in the expected Mendelian distribution of one *Cyp1a2*(+/+) to two *Cyp1a2*(+/−) to one *Cyp1a2*(−/−), indicating no *in utero* lethality due to loss of both functional alleles of the *Cyp1a2* gene.

Homozygous *Cyp1a2*(−/−) null mutants were identified by the presence of only the 0.9-kb band upon PCR analysis (Fig. 3). Genotype was confirmed by Southern blotting. We found the homozygous *Cyp1a2*(−/−) mouse to be completely viable, fertile, and indistinguishable from its *Cyp1a2*(+/+) or *Cyp1a2*(+/−) littermates by appearance, mortality rate, reproductive capacity, and histologic examination of many organs and tissues; this has remained true—currently beyond 15 months of age. The organs and tissues examined histologically included: liver, lung, kidney, stomach, duodenum, small and large intestine, spleen, thymus, lymph nodes, heart, and brain.

CYP1A2 mRNA Analysis. The absence of CYP1A2 mRNA in *Cyp1a2*(−/−) mice was confirmed by Northern blot analysis of liver RNA from both control and β-naphthoflavone-treated animals. Fig. 4 *Left* shows a gene-dose effect: constitutive CYP1A2 mRNA levels in the heterozygote were intermediate between the null mutant, in which no mRNA was detectable even with 21-day exposures of the filter to x-ray film, and the wild type, which showed abundant mRNA. Induction by β-naphthoflavone treatment was found to increase the

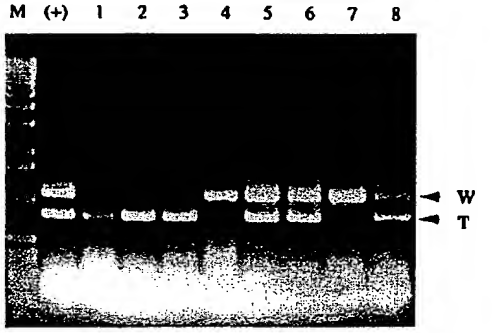

FIG. 3. PCR analysis of tail DNA from eight pups in the same litter generated from a *Cyp1a2*(+/−) × *Cyp1a2*(+/−) intercross. PCR products are 1.2 and 0.9 kb for the wild-type (W) and targeted (T) alleles, respectively. M, 1-kb nucleic acid markers. (+), targeted ES cell DNA.

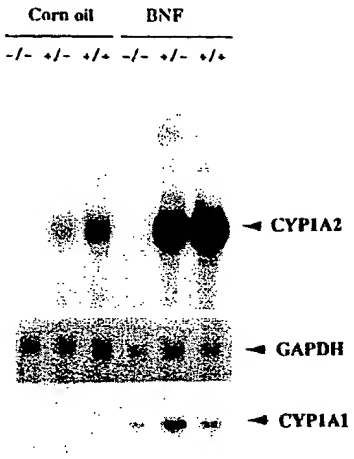

FIG. 4. Northern hybridization analysis of liver RNA from *Cyp1a2*(−/−), *Cyp1a2*(+/−), and *Cyp1a2*(+/+) mice. Probes include the CYP1A2-specific cDNA, the CYP1A1-specific cDNA as a positive control, and GAPDH cDNA to assess RNA loading in each lane. Sizes of the CYP1A2 and CYP1A1 mRNAs are 2.1 and 2.8 kb, respectively (17). Animals were treated with corn oil alone (controls) or β-naphthoflavone (BNF) 36 hr prior to sacrifice. When standardized for GAPDH, CYP1A1 mRNA levels are not significantly different in the three BNF lanes.

CYP1A2 mRNA 4- to 6-fold in the heterozygote and wild-type mouse (Fig. 4 *Right*), whereas no CYP1A2 mRNA was detected in the β-naphthoflavone-treated *Cyp1a2*(−/−) mouse.

CYP1A1 mRNA levels, detectable in liver only after β-naphthoflavone induction, were virtually identical in the *Cyp1a2*(+/+), *Cyp1a2*(+/−), and *Cyp1a2*(−/−) mice (Fig. 4 *Bottom*). These data indicate that expression of this other member of the mouse *Cyp1a* subfamily does not appear to compensate, or to be altered, by absence of the *Cyp1a2* gene.

Zoxazolamine Paralysis Test. The muscle relaxant zoxazolamine is a known CYP1A2 substrate, as well as a CYP2E1 substrate (28), and has been used for more than two decades to phenotype individual recombinant inbred or congenic mice having had CYP1A2 induced by β-naphthoflavone, benzo[*a*]pyrene, or 2,3,7,8-tetrachloro-*p*-dioxin (26, 29). It was expected that mice lacking any CYP1A2 enzyme would metabolize zoxazolamine more slowly and therefore remain paralyzed for a longer period of time and that β-naphthoflavone treatment—while inducing CYP1A2 in *Cyp1a2*(+/+) and *Cyp1a2*(+/−) mice—would have no effect on the *Cyp1a2*(−/−) mouse. The results of the zoxazolamine paralysis test (Table 1) show these expectations to be correct. Interestingly, the data are also correlated with the gene-dose mRNA data of Fig. 4 in that *Cyp1a2*(+/−) animals exhibited an intermediate paralysis time, when compared with the *Cyp1a2*(+/+) wild type and the *Cyp1a2*(−/−) null mutant. The CYP1A2-deficient mouse was paralyzed at least 9 times longer than the wild-type mouse. These results clearly illustrate the major role of CYP1A2 in zoxazolamine metabolism.

Table 1. Results of the zoxazolamine paralysis test in mice of the three genotypes

Genotype	Time paralyzed, min	
	Control	β-Naphthoflavone pretreatment
Cyp1a2(−/−)	>960	>960
Cyp1a2(+/−)	534 ± 225	309 ± 69
Cyp1a2(+/+)	498 ± 121	103 ± 59

The zoxazolamine paralysis test was performed as described (26). Zoxazolamine (chlorzoxazone) was given to all mice 36 hr after a single intraperitoneal dose of β-naphthoflavone (in corn oil); controls received corn oil alone. Paralysis times were assessed as the time taken for mice to right themselves three times. Values (mean ± SEM) are for four mice for each condition.

DISCUSSION

Evolutionary Considerations. We had anticipated that homozygous *Cyp1a2*(−/−) mutant mice would be viable and healthy, yet phenotypically different from wild-type *Cyp1a2*(+/+) and heterozygous *Cyp1a2*(+/−) mice toward CYP1A2-specific substrates such as zoxazolamine, based on several criteria. (*i*) Whereas constitutive expression of the *Cyp1a1* gene and its induction by polycyclic aromatic compounds occur very early during embryogenesis, increases in expression of the *Cyp1a2* gene are not detectable until the neonatal period (1, 30–32). These observations suggest that the *Cyp1a2* gene might not be critical for mouse embryogenesis but more likely is involved in metabolism of dietary and other foreign chemicals encountered after birth. (*ii*) Mammalian *CYP1A2* genes are extinguished in virtually all established and transformed cell lines examined, indicating that absence of CYP1A2 does not affect viability of cells in culture (1, 33, 34). (*iii*) Evolutionary analysis of the *CYP1A* family in trout and mammalian species (5) suggests that, while *CYP1A1* most likely encodes an enzyme critical to life, the *CYP1A2* gene is likely to be the result of a relatively recent gene duplication event in response to dietary selective pressures (35). Whereas trout appears to have only the *CYP1A1* gene, birds and mammals possess both *CYP1A1* and *CYP1A2*. It was therefore proposed that the *CYP1A2* gene originated ≈350 million years ago via a gene duplication event—after the divergence of land animals from sea animals, and before divergence of land animals from birds (5, 35, 36). This duplication event may have been driven by evolutionary pressures caused by animal–plant interactions (35). Thus, it appears more likely that CYP1A2 might play an important role in protecting newborns from the insults of foreign (particularly dietary) chemicals during and after the neonatal period. We therefore had expected that the *Cyp1a2*-deficient mouse would develop normally, be viable, and display normal fertility, and this is what the present study shows.

Comparison of Two CYP1A2-Deficient Mouse Lines. The normal phenotype of the *Cyp1a2*(−/−) mouse line described in our study contrasts sharply with the phenotype of respiratory distress and neonatal lethality observed in another *Cyp1a2*(−/−) mouse line recently described (37). One possibility to explain the differences in phenotype would be differences in genetic background. This is not without precedent: for example, in studies of the insulin-like growth factor (*Igf1*) gene, differences in the phenotype of knockout mouse lines were found to be caused by differences in genetic background (38). In the present study, chimeric males in this laboratory were bred to CF-1 females or Swiss Black females, whereas chimeric males in the other laboratory were bred to C57BL/6J females (37).

Another possible explanation for differences in the phenotype of CYP1A2-deficient mice between the present study and a recent study (37) is a combination of genetic and nongenetic factors—i.e., presence of viral or other respiratory pathogens in a genetically susceptible host. In support of this possibility is that 19 of their 599 *Cyp1a2*(−/−) null mutants did survive to adulthood and are fertile (37).

An additional possible explanation has to do with the gene construct electroporated into the ES cells. It is not without precedent that different genomic approaches to knockouts of the same gene can lead to different phenotypes. For example, several laboratories engineered mutations that created null alleles with no residual expression of the cystic fibrosis transmembrane conductance regulator (*Cftr*) gene (39–41),

whereas a different laboratory created a "leaky" insertional mutation in exon 10 leading to an only mildly affected phenotype (42). It is exciting that both the mild and severe phenotypes of the *Cftr* gene knockout are proving to be valuable experimental model systems. Pineau *et al.* (37) disrupted the *Cyp1a2* gene by inserting the *neo* selection marker into exon 2, whereas we removed much of exon 2 and all of exons 3–5.

Conclusions. We have produced a *Cyp1a2*(−/−) null mutant mouse that develops normally, and is completely viable and fertile, yet exhibits altered drug metabolism. The generation of the *Cyp1a2*(−/−) mouse line described herein will provide an invaluable tool for researchers seeking to define the precise role of the CYP1A2 enzyme in numerous metabolic processes. Such a model will be particularly useful for further investigation of the CYP1A2 enzyme in terms of drug metabolism and toxicity, as well as cancer caused by environmental arylamines. Extrapolation of studies in this mouse line to human populations should also enable more educated predictions of the risk assessment associated with toxic exposures to chemicals via diet, life style, and occupation.

This project was supported by National Institutes of Health Grants RO1-ES06321 (D.W.N.) and P30 ES06096 (J.J.D., D.W.N., and S.S.P.).

1. Nebert, D. W. & Gonzalez, F. J. (1987) *Annu. Rev. Biochem.* 56, 945–993.
2. Nebert, D. W. (1990) *Nature (London)* 347, 709–710.
3. Nebert, D. W. (1991) *Mol. Endocrinol.* 5, 1203–1214.
4. Nebert, D. W. (1994) *Biochem. Pharmacol.* 47, 25–37.
5. Nelson, D. R., Koymans, L., Kamataki, T., Stegeman, J. J., Feyereisen, R., Waxman, D. J., Waterman, M. R., Gotoh, O., Coon, M. J., Estabrook, R. W., Gunsalus, I. C. & Nebert, D. W. (1996) *Pharmacogenetics* 6, in press.
6. Nebert, D. W. & McKinnon, R. A. (1994) *Prog. Liver Dis.* 14, 63–97.
7. Hildebrand, C. E., Gonzalez, F. J., Kozak, C. A. & Nebert, D. W. (1985) *Biochem. Biophys. Res. Commun.* 130, 396–406.
8. Cobb, R. R., Stoming, T. A. & Whitney, J. B., III (1987) *Biochem. Genet.* 25, 401–412.
9. Poland, A. P., Glover, E. & Taylor, B. A. (1988) *Mol. Pharmacol.* 32, 471–478.
10. Burbach, K. M., Poland, A. & Bradfield, C. A. (1992) *Proc. Natl. Acad. Sci. USA* 89, 8185–8189.
11. Ema, M., Sogawa, K., Watanabe, N., Chujoh, Y., Matsushita, N., Gotoh, O., Funae, Y. & Fujii-Kuriyama, Y. (1992) *Biochem. Biophys. Res. Commun.* 184, 246–253.
12. Fernandez-Salguero, P., Pineau, T., Hilbert, D. M., McPhail, T., Lee, S. S. T., Kimura, S., Nebert, D. W., Rudikoff, S., Ward, J. M. & Gonzalez, F. J. (1995) *Science* 268, 722–726.
13. Schweikl, H., Taylor, J. A., Kitareewan, S., Linko, P., Nagorney, D. & Goldstein, J. A. (1993) *Pharmacogenetics* 3, 239–249.
14. Guengerich, F. P., Shimada, T., Raney, K. D., Yun, C.-H., Meyer, D. J., Ketterer, B., Harris, T. M., Groopman, J. D. & Kadlubar, F. F. (1992) *Environ. Health Perspect.* 98, 75–80.
15. Butler, M. A., Lang, N. P., Young, J. F., Caporaso, N. E., Vineis, P., Hayes, R. B., Teitel, C. H., Massengill, J. P., Lawsen, M. F. & Kadlubar, F. F. (1992) *Pharmacogenetics* 2, 116–127.
16. Tang, B. K., Zhou, Y. & Kalow, W. (1994) *Pharmacogenetics* 4, 117–124.
17. Kimura, S., Gonzalez, F. J. & Nebert, D. W. (1984) *J. Biol. Chem.* 259, 10705–10713.
18. Ausubel, F. M., Brent, R., Kingston, R. E., Moore, D. D., Smith, J. A., Seidman, J. G. & Struhl, K. (1991) *Current Protocols in Molecular Biology* (Greene/Wiley-Interscience, New York).
19. Li, H., Zeitler, P. S., Valerius, M. T., Small, K. & Potter, S. S. (1996) *EMBO J.*, in press.
20. Small, K. M. & Potter, S. S. (1993) *Genes Dev.* 7, 2318–2328.
21. Doetschman, T., Eistetter, H., Katz, M., Schmidt, W. & Kemler, R. (1985) *J. Embryol. Exp. Morphol.* 87, 27–45.
22. Hooper, M., Handy, K., Handyside, A., Hunter, S. & Monk, M. (1987) *Nature (London)* 326, 292–295.
23. Doetschman, T. (1994) in *Transgenic Animal Technology: A Laboratory Handbook*, ed. Pinkert, C. (Academic, New York), pp. 115–146.
24. Li, H., Witte, D. P., Brandford, W. W., Aronow, B. J., Weinstein, M., Kaur, S., Wert, S., Singh, G., Schreiner, C. M., Whitsett, J. A., Scott, W. J. & Potter, S. S. (1994) *EMBO J.* 13, 2876–2885.
25. Chomczynski, O. & Sacchi, N. (1987) *Anal. Biochem.* 162, 156–159.
26. Robinson, J. R. & Nebert, D. W. (1974) *Mol. Pharmacol.* 10, 484–493.
27. Ozols, J., Heinemann, F. S. & Johnson, E. F. (1981) *J. Biol. Chem.* 256, 11405–11408.
28. Ono, S., Hatanaka, T., Hotta, H., Tsutsui, M., Satoh, T. & Gonzalez, F. J. (1995) *Pharmacogenetics* 5, 143–150.
29. Nebert, D. W. (1980) *J. Natl. Cancer Inst.* 64, 1279–1290.
30. Tuteja, N., Gonzalez, F. J. & Nebert, D. W. (1985) *Dev. Biol.* 112, 177–184.
31. Kimura, S., Donovan, J. C. & Nebert, D. W. (1987) *J. Exp. Pathol.* 3, 61–74.
32. Dey, A., Westphal, H. & Nebert, D. W. (1989) *Proc. Natl. Acad. Sci. USA* 86, 7446–7450.
33. Pasco, D. S., Boyum, K. W., Merchant, S. N., Chalberg, S. C. & Fagan, J. B. (1988) *J. Biol. Chem.* 263, 8671–8676.
34. Silver, G. J. & Krauter, K. S. (1988) *J. Biol. Chem.* 263, 11802–11807.
35. Gonzalez, F. J. & Nebert, D. W. (1990) *Trends Genet.* 6, 182–186.
36. Heilmann, L. J., Sheen, Y. Y., Bigelow, S. W. & Nebert, D. W. (1988) *DNA* 7, 379–387.
37. Pineau, T., Fernandez-Salguero, P., Lee, S. T. T., McPhail, T., Ward, J. M. & Gonzalez, F. J. (1995) *Proc. Natl. Acad. Sci. USA* 92, 5134–5138.
38. Liu, J. P., Baker, J., Perkins, A. S., Robertson, E. J. & Efstratiadis, A. (1993) *Cell* 75, 59–72.
39. Ratcliff, R., Evans, M. J., Cuthbert, A. W., MacVinish, L. J., Foster, D., Anderson, J. R. & Colledge, W. H. (1993) *Nat. Genet.* 4, 35–41.
40. O'Neal, W. K., Hasty, P., McCray, Jr., J. B., Casey, B., Rivera-Perez, J., Welsh, P. J., Beaudet, A. L. & Bradley, A. (1993) *Hum. Mol. Genet.* 2, 1561–1569.
41. Hyde, S. C., Gill, D. R., Higgins, C. F., Trezise, A. E., MacVinish, L. J., Cuthbert, A. W., Ratcliff, R., Evans, M. J. & Colledge, W. H. (1993) *Nature (London)* 362, 250–255.
42. Dorin, J. R., Dickinson, P., Alton, E. W., Smith, S. N., Geddes, D. M., Stevenson, B. J., Kimber, W. L., Fleming, S., Clark, A. R., Hooper, M. L., Anderson, L., Beddington, R. S. P. & Porteous, D. J. (1993) *Nature (London)* 359, 211–215.
43. Liang, H. C., Li, H., Potter, S. S., Duffy, J. J., Puga, A., McKinnon, R. A. & Nebert, D. W. (1995) *Toxicologist* 15, 59 (abstr.).

THE JOURNAL OF BIOLOGICAL CHEMISTRY

Vol. 271, No. 20, Issue of May 17, pp. 12063–12067, 1996
Printed in U.S.A.

Role of CYP2E1 in the Hepatotoxicity of Acetaminophen*

(Received for publication, January 29, 1996)

Susanna S. T. Lee‡, Jeroen T. M. Buters, Thierry Pineau§, Pedro Fernandez-Salguero, and Frank J. Gonzalez¶

From the Laboratory of Molecular Carcinogenesis, NCI, National Institutes of Health, Bethesda, Maryland 20892

CYP2E1, a cytochrome P-450 that is well conserved across mammalian species, metabolizes ethanol and many low molecular weight toxins and cancer suspect agents. The *cyp2e1* gene was isolated, and a mouse line that lacks expression of CYP2E1 was generated by homologous recombination in embryonic stem cells. Animals deficient in expression of the enzyme were fertile, developed normally, and exhibited no obvious phenotypic abnormalities, thus indicating that CYP2E1 has no critical role in mammalian development and physiology in the absence of external stimuli. When *cyp2e1* knockout mice were challenged with the common analgesic acetaminophen, they were found to be considerably less sensitive to its hepatotoxic effects than wild-type animals, indicating that this P-450 is the principal enzyme responsible for the metabolic conversion of the drug to its active hepatotoxic metabolite.

Cytochromes P-450 (P-450)[1] are a superfamily of hemoproteins that carry out oxidative metabolism of many endogenous and foreign chemicals (1). In mammals, P-450s can be functionally segregated into two groups, those that participate in biochemical pathways leading to the synthesis of steroid hormones and those that primarily metabolize foreign chemicals or xenobiotics such as drugs. The latter enzymes are included in the CYP1, CYP2, CYP3, and CYP4 families (2). Many of the hepatic xenobiotic-metabolizing P-450s also metabolize endogenous compounds, but the significance of these reactions is questionable. A clue to the lack of a critical role for many of the P-450s, particularly those in family 2, in development, reproduction, and longevity, is the marked species differences in their expression and catalytic activities (3). However, some of the xenobiotic-metabolizing P-450s are well conserved, including those in the CYP1 family and CYP2E1, suggesting that they may perform an important physiological function.

CYP2E1 is the principal P-450 responsible for the metabolism of ethanol and is considered as a major component of the microsomal ethanol-oxidizing system (4, 5). Among xenobiotics metabolized by CYP2E1 are acetaldehyde, acetaminophen, acrylamide, aniline, benzene, butanol, carbon tetrachloride, diethylether, dimethyl sulfoxide, ethyl carbamate, ethylene chloride, halothane, glycerol, ethylene glycol, *N*-nitrosodimethylamine, 4-nitrophenol, pyrazole, pyridine, and vinyl chloride (6). Many of these chemicals are known toxins, established chemical carcinogens, or suspected carcinogens. CYP2E1-mediated oxidation of a variety of substrates is also believed to liberate a substantial amount of reactive oxygen that can lead to membrane lipid peroxidation and cell toxicity (7).

CYP2E1 is also capable of metabolizing endogenous chemicals including acetone and acetol, which are key metabolites in the methylglyoxal and propanediol pathways of gluconeogenesis (8, 9). CYP2E1 can also carry out the metabolism of arachidonic acid, resulting in the production of several hydroxyeicosatetraenoic acids (10), some of which may have physiological and pharmacological properties (11).

CYP2E1 is inducible by ethanol and other low molecular weight substrates (5, 12). This induction is primarily due to a postranscriptional mechanism where presence of the substrate stabilizes the enzyme from degradation (13). However, transcriptional mechanisms have not been ruled out (14). This enzyme is also induced by starvation and in uncontrolled diabetes (15, 16).

P-450s have been implicated in the hepatotoxicity of acetaminophen (also called paracetamol), an over-the-counter analgesic and antipyretic that is commonly used worldwide as a substitute for acetylsalicylic acid (aspirin®) due to its lack of gastric ulceration and general low toxicity when used within the recommended dose range (17–19). Acetaminophen causes hepatotoxicity at a low frequency. It is metabolized to *N*-acetyl-*p*-benzoquinoneimine, a metabolite that is capable of reacting with cellular nucleophiles. The bulk of this metabolite is either reduced back to acetaminophen or conjugated with glutathione. It was postulated that toxicity results from low cellular glutathione leaving an excess of active metabolite that can cause cell toxicity (19–22).

The P-450s responsible for acetaminophen activation have been investigated. Ethanol was reported to increase the toxicity of acetaminophen in mice (20, 23), thus suggesting the involvement of CYP2E1 *in vivo*. *In vitro* studies have also implicated human CYP1A2 in addition to CYP2E1 in acetaminophen metabolism, although the latter P-450 had a lower K_m than CYP1A2 (24, 25).

The conservation across species in expression and catalytic activities of CYP2E1 and its ability to metabolize and be induced by chemicals that are generated endogenously, such as acetone and ethanol, suggests that it has an important physiological role in mammals. To investigate this possibility and to determine if this P-450 is involved in the hepatotoxicities and carcinogenesis potential of many of its substrates, mice lacking CYP2E1 expression were produced and characterized.

MATERIALS AND METHODS

Construction of the Targeting Vector—Genomic clones corresponding to *cyp2e1* were obtained by screening a 129/SV genomic library (Stratagene) with a rat CYP2E1 cDNA (26). A clone spanning 14.2 kb and containing all nine exons of the gene was subcloned as a *Sal*I fragment. To disrupt the gene, a 1.9-kb *Hin*dIII fragment containing exon 2 and

* The costs of publication of this article were defrayed in part by the payment of page charges. This article must therefore be hereby marked "*advertisement*" in accordance with 18 U.S.C. Section 1734 solely to indicate this fact.

‡ Present address: Dept. of Biochemistry, The Chinese University of Hong Kong, Shatin, New Territories, Hong Kong.

§ Present address: Laboratory of Pharmacology and Toxicology, INRA, BP3 31931 Toulouse Cedex, France.

¶ To whom correspondence should be addressed: Bldg. 37, Rm. 3E-24, NIH, Bethesda, MD 20892. Tel.: 301-496-9067; Fax: 301-496-8419; E-mail: fjgonz@helix.nih.gov.

[1] The abbreviations used are: P-450, cytochrome P-450; kb, kilobase pair(s); PGK, phosphoglycerate kinase 1; ES, embryonic stem.

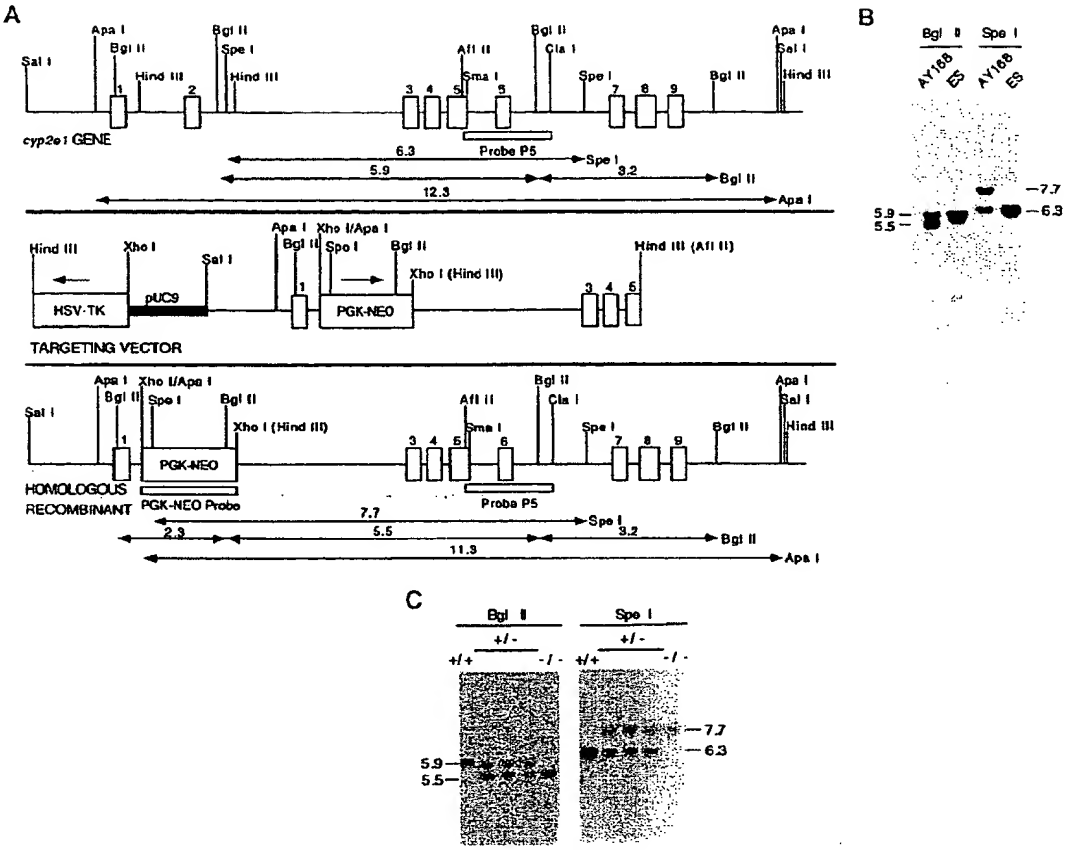

FIG. 1. *Panel A* displays the restriction map of the *cyp2e1* gene, the targeting vector, and the predicted homologous recombinant locus. The *numbers over* the *horizontal double arrows* are the predicted sizes of restriction fragments in kb. *Panel B* shows a Southern blot of the specific ES clone and wild-type ES cells, and *panel C* displays a Southern blot of a typical screen of tail clipping DNA from mice with different genotypes. The sizes of the fragments are in kb.

spanning from intron 1 to intron 2 was deleted and replaced with the bacterial phosphoribosyltransferase II gene, under control of the phosphoglycerate kinase-1 promoter (PGK-NEO), that confers resistance to the neomycin derivative G418 (Life Sciences Inc.). This gene was derived from the plasmid pPNT (27). The PGK-NEO cassette was inserted in the same transcriptional orientation as the *cyp2e1* gene. The herpes simplex virus thymidine kinase gene was inserted at the 3′ end of the *cyp2e1* gene as a negative selection against random integration of the construct (28). The construct used for targeting (see Fig. 1*A*), contained 2.3 kb of 5′ and 3.6 kb of 3′ genomic DNA flanking the PGK-NEO cassette.

The construct was made in six cloning steps (see Fig. 1A). 1) The *Hin*dIII site in the polylinker region of pGEM-3Z (Promega) was destroyed by *Hin*dIII digestion, Klenow polymerase treatment, and religation. 2) An 8-kb *Sal*I-*Sma*I *cyp2e1* genomic fragment was subcloned into the same sites in the modified pGEM-3Z. 3) The plasmid made in step 2 was digested with *Hin*dIII, treated with Klenow polymerase, and ligated with *Xho*I linkers in order to remove the 1.8-kb fragment containing exon 2 and add a restriction site compatible with the PGK-NEO cassette. This 1.9-kb cassette was previously modified by changing the *Bam*HI site at its 3′ end to an *Xho*I site by use of Klenow polymerase and *Xho*I linkers. 4) The *Xho*I fragment containing the PGK-NEO cassette was subcloned into the *cyp2e1* gene at the *Xho*I site. 5) The *cyp2e1* construct, containing the PGK-NEO cassette was digested with *Aff*II, treated with Klenow polymerase, and ligated with *Hin*dIII linkers. 6) The *cyp2e1* gene was released from this construct by digestion with *Sal*I and *Hin*dIII and inserted into the corresponding sites of pMC1TK plasmid (29) containing the herpes simplex virus thymidine kinase gene. The resulting plasmid was used as a targeting vector.

Production of Chimeric Mice—The plasmid DNA used for targeting was purified by banding twice on cesium chloride. After linearization with *Hin*dIII, 40 μg was electroporated into J1 embryonic stem (ES) cells (30) using conditions described previously (31). ES cell clones resistant to both G418 and ganciclovir (gift of Syntex) were selected and screened for homologous recombination, and clones having the expected Southern blot pattern for a homologous recombinant (see below) were regrown and injected into C57BL/6N blastocysts. The blastocysts were transferred into the uterus of a pseudopregnant recipient NIH Swiss mouse in order to produce an animal exhibiting chimerism (32). Male chimeras presenting greater than 95% 129/SV contribution, as determined by coat color, were bred with C57BL/6N females to determine if the trait was transmitted to the germ line. Southern blot genotyping performed on DNA extracted from tail clips, was used to score for the presence of the mutated *cyp2e1* gene in the progeny. Homozygotes were produced by crossing the F1 generation.

Genotyping of ES Cells and Mice—DNA was isolated from ES cells and mouse tail clips as described previously (33) and digested with either *Bgl*I or *Spe*I. The digested DNAs were subjected to electrophoresis in 0.6% agarose gels and transferred to GeneScreen Plus nylon membranes (DuPont) using 0.4 N NaOH. The conditions for hybridization and washing were described previously (31). A 3′-flanking probe derived from a *Aff*II-*Cla*I genomic fragment (see probe P5, Fig. 1*A*) was labeled with [^{32}P]dCTP using random primers. This probe hybridizes with 5.9- and 3.2-kb *Bgl*I fragments and with a 6.3 kb *Spe*I diagnostic fragment for the wild-type *cyp2e1* allele. The homologous recombinant allele generated fragments of 5.5 and 7.7 kb corresponding to digestions with *Bgl*I and *Spe*I, respectively (see Fig. 1, *A–C*). Mice homozygous for the disrupted *cyp2e1* allele were designated cyp2e1$^{-/-}$.

Analysis of CYP2E1 Expression—Mice were killed by carbon monoxide asphyxiation, and 400 mg of liver tissue was disrupted using a

Teflon-glass homogenizer in 3 ml of a buffer containing 20 mM Tris-HCl, pH 7.5, 1 mM EDTA, 25 mM KCl, 1 mM phenylmethylsulfonyl fluoride, 1 mM dithiothreitol, and 10% (v/v) glycerol. The homogenate was centrifuged for 20 min at 10,000 × *g*, and the supernatant was centrifuged for 12 min at 500,000 × *g* in a Beckman Optima TL tabletop ultracentrifuge to recover microsomes. All operations were performed at 4 °C. The microsome pellets were resuspended by homogenization in 0.1 M sodium potassium phosphate buffer, pH 7.4, containing 20% (v/v) glycerol and stored at −80 °C until use. Protein concentrations were determined with the bichinchoninic acid reagent (Pierce) using bovine serum albumin as a standard. SDS-polyacrylamide gel electrophoresis was carried out according to Laemmli (34) using 10 μg of microsomal protein. Proteins were electroblotted to nitrocellulose membranes by semi-dry transfer. Immunoblotting was performed according to Towbin *et al.* (35). Rabbit antibodies against CYP1A2 (36), CYP2A1 (37), CYP2B1 (38), and CYP3A1 (39) were produced as described earlier. Rabbit antisera against CYP2C6 was produced by Dr. Kiyoshi Nagata (Tohoku University, Sendai Japan). Antibody to CYP2E1, produced in goat, was obtained from the Gentest Corp. The secondary antibodies, labeled with horseradish peroxidase, were from Amersham Corp.

Messenger RNA was analyzed by Northern blots using liver RNA and the rat CYP2E1 cDNA as a probe. Total RNA was isolated from liver tissue using guanidinium thiocyanate extraction (40) and cesium trifluoroacetic acid centrifugation as described previously (31). Ten μg of total RNA was subjected to electrophoresis on 1% agarose gels containing 2.2 M formaldehyde (41) and blotted to GeneScreen Plus (DuPont) nylon membranes using 3 M NaCl and 0.15 M sodium citrate, pH 7.0. The CYP2E1 cDNA was labeled using random primers and [^{32}P]dCTP. The conditions for prehybridization, hybridization, and

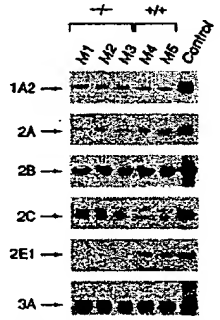

FIG. 2. Western immunoblots of different P-450s in cyp2e1$^{-/-}$ mice. Each lane was loaded with 10 μg of microsomal protein from a single mouse.

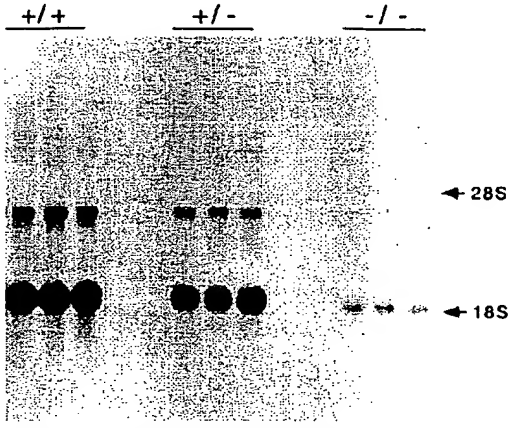

FIG. 3. Analysis of RNA in livers of cyp2e1$^{-/-}$ mice. Each lane was loaded with 10 μg of total liver RNA from a single mouse. The blot was exposed for 24 h with aid of an intensifying screen.

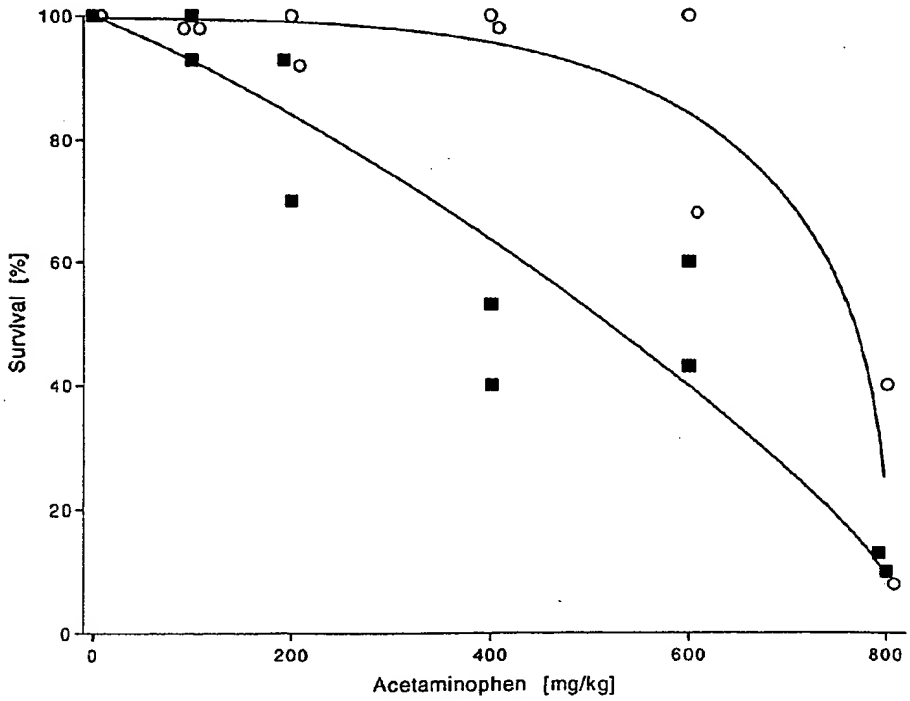

FIG. 4. Survival rate of cyp2e1−/− (○) and wild-type (■) mice as a function of the dose of acetaminophen administered. Groups of 10 mice were injected intraperitoneally with acetaminophen in alkaline saline and survival scored after 48 h. Two complete and independent experiments were performed. The curves were manually fit to the data points.

washing were described previously (31).

Acetaminophen Toxicity—The protocol for dosing mice with acetaminophen was approved by the National Cancer Institute's Animal Care and Use Committee (Protocol LMCE-023). Male cyp2e1$^{-/-}$ and wild-type strains, from 2 to 4 months of age, were administered acetaminophen by intraperitoneal injection at doses ranging from 0 to 800 mg/kg in alkaline saline solution. Each dose group consisted of 10 mice. To score toxicities, the number of surviving animals at 48 h were quantified. Two complete and independent experiments were conducted over the same dose range. From the remaining mice, blood was collected and serum was used to determine the levels of bilirubin, creatinine, alkaline phosphatase, aspartate aminotransferase, and alanine aminotransferase. These measurements were performed by the Diagnostic Services and Clinical Pathology Laboratory of the Uniformed Services University of the Health Sciences Clinical Chemistry Department using a Kodac Ektachem 250 automated plasma analyzer.

RESULTS AND DISCUSSION

Production and Characterization of the cyp2e1$^{-/-}$ Mice—The *cyp2e1* gene was isolated from a 129/SV mouse genomic library. The genomic clone spanned 14.2 kb and contained the complete coding region (Fig. 1*A*). The gene was disrupted by the replacement of exon 2 with the PGK-NEO cassette. A diagnostic probe, designated probe P5 and shown in Fig. 1*A*, was generated that detects homologous integrations of the targeting construct into the gene. Mice having the wild-type allele are expected to yield a 5.9-kb *Bgl*II and a 6.3-kb *Spe*I fragments. A typical autoradiography of a Southern blot of DNA from the ES cell clone AY168 and control ES cells hybridized with the probe P5 is shown in Fig. 1*B*. Upon longer exposure of the blot, an expected 3.2-kb *Bgl*II fragment was also detected. Specific recombinants had diagnostic 5.5- and 7.7-kb fragments from *Bgl*II and *Spe*I, respectively. Screening of mice generated by breeding for heterozygotes for the disrupted *cyp2e1* allele is shown in Fig. 1*C*. Heterozygous mice have the diagnostic fragments corresponding to the wild-type and disrupted alleles, whereas mice that have two copies of the disrupted allele yielded the 5.5- and 7.7-kb fragments after digestion with *Bgl*II and *Spe*I, respectively. Hybridization with the PGK-NEO gene as a probe revealed only a single hybridizing fragments of 2.3, 7.7, and 11.3 kb for the *Bgl*II-, *Spe*I-, and *Apa*I-digested DNA (data not shown), demonstrating that this clone did not contain any additional random integration of the targeting construct.

Mice homozygous for the disrupted allele, designated cyp2e1$^{-/-}$, were born normally and appeared indistinguishable from their wild-type counterparts. No differences were found between litter size and growth rates for the cyp2e1$^{-/-}$ animals as compared with wild-type littermate controls. The expression of CYP2E1 was determined by immunoblotting with anti-rat CYP2E1 antibody. As expected, a complete absence of protein expression was found in the livers of cyp2e1$^{-/-}$ mice (Fig. 2). The liver is the primary site of expression of this P-450 (16). P-450s in the CYP1A, CYP2A, CYP2B, CYP2C, and CYP3A subfamilies were expressed in the cyp2e1$^{-/-}$ mice at similar levels to those found in control animals, thus indicating that the loss of CYP2E1 was not compensated by an increase in expression of other P-450s, although it remains a possibility that a P-450 not detected with our anti-rat P-450 antibodies is overexpressed.

The expression of CYP2E1 mRNA was also analyzed in the cyp2e1$^{-/-}$ mice. Two transcripts were detected in the liver of normal mice and mice heterozygous for the disrupted allele (Fig. 3). In the cyp2e1$^{-/-}$ mice, neither of these two RNA transcripts were found. Instead, two lower abundance RNAs slightly smaller than the transcripts present in wild-type animals were detected. These may be transcripts from the disrupted allele that should be smaller than a transcript from the normal allele since exon 2 is deleted in the disrupted allele. The lower abundance of these RNAs, as compared with those from the wild-type allele, is not surprising since mRNAs that do not encode a normal protein are usually not stable. In any case, the protein and RNA establish with certainty that the *cyp2e1* gene is not expressed in the knockout animals. The change in size and abundance of the high molecular weight transcript annealing with the CYP2E1 cDNA in the cyp2e1$^{-/-}$ mice suggest that it is not due to a cross-hybridizing mRNA derived from another gene but is most likely a read-through transcript of the *cyp2e1* gene with an alternate polyadenylation signal.

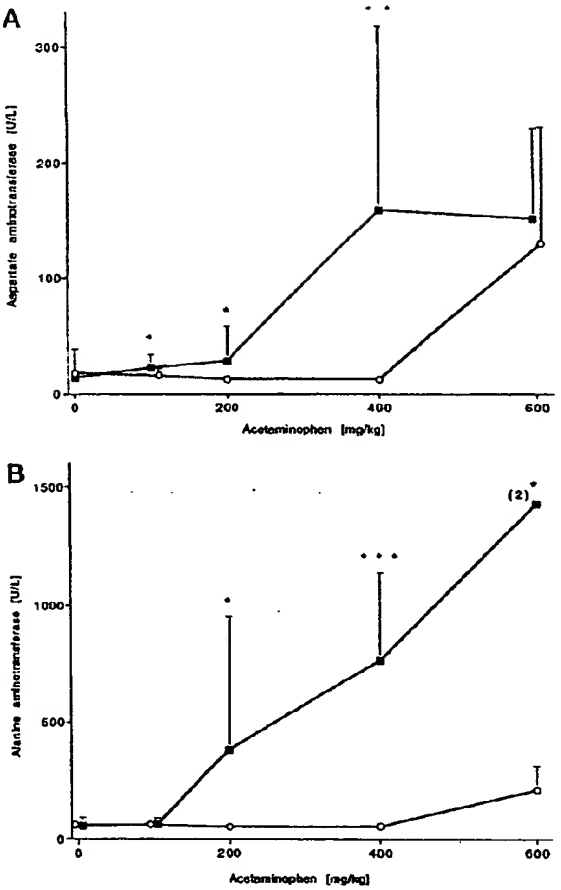

FIG. 5. **Determinations of aspartate aminotransferase (*panel A*) and alanine aminotransferase (*panel B*) activities in serum of cyp2e1$^{-/-}$ (○) and wild-type (■) mice as a function of the dose of acetaminophen administered.** The mean + standard deviations are shown with $n = 3$ (* $p < 0.05$, ** $p < 0.01$, *** $p < 0.001$). At the 600 mg/kg dose group for the wild-type mice in *panel B*, two animals were analyzed.

Acetaminophen Toxicity—P-450s have been implicated in the hepatotoxicity of acetaminophen. To determine whether CYP2E1 influences the toxicity of this compound in mice, the cyp2e1$^{-/-}$ animals were administered the drug and compared with wild-type mice. Survival curves indicated that the cyp2e1$^{-/-}$ mice were more resistant to acetaminophen toxicity than wild-type animals (Fig. 4). Levels of 400 mg of acetaminophen/kg producing toxicity in wild-type mice in this study were similar to those that produced toxicity in other studies (20, 23). Cyp2e1$^{-/-}$ mice survived at doses up to 400 mg/kg, whereas over 50% of wild-type animals died at these doses.

To determine the mechanism of toxicity, levels of enzymes and other serum components, some of which are diagnostic for liver and kidney injury, were measured in serum of treated mice that survived in the experiments described above. At all doses, levels of creatinine, bilirubin, and alkaline phosphatase were within the normal range for mice and were not significantly different between the cyp2e1$^{-/-}$ and wild-type mice. In contrast, liver enzymes aspartate aminotransferase and alanine aminotransferase were elevated at high doses of acetaminophen (Fig. 5). Elevation of these liver enzymes, which are considered a measure of liver cell death, were detected at doses of 200 and 400 mg/kg in wild-type animals but were unchanged at these doses in the cyp2e1$^{-/-}$ mice. These data indicate that liver damage is involved in mediating the toxicity of acetaminophen. This was confirmed by analysis of liver histology of acetaminophen-treated mice (data not shown). At doses higher than 600 mg/kg, a significant level of toxicity was also found in the cyp2e1$^{-/-}$ mice. These data suggest that CYP2E1 mediates the hepatotoxicity of acetaminophen. Other P-450s such as CYP1A2 having a higher K_m for acetaminophen may be responsible for the toxicity in cyp2e1$^{-/-}$ mice at high doses of the drug.

The present study using mice lacking expression of CYP2E1 establish that although this P-450 is highly conserved in mammals, it does not appear to play a significant role in development, reproductive vitality, and physiology. Under conditions of exposure to certain chemicals, CYP2E1 accentuates toxicity. Efforts are underway to use this animal model to determine whether this enzyme is responsible for the carcinogenicity of a number of its chemical substrates including *N*-nitrosodimethylamine and phenacetin.

CYP2E1 may also exert a role in alcoholic liver disease. Lipid peroxidation was found to be associated with alcoholic liver injury in humans and experiment animals (42). This could be the result, in part, of increased oxygen radical production by ethanol-induced CYP2E1 (7). The cyp2e1$^{-/-}$ mice could be used to test this possibility.

During fasting and diabetic ketosis, serum acetone, acetol, and 1,2-propanediol are elevated. CYP2E1 is concommitantly induced due to protein stabilization by acetone (16). Acetone is primarily oxidized to acetol by CYP2E1. Acetol is further metabolized to 1,2-propanediol by the same P-450 in a pathway of gluconeogenesis, suggesting a physiological role for this P-450 during pathophysiological and dietary stress (8). The cyp2e1$^{-/-}$ mice should be of use to determine if CYP2E1 plays an essential role in survival under conditions of starvation.

REFERENCES

1. Gonzalez, F. J. (1988) *Pharmacol. Rev.* **40**, 243-248
2. Nelson, D. R., Koymans, L., Kamataki, T., Stegeman, J. J., Feyereisen, R., Waxman, D. J., Waterman, M. R., Gotoh, O., Coon, M. J., Estabrook, R. W., Gunsalus, I. C., and Nebert, D. W. (1996) *Pharmacogenetics* **6**, 1-41
3. Gonzalez, F. J., and Nebert, D. W. (1989) *Trends Genet.* **6**, 182-187
4. Lieber, C. S., and DeCarli, L. M. (1970) *J. Biol. Chem.* **245**, 2505-2512
5. Koop, D. R., Morgan, E. T., Tarr, G. E., and Coon, M. J. (1982) *J. Biol. Chem.* **257**, 8472-8480
6. Guengerich, F. P., Kim, D. H., and Iwasaki, M. (1991) *Chem. Res. Toxicol.* **4**, 168-179
7. Coon, M. J., Roberts, E. S., and Vaz, A. D. N. (1991) in *Oxidative Damage and Repair: Chemical, Biological and Medical Aspects* (Davies, K. J. A., ed) Pergamon, New York, pp. 726-731
8. Casazza, J. P., Felver, M. E., and Veech, R. L. (1984) *J. Biol. Chem.* **259**, 231-236
9. Koop, D. R., and Casazza, J. P. (1985) *J. Biol. Chem.* **260**, 13607-13612
10. Laethem, R. M., Balazy, M., Falck, J. R., Laethem, C. L., and Koop, D. R. (1993) *J. Biol. Chem.* **268**, 12912-12918
11. Fitzpatrick, F. A., and Murphy, R. C. (1988) *Pharmacol. Rev.* **40**, 229-241
12. Koop, D. R., and Coon, M. J. (1984) *Mol. Pharmacol.* **25**, 494-501
13. Song, B. J., Matsunaga, T., Hardwick, J. P., Veech, R. L., Yang, C. S., Gelboin, H. V., and Gonzalez, F. J. (1987) *Mol. Endocrinol.* **1**, 542-547
14. Song, B. J. (1995) in *Drug and Alcohol Abuse Reviews, Vol. 6: Alcohol and Hormones* (Watson, R. R., ed) pp. 277-192, Human Press Inc., Totowa, NJ
15. Hong, J., Pan, J., Gonzalez, F. J., Gelboin, H. V., and Yang, C. S. (1987) *Biochem. Biophys. Res. Commun.* **142**, 1077-1083
16. Song, B. J., Gelboin, H. V., Park, S. S., Yang, C. S., and Gonzalez, F. J. (1986) *J. Biol. Chem.* **261**, 16689-16697
17. Jollow, D. J., Mitchell, J. R., Potter, W. Z., Davis, D. C., Gillette, J. R., and Brodie, B. B. (1973) *J. Pharmacol. Exp. Ther.* **187**, 195-202
18. Mitchell, J. R., Jollow, D. J., Potter, W. Z., Davis, D. C., Gillette, J. R., and Brodie, B. B. (1973) *J. Pharmacol. Exp. Ther.* **187**, 211-217
19. Potter, W. Z., Davis, D. C., Mitchell, J. R., Jollow, D. J., Gillette, J. R., and Brodie, B. B. (1973) *J. Pharmacol. Exp. Ther.* **187**, 203-210
20. Peterson, F. J., Holloway, D. E., Erickson, R. R., Duquette, P. H., McCain, C. J., and Holtzman, J. L. (1980) *Life Sci.* **27**, 1705-1711
21. Dahlin, D. C., Miwa, G. T., Lu, A. Y. H., and Nelson, S. D. (1984) *Proc. Natl. Acad. Sci. U. S. A.* **81**, 1327-1331
22. Prasad, J. S., Chen, N. Q., Liu, Y. X., Coon, D. J. W., and Holtzman, J. L. (1990) *Biochem. Pharamacol.* **40**, 1989-1995
23. Snawder, J. E., Roe, A. L., Benson, R. W., and Roberts, D. W. (1994) *Biochem. Biophys. Res. Commun.* **203**, 532-539
24. Raucy, J. L., Lasker, J. M., Lieber, C. S., and Black, M. (1989) *Arch. Biochem. Biophys.* **271**, 270-283
25. Snawder, J. E., Roe, A. L., Benson, R. W., Casciano., D. A., and Roberts, D. W. (1994) *Pharmacogenetics* **4**, 43-46
26. Song, B. J., Veech, R. L., Park, S. S., Gelboin, H. V., and Gonzalez, F. J. (1989) *J. Biol. Chem.* **264**, 3568-3572
27. Tybulewicz, V. L. J., Crawford, C. E., Jackson, P. K., Bronson, R. T., and Mulligan, R. C. (1991) *Cell* **65**, 1153-1163
28. Bradley, A. (1987) in *Teratocarcinoma and Embryonic Stem Cells: A Practical Approach* (Robertson, E. J., ed) pp. 133-151, IRL Press, Oxford
29. Mansour, S. L., Thomas, K. R., and Capecchi, M. R. (1988) *Nature* **336**, 348-352
30. Li, E., Bestor, T. H., and Jaenisch, R. (1992) *Cell* **69**, 915-926
31. Lee, S. S. T., Pineau, T., Drago, J., Lee, E. J., Owens, J. W., Kroetz, D. L., Fernandez-Salguero, P., Westphal, H., and Gonzalez, F. J. (1995) *Mol. Cell. Biol.* **15**, 3012-3022
32. Hogan, B., Costantini, F., and Lacy, E. (eds) (1986) *Manipulating the Mouse Embryo: A Laboratory Manual*, Cold Spring Harbor Laboratory, Cold Spring Harbor, NY
33. Laird, P. W., Zijderveld, A., Linders, K., Rudnicki, M. A., Jaenisch, R., and Berns, A. (1991) *Nucleic Acids Res.* **19**, 4293
34. Laemmli, U. K. (1970) *Nature* **227**, 680-685
35. Towbin, H., Staehelin, T., and Gordon, J. (1979) *Proc. Natl. Acad. Sci. U. S. A.* **76**, 4350-4354
36. Aoyama, T., Gonzalez, F. J., and Gelboin, H. V. (1989) *Mol. Carcinogen.* **1**, 253-259
37. Nagata, K., Matsunaga, T., Gillette, J., Gelboin, H. V., and Gonzalez, F. J. (1987) *J. Biol. Chem.* **262**, 2787-2793
38. Yamano, S., Nhamburo, P. T., Aoyama, T., Meyer, U. A., Inaba, T., Kalow, W., Gelboin, H. V., McBride, O. W., and Gonzalez, F. J. (1989) *Biochemistry* **28**, 7340-7348
39. Gonzalez, F. J., Song, B. J., and Hardwick, J. P. (1986) *Mol. Cell. Biol.* **6**, 2969-2976
40. Chirgwin, J. M., Przybyla, A. E., MacDonald, R. J., and Rutter, W. J. (1979) *Biochemistry* **18**, 5294-5299
41. Lehrach, H., Diamond, D., Wozney, J. M., and Boedtker, H. (1977) *Biochemistry* **16**, 4743-4751
42. Shaw, S., Rubin, K. P., and Lelber, C. S. (1983) *Dig. Dis. Sci.* **28**, 585-589

BREVIA

NEUROSCIENCE

Synthesis of Serotonin by a Second Tryptophan Hydroxylase Isoform

Diego J. Walther,[1]* Jens-Uwe Peter,[1] Saleh Bashammakh,[1] Heide Hörtnagl,[2] Mechthild Voits,[2] Heidrun Fink,[3] Michael Bader[1]*

The neurotransmitter serotonin [5-hydroxytryptamine (5-HT)] is causally involved in multiple central nervous facets of mood control and in regulating sleep, anxiety, alcoholism, drug abuse, food intake, and sexual behavior (*1*). In peripheral tissues, 5-HT regulates vascular tone, gut motility, primary hemostasis, and cell-mediated immune responses (*1*). 5-HT is synthesized in two steps, with tryptophan hydroxylase (TPH) as the rate-limiting enzyme (*2*). TPH belongs to a superfamily of aromatic amino acid hydroxylases, together with phenylalanine (PAH) and tyrosine hydroxylases (TH), and has been detected mainly in the brain stem and gut enterochromaffin cells (*2*).

To study the physiological impact of the loss of 5-HT synthesis, we generated mice genetically deficient for TPH (*Tph*−/−). Like wild-type (*Tph*+/+) siblings and the mouse strains from which the *Tph*−/− animals were derived, *Tph*−/− mice still expressed normal amounts of 5-HT in classical serotonergic brain regions. However, *Tph*−/− mice lacked 5HT in the periphery except for in the duodenum (Fig. 1A), which contained about 4% of normal 5-HT levels, probably because of the serotonergic neurons in this tissue (*3*). Concordantly, *Tph*−/− mice exhibited no significant behavioral differences in elevated plus maze and hole board tests (table S1), which are indicative for 5-HT–related behavior.

Despite suggestions of a possible second TPH isoform (*4*), molecular verification has been lacking. Therefore, we screened the High Throughput Genomic Sequences database of GenBank with short translated sequences of *Tph* and obtained a human genomic clone on chromosome 12, with an open reading frame similar to *Tph* exon 4, but different from *Pah*, which is located on the same chromosome. On the basis of this sequence, we performed 5′- and 3′-RACE experiments with brain RNA of *Tph*−/− mice and obtained the full-length cDNA (referred to as *Tph2*; GenBank: AY090565; fig. S1), which was different from the known Tph (referred to here now as *Tph1*), *Pah*, and *Th* of the mouse.

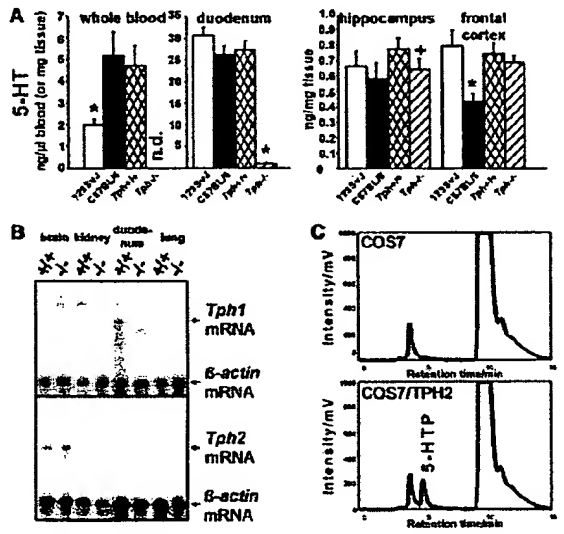

Fig. 1. (A) 5-HT in whole blood, duodenum, hippocampus, and frontal cortex of 129Sv/, C57BL/6, *Tph*+/+, and *Tph*−/− mice. n.d., below the detection limit of the assay (<5 pg/µl). *, statistically significant ($P < 0.05$), as compared with all other investigated mouse lines. +, statistically significant ($P < 0.05$), as compared with *Tph*+/+ mice, but not with other laboratory mouse lines. (B) RNase protection assays with probes specific for the two isoforms reveal the presence of *Tph1* mRNA in duodenum of wild-type animals, but not in *Tph*−/− mice. *Tph2* mRNA is present exclusively in brain, irrespective of the genotype. (C) Reversed-phase HPLC-FD chromatograms of TPH activity assays. (Top) Untransfected COS7 cells. (Bottom) COS7 cells transiently transfected with a eukaryotic expression vector containing the mouse *Tph2* cDNA. 5-Hydroxylated tryptophan (5-HTP) elutes with a retention time of 5 min.

We detected *Tph1* mRNA in the duodenum, but not in the brain, by ribonuclease (RNase) protection assays (RPAs) specific for each *Tph* isoform (Fig. 1B). In contrast, *Tph2* was detected exclusively in the brain (Fig. 1B). Brain stem total RNA samples from wild-type mice revealed about 150 times more *Tph2* than *Tph1* mRNA by RPAs (*5*).

Transfected COS7 cells expressing TPH2 acquired tryptophan-hydroxylating activity, confirming the identity of this enzyme (Fig. 1C). Moreover, commercially available antibodies against TPH1 also detected TPH2 in transfected cells (*5*), thus explaining previous detection of TPH in the brain.

We also cloned and sequenced the rat and human TPH2 homologs (GenBank: AY098915 and AY098914; fig. S1) and detected TPH2 expression in rat brain (*5*). By searching GenBank, we found one homologous expressed sequence tag from chicken and several from zebrafish brain, in addition to a sequence from zebrafish ovary with high homology to the mammalian TPH1 (*6*).

The discovered duality of the serotonin system in vertebrates may open up new avenues for specific therapeutic approaches exclusively affecting central or peripheral 5-HT actions. This is particularly important, because of efforts to find diagnostically useful correlations between peripheral levels of 5-HT and its metabolites and 5-HT function in the central nervous system of human patients suffering from psychiatric disorders (*7*). Also, numerous attempts linking polymorphisms in the *Tph1* gene with such diseases (*1*) have to be reconsidered now that it is known that this gene is hardly expressed in the brain.

References and Notes

1. J. Veenstra-VanderWeele, G. M. Anderson, E. H. Cook Jr., *Eur. J. Pharmacol.* **410**, 165 (2000).
2. P. F. Fitzpatrick, *Annu. Rev. Biochem.* **68**, 355 (1999).
3. J. J. Chen *et al.*, *J. Neurosci.* **21**, 6348 (2001).
4. D. M. Kuhn, M. A. Meyer, W. Lovenberg, *Arch. Biochem. Biophys.* **199**, 355 (1980).
5. D. J. Walther *et al.*, data not shown.
6. Accession numbers of vertebrate *Tph* sequences are provided in the supplementary material available on *Science* Online.
7. M. Humble, S. Bejerot, P. B. F. Bergqvist, F. Bengtsson, *Biol. Psychiatry* **49**, 360 (2001).

Supporting Online Material
www.sciencemag.org/cgi/content/full/299/5603/76/DC1
Materials and Methods
Fig. S1
Table S1

[1]Max Delbrück Center for Molecular Medicine (MDC), Robert-Rössle-Strasse 10, D-13092 Berlin-Buch, Germany. [2]Institute of Pharmacology and Toxicology of the Medical Faculty, Charité, Humboldt University Berlin, Dorotheenstrasse 94, D-10117 Berlin, Germany. [3]Institute of Pharmacology and Toxicology of the School of Veterinary Medicine, Free University Berlin, Koserstrasse 20, D-14195 Berlin, Germany.

*To whom correspondence and requests for materials should be addressed. E-mail: dwalther@mdc-berlin.de or mbader@mdc-berlin.de

MOLECULAR AND CELLULAR BIOLOGY, Jan. 2001, p. 148–155 Vol. 21, No. 1
0270-7306/01/$04.00+0 DOI: 10.1128/MCB.21.1.148–155.2001

Gene Disruption of Tissue Transglutaminase

VINCENZO DE LAURENZI AND GERRY MELINO*

IDI-IRCCS Biochemistry Lab, Department of Experimental Medicine, University Tor Vergata, Rome, Italy

Received 20 July 2000/Returned for modification 12 September 2000/Accepted 28 September 2000

Transglutaminase 2 (TGase 2), or tissue transglutaminase, catalyzes either ε-(γ-glutamyl)lysine or N^1,N^8-(γ-glutamyl)spermidine isopeptide bonds. TGase 2 expression has been associated with apoptosis, and it has been proposed that its activation should lead to the irreversible assembly of a cross-linked protein scaffold in dead cells. Thus, TGase 2-catalyzed protein polymerization contributes to the ultrastructural changes typical of dying apoptotic cells; it stabilizes the integrity of the apoptotic cells, preventing the release of harmful intracellular components into the extracellular space and, consequently, inflammation and scar formation. In order to perform a targeted disruption of the enzyme, we prepared a construct deleting part of exons 5 and 6, containing the active site, and intron 5. Complete absence of TGase 2 was demonstrated by reverse transcription-PCR and Western blot analysis. TGase activity measured on liver and thymus extracts showed, however, a minimal residual activity in TGase $2^{-/-}$ mice. PCR analysis of mRNA extracted from the same tissues demonstrated that at least TGase 1 (normally present in the skin) is also expressed in these tissues and contributes to this residual activity. TGase $2^{-/-}$ mice showed no major developmental abnormalities, and histological examination of the major organs appeared normal. Induction of apoptosis ex vivo in TGase $2^{-/-}$ thymocytes (by CD95, dexamethasone, etoposide, and H_2O_2) and in vitro on TGase $2^{-/-}$ mouse embryonal fibroblasts (by retinoids, UV, and H_2O_2) showed no significant differences. A reduction in cross-linked apoptotic bodies with a modestly increased release of lactate dehydrogenase has been detected in some cases. Together our results show that TGase 2 is not a crucial component of the main pathway of the apoptotic program. It is possible that the residual enzymatic activity, due to TGase 1 or redundancy of other still-unidentified TGases, can compensate for the lack of TGase 2.

Transglutaminase 2 (TGase 2; also called tissue transglutaminase or TG C) belongs to the transglutaminase (EC 2.3.2.13) family, which includes intracellular and extracellular enzymes catalyzing Ca^{2+}-dependent reactions resulting in the formation of ε-(γ-glutamyl)lysine cross-links and/or in the covalent incorporation of di- and polyamines and histamine (25, 26). The establishment of these covalent cross-links leads to the posttranslational modification and, in many instances, the oligomerization of substrate proteins. The resulting protein polymers are resistant to breakage and chemical attack and can release polypeptides only through the proteolytic degradation of protein chains. At least seven distinct types of TGases in mammals have been characterized: TGase 1 (or TG K), TGase 2, TGase 3 (or TG E), TGase X, coagulation factor XIII, band 4.2., and prostate TGase. At least four transglutaminases (TGases 1, 2, 3, and X) are expressed and synthesized during terminal differentiation and death of human epidermal keratinocytes (44, 45), where they contribute to the formation of the cornified envelope.

The TGase 2 gene is constitutively expressed both during development (29, 48) and in adult tissues (for a review, see reference 36). In both cases a tight correlation between TGase 2 expression and occurrence of apoptosis has been found. This includes, for example, interdigital web formation (29), implantation of the embryo in utero (35), and mammary gland regression (31, 46). In addition, the presence and activity of the enzyme have been shown to increase in cells undergoing apoptosis in several models (2, 9, 10, 21, 23–25, 32–34, 37, 40). Indeed, during apoptosis de novo transcription of the TGase 2 gene is induced by several factors (e.g., retinoic acid [RA], prostaglandin E2, interleukin 6, and tumor growth factor β). Moreover, in addition to transcriptional regulation (24, 28, 41), TGase 2 can also be modulated posttranscriptionally (1, 23, 50) during apoptosis. TGase 2 activation leads to the assembly of intracellular cross-linked protein polymers, which irreversibly modifies cell organization, contributing to the wide ultrastructural changes occurring in cells undergoing apoptosis (9, 10, 39). This extensive TGase 2-dependent protein polymerization stabilizes apoptotic cells before their clearance by phagocytosis, thus contributing to the prevention of inflammation in the surrounding tissues (39).

In addition to its cross-linking activity, TGase 2 acts as the Gαh subunit, associated with the 50-kDa β subunit (Gβh), of the GTP-binding protein (Gh) in a ternary complex associated with the rat liver α1-adrenergic receptor (30). Thus, TGase 2-Gαh is a multifunctional protein, which by binding GTP in a Gαh-GTP complex can modulate receptor-stimulated phospholipase C activation.

In order to clarify the role of TGase 2 in apoptosis we have generated mice lacking TGase 2 by homologous recombination techniques. Our results, however, show that the disruption of TGase 2 does not produce a major phenotype and that apoptosis still occurs normally in the absence of TGase 2.

* Corresponding author. Mailing address: IDI-IRCCS, Biochemistry Lab, c/o Dep. Experimental Medicine, D26/F153, University of Rome Tor Vergata, Via Tor Vergata 135, 00133 Rome, Italy. Phone: 39 6 20427299. Fax: 39 6 20427290. E-mail: gerry.melino@uniroma2.it.

MATERIALS AND METHODS

Reagents. Ham's F-12 and minimal essential media were from Gibco (Berlin, Germany), and fetal calf serum was from HyClone (Oud-Beijerland, The Neth-

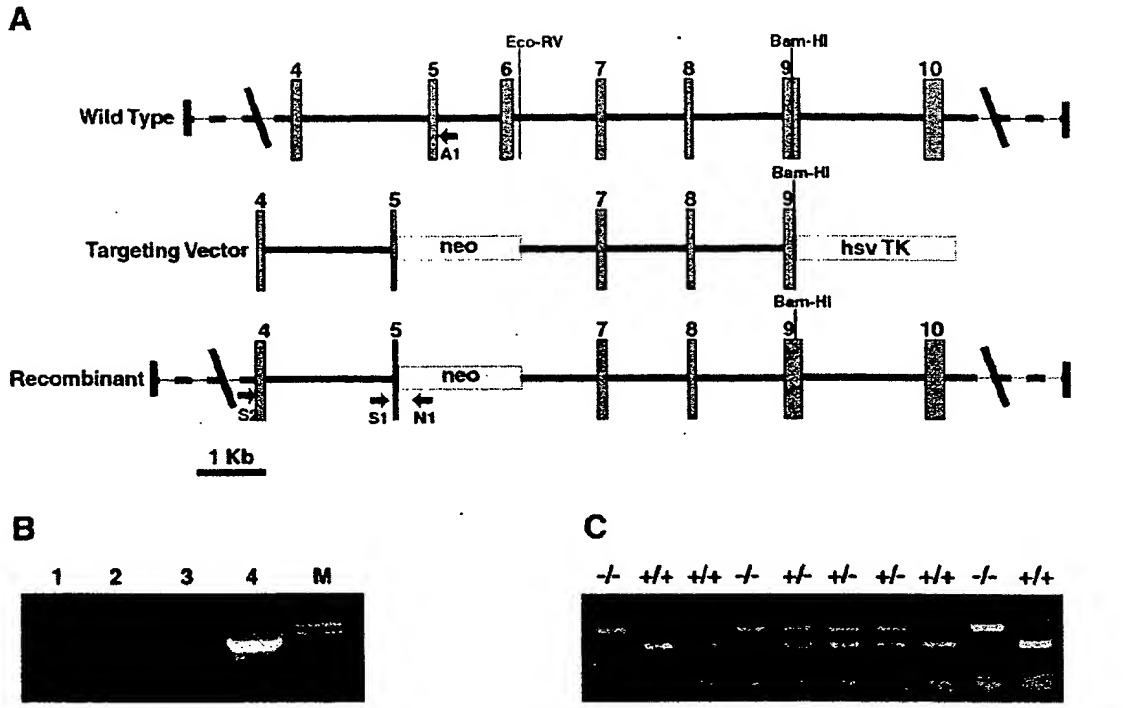

FIG. 1. (A) Schematic representation of the targeting construct used to generate TGase 2 knockout mice. An *Eco*RV/*Bam*HI genomic fragment (from intron 6 to exon 9) was cloned at the 5′ end of the neomycin resistance gene into the pPNT vector (49). Subsequently, a PCR fragment from exon 4 to exon 5 was cloned into this vector at the 5′ end of the neomycin resistance gene, using an *Xho*I site. As a result, part of exon 5 and the totality of exon 6 (containing the active site) and intron 5 were deleted. The arrows show the positions of the primers used for the screening of the recombinant clones (N1 and S2) and the genotyping of the mice (A1, N1, and S1). Intron positions were obtained by direct sequencing or PCR analysis with primers located in the flanking exons. The position of exon 7 was not determined, and therefore its position in the scheme is arbitrary. hsv TK, herpes simplex virus thymidine kinase. (B) PCR screening for the recombinant clone using a primer in the neomycin resistance gene (N1) and a primer on the TGase sequence (S2) in a region upstream of the fragment used to generate the targeting vector. Lanes 1 to 3 contain wild-type clones, and lane 4 contains the recombinant clone used to generate chimeras. (C) PCR screening for the genotyping of the mice. Three different primers (see Materials and Methods) were used at the same time: an antisense primer on the neomycin resistance gene (N1), an antisense primer in intron 5 (A1) deleted in the targeted alleles, and a sense primer in intron 4 (S1) present in both wild-type and targeted alleles.

erlands). HEPES, bovine serum albumin (BSA), RNase A, propidium iodide (PI), Triton X-100, RA, *N,N′*-dimethylcasein, and putrescine were obtained from Sigma Chemical (St. Louis, Mo.). The mouse monoclonal anti-TGase 2 antibodies (clone CUB 7402 and clone CUB 7402+TG100) were purchased from Neo-Markers (Union City, Calif.). All electrophoresis reagents and secondary antibodies were from Bio-Rad (Richmond, Calif.). [^{3}H]putrescine was obtained from Amersham (Arlington Heights, Ill.).

Generation of TGase 2-deficient mice. A genomic clone containing the genomic sequence 3′ of exon 5 was isolated by screening a 129/SvJ mouse genomic library (Stratagene, La Jolla, Calif.). The targeting vector (Fig. 1A) was constructed by cloning an ~4-kb *Eco*RV/*Bam*HI fragment of this clone, containing the sequence from intron 6 to exon 9, into the pPNT vector (49) 3′ of the neomycin resistance gene between the *Xba*I and *Bam*HI unique sites. An ~2-kb fragment containing intron 3 was generated by PCR using primers designed on the basis of the sequence of exons 4 and 5. This fragment was cloned into the *Xho*I site of the pPNT vector 5′ of the neomycin resistance gene. This construct deletes 1.2 kb containing part of exon 5, intron 5, exon 6, and a small piece of intron 6 up to the *Eco*RV site.

The targeting vector was linearized by *Not*I and electroporated into embryonic stem cells. Cells were selected with G418 and ganciclovir. Surviving clones were screened by PCR using the following primers: S2 (5′AGCCGATGATGTGTA CCTAGAC3′) and N1 (5′ACGAGACTAGTGAGACGTGC3′) (Fig. 1B). The following PCR program was used: 95°C for 5 min, followed by 40 cycles of 94°C for 1 min, 58°C for 1 min, and 72°C for 1 min. PCR products were resolved on a 0.8% agarose gel and stained with ethidium bromide. The positive clone was then confirmed by Southern blotting.

Cells from the positive clone were microinjected into C57BL/6 blastocysts and transferred into pseudopregnant recipients by Genome Systems, St. Louis, Mo. The six chimeric animals obtained were bred with C57BL/6 mice. The genotype of the subsequent offspring was determined by PCR using the following primers: S1 (5′TACTCCAGCTTCCTGTTCTG3′), A1 (5′TCCTGACCTGAGTCCTCG TC3′), and N1 (Fig. 1). The following PCR program was used: 95°C for 5 min, followed by 30 cycles of 94°C for 1 min, 56°C for 45 s, and 72°C for 1 min. PCR products were resolved on a 1% agarose gel and stained with ethidium bromide. Each mouse was individually genotyped before every experiment.

Cell cultures. Mouse embryonic fibroblasts (MEFs) and thymocytes were grown in a 1:1 mixture of minimal essential medium and Ham's F-12 medium supplemented with 10% heat-inactivated fetal calf serum, 1.2 g of sodium bicarbonate per liter, and 15 mM HEPES at 37°C with 5% CO_2 in a humidified atmosphere.

Western blotting. Livers were homogenized in 3 ml of cold lysis buffer containing 100 mM Tris-HCl (pH 7.4), 10 mM KCl, 2 mM $MgCl_2$, 0.1% Triton X-100, 1 mM EDTA, and 1 mM phenylmethylsulfonyl fluoride. They were then centrifuged, and the protein content of the supernatants was determined using the Bradford method (Bio-Rad). Proteins were normalized to 30 μg/lane, separated on sodium dodecyl sulfate (SDS)–12% polyacrylamide gels, and blotted onto nitrocellulose sheets. Filters were washed twice with phosphate-buffered saline (PBS) containing 0.1% Tween 20 before blocking nonspecific binding

overnight with 10% nonfat milk and 5% BSA dissolved in PBS–0.1% Tween 20. The TGase 2 antigen was detected by incubation for 2 h with a 1:1 mixture of mouse monoclonal anti-TGase 2 antibodies (1:300 in PBS–0.1% Tween 20). Nitrocellulose filters were washed five times, and detection was performed by horseradish peroxidase-conjugated goat anti-mouse monoclonal antibody (1:2,500 in PBS–0.1% Tween 20 with 10% milk and 5% BSA) for 1 h at room temperature, using the ECL method (Amersham).

Enzyme assay. TGase activity was determined by measuring the incorporation of [^{3}H]putrescine into *N,N'*-dimethylcasein (22, 26). The reaction mixture contained 150 mM Tris-HCl buffer (pH 8.3), 90 mM NaCl, 10 mM dithiothreitol, 15 mM $CaCl_2$, 12.5 mg of *N,N'*-dimethylcasein/ml, and 0.2 mM putrescine containing 1 μCi of [^{3}H]putrescine. Proteins from different tissue and cellular extracts (0.1 to 0.3 mg) were incubated with the reaction mixture in a final volume of 150 μl at 37°C. After 20 min of incubation, the reaction was stopped by spotting 100-μl quadruplicate aliquots onto Whatman 3MM filter paper. Unbound [^{3}H]putrescine was removed by washing with large volumes of 15, 10, and 5% trichloroacetic acid and absolute ethanol. Filters were then air dried and the radioactivity was measured by liquid scintillation counting.

PCR analysis of TGases 2 and 1. Total RNA was extracted from mouse livers, using the RNeasy minikit from Qiagen (Crawley, United Kingdom). Reverse transcription (RT)-PCRs were performed with the RT-PCR One Step System (Life Technologies, Paisley, United Kingdom), using 100 ng of total RNA according to the manufacturer's instructions. The primers used for the amplification of TGase 2 were TG30 (5'GACAACAACTATGGGGATGGT3') and TG9B (5'ATCATCTCGCTCTTGTTCGTC3'). The primers used for the amplification of TGase 1 were MTG1F (5'ACCACCACAGTGCTCCGATG3') and MTG1R (CCACACGTGGAAGTTCCAAAC3'). The following PCR program was used in all cases: 42°C for 30 min and 94°C for 2 min, followed by 35 cycles of 94°C for 30 s, 57°C for 30 s, and 70°C for 30 s. PCR products were resolved on a 1.6% agarose gel and stained with ethidium bromide.

Determination of cell death. To estimate DNA fragmentation, a mixture of floating cells and cells mechanically recovered from flasks, which had been subjected to different treatments, were collected at 800 × *g* for 10 min and fixed with a 1:1 solution of PBS and methanol-acetone (4:1, vol/vol) at −20°C. The cell cycle was evaluated by flow cytometry using PI staining (40 mg/ml) (22) in the presence of 13 kU of RNase A per ml (20 min of incubation at 37°C) on a FACS-Calibur flow cytometer (Becton Dickinson, San Jose, Calif.). Cells were excited at 488 nm using a 15-mW argon laser, and the fluorescence was monitored at 578 nm at a rate of 150 to 300 events/s. Ten thousand events were evaluated using the Cell Quest program (Becton Dickinson). Electronic gating (FSC-a/vs/FSC-h) was used, when appropriate, to eliminate cell aggregates.

LDH release. For measurement of lactate dehydrogenase (LDH) levels, a kit was used according to the manufacturer's instructions (Sigma Chemical). Briefly, the cell culture supernatant was incubated with pyruvate and NADH, and the LDH activity was determined photometrically at 340 nm.

Quantification of cross-linked apoptotic bodies. Cross-linked apoptotic bodies were estimated on cells cultured in 175-cm^2 flasks, as previously described (26). Cells floating in the culture medium were collected by centrifugation at 800 × *g* for 10 min and pooled with the cells mechanically recovered from flasks. After being washed in PBS, cells were suspended in 1 ml of lysis buffer (10 mM KCl, 2 mM $MgCl_2$, and 0.5% Triton X-100 in 10 mM Tris-HCl, pH 7.4) containing 1 mM phenylmethylsulfonyl fluoride and 2 mM iodoacetamide. After centrifugation the pellet was washed in lysis buffer, suspended in a 2% sodium dodecyl sulfate solution containing 5% β-mercaptoethanol, and boiled, and the number of detergent-insoluble apoptotic bodies was scored using a phase-contrast microscope (Diaphot; Nikon) and normalized to milligrams of protein.

RESULTS

Generation of TGase 2-deficient mice. The TGase 2 gene was disrupted by homologous recombination. The targeting vector deletes 1,200 bp of the TGase gene from exon 5 to intron 6. This deletion includes exon 6, which contains the active site. The loss of the catalytic site abolishes the protein cross-linking activity of TGase 2, consequently removing its presumed role in the formation of the apoptotic body. Figure 1 shows the targeting vector and the screening strategy.

TGase $2^{-/-}$ mice show no clear phenotypic abnormality (macroscopic or microscopic); they develop normally and are capable of reproducing at the expected frequency.

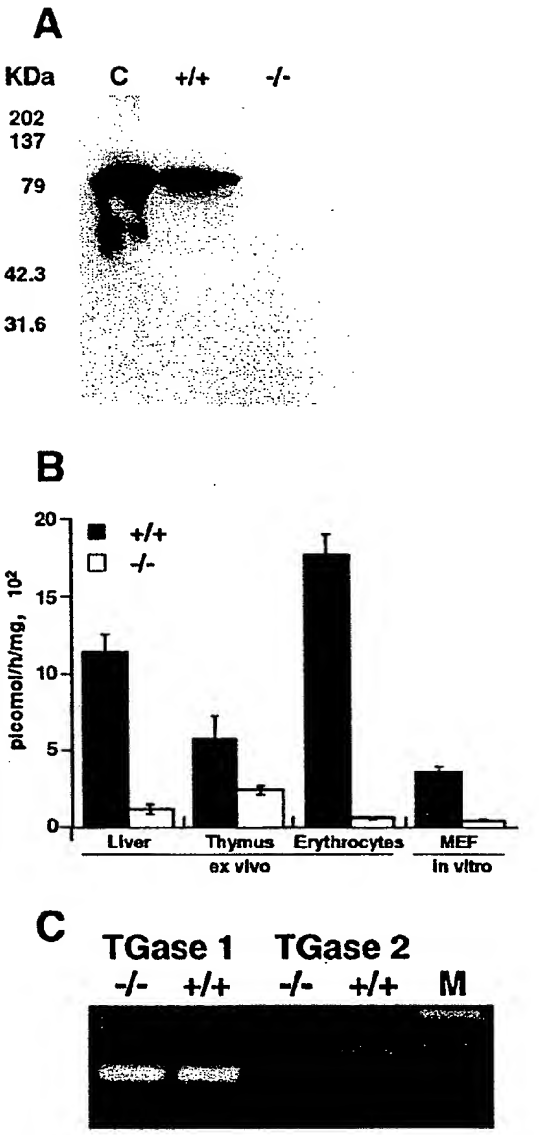

FIG. 2. (A) Western blotting performed on liver extracts from wild-type and TGase-knockout mice with anti-TGase 2 antibody. Thirty micrograms of total protein was loaded in each lane. Recombinant guinea pig TGase 2 (0.1 μg) was used as a positive control (C). This blot is representative of experiments performed on different tissues from four different animals per group. (B) TGase enzymatic activity measured in extracts from different mouse tissues and cultured MEFs in both wild-type and TGase-knockout mice. Activity was measured as incorporation of [^{3}H]putrescine into casein. Standard deviations for 10 different evaluations are shown. (C) RT-PCR performed on RNA extracted from thymus tissues of wild-type and TGase-knockout mice using primers for TGase 2 and TGase 1.

In order to confirm that no TGase 2 protein is produced in TGase 2-deficient mice, we performed Western blot analysis on liver, thymus, brain, and erythrocyte extracts from wild-type animals (TGase $2^{+/+}$) and from TGase $2^{-/-}$ mice. Our results

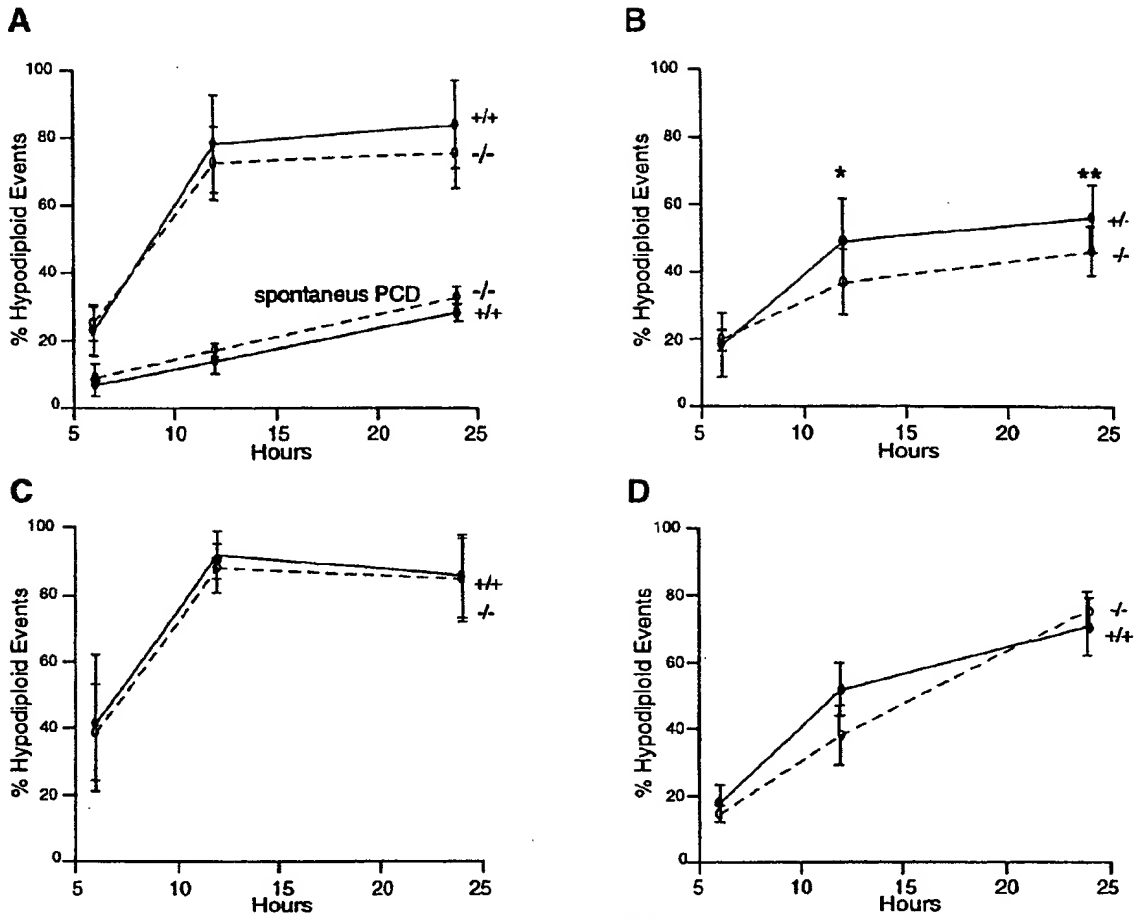

FIG. 3. Hypodiploid events in wild-type and knockout mouse thymocytes, either left untreated (spontaneous programmed cell death [PCD]) (bottom curves in panel A) or treated with etoposide (25 μM) (top curves in panel A), anti-CD95 agonist antibody (1 μg/ml) (B), dexamethasone (10 μM) (C), and H_2O_2 (30 μM) (D). Cells were treated for 6, 12, and 24 h, then fixed with a 1:1 solution of PBS and methanol-acetone (4:1, vol/vol) at −20°C and stained with PI. The number of events (10,000 collected) with hypodiploid DNA was measured by flow cytometry. The data reported are averages of four independent experiments performed on different mice. *, $P = 0.0352$ for +/+ versus −/− mice; **, $P = 0.0451$ for +/+ versus −/− mice (according to the Student t test). Differences not indicated are not statistically significant.

show the absence of TGase 2 protein in the −/− animals (Fig. 2A shows liver extracts). However, measurement of TGase activity (Fig. 2B) in different tissues extracted from TGase $2^{-/-}$ animals showed that some residual TGase enzyme activity was still present. Indeed, while erythrocytes showed a reduction in activity close to 100%, thymocytes showed the highest level of residual TGase activity, which is quite significant compared with the activity of TGase $2^{+/+}$ animals. RT-PCR of RNA extracted from thymus tissues of both +/+ and −/− animals showed that no transcript for TGase 2 was present in −/− animals (Fig. 2C).

In order to detect and identify TGases different from type 2, we performed RT-PCRs using both specific and degenerate primers for the catalytic site region of TGases. Figure 2C shows that similar amounts of TGase 1 were expressed in −/− and +/+ animals. This should account for the residual TGase enzymatic activity.

TGase $2^{-/-}$ thymocytes and MEFs show normal induction of apoptosis. Since a large number of reports suggest a role for TGase 2 in apoptosis, including in vivo in the thymus (47), we studied apoptosis induced ex vivo in mouse thymocytes and in vitro in MEFs.

Apoptosis was induced with different stimuli, namely, etoposide (Fig. 3A), CD95 ligation (Fig. 3B), dexamethasone (Fig. 3C), and H_2O_2 (Fig. 3D). Figure 3A shows also the spontaneous level of apoptosis of thymocytes ex vivo. No relevant difference in the number of cells undergoing apoptosis was observed between +/+ and −/− animals with any of the treatments.

The evaluation of apoptosis ex vivo was performed on cells presenting a significant TGase enzymatic activity (Fig. 2B), at least in part due to TGase 1. We therefore performed similar experiments on cultured MEFs, which show the lowest residual enzymatic activity (Fig. 2B).

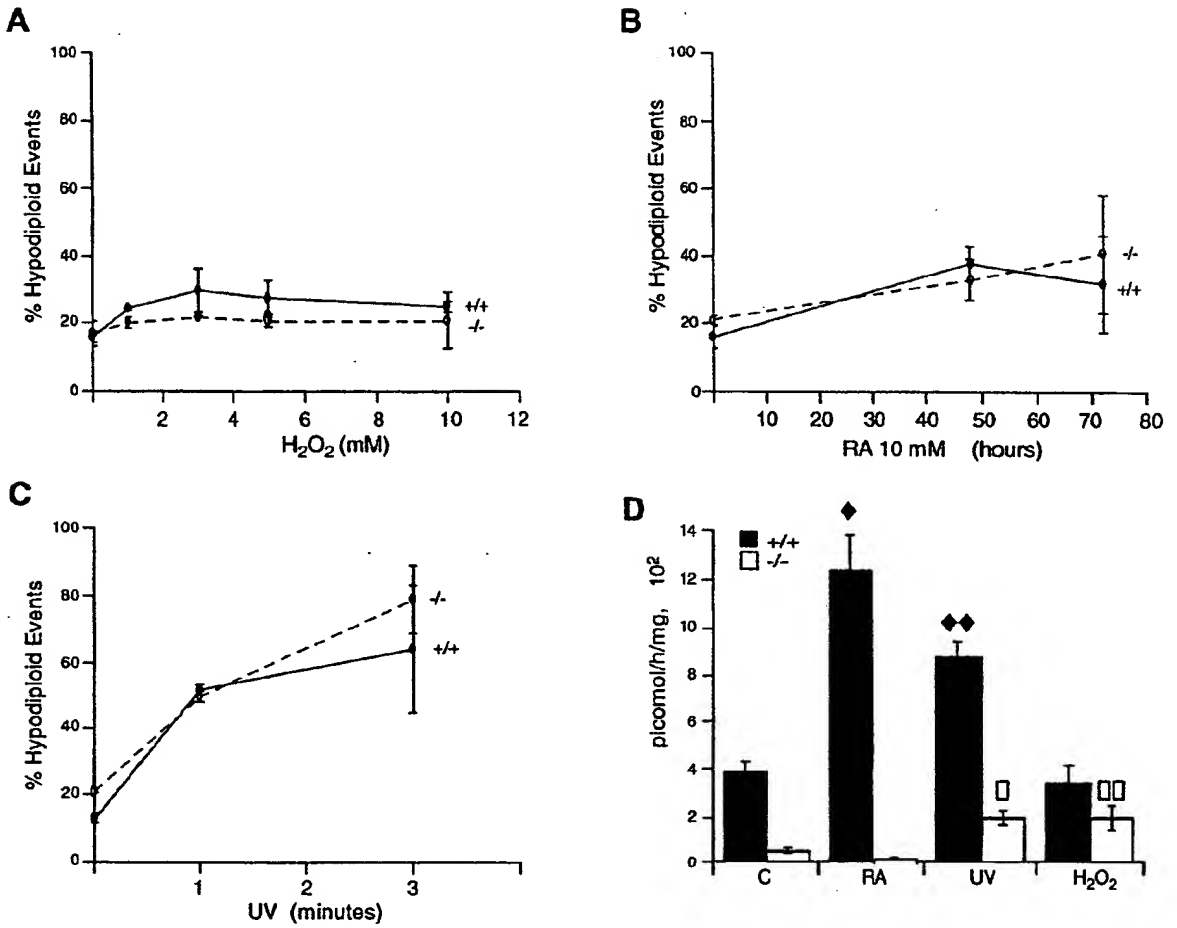

FIG. 4. Hypodiploid events in wild-type and knockout MEFs treated with 1, 3, 5, and 10 mM H_2O_2 for 15 min in PBS, washed, and then cultured in medium for 24 h (A); treated with 10 μM RA for 48 and 72 h (B); or treated with UV irradiation for 1 or 3 min in PBS and then cultured in medium for 24 h (C). Cells were fixed with a 1:1 solution of PBS and methanol-acetone (4:1, vol/vol) at −20°C and stained with PI. The number of events with hypodiploid DNA was measured by flow cytometry (see Materials and Methods). The data reported are averages of four independent experiments. (D) Corresponding transglutaminase activity in wild-type and knockout MEFs, untreated (C) or treated with 10 μM RA for 48 h, UV irradiation for 3 min followed by 24 h of culture, and 5 mM H_2O_2 followed by 24 h of culture. The data reported are averages of four independent experiments. Statistical differences between treated cells and the corresponding controls were evaluated. In detail, differences were statistically significant as follows: ◆, $P = 0.0189$ for control and RA-treated +/+ cells; ◆◆, $P = 0.0013$ for control and UV-treated +/+ cells; □, $P = 0.0294$ for control and UV-treated −/− cells; and □□, $P = 0.0475$ for control and H_2O_2-treated −/− cells. Differences not indicated were not statistically significant. All differences between +/+ and −/− cells are statistically significant.

As in the ex vivo studies, no difference was observed when +/+ and −/− MEFs were treated in vitro with H_2O_2 (Fig. 4A), RA (Fig. 4B), or UV (Fig. 4C). Treatment of +/+ MEFs with RA and UV resulted in an increase in TGase activity; −/− MEFs had a much lower basal activity that increased with UV and H_2O_2 treatment, while RA treatment resulted in a decrease of TGase activity (Fig. 4D). Since TGase 1 is negatively regulated by retinoids, while TGase 2 is upregulated (50), these results are in keeping with the evidence that the minimal residual activity observed in MEFs is due to TGase 1 (Fig. 4D). Indeed, as for thymocytes, mRNA for TGase 1 was also detected in MEFs by RT-PCR (data not shown).

Cross-linked apoptotic body formation is present in TGase $2^{-/-}$ mice. It has been consistently suggested that TGase 2 induction during apoptosis results in the formation of cross-linked insoluble apoptotic bodies. In order to investigate the possibility that the formation of cross-linked apoptotic bodies is impaired in TGase $2^{-/-}$ mice, we measured the number of insoluble apoptotic bodies in control or RA-, UV-, and H_2O_2-treated MEFs. Figure 5A shows that apoptotic bodies also formed in TGase $2^{-/-}$ cells, even though the number of cross-linked apoptotic bodies was significantly reduced in UV- and H_2O_2-treated −/− MEFs.

The reduction of cross-linked apoptotic bodies could be

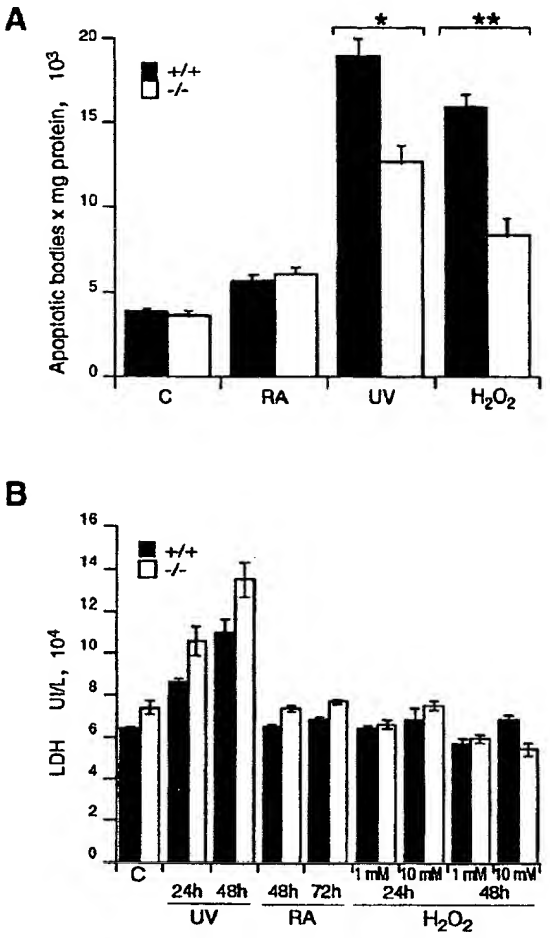

FIG. 5. (A) Cross-linked apoptotic body formation in wild-type and knockout MEFs. Cells were treated with 10 μM RA for 48 h, UV irradiation for 3 min followed by culture for 24 h, or 3 mM H_2O_2 for 15 min followed by culture for 24 h. See Materials and Methods for details. (B) LDH release in wild-type and knockout MEFs. Cells were left untreated (C) or treated with UV irradiation for 3 min followed by culture for 24 and 48 h, 10 μM RA for 48 and 72 h, or 1 and 10 mM H_2O_2 for 15 min followed by culture for 24 and 48 h. The data reported are averages of four independent experiments. Statistical analysis was performed according to the Student *t* test to compare +/+ and −/− cells: *, $P = 0.0014$; **, $P = 0.0003$. Differences not indicated are not statistically significant.

accompanied by an increased release of cytoplasmic material from cells undergoing apoptosis. In order to evaluate this aspect, we measured the release of LDH from +/+ and −/− MEFs after induction of apoptosis with UV, RA, and H_2O_2. Figure 5B shows that LDH release was only moderately increased (not statistically significant) in +/+ versus −/− MEFs. Treatment with UV, with which some necrosis was expected, showed a significant increase in LDH release in both +/+ and −/− cells. Therefore, our results are consistent with an essentially normal induction of apoptosis.

DISCUSSION

We have generated TGase 2-deficient mice through homologous recombination techniques. No TGase 2 was detectable in these mice by RT-PCR or Western blotting. The mice were viable and fertile and showed no developmental abnormalities. Apoptosis induced with different agents in both fibroblasts and thymocytes is normal. The reduction in enzymatic activity in −/− mice showed only a minor effect on both cross-linked apoptotic body formation (Fig. 5A) and LDH release (Fig. 5B), with no major consequences for the mice. Although we cannot exclude the possibility that TGase 2 deficiency may play a role in pathological situations (11, 38), aged mice (up to 20 months of age) do not show abnormalities such as cancer development and generation of autoimmunity (data not shown). It might be necessary to cross the mice into a more permissive genetic background in order to reveal an overt phenotype.

Deletion of various genes involved in apoptosis does not always produce an evident phenotype. Mice with deleted caspases 1, 2, 6, and 11 do not show evident developmental abnormalities (51), while in other cases a very specific or minimal phenotype is observed. Disruptions of other genes produce a phenotype only when animals are stressed with specific inducers requiring that protein, namely, radiation on $p53^{-/-}$ (8) or liposaccharides on caspase $1^{-/-}$ (16, 18) cells. Even though the accredited model for apoptosis indicates the requirement for the apoptosome and in particular for apaf-1 and caspases 3 and 9 (for a review, see references 6 and 17), the knockout of the genes for these proteins shows that thymocytes are still able to undergo apoptosis (for a review, see references 5 and 51). This has elicited various explanations, including the existence of additional unknown pathways or compensation mechanisms.

Similarly, there are different possible interpretations for the lack of phenotype in TGase 2 animals: (i) TGase 2 is not involved in apoptosis; (ii) it is not involved in the central, essential apoptotic machinery, but it is part of a regulatory or side pathway elicited only by specific inducers or only in specific tissues; or (iii) there is redundancy in the system.

The lack of effect on apoptosis of targeted disruption of the TGase 2 gene is in apparent contrast to previous evidence in favor of a role for TGase 2 in the apoptotic program. Indeed, it has been shown previously that transfection of an antisense TGase 2 construct into cell lines confers resistance to apoptosis induction, while sense transfectants show enhanced spontaneous apoptosis (22). There are several reasons for this disparity. First, not all models of apoptosis require TGase 2. For example, CD95 ligation elicits apoptosis independently of the steady-state levels of TGase 2 protein (3); correspondingly, there is no change in TGase enzymatic activity during CD95-induced apoptosis (3). Second, other TGases may assume the protein cross-linking role of TGase 2. Indeed, the TGase $2^{-/-}$ mice showed different degrees of TGase enzymatic activity in different tissues. Our data show the presence of TGase 1 in both +/+ and −/− mice. Recently, TGase 1 has been shown to exist in tissues different from the skin, namely, in the central nervous system (15). Furthermore, the TGase activity levels in −/− thymocytes is inhibited by GTP, a property of TGase X (E. Candi, G. Melino, et al., unpublished observation), sug-

gesting its expression in lymphoid tissue. Therefore, the possibility that other TGases, and particularly TGase 1, can compensate for TGase 2 loss cannot be excluded. TGases show very different biochemical properties, such as k_{cat}/K_m ratio, residue preference, and yield (26). Therefore, it is unlikely that there is a perfect compensation among distinct TGases. In fact, TGase 1 knockout animals show a lethal phenotype, despite the presence of four distinct TGases in the skin (20). However, point mutations for TGase 1 in humans, with complete loss of TGase enzymatic activity (4), are compatible with life but cause a skin disease known as lamellar ichthyosis (12, 42), suggesting a different degree of compensation in humans.

Despite the large body of data suggesting an involvement of TGase 2 in apoptosis, its precise role in this process is not evident from the present gene disruption study. While the TGase $2^{-/-}$ animals could be used to study other functions of the enzyme, particularly by further crossbreeding to evaluate its contribution in pathologies such as celiac (7, 27) and Huntington (13, 14, 19, 43) diseases, clarification of the importance of TGase 2 in apoptosis may well require the generation of animals deficient in multiple TGases.

ACKNOWLEDGMENTS

We thank Mauro Piacentini, Gennaro Ciliberto, and Richard A. Knight for generous support, critical discussions, and helpful suggestions. This work could not have been completed without the generous help of Francesca Bernassola, Eleonora Candi, Marco Corazzari, Daniela Barcaroli, and Marco Ranalli. We thank Giuseppe Bertini, Giancarlo Cortese, and Pierino Piccoli (S.S.D. SAFU, Instituto Fisioterapici Ospedalieri, Rome, Italy) for technical assistance and mouse husbandry.

The work was partially supported by grants from MURST, MinSan, Associazione Neuroblastoma, AIRC, Telethon (E 872 and E 1257), and EU (QLG1-1999-00739).

REFERENCES

1. Achyuthan, K. E., and C. S. Greenberg. 1987. Identification of a guanosine triphosphate-binding site on guinea pig liver transglutaminase. Role of GTP and calcium ions in modulating activity. J. Biol. Chem. 262:1901–1906.
2. Amendola, A., M. L. Gougeon, F. Poccia, A. Bondurand, L. Fesus, and M. Piacentini. 1996. Induction of "tissue" transglutaminase in HIV-pathogenesis: evidence for high rate of apoptosis of CD4+ T lymphocytes and accessory cells in lymphoid tissues. Proc. Natl. Acad. Sci. USA 93:11057–11062.
3. Bernassola, F., C. Schenrpflug, I. Herr, P. H. Krammer, K. M. Debatin, and G. Melino. 1999. Induction of apoptosis by IFNgamma in human neuroblastoma cell lines through the CD95/CD95L autocrine circuit. Cell Death Differ. 6:652–660.
4. Candi, E., G. Melino, A. Lahm, R. Ceci, A. Rossi, I.-G. Kim, B. Ciani, and P. M. Steinert. 1998. Transglutaminase 1 mutations in lamellar ichthyosis. J. Biol. Chem. 273:13693–13702.
5. Cecconi, F. 1999. Apaf1 and the apoptotic machinery. Cell Death Differ. 6: 1087–1098.
6. De Laurenzi, V., and G. Melino. 2000. Apoptosis. The little devil of death. Nature 406:135–136.
7. Dieterich, W., T. Ehnis, M. Bauer, P. Donner, U. Volta, E. O. Riecken, and D. Schuppan. 1997. Identification of tissue transglutaminase as the autoantigen of celiac disease. Nat. Med. 3:797–801.
8. Donehower, L. A., M. Harvey, B. L. Slagle, M. J. McArthur, C. A. Montgomery, Jr., J. S. Butel, and A. Bradley. 1992. Mice deficient for p53 are developmentally normal but susceptible to spontaneous tumours. Nature 356:215–221.
9. Fesus, L., V. Thomazy, F. Autuori, M. P. Ceru', E. Tarcsa, and M. Piacentini. 1989. Apoptotic hepatocytes become insoluble in detergents and chaotropic agents as a result of transglutaminase action. FEBS Lett. 245:150–154.
10. Fesus, L., P. J. A. Davies, and M. Piacentini. 1991. Apoptosis: molecular mechanisms in programmed cell death. Eur. J. Cell Biol. 56:170–177.
11. Hettasch, J. M., N. Bandarenko, J. L. Borchette, T. S. Lai, J. R. Marks, Z. A. Haroon, K. Peters, M. W. Dewhirst, J. D. Iglehart, and C. S. Greenberg. 1996. Tissue transglutaminase expression in human breast cancer. Lab. Investig. 75:637–645.
12. Huber, M., I. Rettler, K. Bernasconi, E. Frenk, S. P. Lavrijsen, M. Ponec, A. Bon, S. Lautenschlager, D. F. Schorderet, and D. Hohl. 1995. Mutations of keratinocyte transglutaminase in lamellar ichthyosis. Science 267:525–528.
13. Igarashi, S., R. Koide, T. Shimohata, M. Yamada, Y. Hayashi, H. Takano, H. Date, M. Oyake, T. Sato, A. Sato, S. Egawa, T. Ikeuchi, H. Tanaka, R. Nakano, K. Tanaka, I. Hozumi, T. Inuzuka, H. Takahashi, and S. Tsuji. 1998. Suppression of aggregate formation and apoptosis by transglutaminase inhibitors in cells expressing truncated DRPLA protein with an expanded polyglutamine stretch. Nat. Genet. 18:111–117.
14. Kahlem, P., H. Green, and P. Djian. 1998. Transglutaminase action imitates Huntington's disease: selective polymerization of Huntingtin containing expanded polyglutamine. Mol. Cell 1:595–601.
15. Kim, S. Y., P. Grant, J. H. Lee, H. C. Pant, and P. M. Steinert. 1999. Differential expression of multiple transglutaminases in human brain. Increased expression and cross-linking by transglutaminases 1 and 2 in Alzheimer's disease. J. Biol. Chem. 274:30715–30721.
16. Kuida, K., J. A. Lippke, G. Ku, M. W. Harding, D. J. Livingstone, M. S.-S. Su, and R. A. Flavell. 1995. Altered cytokine export and apoptosis in mice deficient in interleukin-1 beta converting enzyme. Science 281:2000–2002.
17. Kumar, S. 1999. Mechanisms mediating caspase activation in cell death. Cell Death Differ. 6:1060–1066.
18. Li, P., H. Allen, S. Banerjee, S. Franklin, L. Herzog, C. Johnstone, J. McDowell, M. Paskind, L. Rodman, J. Salfeld, E. Townes, D. Tracey, S. Wardwell, F.-Y. Wei, W. W. Wong, R. Kamen, and T. Seshadri. 1995. Mice deficient in IL-1 beta-converting enzyme are defective in production of mature IL beta and resistant to endotoxic shock. Cell 80:401–411.
19. Lorand, L. 1998. DRPLA aggregation and transglutaminase, revisited. Nat. Genet. 20:231.
20. Matsuki, M., F. Yamashita, A. Ishida-Yamamoto, K. Yamada, C. Kinoshita, S. Fushiki, E. Ueda, Y. Morishima, K. Tabata, H. Yasuno, M. Hashida, H. Iizuka, M. Ikawa, M. Okabe, G. Kondoh, T. Kinoshita, J. Takeda, and K. Yamanishi. 1998. Defective stratum corneum and early neonatal death in mice lacking the gene for transglutaminase 1 (keratinocyte transglutaminase). Proc. Natl. Acad. Sci. USA 95:1044–1049.
21. Melino, G., M. G. Farrace, M. P. Ceru', and M. Piacentini. 1988. Correlation between transglutaminase activity and polyamine levels in human neuroblastoma cells. Effect of retinoic acid and alpha-difluoromethylornithine. Exp. Cell Res. 179:429–445.
22. Melino, G., M. Annicchiarico-Petruzzelli, L. Piredda, E. Candi, V. Gentile, P. J. A. Davies, and M. Piacentini. 1994. Tissue transglutaminase and apoptosis: sense and antisense transfection studies with human neuroblastoma cells. Mol. Cell. Biol. 14:6584–6596.
23. Melino, G., F. Bernassola, M. T. Corasaniti, R. A. Knight, G. Nistico, and A. Finazzi-Agro. 1997. S-nitrosylation regulates apoptosis. Nature 388:432–433.
24. Melino, G., M. Draoui, M. Piacentini, L. Bellincampi, F. Bernassola, U. Reichert, and P. Cohen. 1997. Retinoic acid receptors a and g mediate tissue-transglutaminase induction in human neuroblastoma cells undergoing apoptosis. Exp. Cell Res. 255:55–61.
25. Melino, G., and M. Piacentini. 1998. Tissue transglutaminase in apoptosis: a downstream or a multifunctional upstream effector? FEBS Lett. 430:59–63.
26. Melino, G., E. Candi, and P. M. Steinert. 2000. Assay for transglutaminases in cell death. Methods Enzymol 322:433–472.
27. Molberg, O., S. N. Mcadam, R. Korner, H. Quarsten, C. Kristiansen, L. Madsen, L. Fugger, H. Scott, O. Noren, P. Roepstorff, K. E. Lundin, H. Sjostrom, and L. M. Sollid. 1998. Tissue transglutaminase selectively modifies gliadin peptides that are recognized by gut-derived T cells in celiac disease. Nat. Med. 4:713–717.
28. Nagy, L., M. Saydak, N. Shipley, S. Lu, J. P. Basilion, Z. H. Yan, P. Syka, R. Chandraratna, R. Heyman, and P. J. A. Davies. 1996. Identification and characterization of a versatile retinoid response element (RARE/RXRE) in the promoter of the mouse tissue transglutaminase gene. J. Biol. Chem. 271: 4355–4365.
29. Nagy, L., V. A. Thomazy, M. M. Soydak, J. P. Stein, and P. J. A. Davies. 1997. The promoter of mouse tissue transglutaminase gene directs tissue-specific, retinoid-regulated and apoptosis-linked expression. Cell Death Differ. 4: 534–547.
30. Nakaoka, H., D. M. Perez, K. J. Baek, T. Das, A. Husain, K. Misono, M. Im, and R. M. Graham. 1994. Gh: a GTP-binding protein with transglutaminase activity and receptor signaling function. Science 264:1593–1596.
31. Nemes, Z., Jr., R. R. Friis, D. Aeschlimann, S. Saurer, M. Paulsson, and L. Fesus. 1996. Expression and activation of tissue transglutaminase in apoptotic cells of involuting rodent mammary tissue. Eur. J. Cell Biol. 70:125–133.
32. Piacentini, M., L. Fesus, M. G. Farrace, L. Ghibelli, L. Piredda, and G. Melino. 1991. The expression of "tissue" transglutaminase in two human cancer cell lines is related with the programmed cell death (apoptosis). Eur. J. Cell Biol. 54:246–254.
33. Piacentini, M., M. Annicchiarico-Petruzzelli, S. Oliverio, L. Piredda, J. L. Biedler, and G. Melino. 1992. Phenotype-specific "tissue" transglutaminase regulation in human neuroblastoma cells in response to retinoic acid: correlation with cell death by apoptosis. Int. J. Cancer 52:271–278.
34. Piacentini, M., L. Fesus, and G. Melino. 1993. Multiple cell cycle access to the apoptotic death programme in human neuroblastoma cells. FEBS Lett. 320:150–154.

35. **Piacentini, M., and F. Autuori.** 1994. Immunohistochemical localization of tissue transglutaminase and Bcl-2 in rat uterine tissues during embryo implantation and post-partum involution. Differentiation 57:51–61.
36. **Piacentini, M.** 1995. Tissue transglutaminase: a candidate effector element of physiological cell death. Curr. Top. Microbiol. Immunol. 200:163–176.
37. **Piacentini, M., L. Piredda, D. Starace, M. Anniechiarico-Petruzzelli, M. Mattei, S. Oliverio, M. G. Farrace, and G. Melino.** 1996. Differential growth properties of S- and N-type human neuroblastoma cell variants transplanted into SCID mice: correlation with apoptosis and effect of ethanol. J. Pathol. 180:415–422.
38. **Piacentini, M., and V. Colizzi.** 1999. Tissue transglutaminase: apoptosis versus autoimmunity. Immunol. Today 20:130–134.
39. **Piredda, L., A. Amendola, V. Colizzi, P. J. A. Davies, M. G. Farrace, M. Fraziano, V. Gentile, I. Uray, M. Piacentini, and L. Fesus.** 1997. Lack of "tissue" transglutaminase protein cross-linking leads to leakage of macromolecules from dying cells: relationship to development of autoimmunity in MRLlpr/lpr mice. Cell Death Differ. 4:463–472.
40. **Piredda, L., M. G. Farrace, M. Lo Bello, W. Malorni, G. Melino, R. Petruzzelli, and M. Piacentini.** 1999. Identification of 'tissue' transglutaminase binding proteins in neural cells committed to apoptosis. FASEB J. 13:355–364.
41. **Ritter, S. J., and P. J. Davies.** 1998. Identification of a transforming growth factor-beta1/bone morphogenetic protein 4 (TGF-beta1/BMP4) response element within the mouse tissue transglutaminase gene promoter. J. Biol. Chem. 273:12798–12806.
42. **Russell, L. J., J. J. DiGiovanna, G. R. Rogers, P. M. Steinert, N. Hashem, J. G. Compton, and S. J. Bale.** 1995. Mutations in the gene for transglutaminase 1 in autosomal recessive lamellar ichthyosis. Nat. Genet. 9:279–283.
43. **Saudou, F., S. Finkbeiner, D. Devys, and M. E. Greenberg.** 1998. Huntingtin acts in the nucleus to induce apoptosis but death does not correlate with the formation of intranuclear inclusions. Cell 95:55–66.
44. **Steinert, P. M.** 1995. A model for the hierarchical structure of the human epidermal cornified cell envelope. Cell Death Differ. 2:33–40.
45. **Steinert, P. M., E. Candi, E. Tarcsa, L. N. Marekov, M. Sette, M. Paci, B. Cianni, P. Guerrieri, and G. Melino.** 1999. Transglutaminase crosslinking and structural studies of the human small proline rich 3 protein. Cell Death Differ. 6:916–930.
46. **Strange, R., F. Li, S. Saurer, A. Bukhard, and R. R. Friis.** 1992. Apoptotic cell death and tissue remodelling during mouse mammary gland involution. Development 115:49–58.
47. **Szondy, Z., P. Molnar, Z. Nemes, M. Boyiardzis, N. Kedei, R. Toth, and L. Fesus.** 1997. Differential expression of transglutaminase during in vivo apoptosis of thymocytes induced via distinct signalling pathways. FEBS Lett. 404:307–313.
48. **Thomazy, V. A., and P. J. Davies.** 1999. Expression of tissue transglutaminase in the developing chicken limb is associated both with apoptosis and endochondral ossification. Cell Death Differ. 6:146–154.
49. **Tybulewicz, V. L., C. E. Crawford, P. K. Jackson, R. T. Bronson, and R. C. Mulligan.** 1991. Neonatal lethality and lymphopenia in mice with a homozygous disruption of the c-abl proto-oncogene. Cell 65:1153–1163.
50. **Zhang, L. X., K. J. Mills, M. I. Dawson, S. J. Collins, and A. M. Jetten.** 1995. Evidence for the involvement of retinoic acid receptor RAR alpha-dependent signaling pathway in the induction of tissue transglutaminase and apoptosis by retinoids. J. Biol. Chem. 270:6022–6029.
51. **Zheng, T. S., S. Hunot, K. Kuida, and R. A. Flavell.** 1999. Caspase knockouts: matters of life and death. Cell Death Differ. 6:1043–1053.

A lupus-like syndrome develops in mice lacking the Ro 60-kDa protein, a major lupus autoantigen

Dahai Xue*, Hong Shi*, James D. Smith*, Xinguo Chen*, Dennis A. Noe*, Tommy Cedervall*, Derek D. Yang†, Elizabeth Eynon†, Douglas E. Brash‡, Michael Kashgarian§, Richard A. Flavell†, and Sandra L. Wolin*¶

*Department of Cell Biology and Howard Hughes Medical Institute, Yale University School of Medicine, New Haven, CT 06536; †Section of Immunobiology and Howard Hughes Medical Institute and §Department of Pathology, Yale University School of Medicine, New Haven, CT 06510; and ‡Departments of Therapeutic Radiology and Genetics, Yale University School of Medicine, New Haven, CT 06520

Communicated by Joan A. Steitz, Yale University, New Haven, CT, April 23, 2003 (received for review March 3, 2003)

Antibodies against a conserved RNA-binding protein, the Ro 60-kDa autoantigen, occur in 24–60% of all patients with systemic lupus erythematosus. Anti-Ro antibodies are correlated with photosensitivity and cutaneous lesions in these patients and with neonatal lupus, a syndrome in which mothers with anti-Ro antibodies give birth to children with complete congenital heart block and photosensitive skin lesions. In higher eukaryotes, the Ro protein binds small RNAs of unknown function known as Y RNAs. Because the Ro protein also binds misfolded 5S rRNA precursors, it is proposed to function in a quality-control pathway for ribosome biogenesis. Consistent with a role in the recognition or repair of intracellular damage, an orthologue of Ro in the radiation-resistant eubacterium *Deinococcus radiodurans* contributes to survival of this bacterium after UV irradiation. Here, we show that mice lacking the Ro protein develop an autoimmune syndrome characterized by anti-ribosome antibodies, anti-chromatin antibodies, and glomerulonephritis. Moreover, in one strain background, $Ro^{-/-}$ mice display increased sensitivity to irradiation with UV light. Thus, one function of this major human autoantigen may be to protect against autoantibody development, possibly by sequestering defective ribonucleoproteins from immune surveillance. Furthermore, the finding that mice lacking the Ro protein are photosensitive suggests that loss of Ro function could contribute to the photosensitivity associated with anti-Ro antibodies in humans.

Patients suffering from systemic rheumatic diseases such as scleroderma, systemic lupus erythematosus, and polymyositis often produce antibodies against highly conserved RNA–protein complexes. A fascinating but poorly understood facet of these diseases is that specific autoantibodies are associated with distinct rheumatic disease syndromes. For example, antibodies against tRNAs and tRNA–synthetase complexes are commonly found in polymyositis, whereas antibodies against nucleolar components are associated with scleroderma (1). This association of particular autoantibodies with specific syndromes has been useful for establishing diagnoses and for predicting sequelae that may accompany the particular rheumatic disorder.

In two rheumatic diseases, systemic lupus erythematosus and Sjögren's syndrome, a major target of the immune response is an RNA-binding protein known as the Ro 60-kDa autoantigen. In lupus patients, anti-Ro antibodies are highly associated with photosensitivity and photosensitive skin lesions, particularly those of subacute cutaneous lupus erythematosus (1, 2). In addition, anti-Ro antibodies are associated with neonatal lupus, a syndrome in which maternal autoantibodies cross the placenta, resulting in infants with photosensitive skin lesions and a cardiac conduction defect, complete congenital heart block (3).

Studies of the Ro 60-kDa protein have revealed that it is present in both the nucleoplasm and cytoplasm of vertebrate cells (4–6). In the cytoplasm, the Ro protein is complexed with one of several small RNAs known as Y RNAs. These Y RNAs are ≈100 nt long, transcribed by RNA polymerase III, and bound almost entirely by the Ro protein (7). The Ro protein/Y RNA complex is conserved evolutionarily, because orthologues have been described in mammals, the frog *Xenopus laevis*, and the nematode *Caenorhabditis elegans*, as well as the radiation-resistant eubacterium *Deinococcus radiodurans* (8–12). Although the function of the Y RNAs remains unknown, genetic depletions of the Ro protein from *C. elegans* and *D. radiodurans* have revealed that Ro protein binding stabilizes Y RNAs from degradation (12, 13). Both mammalian cells and *Xenopus* oocytes contain a nuclear pool of Ro protein, which is not complexed with Y RNAs (4–6).

Experiments in *X. laevis* and *C. elegans* have led to the proposal that the Ro 60-kDa protein functions in a quality-control pathway for ribosome biogenesis (6, 13). In *Xenopus* oocyte nuclei, the Ro protein associates with a large class of variant 5S rRNA precursors. To synthesize the large numbers of ribosomes needed for early development, *X. laevis* contains ≈20,000 genes encoding the oocyte 5S rRNA, many of which diverge from the consensus 5S rRNA sequence (14). The 5S rRNA variants bound by the Ro protein contain additional gene-encoded nucleotides at their 3′ ends, suggesting that they are generated by read-through of the first termination signal for RNA polymerase III. The variants also contain one or more changes from the consensus 5S rRNA sequence that cause the RNAs to misfold into a structure recognized by the Ro protein (15). Because these variant pre-5S rRNAs are processed inefficiently to mature 5S rRNA and eventually degraded, the Ro protein is proposed to function in a quality-control pathway for 5S rRNA biogenesis (6, 15). Consistent with a role in ribosomal quality control, nematodes lacking the Ro protein have increased numbers of variant 5S rRNAs (13).

Genetic analyses in *C. elegans* and *D. radiodurans* have implicated the Ro 60-kDa protein in the resistance to environmental stress. *C. elegans* lacking the Ro protein are defective in the formation of dauer larvae, a stress-resistant stage formed when environmental conditions are unfavorable for growth (16). *D. radiodurans* lacking the Ro protein exhibit decreased survival after UV irradiation. Moreover, both the *D. radiodurans* Ro protein and a Y RNA orthologue are up-regulated after UV irradiation, suggesting a role for the Ro ribonucleoproteins (RNPs) in the recognition and/or repair of intracellular damage (12).

To examine the role of Ro RNPs in a mammalian organism, we created mice lacking the Ro 60-kDa protein. We report that mice lacking the Ro autoantigen develop an autoimmune syndrome that shares several features with the human disease systemic lupus erythematosus. Similar to lupus patients, $Ro^{-/-}$ mice exhibit anti-ribosome and anti-chromatin antibodies, glomerulonephritis, and sensitivity to sunlight. Thus, one normal

BIOCHEMISTRY

Abbreviation: RNP, ribonucleoprotein.

¶To whom correspondence should be addressed at: Department of Cell Biology and Howard Hughes Medical Institute, Boyer Center for Molecular Medicine, Yale University School of Medicine, 295 Congress Avenue, New Haven, CT 06536. E-mail: sandra.wolin@yale.edu.

function of this major lupus autoantigen may be to protect against the development of autoimmune disease.

Materials and Methods

Generation and Characterization of $Ro^{-/-}$ Mice. DNAs corresponding to the first 10 kb of the mouse *Ro* gene (17) were isolated from a λFIXII mouse genomic library (129/Sv strain; Stratagene) by using human cDNA (18) as a hybridization probe. To construct the targeting vector shown in Fig. 1*A*, we used plasmids (19) in which the PGKneo cassette (pBS-neo) and herpes simplex virus thymidine kinase genes (pBS-TK) were cloned into pBluescript SK (Stratagene). First, a 2.3-kb *Pst*I fragment containing intronic sequences between the second and third coding exons was inserted into the pBS-neo vector at the *Eco*RI site. Next, a 3-kb *Not*I/*Eco*RI fragment containing the 1.6-kb PGKneo cassette and 1.4 kb of Ro sequences was excised from the plasmid and inserted into the corresponding sites of pBS-TK. Last, a 4.7-kb *Not*I/*Xba*I fragment derived from the 5′ end of the Ro genomic clone was ligated into the corresponding sites of the TK/PGKneo/Ro-containing plasmid. The resulting plasmid was linearized with *Not*I and electroporated into W9.5 embryonic stem cells. Genomic DNA from transformants resistant to G418 (200 μg/ml) and ganciclovir (2 μM) was digested with *Pst*I and subjected to Southern blot analysis. Clones containing the targeted mutation were injected into C57BL/6 blastocysts, followed by implantation into pseudopregnant foster mothers. Male chimeric mice were mated with C57BL/6 female mice, and germ-line-transmitted progeny were obtained. Light and electron microscopic examination of kidneys was performed as described (20).

For Northern blot analyses to detect Y RNAs, total brain tissue was lysed in TRIzol (Invitrogen), and RNA was isolated as described by the supplier. After fractionation in 5% polyacrylamide/8 M urea gels, the RNA was transferred to Zeta-probe GT nylon membranes (Bio-Rad) in 0.5× TBE (1× TBE = 89 mM Tris/89 mM boric acid/2.0 mM EDTA, pH 8.3) at 150 mA for 16 h. Oligonucleotides used to detect mY1 and mY3 RNA were 5′-AAGGGGGGAAAGTGTAGAACAGGA-3′ and 5′-GAGCGGAGAAGGAACAAAGAAATCTG-3′, respectively.

For Western blot analyses, brain extracts were fractionated in SDS/polyacrylamide gels, transferred to nitrocellulose as described (21), and probed with a monoclonal anti-mouse Ro antibody. To prepare the antibody, oligonucleotides 5′-GGCGCGGGATCCGAAGGATCTGCAAACCAGTTGC-3′ and 5′-GCCGCGGAGCTCTTAAATGACATCCAATGTGAAATTCCG-3′ were used to amplify the mouse Ro protein-coding sequence. The DNA was digested with *Bam*HI and *Sac*I and inserted into pTrcHisA (Invitrogen). Because the recombinant protein was insoluble, it was solubilized in guanidine·HCl, purified from *Escherichia coli* lysates, and renatured as described (12). After renaturation, the protein was used to immunize $Ro^{-/-}$ mice. Spleen cells were fused to Ag8.653 cells by using standard methods. Antiserum against human Uch-L5 was a generous gift of R. Cohen (University of Iowa, Iowa City).

Analysis of T and B Cell Function. Thymus, spleen, lymph nodes, and bone marrow were isolated from $Ro^{-/-}$ and wild-type mice, stained with the appropriate antibodies [CD4, CD8, T cell receptor, CD69, CD44, CD25, CD45R, CD43, IgM, and IgD antibodies (Pharmingen)] and analyzed by using a FACSCalibur analysis instrument (Becton Dickinson). Adult $Ro^{-/-}$, $Ro^{+/-}$, and wild-type mice were immunized s.c. with keyhole limpet hemocyanin (Calbiochem) that was emulsified in complete Freund's adjuvant. After 10 days, mice were killed and lymph node cells were assayed for proliferation by [^{3}H]thymidine incorporation (New England Nuclear) and cytokine production by ELISA (Pharmingen). Blood was collected at this time, and anti-keyhole limpet hemocyanin antibodies were measured by ELISA (Southern Biotechnology Associates). Ig levels were measured by ELISA in unimmunized mice and in age-matched $Ro^{-/-}$, $Ro^{+/-}$, and wild-type mice.

Characterization of Autoantibodies. Mouse NIH 3T3 cells were fixed in 3% formaldehyde/120 mM sodium phosphate, pH 7.4, and subjected to immunofluorescence analysis. Sera were used at dilutions between 1:125 and 1:1,000. Antibodies against RNA-containing antigens were detected by performing immunoprecipitations from mouse L1210 cells as described (8, 22). RNAs contained within immunoprecipitates were labeled with [^{32}P]pCp and T4 RNA ligase (23) and fractionated in 5% polyacrylamide/8 M urea gels. Reference sera were anti-Sm and anti-ribosome mouse monoclonal antibodies (24) and human anti-P antibodies (a gift of K. Elkon, University of Washington, Seattle). Antibodies against histones were detected by Western blotting extracts of mouse L1210 cells as described (21) by using sera diluted to 1:500 and 1:1,000. Antibodies against double-stranded and single-stranded DNA (Euroimmun, Lübeck, Germany) and nucleosomes (Medizym, Medipan Diagnostics, Selchow, Germany) were detected by ELISA using precoated plates. For ELISAs, the mean reactivity for 18 wild-type antinuclear antibody (ANA)-negative mice was determined. Values higher than three standard deviations above the mean were considered positive.

To identify the ≈30-kDa doublet recognized by many sera, L1210 cells were sonicated in 40 mM Tris·HCl, pH 7.5/150 mM NaCl/2 mM $MgCl_2$ by using a Branson sonifier (twice for 20 sec at setting 3). After sedimentation at 10,000 × *g* for 10 min, the 30-kDa doublet was found in the pellet. The pellet was subjected to sequential salt extraction using 300 and 600 mM NaCl. The doublet corresponded to two bands in the 600 mM NaCl supernatant, which were microsequenced at the Yale Keck Facility. For the ≈15-kDa band, embryonic stem cells were lysed in a Dounce homogenizer in 40 mM Tris·HCl, pH 7.5/150 mM NaCl/2 mM $MgCl_2$/0.1% Nonidet P-40/10 mM DTT, and nuclei were sedimented at 10,000 × *g* for 10 min. After resuspension in the same buffer, nuclei were disrupted by sonication and the lysate was sedimented at 10,000 × *g* for 10 min. After washing the pellet with 300 mM NaCl in the above buffer, the pellet was incubated in 0.2 M HCl for 30 min on ice to extract histones, followed by sedimentation at 10,000 × *g* for 10 min. The supernatant was applied to a PD-10 column (Amersham Biosciences) equilibrated in 50 mM sodium phosphate, pH 8.5. The column eluate was applied to an SP Sepharose column equilibrated in the same buffer. Histones were eluted with 1 M NaCl.

UV Sensitivity. Mice (6–8 weeks old) were shaved on the back and irradiated 24 h later by using UVB lamps (FS20T12/UVB, National Biological, Twinsburg, OH; ref. 25). After 24 h, animals were killed and the exposed skin was excised, fixed, and examined for sunburn cells as described (25).

Results

Generation of Mice Lacking the Ro 60-kDa Autoantigen. Ro-deficient mice were generated through homologous recombination in embryonic stem cells. The targeting vector replaced the first coding exon of the Ro gene and parts of the adjacent introns with a *neo* gene cassette (Fig. 1 *A* and *B*). Targeted embryonic stem cells were injected into C57BL/6 blastocysts, and the resulting chimeric males were bred with C57BL/6 females to generate F_1 hybrid (129/Sv × C57BL/6) heterozygotes. The F_1 hybrid mice were inbred to generate F_2 and F_3 hybrid progeny. In addition, $Ro^{-/-}$ F_3 hybrid progeny were backcrossed three generations to C57BL/6 mice and then inbred to generate F_1 progeny. $Ro^{-/-}$ mice from both backgrounds were viable and fertile. Western

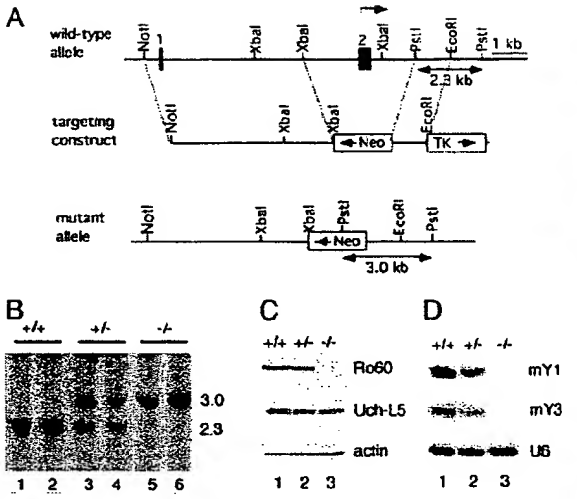

Fig. 1. Disruption of the *Ro* gene. (*A*) Diagram showing the *Ro* gene locus, the targeting construct, and the recombined mutant allele. The first two exons are indicated by filled boxes, and the translation initiation site is indicated (arrow). (*B*) Southern analysis of *Pst*I-digested DNA from wild-type (lanes 1 and 2), $Ro^{+/-}$ (lanes 3 and 4), and $Ro^{-/-}$ (lanes 5 and 6) mice. (*C*) Western blots of brain extracts with a rabbit anti-Ro serum. The blot was reprobed to detect Uch-L5, which runs as a doublet (*Middle*), and actin (*Bottom*). (*D*) Northern blot analyses of brain RNA reveal that Y RNAs are reduced in $Ro^{+/-}$ and $Ro^{-/-}$ mutant mice.

blotting of brain extracts confirmed that Ro protein levels were reduced in $Ro^{+/-}$ mice and undetectable in $Ro^{-/-}$ mice (Fig. 1*C*). Reprobing of the blot revealed that expression of the neighboring Uch-L5 gene, whose transcription start site is 2.9 kb from the *neo* insertion, was unaffected (Fig. 1*C*). Northern analyses revealed that the levels of the two mouse Y RNAs, mY1 and mY3 (26, 27), were reduced in $Ro^{+/-}$ mice and undetectable in $Ro^{-/-}$ mice (Fig. 1*D*), consistent with previous reports that Ro protein binding is required for stable accumulation of these RNAs (12, 13).

Mice Lacking the Ro Protein Develop Membranoproliferative Glomerulonephritis. Although histologic examination of 6-week-old $Ro^{-/-}$ mice revealed no significant abnormalities, ≈10% of the original F_2 and F_3 hybrid $Ro^{-/-}$ mice (8 of 74), but none of the wild-type mice (0 of 55), were dead within 6 months. By 12 months, this mortality had increased to 28% (21 of 74) of the $Ro^{-/-}$ mice, compared with 4% (2 of 55) of the wild-type mice. Mice showing signs of distress, such as fur ruffling and lethargy, were killed and subjected to histologic examination. All had evidence of membranoproliferative glomerulonephritis (Fig. 2). Examination of asymptomatic mice revealed that most (8 of 9) $Ro^{-/-}$ mice between 6 and 8 months of age showed changes characteristic of membranoproliferative glomerulonephritis. Inspection of other organs revealed no apparent differences compared with wild-type littermates. After three backcrosses to C57BL/6 mice, the $Ro^{-/-}$ mice no longer exhibited increased mortality compared with their wild-type counterparts. Nevertheless, examination of kidneys revealed that all $Ro^{-/-}$ mice >6 months of age exhibited histologic changes. The glomeruli were hypercellular with leukocytes in the capillary lumens (Fig. 2*B*), and immunofluorescence microscopy demonstrated the presence of IgG in a granular pattern (data not shown). Electron microscopy confirmed the presence of electron-dense deposits consistent with immune

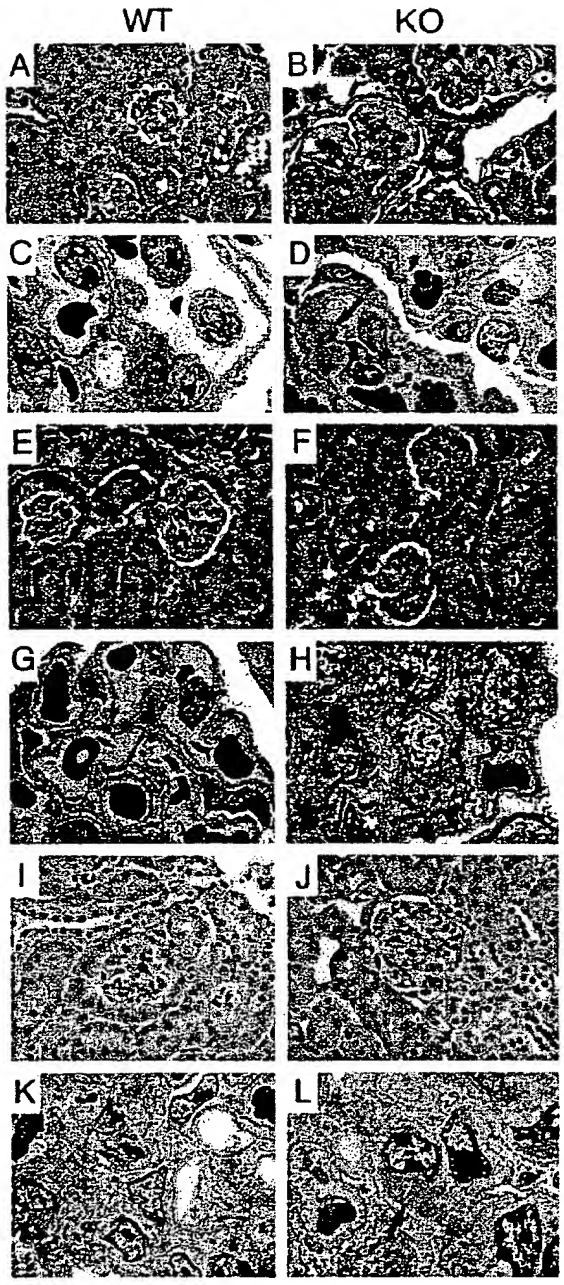

Fig. 2. Glomerulonephritis in $Ro^{-/-}$ mice. Light (*A*, *B*, *E*, *F*, *I*, and *J*; ×200) and electron (*C*, *D*, *G*, *H*, *K*, and *L*; ×5,000) microscopy of kidneys from $Ro^{-/-}$ mice and age-matched controls. $Ro^{-/-}$ and wild-type mice from the original hybrid strain (*A–D*) were examined at 16.5 months, and backcrossed mice were examined at 7 (*E–H*) and 12.5 (*I–L*) months. Age-matched controls show essentially normal histology. The hybrid $Ro^{-/-}$ mice show glomerular hypercellularity with large eosinophilic capillary deposits (*B*, arrow), which correspond to subendothelial immune complexes (*D*, arrow). Lesions in the backcrossed mice are less severe, with mesangial immune complexes at 7 months (*H*, arrow) and larger subendothelial complexes at 12.5 months (*L*, arrow).

BIOCHEMISTRY

Table 1. Autoantibodies in $Ro^{-/-}$, $Ro^{+/-}$, and wild-type mice

Age, months	No. of mice with autoantibodies		
	$Ro^{-/-}$	$Ro^{+/-}$	Wild type
129/Sv × C57BL/6 hybrid mice (ANA ≥1:1,000)			
6–7	5/6 (83%)	ND	ND
12–14	18/22 (82%)	ND	1/17 (6%)
After three backcrosses to C57BL/6 (ANA ≥1:125)			
9	17/25 (68%)	10/26 (38%)	2/24 (8%)

ANA, anti-nuclear antibody; ND, not done.

complexes (Fig. 2*D*). Deposits initially were seen predominantly in the glomerular mesangium (Fig. 2*H*) but, with increasing age, became larger and extended into the subendothelial region (Fig. 2*L*). These lesions were not as severe in the backcrossed mice as they were in the original, mixed background $Ro^{-/-}$ mice, suggesting the presence of modifier loci in the C57BL/6 background. Heterozygotes showed essentially normal histology by light microscopy, but those mice that developed antibodies (see below) demonstrated mild lesions characterized by the presence of small, electron-dense deposits by electron microscopy.

Anti-Chromatin and Anti-Ribosome Antibodies in $Ro^{-/-}$ Mice and Heterozygotes. To confirm the presence of autoantibodies, sera from the mice were analyzed by performing indirect immunofluorescence on NIH 3T3 cells. Autoantibodies (antinuclear and/or anticytoplasmic) with titers of at least 1:1,000 were detectable by 6 months of age in five of six (83%) $Ro^{-/-}$ mice from the original hybrid strain (Table 1; also see Fig. 3 *A–D*). After three backcrosses to C57/BL6 mice, antibodies remained detectable in the majority of $Ro^{-/-}$ mice (68%; 17 of 25). Autoantibodies also were detected in 10 of 26 (38%) $Ro^{+/-}$ heterozygotes but only 2 of 24 (8%) wild-type mice (Table 1). Although these antibodies tended to be of lower titer, between 1:125 and 1:500, high-titer antibodies (≥1:1,000) were detected in 7 of 25 (28%) backcrossed $Ro^{-/-}$ mice and 5 of 26 (19%) $Ro^{+/-}$ heterozygotes but were not detected in wild-type mice. Western blotting of mouse whole-cell extracts revealed that many sera detected a prominent doublet of 30 kDa and a second band of ≈16 kDa (Fig. 3*E*, lanes 3–6). Purification of these antigens, followed by protein microsequencing, revealed that they were histones H1 and H2b. Consistent with a prominent anti-chromatin response, characterization of the sera by ELISA revealed that many sera contained antibodies against nucleosomes, single-stranded DNA, and double-stranded DNA (Table 2).

To characterize further the targeted antigens, sera were used to immunoprecipitate from mouse whole-cell extracts, and the RNAs within the immunoprecipitates were labeled at the 3′ end. This assay detects many RNA-containing lupus antigens, including Sm, Ro, La, tRNA/synthetase complexes, and ribosomes (22). Although none of the mice contained detectable anti-Sm, anti-Ro, anti-La, or anti-tRNA/synthetase antibodies, a large fraction of the $Ro^{-/-}$ mice contained anti-ribosome antibodies, because both 5S and 5.8S rRNAs were contained within the immunoprecipitates (Fig. 3*F*, lanes 13–15). In addition, one mouse had antibodies directed against the U1 small nuclear RNP (snRNP; Fig. 3*F*, lane 9, asterisk), a common lupus antigen (1). For the original hybrid strain, anti-ribosome antibodies were detected in 50% of $Ro^{-/-}$ mice older than 6 months (Table 2). This was also a major specificity in sera from the backcrossed mice, as 43% of $Ro^{-/-}$ mice possessed these antibodies (Table 2). The majority of sera positive for anti-ribosome antibodies detected a doublet migrating below the histone H1 band (Fig. 3*E*, lane 3, asterisk).

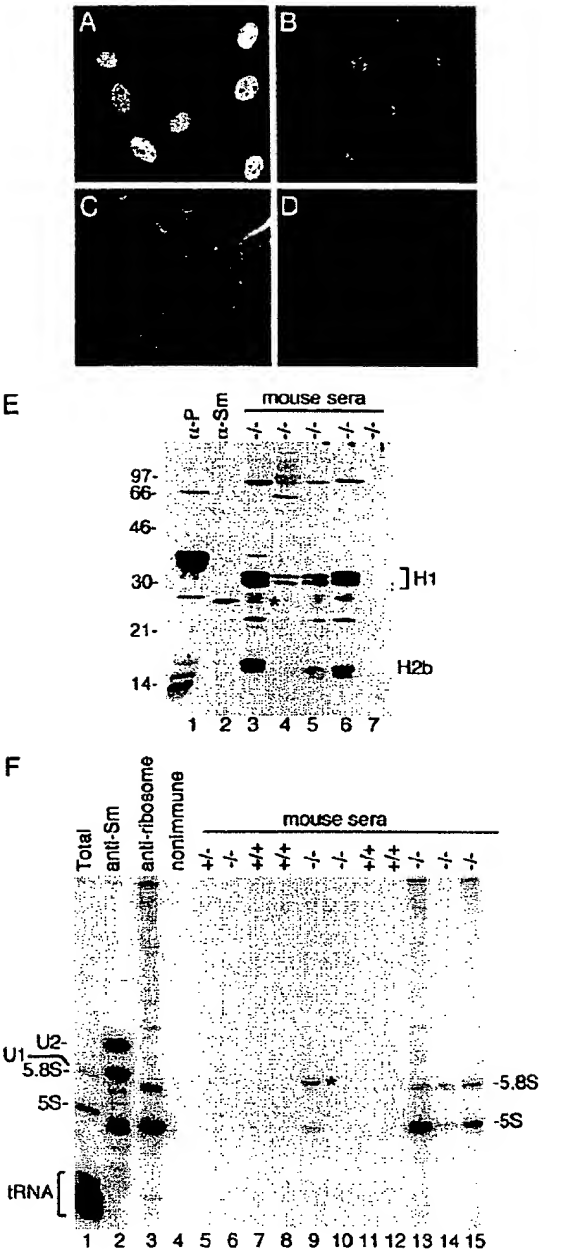

Fig. 3. Autoantibodies in Ro mutant mice. NIH 3T3 cells were stained with sera (diluted 1:1,000) from 6- to 7-month-old $Ro^{-/-}$ mice (*A–C*) and a 12-month-old wild-type mouse (*D*). (*E*) Reference sera (lanes 1 and 2) and sera from $Ro^{-/-}$ mice were used to probe Western blots of L1210 cell extracts. *, Doublet detected by most sera containing anti-ribosomal antibodies. (*F*) Reference sera (lanes 2–4) and sera from 129/Sv × C57BL/6 hybrid mice were used to immunoprecipitate from L1210 cell extracts. RNAs in immunoprecipitates were labeled with [^{32}P]pCp. *, Band identified as U1 RNA by cDNA sequencing.

Fractionation of cell extracts revealed that the doublet was found in the pellet after sedimentation at 100,000 × *g* for 1 h, consistent with a ribosomal protein (data not shown). None

Table 2. Subclassification of autoantibodies in $Ro^{-/-}$ and wild-type mice

Antigen	No. of mice with autoantibodies				
	(129/Sv × C57BL/6)		C57BL/6 backcross		
	Wild type (n = 18)	$Ro^{-/-}$ (n = 18)	Wild type (n = 19)	$Ro^{+/-}$ (n = 23)	$Ro^{-/-}$ (n = 23)
Histones	0	10	0	1	9
Ribosomes	1	9	0	3	10
Sm	0	0	0	0	0
U1 snRNP	0	1	0	0	0
Ro	0	0	0	0	0
La	0	0	0	0	0
dsDNA	2	9	0	3	6
ssDNA	2	6	1	3	5
Nucleosomes	2	10	1	8	6

snRNP, small nuclear RNP; dsDNA, double-stranded DNA; ssDNA, single-stranded DNA.

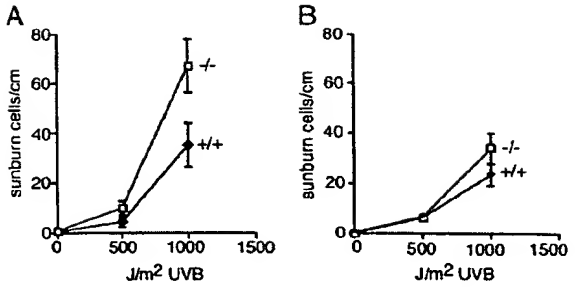

Fig. 4. $Ro^{-/-}$ mice are more sensitive to UVB irradiation. (*A*) After six backcrosses to C57BL/6 mice, the backs of wild-type (n = 8) and $Ro^{-/-}$ (n = 6) mice were shaved and exposed to the indicated doses of UVB. After 24 h, apoptotic keratinocytes (sunburn cells) were counted. (*B*) The backs of mice from the original hybrid 129/Sv × C57BL/6 strain were shaved and exposed to UVB, and apoptotic keratinocytes were counted. For the 1,000-J/m^2 dose, 14 wild-type and 13 $Ro^{-/-}$ mice were examined.

of the anti-ribosome antibodies recognized the ribosomal P proteins, which are common autoantigens in lupus patients (Fig. 3*E*, lane 1; ref. 1).

Evaluation of T and B Cell Populations and Function. T and B cell surface markers were evaluated in $Ro^{-/-}$ and wild-type mice by flow cytometric analysis. No obvious changes were found in mature T cell markers (CD4/CD8 ratios) or in the most immature (T cell antigen receptor-negative CD25/CD44 populations) cells in the thymus. Likewise in the bone marrow, B cell development appeared normal (using CD43/CD45R and IgM markers). Lymph node and spleen populations did not reveal differences in T and B cell activation status (using CD69 and CD25 markers). To determine whether $Ro^{-/-}$ mice respond abnormally to challenge with protein antigens, animals were immunized with the T cell-dependent antigen keyhole limpet hemocyanin. No significant differences in T cell proliferation, cytokine production, or anti-keyhole limpet hemocyanin antibody production were detected. However, total Ig levels in unimmunized 8-week-old $Ro^{-/-}$ mice were elevated slightly (1.4-fold). Among the Ig isotypes, increases were found in IgM (1.5-fold in the $Ro^{-/-}$ mice) and IgG2a (3-fold in $Ro^{+/-}$ mice and 3- to 29-fold in $Ro^{-/-}$ mice) (data not shown).

Sensitivity of $Ro^{-/-}$ Mice to UV Irradiation. Because a prokaryotic orthologue of the Ro protein is important for survival of the eubacterium *D. radiodurans* after UV irradiation (12), we examined the sensitivity of $Ro^{-/-}$ mice to UV light. The backs of wild-type and $Ro^{-/-}$ mice were shaved and the dorsal skin was exposed to UVB light at the physiologically relevant doses of 500 and 1,000 J/m^2. Twenty-four hours later, histological sections were prepared. For mice that had been backcrossed six times to C57BL/6 mice, the number of apoptotic keratinocytes (sunburn cells) in the $Ro^{-/-}$ mice after 1,000 J/m^2 UVB light was twice that of wild-type littermates (P = 0.02; Fig. 4*A*). Examination of mice from the original (129/Sv × C57BL/6) hybrid strain revealed that both wild-type and $Ro^{-/-}$ mice were less sensitive to irradiation than the backcrossed mice (Fig. 4*B*). However, although $Ro^{-/-}$ mice from the original hybrid strain also had higher numbers of apoptotic keratinocytes than did wild-type controls (Fig. 4*B*), the difference was not statistically significant (P = 0.08). Nonetheless, in at least one genetic background, the absence of the Ro protein results in significant photosensitivity, although modifier loci also may contribute.

Discussion

Although small RNA–protein complexes are major autoantigens in patients suffering from systemic lupus erythematosus, there have been few links between the RNP antigens and the disease pathology. We have shown that mice lacking the Ro 60-kDa autoantigen develop a lupus-like syndrome consisting of anti-ribosome and anti-chromatin antibodies, glomerulonephritis with subendothelial immune deposits, and photosensitivity. Thus, the Ro autoantigen may not be simply a passive target in the lupus immune response but, instead, may be important for the prevention of autoimmune disease.

Although a number of gene disruptions result in at least some degree of autoimmunity (28), our work is unique in several ways. First, we report that disruption of an RNA-binding protein can result in autoimmunity. Second, although photosensitivity occurs in a significant fraction of lupus patients, our backcrossed mice are unusual in displaying both autoimmune disease and sensitivity to sunlight. Although the observed difference is only 2-fold, similar changes in cell survival after UV are seen in cells from patients with the XP-E, XP-F, and XP-V forms of xeroderma pigmentosum, hereditary syndromes in which patients are predisposed to sunlight-induced skin cancers (29, 30). Last, our finding that mice lacking a major lupus autoantigen develop autoimmune disease raises the possibility that the anti-Ro antibodies seen in patients may not be an epiphenomenon but, instead, may contribute to the development or perpetuation of the autoimmune response and/or the observed photosensitivity.

How might the absence of an intracellular RNA-binding protein result in autoimmunity? Because the Ro protein binds misfolded, defective pre-5S rRNAs in *X. laevis* oocytes, it has been proposed to function in a quality-control pathway for ribosome biogenesis (6, 13, 15). Thus, one possibility is that the release of intracellular contents from $Ro^{-/-}$ cells that occurs normally during cell turnover triggers the autoimmune response. In this model, the presence of a small fraction of ribosomes containing subtle structural alterations resulting from the presence of misfolded 5S rRNAs causes a breach of tolerance by exposing normally cryptic determinants to the immune system. In support of this hypothesis, it often has been proposed that autoimmunity can be triggered by presentation of cryptic epitopes (31, 32). Such a mechanism would be reminiscent of the lupus-like syndromes that develop in mice lacking components of pathways involved in clearing extracellular debris, in that failure to remove cellular detritus triggers an autoimmune response (33–36). Alternatively, it remains possible that the absence of the Ro protein results in a subtle defect in immune system function that we have not yet uncovered.

In lupus patients, photosensitivity occurs in up to 90% of patients with anti-Ro autoantibodies (2). Moreover, maternal

anti-Ro antibodies that cross the placenta are highly associated with photosensitive skin lesions in infants. Because the disappearance of the skin lesions coincides with the loss of maternal antibodies from the circulation, it has been assumed that the antibodies play a direct role in the pathogenic process (37, 38). Our result that the absence of the Ro protein in one genetic background is associated with photosensitivity suggests that the photosensitivity long observed in patients could be related to a loss of Ro protein function in keratinocytes. However, although there are many reports that antibodies can enter cells (39–44), it is unlikely that they access the cytosol in quantities sufficient to ablate function of abundant target molecules (45). Nonetheless, inefficient entry of anti-Ro antibodies into a small fraction of patient keratinocytes potentially could enhance the sensitivity of these cells to sunlight, resulting in increased apoptotic cell death.

In summary, our genetic experiments have uncovered a new and surprising way in which the lack of an RNA-binding protein leads to an immune response to specific components of the subcellular machinery. Moreover, our experiments reveal that the Ro 60-kDa protein plays a critical role in the prevention of autoimmunity, possibly by removing defective RNPs from cells, allowing them to escape immune surveillance. In this regard, it is interesting that the human Ro protein maps to chromosome 1q31 (46), which has been linked to lupus (47–49).

We thank C. Delvecchio for technical assistance; R. Cohen, K. Elkon, and J. Steitz for providing antibodies; and J. Craft, R. Lifton, and M. Shlomchik for comments on the manuscript. Parts of this work were supported by grants from the National Institutes of Health (to M.K. and D.E.B.). R.A.F. is an Investigator and S.L.W. is an Associate Investigator of the Howard Hughes Medical Institute.

1. von Muhlen, C. A. & Tan, E. M. (1995) *Semin. Arthritis Rheum.* **24**, 323–358.
2. Provost, T. T., Watson, R. & Simmons-O'Brien, E. (1996) *J. Am. Acad. Dermatol.* **35**, 147–169.
3. Silverman, E. D. & Laxer, R. M. (1997) *Rheum. Dis. Clin. North Am.* **23**, 599–618.
4. Peek, R., Pruijn, G. J. M., van der Kemp, A. & van Venrooij, W. J. (1993) *J. Cell Sci.* **106**, 929–935.
5. Simons, F. H. M., Pruijn, G. J. M. & van Venrooij, W. J. (1994) *J. Cell Biol.* **125**, 981–988.
6. O'Brien, C. A. & Wolin, S. L. (1994) *Genes Dev.* **8**, 2891–2903.
7. Wolin, S. L. & Steitz, J. A. (1983) *Cell* **32**, 735–744.
8. Wolin, S. L. & Steitz, J. A. (1984) *Proc. Natl. Acad. Sci. USA* **81**, 1996–2000.
9. O'Brien, C. A., Margelot, K. & Wolin, S. L. (1993) *Proc. Natl. Acad. Sci. USA* **90**, 7250–7254.
10. Farris, A. D., O'Brien, C. A. & Harley, J. B. (1995) *Gene* **154**, 193–198.
11. Van Horn, D. J., Eisenberg, D., O'Brien, C. A. & Wolin, S. L. (1995) *RNA* **1**, 293–303.
12. Chen, X., Quinn, A. M. & Wolin, S. L. (2000) *Genes Dev.* **14**, 777–782.
13. Labbe, J. C., Hekimi, S. & Rokeach, L. A. (1999) *Genetics* **151**, 143–150.
14. Peterson, R. C., Doering, J. L. & Brown, D. D. (1980) *Cell* **20**, 131–141.
15. Shi, H., O'Brien, C. A., Van Horn, D. J. & Wolin, S. L. (1996) *RNA* **2**, 769–784.
16. Labbe, J. C., Burgess, J., Rokeach, L. A. & Hekimi, S. (2000) *Proc. Natl. Acad. Sci. USA* **97**, 13233–13238.
17. Kaufman, K. M., Farris, A. D., Gross, J. K., Kirby, M. Y. & Harley, J. B. (2000) *Genes Immunol.* **1**, 265–270.
18. Deutscher, S. L., Harley, J. B. & Keene, J. D. (1988) *Proc. Natl. Acad. Sci. USA* **85**, 9479–9483.
19. Yang, D., Tournier, C., Wysk, M., Lu, H. T., Xu, J., Davis, R. J. & Flavell, R. A. (1997) *Proc. Natl. Acad. Sci. USA* **94**, 3004–3009.
20. Liang, B., Gee, R. J., Kashgarian, M. J., Sharpe, A. H. & Mamula, M. J. (1999) *J. Immunol.* **163**, 2322–2329.
21. Yoo, C. J. & Wolin, S. L. (1994) *Mol. Cell. Biol.* **14**, 5412–5424.
22. Hardin, J. A., Rahn, D. R., Shen, C., Lerner, M. R., Wolin, S. L., Rosa, M. D. & Steitz, J. A. (1982) *J. Clin. Invest.* **70**, 141–147.
23. England, T. E., Bruce, A. G. & Uhlenbeck, O. C. (1980) *Methods Enzymol.* **65**, 65–74.
24. Lerner, E. A., Lerner, M. R., Janeway, C. A. & Steitz, J. A. (1981) *Proc. Natl. Acad. Sci. USA* **78**, 2737–2741.
25. Ziegler, A., Jonason, A. S., Leffell, D. J., Simon, J. A., Sharma, H. W., Kimmelman, J., Remington, L., Jacks, T. & Brash, D. E. (1994) *Nature* **372**, 773–776.
26. Hendrick, J. P., Wolin, S. L., Rinke, J., Lerner, M. R. & Steitz, J. A. (1981) *Mol. Cell. Biol.* **1**, 1138–1149.
27. Farris, A. D., Gross, J. K., Hanas, J. S. & Harley, J. B. (1996) *Gene* **174**, 35–42.
28. Wakeland, E. K., Liu, K., Graham, R. R. & Behrens, T. W. (2001) *Immunity* **15**, 397–408.
29. Andrews, A. D., Barrett, S. F. & Robbins, J. H. (1978) *Proc. Natl. Acad. Sci. USA* **75**, 1984–1988.
30. Bootsma, D., Kraemer, K. H., Cleaver, J. E. & Hoeijmakers, J. H. J. (2001) in *The Metabolic and Molecular Bases of Inherited Disease*, eds. Scriver, C. R., Beaudet, A. L., Sly, W. S. & Valle, D. (McGraw-Hill, New York), Vol. 1, pp. 677–703.
31. Lanzavecchia, A. (1995) *J. Exp. Med.* **181**, 1945–1948.
32. Andrade, F., Casciola-Rosen, L. & Rosen, A. (2000) *Rheum. Dis. Clin. North Am.* **26**, 215–227.
33. Botto, M., Dell'Agnola, C., Bygrave, A. E., Thompson, E. M., Cook, H. T., Petry, F., Loos, M., Pandolfi, P. P. & Walport, M. J. (1998) *Nat. Genet.* **19**, 56–59.
34. Bickerstaff, M. C., Botto, M., Hutchinson, W. L., Herbert, J., Tennent, G. A., Bybee, A., Mitchell, D. A., Cook, H. T., Butler, P. J., Walport, M. J., *et al.* (1999) *Nat. Med.* **5**, 694–697.
35. Napirei, M., Karsunky, H., Zevnik, B., Stephan, H., Mannherz, H. G. & Moroy, T. (2000) *Nat. Genet.* **25**, 177–181.
36. Scott, R. S., McMahon, E. J., Pop, S. M., Reap, E. A., Caricchio, R., Cohen, P. L., Earp, H. S. & Matsushima, G. K. (2001) *Nature* **411**, 207–211.
37. Lee, L. A. (2001) *Curr. Rheumatol. Rep.* **3**, 391–395.
38. Patel, P. & Werth, V. (2002) *Dermatol. Clin.* **20**, 373–385.
39. Alarcon-Segovia, D., Ruiz-Arguelles, A. & Fishbein, E. (1978) *Nature* **271**, 67–69.
40. Ma, J., Chapman, G. V., Chen, S. L., Melick, G., Penny, R. & Breit, S. N. (1991) *Clin. Exp. Immunol.* **84**, 83–91.
41. Yanase, K., Smith, R. M., Cizman, B., Foster, M. H., Peachey, L. D., Jarett, L. & Madaio, M. P. (1994) *Lab. Invest.* **71**, 52–60.
42. Zack, D. J., Stempniak, M., Wong, A. L., Taylor, C. & Weisbart, R. H. (1996) *J. Immunol.* **157**, 2082–2088.
43. Koscec, M., Koren, E., Wolfson-Reichlin, M., Fugate, R. D., Trieu, E., Targoff, I. N. & Reichlin, M. (1997) *J. Immunol.* **159**, 2033–2041.
44. Deng, S. X., Hanson, E. & Sanz, I. (2000) *Int. Immunol.* **12**, 415–423.
45. Musunuru, K. & Darnell, R. B. (2001) *Annu. Rev. Neurosci.* **24**, 239–262.
46. Chan, E. K., Tan, E. M., Ward, D. C. & Matera, A. G. (1994) *Genomics* **23**, 298–300.
47. Moser, K. L., Neas, B. R., Salmon, J. E., Yu, H., Gray-McGuire, C., Asundi, N., Bruner, G. R., Fox, J., Kelly, J., Henshall, S., *et al.* (1998) *Proc. Natl. Acad. Sci. USA* **95**, 14869–14874.
48. Lindqvist, A. K., Steinsson, K., Johanneson, B., Kristjansdottir, H., Arnasson, A., Grondal, G., Jonasson, I., Magnusson, V., Sturfelt, G., Truedsson, L., *et al.* (2000) *J. Autoimmun.* **14**, 169–178.
49. Johanneson, B., Lima, G., Von Salome, J., Alarcon-Segovia, D. & Alarcon-Riquelme, M. E. (2002) *Am. J. Hum. Genet.* **71**, 1060–1071.

ICA69^{null} Nonobese Diabetic Mice Develop Diabetes, but Resist Disease Acceleration by Cyclophosphamide[1]

Shawn Winer,[2*] Igor Astsaturov,[2*] Roger Gaedigk,[2*] Denise Hammond-McKibben,* Marc Pilon,* Aihua Song,* Violetta Kubiak,* Wolfram Karges,* Enrico Arpaia,* Colin McKerlie,[†] Peter Zucker,[‡] Bhagirath Singh,[‡] and H.-Michael Dosch[3*]

ICA69 (islet cell Ag 69 kDa) is a diabetes-associated autoantigen with high expression levels in β cells and brain. Its function is unknown, but knockout of its *Caenorhabditis elegans* homologue, *ric-19*, compromised neurotransmission. We disrupted the murine gene, *ica-1*, in 129-strain mice. These animals aged normally, but speed-congenic ICA69^{null} nonobese diabetic (NOD) mice developed mid-life lethality, reminiscent of NOD-specific, late lethal seizures in glutamic acid decarboxylase 65-deficient mice. In contrast to wild-type and heterozygous animals, ICA69^{null} NOD congenics fail to generate, even after immunization, cross-reactive T cells that recognize the dominant Tep69 epitope in ICA69, and its environmental mimicry Ag, the ABBOS epitope in BSA. This antigenic mimicry is thus driven by the endogenous self Ag, and not initiated by the environmental mimic. Insulitis, spontaneous, and adoptively transferred diabetes develop normally in ICA69^{null} NOD congenics. Like glutamic acid decarboxylase 65, ICA69 is not an obligate autoantigen in diabetes. Unexpectedly, ICA69^{null} NOD mice were resistant to cyclophosphamide (CY)-accelerated diabetes. Transplantation experiments with hemopoietic and islet tissue linked CY resistance to ICA69 deficiency in islets. CY-accelerated diabetes involves not only ablation of lymphoid cells, but ICA69-dependent drug toxicity in β cells that boosts autoreactivity in the regenerating lymphoid system. *The Journal of Immunology*, 2002, 168: 475–482.

Type I diabetes (T1D)[4] is the consequence of chronic progressive autoimmunity that targets pancreatic islets of Langerhans, selectively eliminating insulin-producing β cells. Causes that underlie the development of diabetic autoimmunity remain obscure. Products of some 20^{+} predisposing genes interact with critical environmental accelerators and decelerators to generate the autoimmune phenotype (1).

Clinical insulin deficiency and its attendant metabolic abnormalities are the end result of a drawn-out prediabetes phase, in which autoreactive T cell pools accumulate in the islet. Prediabetes proceeds in a stepwise fashion (2, 3), from benign periinsulitis to islet invasion and progressively rising rates of β cell death, as signaled by the generation of autoantibodies (4, 5). Because of the difficulty of tissue access in humans, much of the current view of autoimmune diabetes derives from the excellent rodent models for the disease, BB rats and nonobese diabetic (NOD) mice (6, 7). However, many years of prediabetes are a reality of the human disease, in which B and T cell autoimmunity arise many years before and can persist for decades after onset of overt disease (see Refs. 8–10).

A similar set of autoantigens is targeted by self-reactive T cells in human and murine diabetes, including insulin/proinsulin, glutamic acid decarboxylase 65 (GAD65), GAD67, ICA69 (islet cell Ag 69 kDa), and IA-2/phogrin (1, 7). Of these, only insulin is (nearly) β cell specific, while others follow generally neuroendocrine gene expression profiles. In NOD mice, immunotherapies with any one of these autoantigens can halt, and in some circumstances accelerate development of overt diabetes, depending on the choice of epitopes and the timing of interventions early or later in prediabetes (11–17).

While there may be a hierarchy among autoimmune targets, in particular early on (18), established prediabetes involves multiple T cell pools that home to the islet, targeting more self epitopes with increasing effectiveness (19–21). The progression of prediabetes is complex and passes through checkpoints that halt progression for some periods of time (2). A single dose of cyclophosphamide (CY), an alkylating cancer pro-drug (22), overcomes these checkpoints and allows rapid diabetes development in a process that is dominated by the local activation of myeloid APCs and their cytokine products (3). In this commonly used diabetes model, CY was suggested to remove regulatory hemopoietic cells (23, 24), in a host whose lymphoid cell lineages are relatively resistant to the drug and able to mount a dramatic recovery of lymphoid mass quickly after drug exposure (25). Data presented in this work suggest that the drug's role in diabetes development is more complex and critically depends on direct islet cell toxicity in a process that appears to require the function of ICA69.

To explore the role of self Ag in prediabetes and its progression to overt disease, we disrupted the genomic locus of the autoantigen, ICA69 (14, 26, 27), and backcrossed the defect onto NOD, using a speed-congenic strategy (28). The conserved ICA69 gene, *ica-1*, maps to human chromosome 7p22 and a synthenic location

*The Hospital For Sick Children, Research Institute, University of Toronto, Toronto, Ontario, Canada; [†]Departments of Pediatrics and Immunology, Sunnybrook and Women's College Health Sciences Center, and [‡]University of Western Ontario, Department of Immunology, John P. Robarts Research Institute, London, Ontario, Canada

Received for publication August 16, 2001. Accepted for publication October 25, 2001.

The costs of publication of this article were defrayed in part by the payment of page charges. This article must therefore be hereby marked *advertisement* in accordance with 18 U.S.C. Section 1734 solely to indicate this fact.

[1] This work was supported by grants from the Canadian Institutes of Health Research and the Juvenile Diabetes Research Foundation.

[2] S.W., I.A., and R.G. contributed equally.

[3] Address correspondence and reprint requests to Dr. H.-Michael Dosch, IIIR Program, The Hospital For Sick Children, 555 University Avenue, Toronto, Ontario, Canada, M5G 1X8. E-mail address: hmdosch@sickkids.ca

[4] Abbreviations used in this paper: T1D, type 1 diabetes; CY, cyclophosphamide; GAD, glutamic acid decarboxylase; ICA69, islet cell Ag 69 kDa; NOD, nonobese diabetic; Tep69, major NOD mouse T cell epitope in ICA69; tet07, artificial promoter tetoperon (×7) + TATA box; tTA, tetracycline transactivator.

0022-1767/02/$02.00

on mouse chromosome 6A1, 2, neither location mapping near known diabetes risk loci (27, 29). The molecule has a neuroendocrine expression pattern with peak levels in brain and β cell lines (30). Its function is unknown, but we found that *Caenorhabditis elegans* deficient for the well-conserved ICA69 homologue, *ric-19*, develops a neurotransmission defect (31).

The protein includes a single, dominant T cell epitope, Tep69 (major T cell epitope in ICA69), targeted by autoreactive T cells in both human and NOD mouse T1D (26). There is well-established antigenic mimicry between this epitope and the ABBOS epitope in the commonly encountered, dietary Ag, BSA (14). Because ABBOS is a highly dominant BSA epitope in NOD mice, it appeared possible that ICA69 autoimmunity might be triggered through mimicry with BSA/ABBOS (10, 14, 32), encountered through exposure to dietary cow milk protein, a risk factor for diabetes development (33–36). Observations in ICA69^{null} NOD congenics now indicate that the routinely generated Tep69/ABBOS mimicry T cell pools require and are driven by the endogenous self Ag, which also dictates the apparent dominance for ABBOS in BSA immune responses of wild-type NOD mice.

The 129SvJ mice with ICA69 deficiency had no obvious phenotype and aged normally. However, speed-congenic ICA69^{null} NOD mice develop sudden lethality beginning in early middle age, reminiscent of GAD65 deficiency that produces mid-life lethal seizures only on the NOD background (37). ICA69^{null} NOD female congenics develop diabetes at essentially wild-type NOD incidence. Like GAD65 (38), ICA69 emerges as a facultative, but not obligate element in diabetes progression. Surprisingly, and challenging current views, ICA69^{null} mice were highly resistant to CY-accelerated diabetes due to a previously unrecognized drug effect on islets, which appears to require the function of ICA69.

Materials and Methods

Animals

NOD/Lt (H-2^{g7}) mice were bred in our rodent facility according to approved facility guidelines and protocols. Experiments were performed in our conventional unit, which presently has an 83–86% diabetes incidence in 36-wk-old female mice.

Adoptive transfer

Spleen cells from three to five recently diabetic NOD females were pooled, and 10^7 cells were transferred i.v. to 6- to 8-wk-old, irradiated NOD male (650 rad) or NOD.*scid* (200 rad) recipients. In all experiments, glucosuria (TesTape, Lilly, Toronto) was used for daily diabetes screens. Diabetes was confirmed through blood glucose measurements on 2 consecutive days (13.8 mM/L, SureStep; Life Technologies, Burnaby, British Columbia, Canada).

CY-accelerated diabetes

To induce accelerated diabetes development, 8- to 10-wk-old wild-type, heterozygous or homozygous ICA69 knockout females received one i.p. injection of 250 mg/kg CY (Sigma, St. Louis, MO). In some experiments, 14-wk-old animals were used, or a second injection was given 3 wk later.

Pancreatic islet transplantation

Islets were isolated from pancreata of 4- to 5-wk-old wild-type NODs by standard digestion and manual picking procedures (39). The grafts were placed under the kidney capsule of anesthetized, 8-wk-old ICA69^{null} NOD females. Sixteen days later, the recipients were treated with 250 mg/kg CY, and diabetes development was monitored for at least 4 wk. Sham-operated and nontransplanted wild-type NOD and ICA69^{null} mice provided controls.

Generation of ICA69^{null} mice

The ICA69 locus occupies approximately 100 kb on mouse chromosome 6 (27, 29). A murine 129SvJ genomic library (gift of T. Mak, Toronto, Canada) was screened with a full-length ICA69-α cDNA probe (26). A 2.7-kb clone containing exon 2 was excised with *Bgl*II and subcloned into pBluescript II-SK upstream of a *herpes simplex* thymidine kinase expression cassette. The aminoglycoside phosphotransferase (*neo*) gene was excised from the pPNT vector and ligated into a *Stu*I site at position 107 of exon 2, thus disrupting the coding region of the Tep69 epitope in ICA69 (27).

The tetracycline transactivator (tTA) coding region (40, 41) (gift of H. Bujard, Heidelberg, Germany) was moved in-frame into an *Age*I restriction site at position 38 of exon 2 in ICA69 (see below, Fig. 1). This was thought to allow future experiments, such as possible rescue of knockout phenotypes through doxycycline-regulatable expression of a tet07-ICA69 transgene (42). The function of the targeting vector, including the tTA knock-in, was confirmed in NIT-1 β cells (43) with one allele replaced by the vector. Transient transfection of these cells with low copy numbers of a tet07-luciferase expression plasmid (40) (gift of H. Bujard) resulted in excellent luciferase expression that was over 98% suppressed in the presence of 1 μM doxycycline (Hammond-McKibben et al., manuscript in preparation).

Targeting vector DNA was linearized with *Not*I and transfected into the R1 ES cell line, and multiple clones were selected in the presence of G418 and gancyclovir (44). Double-resistant embryonic stem cell clones (19 of 482 screened) were expanded for use in morula aggregations with fertilized NOD eggs (44), and chimeric male offspring were bred with NOD females. Transmission was analyzed by standard Southern blots (27). Offspring with germline transmission of the ICA69^{null} allele were backcrossed to NOD in a speed-congenic strategy (28). One founder repeatedly generated offspring with germline transmission of the null allele, and one of these ICA69$^{+/-}$ heterozygous offspring was homozygous for NOD variants of *D6 Mit52* and *D6 Mit339* on chromosome 6, suggesting a crossover event that replaced a considerable stretch of 129SvJ strain chromosome 6 with NOD genomic DNA. This male was mated to wild-type NOD females (backcross generation 2). Several offspring from backcross 5 were homozygous NOD for all 17 *Idd* loci, according to microsatellite markers (28). The ICA69-deficient mice analyzed in the present study were derived from backcross 7.

Subcellular fractionation of mouse brain

Mouse brain tissue was fractionated as described (31). Briefly, brains were homogenized in ice-cold, supplemented HBSS buffer. Nuclei and cell debris were removed, and supernatant (S1) was centrifuged at 13,000 × *g* for 13 min. Supernatant was collected and spun at 100,000 × *g* for 30 min to yield S3 (the cytosol) and P3 (the microsomal pellet). The synaptosome fraction was washed with HBSS buffer and centrifuged at 13,000 × *g* for 13 min. The pellet was lysed, buffered (10 mM HBSS, pH 7.4), and centrifuged at 45,000 × *g* for 20 min. The pellet (LP1) was resuspended in HKA buffer (10 mM HEPES-KOH, pH 7.4, 140 mM KoAC, 1 mM $MgCl_2$, 0.1 mM EGTA, 0.3 mM PMSF), while the crude synaptic vesicles were pelleted by further centrifugation of the supernatant at 150,000 × *g* for 1 h, then resuspended in HKA buffer. All procedures were performed on ice.

Western blots

Rabbit anti-ICA69 (gift from M. Pietropaolo, Pittsburgh, PA) was used at a final dilution of 1/7500 (30). Each subcellular fraction (40 μg) was separated on SDS polyacrylamide gels and transferred to nitrocellulose. Peroxidase-conjugated goat anti-rabbit Ab (The Jackson Laboratory, Bangor, ME; 1/15,000) was used to detect bound primary Ab. Rabbit anti-VAMP-2 provided a marker of synaptic vesicles (gift from W. Trimble, The Hospital For Sick Children).

Histology

Tissues for histological sections were fixed in 10% neutral buffered Formalin and stained with H&E. The degree of insulitis was scored blindly by two observers, using the following scale: 0, normal islet; 1, periinsulitis; 2, invasive infiltration of 25%–50% of islet surface area; 3, invasive infiltration of greater than 50% of islet surface area or a small retracted islet. Immunohistochemistry for insulin was performed on Formalin-fixed, paraffin-embedded tissue sections using guinea pig anti-insulin Ab and rabbit HRP-conjugated secondary Ab (Dako Diagnostics, Mississauga, Ontario, Canada). Reactions were visualized using diaminobenzidine peroxidase substrate, and sections were counterstained with hematoxylin.

Proliferative T cell responses

In vitro T cell proliferation was measured as described recently for immunized and nonimmunized NOD mice (16). Immunizations employed s.c. injection of a given Ag, 100 μg emulsified in CFA. Regional lymph nodes were removed 9–10 days after immunization, and 4 × 10^5 cells/well were cultured in serum-free AIM V medium (Life Technologies) to measure recall responses to 0.01–100 μM Ag. After 60 h, cultures were pulsed overnight with 1 μCi [^{3}H]thymidine and subjected to scintillation counting. Spontaneous T cell proliferation in spleen cells from unimmunized naive or adoptively transferred mice was similarly measured, except for the addition of 10 U human rIL-2 (45). Synthetic peptides were highly purified and confirmed by mass spectroscopy: Tep69, AFIKATGKKEDE, ABBOS,

FKADEKKFWGKYLYE. Grade V BSA and OVA were purchased from Sigma. Purified, mouse rICA69-β was prepared as described (26); rGAD65 was purchased (Diamyd Diagnostics, Stockholm, Sweden).

Statistics

Numeric values were compared by Mann-Whitney or Welsh tests; significance was set at 5%; and all tests were two tailed. Tables were used to compare diabetes incidence in different groups of animals (Fisher's exact test); odds ratios were calculated with Woolf's approximation.

Results

Generation of ICA69^{null} mice

The targeting construct (Fig. 1*A*) introduces a neomycin resistance cassette to disrupt the Tep69 epitope in exon 2 of ICA69, and inserts the tTA coding region in-frame after the leading 9 ICA69 aa residues, followed by poly(A) and stop sites. Homologous recombination of this vector in its genomic target locale introduces an additional *Xba*I site that produces a 3.2-kb *Xba*I restriction fragment, while the corresponding wild-type fragment is 3.6 kb in length (Fig. 1*A*). Homologous recombination of the targeting construct was confirmed in genomic DNA of progeny from several chimeric founders, using a 5′-end probe and *Xba*I restriction (Fig. 1*B*) and a neo probe and *Hin*dIII restriction (not shown). Several litters of this generation of *129SvJ x NOD* offspring were monitored for up to 26 mo, including 17 ICA69^{null} animals derived from brother-sister matings. No spontaneous deaths or obvious abnormalities were observed.

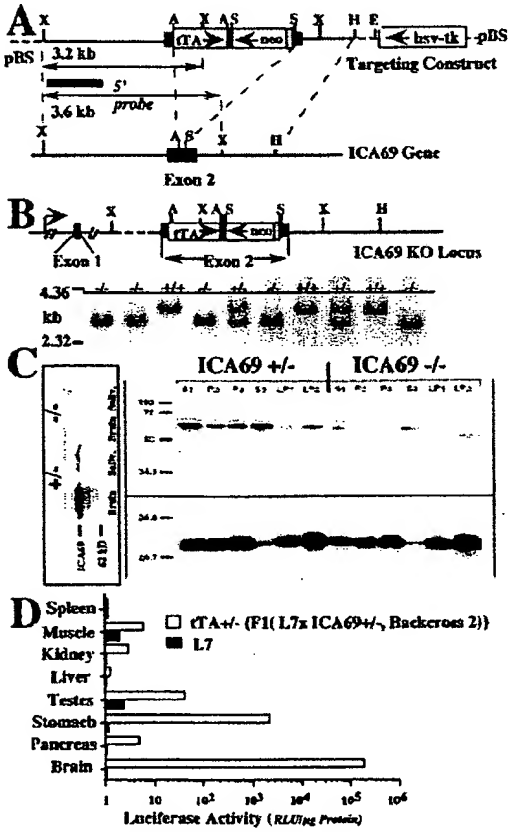

FIGURE 1. Development of ICA69^{null} mice. *A*, The ICA69 locus was genetically disrupted by insertion of tTA and neo genes into exon 2 of the ICA69 gene. The *top diagram* shows the targeting construct that targeted the ICA69 gene (*bottom*) and generated the knockout allele shown at the *top* of *B*. *B*, Southern blot of *Xba*I-restricted genomic DNA from *129vJ x NOD* mice backcross 2. The knockout allele generates a shortened 3.2-kb exon 2 fragment. *C*, Western blots of brain and salivary gland tissue extracts (backcross 11 mice, *left panel*) and fractionated brain protein from wild- type and homozygous ICA69 knockout mice (backcross 7) were probed with anti-ICA69 polyclonal Ab. A 23-kDa synaptic vesicle marker, VAMP2, is shown *below*. S1, postnuclear supernatant; P2, synaptosomes; S3, cytosol; P3, microsomes; LP1, plasma membrane; LP2, synaptic vesicles. *D*, Luciferase activity (relative light units/μg protein) in different tissues from L7 (tet07-luciferase transgenic) mice carrying a single ICA69 knockout/tTA-knock-in allele from backcross 2 mice (open bars). Expression patterns follow the tissue expression of ICA69. L7 mice without the tTA transgene express only background activities (filled bars, note the logarithmic scale).

ICA69 is expressed at low to very low levels in a variety of tissues, with its major expression locale in the brain, and highest levels found in β cell lines (30). Almost certainly reflecting post-translational modifications, Western blots resolve ICA69 as a doublet band of approximately 69 kDa, despite its calculated mass of 55 kDa (30, 46). There was no detectable ICA69 in Western blots of brain and salivary gland extracts from backcross 7 (not shown) or backcross 11 mice (Fig. 1*C*, *left panel*), but there were occasional ghost bands in brain subcellular fractions (*right panel*). These bands were not consistent, and could be detected only with one rabbit Ab raised against a C-terminal peptide (46) (Fig. 1*C*), but not with another rabbit Ab raised against a large, truncated ICA69 fragment (not shown). We were unable to obtain sufficient material for mass spectrography and sequencing studies of these ghost bands. As described below, the distinct phenotypes of these mice, results of extensive RT-PCR, Southern blot, and genomic PCR studies of the disrupted gene locus, and in particular the silencing of the natural ICA69 promoter (see below) make a hypomorphic phenotype with remnant gene expression of gene fragments from this locus unlikely.

Heterozygous (ICA69$^{+/-}$) progeny from backcross 2 were mated with the L7 transgenic mouse that carries a tet07-luciferase transgene (40). Offspring carrying the L7 transgene as well as one ICA69^{null}/tTA^{+} allele demonstrated high luciferase activity in brain (note the logarithmic scale), low levels in stomach and testes, and borderline levels in pancreas, in which β cells contribute 0.1% of total pancreas tissue (Fig. 1*D*). The latter observation is consistent with the fact that ICA69 expression in exocrine pancreas is at best minuscule (47). In mice receiving doxycycline ad libitum in drinking water (0.1 mg/ml), luciferase activity was suppressed to background levels (not shown). These observations provided an excellent readout of ICA69 promoter activity.

However, similar experiments with mice from backcross 3 showed a >10-fold reduction in luciferase activity, and no activity at all could be detected in offspring from L7 matings with knockout animals from backcross 5 and 7. While Southern blots and genomic PCR gave expected results, transcripts of tTA could be demonstrated by RT-PCR of brain RNA in backcross 2-derived, but not in animals from these latter experiments, indicating loss of ICA69 promoter activity. Transcriptional silencing is not rare among neuronal genes (48), and has been described for GAD65 (49).

Autoantigen skews the specificity of autoreactive T cells

Autoreactive T cells in wild-type NOD mice (like patients with T1D) recognize the dominant ICA69 epitope Tep69 (10, 26). These T cells show antigenic mimicry with the ABBOS epitope in BSA, and T cell hybridoma as well as alanine replacement studies indicated that these mimicry T cells represent the bulk of ICA69-specific NOD repertoires (16). ICA69^{null} NOD congenics allowed

us to determine the role of endogenous self Ag in the development of these self-reactive T cell pools. Immunization with BSA had divergent consequences in heterozygous and homozygous ICA69 knockout mice (Fig. 2*A*). Both lines of mice generated good and similar proliferative recall responses after a single BSA immunization in complete adjuvant. However, only heterozygous (+/−) animals generated the coordinate ABBOS and Tep69 mimicry responses typical for wild-type NODs (14, 16). In homozygous ICA69^{null} NOD congenics, ABBOS was no longer a prominent epitope, despite the fact that it binds to NOD I-A^{g7} with high affinity (16). Only some low affinity ABBOS responses were observed at a very high peptide dose. No mimicry responses to Tep69 were seen in BSA-immunized ICA69^{null} animals. Thus, the endogenous self Ag is required for the recruitment of precursor T cell pools that recognize both Tep69 and ABBOS, and the presence of these T cell pools is responsible for the strong immunodominance (14) of the ABBOS epitope in BSA.

Endogenous self Ag (and not dietary ABBOS) was also critical for the maintenance of these autoreactive mimicry T cell pools. Thus, when knockout mice were adoptively transferred with splenocytes from diabetic wild-type NODs, Tep69/ABBOS-specific T lymphocytes were specifically lost (Fig. 2*B*, filled bars), while other islet-reactive T cells, such as GAD65-specific pools, were maintained. Consistent with this critical role of the endogenous self Ag, Tep69/ABBOS-specific T cells were maintained in heterozygous ICA69$^{+/-}$ mice adoptively transferred with the same wild-type splenocyte grafts (Fig. 2*B*, open bars).

ICA69^{null} NOD mice develop diabetes

Autoimmunity to ICA69 is a routine element of prediabetes and of diabetes in wild-type NOD mice and humans (10, 14, 16). Spontaneously diabetic knockout females were observed beginning by wk 20, ~4 wk later than in wild-type or heterozygous animals (Fig. 3*A*). This difference was not quite significant ($p = 0.058$). The consecutive disease development in knockout mice paralleled that in heterozygous and wild-type NOD females ($p > 0.3$). There was a tendency for slightly less or slower development of invasive insulitis (Fig. 3*B*), but this again failed to reach significance. Thus, ICA69 appears to be a facultative, but not obligate element in NOD diabetes development.

This conclusion is somewhat tempered by the unexpected observation of spontaneous lethality in middle-aged NOD female congenics at 4–5 mo of age (Fig. 3*C*). A subset of these animals died suddenly without prodromal symptoms. These animals had no significant histopathology, except for insulitis commensurate with prediabetes progression and a severed tongue in one animal. This phenotype is reminiscent of GAD65 deficiency, which leads to lethal mid-life seizures on the NOD background (37). Neuropharmacological studies have to date failed to unmask a consistent abnormality in the CNS electrophysiology of ICA69^{null} mice. In our assessment of the spontaneous diabetes incidence in ICA69^{null} mice, we removed the prematurely dead animals from calculation. The implicit assumption that these animals would have developed diabetes at the same rate as survivors is based on the presence of invasive insulitis.

Adoptive transfer of diabetes

Accelerated models of diabetes such as adoptive transfer of diabetic spleen cells circumvent natural checkpoints in prediabetes progression (50). We asked whether the slight delay in spontaneous diabetes development would be amplified or eliminated following adoptive transfer of wild-type diabetic spleen cells into irradiated knockout recipients. The latter was observed: transferred animals developed disease at the same rate and incidence as heterozygous littermates or wild-type controls (Fig. 3*D*), unhindered by the fact that the knockout mice lost ICA69-specific T cells during disease development (see above, Fig. 2*B*), and lacked this target autoantigen.

Acceleration of diabetes with CY

In striking contrast to wild-type and heterozygous animals, injection of CY (250 mg/kg) failed to induce accelerated diabetes in ICA69^{null} mice (Fig. 4). Heterozygous littermates began to develop overt disease by 10–11 days post-CY, reaching a high disease incidence by 3 wk ($p < 0.0001$, odds ratio 27.4 vs knockout (Fig. 4*A*), $p > 0.3$ vs wild-type mice, not shown). ICA69 protein is not expressed in hemopoietic cells (30) (see Fig. 1*D* for splenocytes). Consistently, there was no detectable effect of ICA69 deficiency in this tissue, with homozygous, heterozygous NOD as well as 129 mice showing the same acute drug-induced fall in spleen weight and cellularity. CY metabolism with generation of, and response to the major toxic intermediates (22) was thus similar in these animals ($p > 0.3$, data not shown).

Curiously, there was only a slight, nonsignificant difference in insulitis severity of CY-treated homozygous and heterozygous animals (Fig. 4*B*, $p = 0.2$), suggesting that effector functions in the islet infiltrate of knockout mice lacked the competence to mediate β cell death. This incompetence was not due to a general delay of prediabetes, since ICA69^{null} NOD mice 14 wk of age, and thus close to the time of overt spontaneous diabetes development, were still protected from CY-induced disease (Fig. 4*C*). These older animals ultimately did develop diabetes, beginning in wk 20 with the incidence rising at wild-type rates (see Fig. 3*A*). The resistance to CY-accelerated diabetes in knockout mice was not absolute, since a second CY injection caused diabetes in nearly half of the

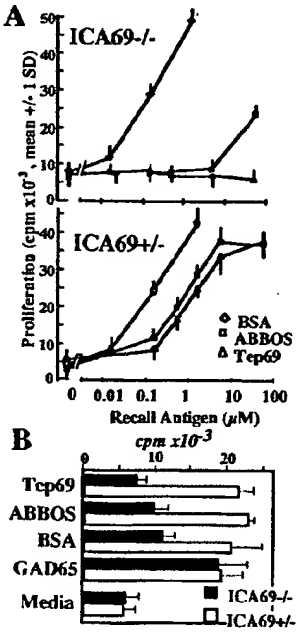

FIGURE 2. In vitro proliferative recall responses. *A*, Homo- and heterozygous knockout NOD congenics were immunized s.c. once with BSA emulsified in CFA, and in vitro lymph node responses to BSA, ABBOS, and Tep69 were elicited 10 days later. *B*, In vitro proliferative response of wild-type, diabetic spleen cells 14 days after transfer to irradiated ICA69$^{-/-}$ (filled columns) or ICA69$^{+/-}$ recipients (open columns).

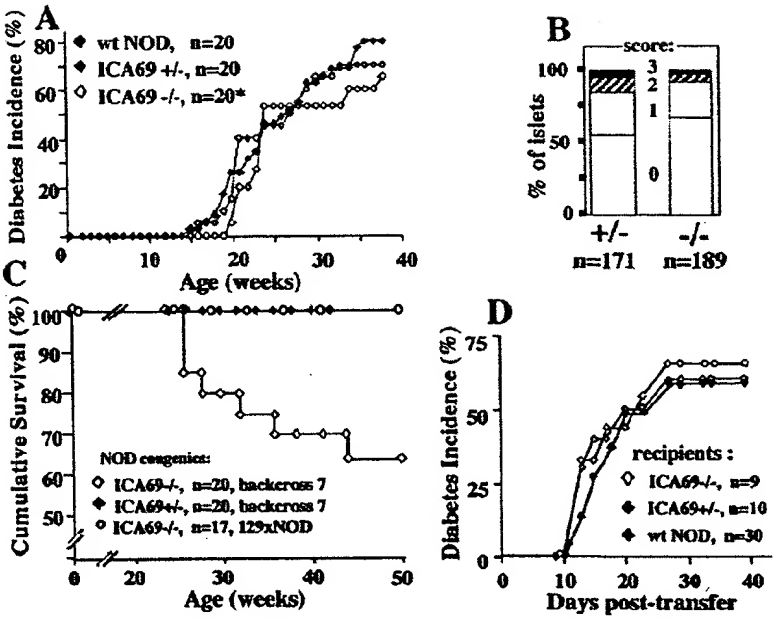

FIGURE 3. Diabetes development and survival of ICA69^{null} NOD mice. *A*, Spontaneous diabetes development; *, a proportion of ICA69^{null} mice died prematurely (see *C*) and were removed from the calculation of disease incidence. *B*, Insulitis in untreated ICA69$^{+/-}$ or ICA69$^{-/-}$ female congenics (seven animals/group) at 10 wk of age. *C*, Mid-life lethality of ICA69^{null} NOD females without prodromal disease symptoms or diagnostic histopathology. *D*, Wild-type diabetes development in irradiated ICA69$^{-/-}$, ICA69$^{+/-}$, or wild-type NOD mice adoptively transferred with spleen cells from diabetic wild-type donors.

homozygous mice (5 of 11), compared with 12 of 13 heterozygous animals (Fig. 4*D*, $p = 0.02$).

CY-accelerated diabetes has been associated with the selective elimination of regulatory T cells and/or with the induction of a massive wave of T cell regeneration that would coexpand diabetogenic pools (23, 24, 51). We more closely examined the CY responses of knockout hemopoietic cells. NOD.*scid* mice were pretreated with CY 2 days before adoptive transfer of spleen cells from 12-wk-old nondiabetic wild-type mice; diabetes did not develop within the observation period (Fig. 4*E*, *CY→Tx*). This confirmed the critical role of acute, drug-induced toxicity in lymphoid cells.

However, when NOD.*scid* mice were reconstituted with 10^7 spleen cells from 8-wk-old homozygous knockout mice, from heterozygous littermates, or wild-type NOD controls, 1 mo before CY treatment (Fig. 4*E*, *Tx→CY*), these transplanted NOD.*scid* animals developed CY-accelerated diabetes at the same rates and incidence ($p > 0.5$). This observation demonstrated that hemopoietic cells were not involved in the CY resistance of knockout mice. Collectively, these two observations delineated two drug targets prerequisite for diabetes development, one in hemopoietic and one in nonhemopoietic tissue.

Since the islet is one target tissue of CY toxicity (52), we asked whether the nonhemopoietic tissue required for disease acceleration by CY might be the islet itself. We therefore provided ICA69^{null} mice with a source of wild-type islets in small, subrenal islet grafts. Sixteen days later, the engrafted mice were injected with CY as before (Fig. 5*A*). The presence of wild-type islets reversed the resistance to CY-accelerated diabetes in ICA69^{null} mice, and allowed diabetes development in engrafted knockout

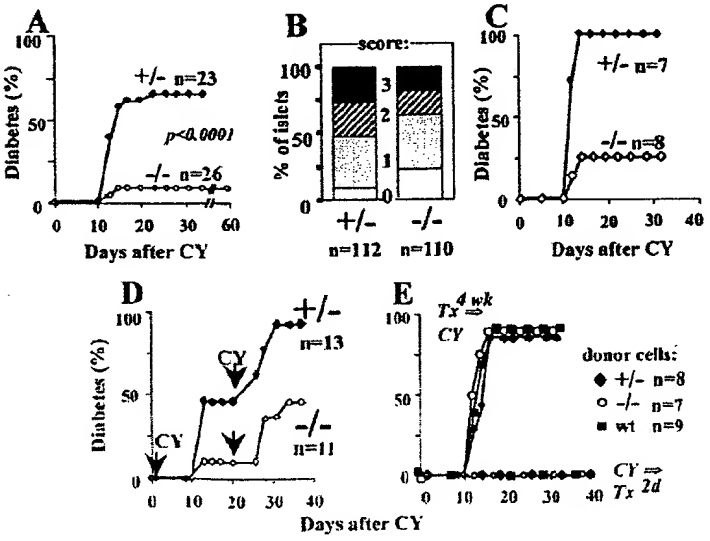

FIGURE 4. ICA69$^{-/-}$ NOD mice resist CY-accelerated diabetes. *A*, Diabetes incidence in CY-treated hetero- and homozygous knockout mice aged 8–10 wk. *B*, Insulitis score in CY-treated, nondiabetic ICA69$^{+/-}$ ($n = 5$) and ICA69$^{-/-}$ mice ($n = 8$) 35 days after drug treatment. The number of nonadjacent islets counted (n) is indicated at the *bottom*. See *Materials and Methods* for scoring scale. About one-half of heterozygote islets and only slightly fewer homozygote islets ($p = 0.2$) had severe, grade 2 and 3 insulitis. *C*, Diabetes incidence in CY-treated hetero- and homozygous knockout mice aged 14 wk. *D*, Dual injections of CY on day 0 and 20 in ICA69$^{-/-}$ and ICA69$^{+/-}$ animals. *E*, Diabetes development in NOD.*scid* mice reconstituted with 10^7 ICA69$^{-/-}$, ICA69$^{+/-}$, or wild-type spleen cells 1 mo before (*Tx→CY*) or 2 days after (*CY→Tx*) CY treatment.

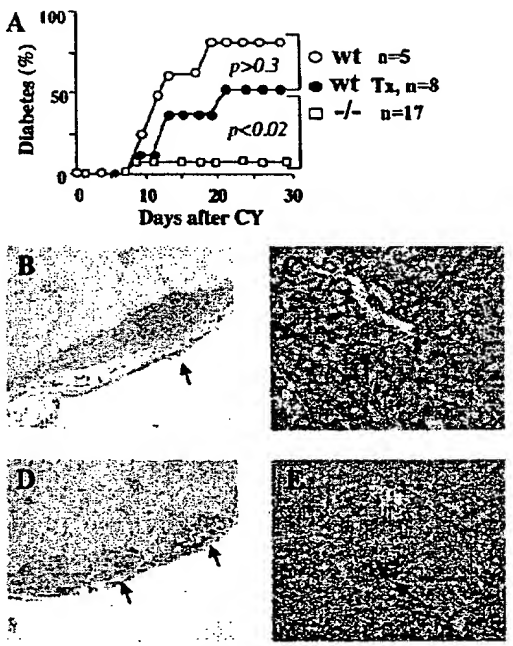

FIGURE 5. Transplantation of wild-type islets reverses CY resistance in ICA69^{null} mice. *A*, Incidence of CY-accelerated diabetes in sham-operated, wild-type mice (O); sham- or nontransplanted ICA69$^{-/-}$ NOD females (□); or ICA69^{null} females with wild-type islet grafts (Tx) under the kidney capsule, transplanted 16 days before CY (●). *B–E*, Immunohistochemical analysis of transplanted or pancreatic islets (×100, insulin stained in brown, counterstained with hematoxylin). *B*, Wild-type islet graft under the kidney capsule with massive inflammatory infiltrate (arrow) and absent insulin staining. *C*, Destroyed pancreatic islet of the same diabetic animal. *D*, Infiltration, but survival of insulin-producing cells in renal wild-type islet grafts (arrows) from a CY-treated, nondiabetic ICA69^{null} mouse. *E*, Infiltration, but survival of insulin-producing cells (arrow) in a pancreatic islet from the same animal.

animals ($p > 0.3$, knockout-operated vs sham-operated wild-type NOD; $p = 0.016$, islet-engrafted vs sham-operated or nontransplanted ICA69^{null} mice). These observations confirm and extend previous, indirect evidence for a duality of CY effects that accelerate diabetes development (53).

Histological examination of transplanted, CY-induced diabetic ICA69^{null} mice showed massive infiltration and complete disappearance of insulin-producing cells in the subrenal, wild-type islet grafts (Fig. 5*B*). Endogenous (pancreatic) islets in these knockout mice were similarly infiltrated and depleted of insulin-producing β cells (Fig. 5*C*). Destruction of wild-type islet grafts was a prerequisite for the destruction of endogenous (knockout) islets in the pancreas: those ICA69^{null} mice that escaped CY-accelerated diabetes showed less infiltration and intact insulin-producing cells in the wild-type islet grafts (Fig. 5*D*). The endogenous islets in these mice were heavily infiltrated, but retained a prominent compartment of insulin-producing β cells (Fig. 5*E*), suggesting that this infiltrate was incompetent to mediate β cell destruction.

These observations suggest that the resistance of ICA69^{null} mice to CY-accelerated diabetes reflects a relative resistance to CY toxicity in β cells, which require ICA69 for an apoptotic drug response (52). Consistently, CY resistance can be bypassed if a source of drug-sensitive islets is present somewhere in the body, suggesting a systemic effect that boosts T cell pools with pathogenic potential during the rapid recovery and expansion of lymphoid cells after CY treatment.

Discussion

Deficiency of ICA69 generated several distinct phenotypes in NOD mice. It answered several core questions about the role of endogenous self Ag in disease-associated antigenic mimicry and the ability of the diabetic autoimmune process to shape disease-relevant T cell pools. The unexpected resistance to CY-accelerated diabetes allowed a reevaluation of its mechanistic basis in vivo. There is previous evidence for acute, CY-mediated islet toxicity that peaks within a day of drug injection and removes a substantial proportion of β cells (52). We have only begun mechanistic studies of how ICA69 might be involved in this process.

The function of ICA69 remains unclear. The neurotransmission defect generated by knockout of its neuron-specific *C. elegans* homologue, *ric-19* (31), requires further study, as does the mid-life lethality of ICA69^{null} NOD mice. Current experiments suggest that possible abnormalities in neurotransmission of ICA69^{null} mice will be subtle. However, we recently observed that NOD mice undergoing the spontaneous NOD autoimmune encephalitis develop seizures with considerable incidence (45), and Kash et al. (37) provided evidence for a rather strong modifier gene that predisposes NOD to seizures. Neurological similarities in GAD65 and ICA69 knockout mice may place ICA69 into the GABAergic pathway of neurotransmission, consistent with its pre- and postsynaptic localization (e.g., see Fig. 1*C*).

We were fortunate to identify a crossover event early in the backcrossing process, which replaced about two-thirds of the 129-derived chromosome 6 with NOD DNA. Nevertheless, a substantial stretch of 129-derived chromosome 6 remains. We had planned rescue experiments with a tet07-controlled ICA69 transgene, driven by the knock-in tTA transactivator. The silencing of the ICA69 promoter and consequent lack of tTA expression precluded this experiment, meant to rule out specific contributions of 129 genes to the knockout phenotype. However, comparing the CY toxicity in 129 and NOD mice failed to delineate differences in acute drug toxicity in spleen as well as testes, a tissue targeted by the drug (54). Although theoretically possible, it is therefore unlikely that the observed CY resistance of knockout mice reflects an unidentified 129 gene near the *ica-1* locus. Nevertheless, whether CY resistance maps to ICA69 (likely) or a 129 gene (unlikely) is immaterial for the major conclusion of these experiments, i.e., that CY-accelerated diabetes involves direct drug toxicity to the islet.

Several and similar T cell autoreactivities appear to participate in murine and human diabetogenesis (7, 10). Immunotherapy of NOD prediabetes with single autoantigens such as GAD65, GAD67, insulin, ICA69, IA-2, and others can each dramatically modify the disease course, provided that they are applied early in life, generally before the islet is breached (7). The exact mechanisms of effective immunotherapy are still elusive (for a discussion, see Ref. 16), but these consistent observations assign important potential, but not necessarily obligate roles to each target Ag. Removal of one player through gene targeting, e.g., ICA69 or GAD65 (37, 38), is the most accurate way to measure the role of an individual autoantigen, and the data available support a model of many facultative, but not obligate autoantigens in the progression to diabetes.

An unresolved question in autoimmunity is whether autoantigens drive autoimmunity, or whether they are more passive elements, perhaps victims of mimicry with exogenous proteins (55, 56). At least in the case of ICA69, the former appears to be correct. There is well-established mimicry between the major T cell epitopes in ICA69 (Tep69) and the commonly encountered BSA

(ABBOS) (10, 14, 16, 26, 32). T cell responses of wild-type NOD mice to BSA are extremely biased toward ABBOS reactivity. The same cells recognize Tep69 in NOD mice (16), and the same appears to apply to diabetes-prone humans (10). We expected that this polarization solely reflected properties of MHC alleles, with a very high ABBOS-binding affinity for diabetes risk-associated human and NOD MHC class II (16). This turned out to be incorrect: ICA69^{null} mice have entirely different BSA responses, in which ABBOS is at best a minor epitope, recognized by low affinity T cells that do not show mimicry with Tep69. Demonstrating antigenic mimicry, therefore, does not per se imply a primary mechanism for loss of tolerance. However, wild-type NOD mice reared on a diet free of BSA also fail to generate mimicry T cell pools (57). The functional outcome of mimicry is thus affected by both endogenous and exogenous Ag.

The resistance of ICA69^{null} mice to CY-induced diabetes was unexpected and has since been reproduced in backcross 11 mice with ICA69 deficiency. This resistance did not reflect a generalized resistance to β cell death or autoimmune attack, since ICA69^{null} mice develop diabetes spontaneously with wild-type incidence, and since alloxan treatment eliminates β cells just as in wild-type mice (unpublished observation). These observations, and the normal, accelerated diabetes development in NOD.*scid* mice reconstituted with spleen cells from either heterozygous or homozygous knockout donors suggested: 1) that CY-induced diabetes had to require effects in a second target tissue, and 2) that the resistance to diabetes acceleration in ICA69^{null} animals could not be attributed solely to the hemopoietic cell compartment. Islet transplant experiments strongly suggest that the second drug target is islet β cells themselves.

If this is substantially correct, then the islet toxicity of CY is dependent on the presence of ICA69. We propose that direct islet toxicity provides a boost to pathogenic T cell pools, providing islet Ags during the rapid, post-CY regeneration. Injury to β cells has also been implicated as a requirement for virus-accelerated diabetes (58, 59). The earliest, CY-induced change previously reported is the rapid accumulation of monokines IL-12, TNF-α, and IL-18 in the pancreas ~2 days after drug treatment (3), 1 day after the peak of drug-induced β cell death (52). While it may ultimately not be trivial to separate cause and effect, the most obvious scenario would be that CY-induced β cell death attracts and activates professional APCs, which then engender pathogenic competence in preexisting T cell pools with islet autoreactivity. Our data demonstrate that without this event, T cells still home to the islet, but are incompetent to mediate β cell death.

Overall, this process would then be analogous to the induction of NOD autoimmune thyroiditis following induction of thyroid cell death by high dose iodide treatment (60). It would differ from the effects of drugs such as streptozotocin, which kill β cells and cause diabetes in any strain, while CY-accelerated diabetes requires the NOD host with established autoimmune T cell repertoires. Consistently, the provision of wild-type islet grafts under the kidney capsule was sufficient to reverse CY resistance in knockout mice, with rapid elimination of endogenous β cells in the pancreas and consequent diabetes. This outcome confirms that islets drive pathogenic, diabetic autoimmunity, as has been suggested for natural disease development (61).

The exact function of ICA69 remains unclear, but knockout mice will provide excellent tools for further study. Collectively, ICA69 knockout mice generated new insights into the role of a typical autoantigen targeted in autoimmune diabetes. The observations make it unlikely that the exogenous ICA69 mimicry Ag, BSA, has a primary triggering role in the loss of tolerance to ICA69. Instead, the highly biased T cell repertoire of NOD mice immunized with BSA now emerges as a function of autoreactive mimicry T cells driven by the endogenous self Ag. The combination of several autoantigen knockout mice should eventually allow a more complete dissection of diabetic autoimmunity. The long, drawn-out character of prediabetes remains a puzzle. The CY resistance in ICA69^{null} mice sheds new light on this process, with a critical role for drug-induced β cell death, probably coupled to autoimmunity through the activation of local APCs. The heavy islet infiltration in CY-treated ICA69^{null} mice vividly illustrates that the endowment of pathogenicity in infiltrating T cells is a critical progression event, which normally does not occur until very late in prediabetes. These observations favor the view that prediabetes progression is not a linear process of gradual β cell destruction (62), but rather a process that culminates late with massive β cell destruction near disease onset (63). If correct and applicable to the human disease, immunotherapy of prediabetes may be effective even late in prediabetes if it avoids precipitation of diabetes in an immune system precariously balanced between pathogenicity and nonpathogenicity.

Acknowledgments

We thank Dr. Xiao Rong Peng (Toronto, Ontario, Canada) for her excellent suggestions and support throughout this project, Dr. H. Bujard (Heidelberg, Germany), Dr. M. Pietropaolo (Pittsburgh, PA), Dr. J. Elliott (Edmonton, Alberta), and Dr. W. Trimble and Dr. Tak Mak (Toronto, Ontario, Canada) for providing valuable reagents.

References

1. Karges, W., J. Ilonen, B. H. Robinson, and H.-M. Dosch. 1995. Self and non-self antigen in diabetic autoimmunity: molecules and mechanisms. *Mol. Aspects Med. 16:79.*
2. Andre, I., A. Gonzalez, B. Wang, J. Katz, C. Benoist, and D. Mathis. 1996. Checkpoints in the progression of autoimmune disease: lessons from diabetes models. *Proc. Natl. Acad. Sci. USA 93:2260.*
3. Andre-Schmutz, I., C. Hindelang, C. Benoist, and D. Mathis. 1999. Cellular and molecular changes accompanying the progression from insulitis to diabetes. *Eur. J. Immunol. 29:245.*
4. Reddy, S., N. Bibby, and R. B. Elliott. 1990. Longitudinal study of islet cell antibodies and insulin autoantibodies and development of diabetes in non-obese diabetic (NOD) mice. *Clin. Exp. Immunol. 81:400.*
5. Yu, L., D. T. Robles, N. Abiru, P. Kaur, M. Rewers, K. Kelemen, and G. S. Eisenbarth. 2000. Early expression of antiinsulin autoantibodies of humans and the NOD mouse: evidence for early determination of subsequent diabetes. *Proc. Natl. Acad. Sci. USA 97:1701.*
6. Schranz, D. B., and A. Lernmark. 1998. Immunology in diabetes: an update. *Diabetes Metab. Rev. 14:3.*
7. Atkinson, M. A., and E. H. Leiter. 1999. The NOD mouse model of type 1 diabetes: as good as it gets? *Nat. Med. 5:601.*
8. Lipton, R. B., M. Kocova, R. E. LaPorte, J. S. Dorman, T. J. Orchard, W. J. Riley, A. L. Drash, D. J. Becker, and M. Trucco. 1992. Autoimmunity and genetics contribute to the risk of insulin-dependent diabetes mellitus in families: islet cell antibodies and HLA DQ heterodimers. *Am. J. Epidemiol. 136:503.*
9. Verge, C. F., D. Stenger, E. Bonifacio, P. G. Colman, C. Pilcher, P. J. Bingley, and G. S. Eisenbarth. 1998. Combined use of autoantibodies (IA-2 autoantibody, GAD autoantibody, insulin autoantibody, cytoplasmic islet cell antibodies) in type 1 diabetes: Combinatorial Islet Autoantibody Workshop. *Diabetes 47:1857.*
10. Dosch, H.-M., R. K. Cheung, W. Karges, M. Pietropaolo, and D. J. Becker. 1999. Persistent T cell anergy in human type 1 diabetes. *J. Immunol. 163:6933.*
11. Kaufman, D. L., M. Clare-Salzler, J. Tian, T. Fortshuber, G. S. P. Ting, P. Robinson, M. A. Atkinson, E. Sercarz, A. J. Tobin, and P. V. Lehman. 1993. Spontaneous loss of T cell tolerance to glutamic acid decarboxylase in murine insulin dependent diabetes. *Nature 366:69.*
12. Daniel, D., and D. R. Wegmann. 1996. Protection of nonobese diabetic mice from diabetes by intranasal or subcutaneous administration of insulin peptide B-(9-23). *Proc. Natl. Acad. Sci. USA 93:956.*
13. Elliott, J. F., H. Y. Qin, S. Bhatti, R. Singh, D. K. Smith, J. Lauzon, and B. Singh. 1994. Immunization with the large isoform of mouse glutamic acid decarboxylase (GAD67) prevents autoimmune diabetes in NOD mice. *Diabetes 43:1494.*
14. Karges, W., D. Hammond-McKibben, R. Gaedigk, N. Shibuya, R. Cheung, and H.-M. Dosch. 1997. Loss of self-tolerance to ICA69 in non-obese diabetic mice. *Diabetes 46:1548.*
15. Tisch, R., B. Wang, and D. V. Serreze. 1999. Induction of glutamic acid decarboxylase 65-specific Th2 cells and suppression of autoimmune diabetes at late stages of disease is epitope dependent. *J. Immunol. 163:1178.*
16. Winer, S., L. Gunaratnam, I. Astsatourov, R. K. Cheung, V. Kubiak, W. Karges, D. Hammond-McKibben, R. Gaedigk, D. Graziano, M. Trucco, et al. 2000. Peptide dose, MHC-affinity and target self-antigen expression are critical for effective immunotherapy of NOD mouse prediabetes. *J. Immunol. 165:4086.*

17. Trembleau, S., G. Penna, S. Gregori, G. Magistrelli, A. Isacchi, and L. Adorini. 2000. Early Th1 response in unprimed nonobese diabetic mice to the tyrosine phosphatase-like insulinoma-associated protein 2, an autoantigen in type 1 diabetes. *J. Immunol. 165:6748.*
18. Wong, F. S., J. Karttunen, C. Dumont, L. Wen, I. Visintin, I. M. Pilip, N. Shastri, E. G. Pamer, and C. A. Janeway, Jr. 1999. Identification of an MHC class I-restricted autoantigen in type 1 diabetes by screening an organ-specific cDNA library. *Nat. Med. 5:1026.*
19. Sercarz, E. E., P. V. Lehmann, A. Ametani, G. Benichou, A. Miller, and K. Moudgil. 1993. Dominance and crypticity of T cell antigenic determinants. In *Annu. Rev. Immunol.*, Vol. 11. W. E. Paul, C. G. Fathman, and H. Metzger, eds. Annual Rev., Palo Alto. p. 729.
20. Bonifacio, E., V. Lampasona, L. Bernasconi, and A. G. Ziegler. 2000. Maturation of the humoral autoimmune response to epitopes of GAD in preclinical childhood type 1 diabetes. *Diabetes 49:202.*
21. Amrani, A., J. Verdaguer, P. Serra, S. Tafuro, R. Tan, and P. Santamaria. 2000. Progression of autoimmune diabetes driven by avidity maturation of a T-cell population. *Nature 406:739.*
22. Ludeman, S. M. 1999. The chemistry of the metabolites of cyclophosphamide. *Curr. Pharm. Des. 5:627.*
23. Yasunami, R., and J. F. Bach. 1988. Anti-suppressor effect of cyclophosphamide on the development of spontaneous diabetes in NOD mice. *Eur. J. Immunol. 18:481.*
24. Charleton, B., A. Baccij, R. M. Slattery, and T. E. Mandel. 1989. Cyclophosphamide-induced diabetes in NOD/Wehi mice: evidence for suppression in spontaneous autoimmune diabetes mellitus. *Diabetes 38:441.*
25. Colucci, F., C. M. Cilio, K. Lejon, C. P. Goncalves, M. L. Bergman, and D. Holmberg. 1996. Programmed cell death in the pathogenesis of murine IDDM: resistance to apoptosis induced in lymphocytes by cyclophosphamide. *J. Autoimmun. 9:271.*
26. Karges, W., R. Gaedigk, M. F. Hui, R. K. Cheung, and H.-M. Dosch. 1997. Molecular cloning of murine ICA69: diabetes-prone mice recognize the human autoimmune-epitope, Tep69, conserved in splice variants from both species. *Biochim. Biophys. Acta 1360:97.*
27. Gaedigk, R., W. Karges, M. F. Hui, and H.-M. Dosch. 1996. Genomic organization of human and mouse ICAp69, a target antigen in in diabetic autoimmunity. *Genomics 38:382.*
28. Serreze, D. V., H. D. Chapman, D. S. Varnum, M. S. Hanson, P. C. Reifsnyder, S. D. Richard, S. A. Fleming, E. H. Leiter, and L. D. Shultz. 1996. B lymphocytes are essential for the initiation of T cell-mediated autoimmune diabetes: analysis of a new "speed congenic" stock of NOD.Ig μ null mice. *J. Exp. Med. 184:2049.*
29. Gaedigk, R., A. M. V. Duncan, I. Miyazaki, B. H. Robinson, and H.-M. Dosch. 1994. ICA1 encoding p69, a protein linked to the development of type 1 diabetes mellitus, maps to chromosome 7p22. *Cytogenet. Cell Genet. 66:274.*
30. Karges, W., M. Pietropaolo, C. Ackerley, and H.-M. Dosch. 1996. Gene expression of islet cell antigen p69 (ICAp69) in man, mouse and rat. *Diabetes 45:513.*
31. Pilon, M., X.-R. Peng, A. M. Spence, R. H. A. Plasterk, and H.-M. Dosch. 2000. ICA69 and its *C. elegans* homolog, ric-19, are novel regulators of neuroendocrine secretion. *Mol. Biol. Cell 11:3277.*
32. Miyazaki, I., R. K. Cheung, R. Gaedigk, M. F. Hui, J. Van der Meulen, R. V. Rajotte, and H.-M. Dosch. 1995. T cell activation and anergy to islet cell antigen in type 1 diabetes. *J. Immunol. 154:1461.*
33. Perez-Bravo, F., E. Carrasco, M. D. Gutierrez-Lopez, M. T. Martinez, G. Lopez, and, M. Garcia de los Rios. 1996. Genetic predisposition and environmental factors leading to the development of insulin-dependent diabetes mellitus in Chilean children. *J. Mol. Med. 74:105.*
34. Karges, W., and H.-M. Dosch. 1996. Environmental factors: cow milk and others. In *Diabetes Prediction, Prevention and Genetic Counselling in IDDM.* J. P. Palmer, ed. John Wiley & Sons, Chichester, p. 167.
35. Verge, C. F., N. J. Howard, L. Irwig, J. M. Simpson, D. Mackerras, and M. Silink. 1994. Environmental factors in childhood IDDM. *Diabetes Care 17:1381.*
36. Hypponen, E., M. G. Kenward, S. M. Virtanen, A. Piitulainen, P. Virta-Autio, J. Tuomilehto, M. Knip, and H. K. Akerblom. 1999. Infant feeding, early weight gain, and risk of type 1 diabetes: Childhood Diabetes in Finland (DiMe) Study Group. *Diabetes Care 22:1961.*
37. Kash, S. F., R. S. Johnson, L. H. Tecott, J. L. Noebels, R. D. Mayfield, D. Hanahan, and S. Baekkeskov. 1997. Epilepsy in mice deficient in the 65-kDa isoform of glutamic acid decarboxylase. *Proc. Natl. Acad. Sci. USA 94:14060.*
38. Kash, S. F., B. G. Condie, and S. Baekkeskov. 1999. Glutamate decarboxylase and GABA in pancreatic islets: lessons from knock-out mice. *Horm. Metab. Res. 31:340.*
39. Ballinger, W. F., and P. E. Lacy. 1972. Transplantation of intact pancreatic islets in rats. *Surgery 72:175.*
40. Furth, P. A., L. St Onge, H. Boger, P. Gruss, M. Gossen, A. Kistner, H. Bujard, and L. Hennighausen. 1994. Temporal control of gene expression in transgenic mice by a tetracycline-responsive promoter. *Proc. Natl. Acad. Sci. USA 91:9302.*
41. Gossen, M., A. L. Bonin, and H. Bujard. 1993. Control of gene activity in higher eukaryotic cells by prokaryotic regulatory elements. *Trends Biochem. Sci. 18:471.*
42. Kistner, A., M. Gossen, F. Zimmermann, J. Jerecic, C. Ullmer, H. Lubbert, and H. Bujard. 1996. Doxycycline-mediated quantitative and tissue-specific control of gene expression in transgenic mice. *Proc. Natl. Acad. Sci. USA 93:10933.*
43. Hamaguchi, K., H. R. Gaskins, and E. H. Leiter. 1991. NIT-1, a pancreatic β-cell line established from a transgenic NOD/Lt mouse. *Diabetes 40:842.*
44. Nagy, A., J. Rossant, R. Nagy, N. W. Abramow, and J. C. Roder. 1993. Derivation of completely cell culture-derived mice from early-passage embryonic stem cells. *Proc. Natl. Acad. Sci. USA 90:8424.*
45. Winer, S., I. Astsaturov, R. K. Cheung, L. Gunaratnam, V. Kubiak, M. A. Moscarello, P. O'Connor, C. McKerlie, D. J. Becker, and H.-M. Dosch. 2001. Type I diabetes and MS patients target islet plus CNS-autoantigens, non-immunized NOD mice can develop autoimmune encephalitis. *J. Immunol. 166:2832.*
46. Pietropaolo, M., L. Castano, S. Babu, R. Buelow, Y.-L. Kuo, S. S. Martin, A. Martin, A. C. Powers, M. Prochazka, J. Naggert, et al. 1993. Islet cell autoantigen 69 kD (ICA69): molecular cloning and characterization of a novel diabetes-associated autoantigen. *J. Clin. Invest. 92:359.*
47. Stassi, G., N. Schloot, and M. Pietropaolo. 1997. Islet cell autoantigen 69 kDa (ICA69) is preferentially expressed in the human islets of Langerhans rather than exocrine pancreas. *Diabetologia 40:120.*
48. Naruse, Y., T. Aoki, T. Kojima, and N. Mori. 1999. Neural restrictive silencer factor recruits mSin3 and histone deacetylase complex to repress neuron-specific target genes. *Proc. Natl. Acad. Sci. USA 96:13691.*
49. Pinal, C. S., V. Cortessis, and A. J. Tobin. 1997. Multiple elements regulate GAD65 transcription. *Dev. Neurosci. 19:465.*
50. Wicker, L. S., B. J. Miller, and Y. Mullen. 1986. Transfer of autoimmune diabetes mellitus with splenocytes from nonobese diabetic (NOD) mice. *Diabetes 35:855.*
51. Colucci, F., M. L. Bergman, C. Penha-Goncalves, C. M. Cilio, and D. Holmberg. 1997. Apoptosis resistance of nonobese diabetic peripheral lymphocytes linked to the Idd5 diabetes susceptibility region. *Proc. Natl. Acad. Sci. USA 94:8670.*
52. O'Brien, B. A., B. V. Harmon, D. P. Cameron, and D. J. Allan. 2000. Nicotinamide prevents the development of diabetes in the cyclophosphamide-induced NOD mouse model by reducing β-cell apoptosis. *J. Pathol. 191:86.*
53. Casteels, K., M. Waer, R. Bouillon, J. Depovere, D. Valckx, J. Laureys, and C. Mathieu. 1998. 1,25-Dihydroxyvitamin D3 restores sensitivity to cyclophosphamide-induced apoptosis in non-obese diabetic (NOD) mice and protects against diabetes. *Clin. Exp. Immunol. 112:181.*
54. Cai, L., B. F. Hales, and B. Robaire. 1997. Induction of apoptosis in the germ cells of adult male rats after exposure to cyclophosphamide. *Biol. Reprod. 56:1490.*
55. Wucherpfennig, K. W., and J. L. Strominger. 1995. Molecular mimicry in T cell-mediated autoimmunity: viral peptides activate human T cell clones specific for myelin basic protein. *Cell 80:695.*
56. Von Herrath, M. G., A. Holz, D. Homann, and M. B. Oldstone. 1998. Role of viruses in type I diabetes. *Semin. Immunol. 10:87.*
57. Karges, W., D. Hammond-McKibben, R. K. Cheung, M. Visconti, N. Shibuya, D. Kemp, and H. M. Dosch. 1997. Immunological aspects of nutritional diabetes prevention in NOD mice: a pilot study for the cow's milk-based IDDM prevention trial. *Diabetes 46:557.*
58. Horwitz, M. S., L. M. Bradley, J. Harbertson, T. Krahl, J. Lee, and N. Sarvetnick. 1998. Diabetes induced by coxsackie virus: initiation by bystander damage and not mimicry. *Nat. Med. 4:781.*
59. Horwitz, M. S., C. Fine, A. Ilic, and N. Sarvetnick. 2001. Requirements for viral-mediated autoimmune diabetes: β-cell damage and immune infiltration. *J. Autoimmun. 16:211.*
60. Many, M. C., S. Maniratunga, I. Varis, M. Dardenne, H. A. Drexhage, and J. F. Denef. 1995. Two-step development of Hashimoto-like thyroiditis in genetically autoimmune prone non-obese diabetic mice: effects of iodine-induced cell necrosis. *J. Endocrinol. 147:311.*
61. Larger, E., C. Becourt, J. F. Bach, and C. Boitard. 1995. Pancreatic islet β cells drive T cell-immune responses in the nonobese diabetic mouse model. *J. Exp. Med. 181:1635.*
62. Augstein, P., A. G. Elefanty, J. Allison, and L. C. Harrison. 1998. Apoptosis and β-cell destruction in pancreatic islets of NOD mice with spontaneous and cyclophosphamide-accelerated diabetes. *Diabetologia 41:1381.*
63. Shimada, A., B. Charlton, E. C. Taylor, and C. G. Fathman. 1996. β-Cell destruction may be a late consequence of the autoimmune process in nonobese diabetic mice. *Diabetes 45:1063.*

Targeted Disruption of the Protein Tyrosine Phosphatase-Like Molecule IA-2 Results in Alterations in Glucose Tolerance Tests and Insulin Secretion

Keiichi Saeki,[1] Min Zhu,[2] Atsutaka Kubosaki,[1] Jingping Xie,[1] Michael S. Lan,[2] and Abner Louis Notkins[1]

IA-2 is a major autoantigen in type 1 diabetes. Autoantibodies to IA-2 appear years before the development of clinical disease and are being widely used as predictive markers to identify individuals at risk for developing type 1 diabetes. IA-2 is an enzymatically inactive member of the transmembrane protein tyrosine phosphatase family and is an integral component of secretory granules in neuroendocrine cells. To study its function, we generated IA-2–deficient mice. Northern and Western blot analysis showed that neither IA-2 mRNA nor protein was expressed. Physical examination of the IA-2$^{-/-}$ animals and histological examination of tissues failed to reveal any abnormalities. Nonfasting blood glucose levels, measured over 6 months, were slightly elevated in male IA-2$^{-/-}$ as compared to IA-2$^{+/+}$ littermates, but remained within the nondiabetic range. Glucose tolerance tests, however, revealed statistically significant elevation of glucose in both male and female IA-2$^{-/-}$ mice and depressed insulin release. In vitro glucose stimulation of isolated islets showed that male and female mice carrying the disrupted gene released 48% ($P < 0.001$) and 42% ($P < 0.01$) less insulin, respectively, than mice carrying the wild-type gene. We concluded that IA-2 is involved in glucose-stimulated insulin secretion. *Diabetes* **51:1842–1850, 2002**

IA-2 is a major autoantigen in type 1 diabetes (1,2). At the time of diagnosis, ~70% of newly diagnosed patients have autoantibodies to IA-2. Because these autoantibodies appear months and years before the onset of clinical symptoms, they have become useful markers for identifying individuals who are at high risk for developing type 1 diabetes (3–7). Individuals with no clinical symptoms, but who have autoantibodies to IA-2 and GAD, have an ~50% risk of developing type 1 diabetes within 5 years and an even higher risk within 7–10 years. For these reasons, the measurement of autoantibodies to recombinant IA-2 and GAD is being widely used to predict risk for type 1 diabetes (8,9).

IA-2 is a 979–amino acid transmembrane protein. It has an extracellular, transmembrane, and intracellular domain consisting of 576, 24, and 379 amino acids, respectively (1). Autoantibodies to IA-2 are directed exclusively to the intracellular domain, primarily to the COOH-terminus and, to a somewhat lesser extent, to the juxtamembrane region (10–12). The gene encoding IA-2 is located on human chromosome 2q35. The coding region extends over ~20 kb and consists of 23 exons (13). Exons 1–12 encode the extracellular domain; exon 13, the transmembrane domain; and exons 14 through 23, the intracellular domain. A region extending ~200 bp 5′-upstream from the translation start site and a region encompassing exon 1 and intron 1 have been shown to have strong promoter activity (R. Alam and A.L.N., unpublished data; 13).

The function of IA-2 is not known. Based on sequence analysis, IA-2 belongs to a subgroup of the transmembrane protein tyrosine phosphatase (PTP) family. Homologs have been found in cows, rats, mice, macaca, zebrafish, *Drosophilia*, and *Caenorhabditis elegans* and show 99, 98, 97, 73, 82, 58, and 46% identity, respectively, to human IA-2 (14). IA-2 differs from other PTPs in that it is enzymatically inactive because of substitution of amino acids (Ala 911→Asp and Asp 877→Ala) at conserved sites known to be critical for enzymatic activity (15). Electron microscopic studies and immunohistochemical studies have localized the IA-2 protein (also known as ICA512) to the secretory vesicles of neuroendocrine cells (16).

The present study was initiated to determine the function of IA-2 by targeted disruption of the mouse IA-2 gene. Mouse IA-2 is very similar to human IA-2. It is 981 amino acids in length, consists of 23 exons, and is located on mouse chromosome 1 (17). A targeting construct, in which the 5′-upstream promoter region, exons 1–3 and introns 1, 2, and most of 3, were replaced with a neomycin cassette, was used to transfect embryonic stem (ES) cells by homologous recombination. ES cells in which the IA-2 construct had become integrated were injected into blastocysts, and the resulting chimeric animals and their offspring were bred and tested for evidence of homologous recombination and germ-line transmission. Here we describe the successful targeted disruption of the IA-2 gene in mice and provide a description of the resulting phenotype.

From the [1]Experimental Medicine Section, Oral Infection and Immunity Branch, National Institute of Dental and Craniofacial Research, National Institutes of Health, Bethesda, Maryland; and the [2]Research Institute for Children, Children's Hospital, and Departments of Pediatrics and Genetics, Louisiana State University Health Sciences Center, New Orleans, Louisiana.

Address correspondence and reprint requests to Abner L. Notkins, National Institutes of Health, Building 30/Room 121, 30 Convent Dr., MSC 4322, Bethesda, MD 20892-4322. E-mail: anotkins@dir.nidcr.nih.gov.

Received for publication 30 November 2001 and accepted in revised form 11 February 2002.

K.S., M.Z., and A.K. contributed equally to the work.

ELISA, enzyme-linked immunosorbent assay; ES, embryonic stem; KRBB, Krebs-Ringer bicarbonate buffer; PTP, protein tyrosine phosphatase.

RESEARCH DESIGN AND METHODS

Generation of IA-2–deficient mice. A 129SvJ mouse genomic library (Stratagene, Cedar Creek, TX) was screened with a mouse IA-2 cDNA probe. A 17-kb fragment of mouse IA-2 containing the coding sequence of exons 1–13 was used to construct a targeting vector. A 3.5-kb *Sal*I-*Eco*RI fragment upstream of the first exon was subcloned into pBluescript SK+ (Stratagene). From this plasmid, the 5′-segment was subcloned as a 3.5-kb *Kpn*I-*Bam*HI fragment into pPNT vector (18), resulting in pPNT-5′IA-2. Subsequently, a 3.3-kb *Xho*I-*Xho*I fragment containing exons 4–6 was subcloned into pPNT-5′IA-2 vector, resulting in pPNT-IA-2. Homologous recombination resulted in the replacement of IA-2 exons 1–3 and introns 1, 2, and most of 3 with the neo-resistant gene cassette from the pPNT-IA-2 vector into the *Eco*RI-*Xho*I site of the targeted locus. The targeting plasmid was linearized using the unique *Not*I site before electroporation. The HSV-tk cassette was used for negative selection.

JI ES cells (19) were transfected with the linearized targeting vector (50 μg/1.5 × 10^7 cells) using a BioRad Gene Pulser and grown under double-selection conditions (350 μg/ml G418, 2 μmol/l ganciclovir). After 7–10 days, G418-ganciclovir–resistant ES cell clones were picked and expanded (20).

Genomic DNA from individual ES cell clones was extracted and analyzed by Southern blot hybridization. A 1.1-kb *Xho*I-*Hin*dIII fragment (outside probe) containing exons 7 and 8 just downstream of the *Xho*I-*Xho*I segment was used for screening. Homologous recombinant clones selected by the outside probe were also analyzed with a 1.9-kb neo cassette probe to check for multiple integrations. Five ES cell clones were injected into C57BL/6 mice blastocysts to generate chimeras. Overt chimeras were backcrossed with C57BL/6 mice to produce germline transmission of the targeted allele. Tail DNA of agouti offspring and subsequent pups was screened for the presence of the mutant IA-2 allele by Southern blot analysis and PCR. All protocols were approved by our institutional animal care and use committees.

Genotyping. Tail DNA-PCR using four primers was designed to discriminate between wild-type (IA-$2^{+/+}$), heterozygous (IA-$2^{+/-}$), and homozygous (IA-$2^{-/-}$) mice. The wild-type allele was detected as a 1.3-kb product using an exon 3 sense primer (5′-TACAAGGTGTGCTCCGGCAACTCATGT-3′) and an exon 4 antisense primer (5′-GGTCCATCTCCTGGGAGATCACATGCT-3′). The recombinant allele was detected as a 3.5-kb product using the PGK-1 primer (5′-GGTGCTGTCCATCTGCACGAGACTAGT-3′) in the promoter of the neo cassette and an exon 7 antisense primer (5′-CAGCAGTCAATCTCTGCA GACTCAATT-3′). PCR was performed with the TaqPlus Precision PCR System (Stratagene) at 35 cycles of 94°C for 0.5 min, 60°C for 1 min, and 72°C for 3 min in a GeneAmp PCR System 9700 (Applied Biosystems, Forest City, CA). Each PCR product was separated on 1% agarose gels containing ethidium bromide and visualized under ultraviolet light.

RNA analysis. Total RNA from brain (10-week-old male IA-$2^{+/+}$, IA-$2^{+/-}$, and IA-$2^{-/-}$ mice) was isolated using TRIZOL reagent (Life Technology, Rockville, MD). For Northern blot analysis, 20 μg of each sample were separated on a 1% (wt/vol) agarose/2.2 mol/l formaldehyde gel and transferred to a Hybond-XL membrane (Amersham Pharmacia Biotech, Piscataway, NJ). The blot was subsequently hybridized with ^{32}P-radiolabeled mouse IA-2 cDNA intracellular and extracellular probes and an IA-2β cDNA 3′ noncoding region probe.

Western blot analysis. Brain samples from IA-$2^{+/+}$ or IA-$2^{-/-}$ mice were homogenized with PBS. After centrifugation at 10,000*g* for 5 min, cell debris was sonicated in lysis buffer (50 mmol/l Tris-HCl [pH 7.4], 150 mmol/l NaCl, 1 mmol/l EDTA, 1% sodium deoxycholate, 1% NP-40, 0.4% SDS, and 1 mmol/l phenylmethylsulfonyl fluoride). Equivalent amounts of protein dissolved in SDS-PAGE sample buffer were subjected to SDS-PAGE on an 8% polyacrylamide gel. Separated proteins were transferred onto polyvinylidine difluoride membranes by electrotransfer. Blots were processed as recommended by the manufacturer (enhanced chemiluminescence detection; Amersham Pharmacia Biotech). Rabbit anti–IA-2 serum made from the intracellular domain of recombinant mouse IA-2 and absorbed with brain lysate from IA-$2^{-/-}$ mice was used as the primary antibody (1:2,000 dilution) followed by anti-rabbit Ig antibody conjugated to horseradish peroxidase (Amersham Pharmacia Biotech).

Histological and immunohistochemical analysis. All the major organs and tissues were collected in 10% neutral-buffer formalin or 4% paraformaldehyde and processed for paraffin embedding. Sections were stained with hematoxylin and eosin. Pancreatic sections were incubated with antibodies to insulin, glucagon, or somatostatin (DAKO, Carpinteria, CA) followed by biotin-conjugated second antibody and streptavidin-horseradish peroxidase.

Intraperitoneal glucose tolerance test and insulin release. Mice aged 10–23 weeks were fasted for 16 h, followed by glucose injection (2 g/kg body wt i.p.). Venous blood was drawn from the tail vein at 0, 15, 30, 60, and 120 min after the injection. Blood glucose was measured using a portable glucometer (Bayer, Elkhart, IN). For acute insulin release, glucose (3 g/kg body wt) was injected intraperitoneally into male and female mice aged 10–23 weeks. Venous blood was collected at 0, 3, 9, and 15 min in heparinized tubes. After centrifugation, plasma was stored in −20°C. Insulin levels were measured with an enzyme-linked immunosorbent assay (ELISA) kit using a mouse insulin standard (ALPCO, Windham, NH).

Isolation of pancreatic islets. IA-$2^{-/-}$ or IA-$2^{+/+}$ mice were anesthetized with ketamine and xylazine. Pancreases were perfused with 3 ml of collagenase IV (2 mg/ml in Hank's solution; Life Technologies) and further digested in a water bath at 37°C for 25 min. The digested pancreases were washed with Hank's solution three times and passed through mesh to remove undigested tissues. The islet preparation was further subjected to percoll density gradient separation (density 1.089–1.062) and handpicked under a stereomicroscope (21). The purity of islets reached >95% and was verified by dithizone staining (22). The purified islets were cultured overnight in RPMI-1640 medium supplemented with 5.5 mmol/l glucose, 100 units/ml benzypenicillin, 100 μg/ml streptomycin, and 10% fetal bovine serum before insulin secretion tests.

Glucose-stimulated insulin secretion of pancreatic islets. Insulin secretion was measured by placing 10 islets in each of five wells (New Transwell Clear; Costar Scientific, Cambridge, MA). Experiments were repeated at least three times. The islets were preincubated in 1 ml oxygenated Krebs-Ringer bicarbonate buffer (KRBB) containing 143.5 mmol/l Na^+, 5.8 mmol/l K^+, 2.5 mmol/l Ca^{2+}, 25 mmol/l HCO_3, 0.3% BSA (Fraction V; ICN, Lisle, IL), and 3.3 mmol/l glucose at 37°C for 30 min. After preincubation, the islets were incubated in 1.0 ml of KRBB supplemented with 3.3 mmol/l glucose for 1 h. Subsequently, the islets were transferred to media containing 27.7 mmol/l glucose and incubated for 1 h. Aliquots were removed and stored at −20°C for quantitation of insulin by ELISA.

Statistical analysis. Statistical analysis was performed using the Student's *t* test for unpaired comparisons. Data are presented as means + SE. $P < 0.05$ was considered significant.

RESULTS

ES cells were transfected with the IA-2 targeting vector pPNT-IA-2 (Fig. 1). By homologous recombination of the targeting vector with the IA-2 wild-type locus, the 5′-upstream promoter region, exons 1–3 and introns 1, 2, and most 3 of the wild-type IA-2 locus were replaced with a neomycin cassette. Successful homologous recombination in ES cells was detected by Southern blot analysis of neomycin-resistant colonies with a 1.1-kb *Xho*I-*Hin*dIII fragment (outside probe) and a 1.9-kb neo probe (data not shown). Three IA-$2^{+/-}$ ES cells clones were injected into blastocysts to make chimeric mice that transmitted the modified IA-2 allele to their offspring. Wild-type (IA-$2^{+/+}$), heterozygous (IA-$2^{+/-}$), and homozygous (IA-$2^{-/-}$) mice were identified by tail DNA PCR with appropriate primers. As seen in Fig. 2*A*, wild-type IA-$2^{+/+}$ mice were identified by a 1.3-kb PCR product; homozygous IA-$2^{-/-}$ mice, by a 3.5-kb PCR product; and heterozygous IA-$2^{+/-}$ mice, by both 1.3- and 3.5-kb PCR products. The identification of these mice was confirmed by Southern blot analysis. As seen in Fig. 2*B*, tail DNA digested with *Kpn*I and hybridized with the 1.1-kb *Xho*I-*Hin*dIII outside probe produced a 6.9-kb band with IA-$2^{+/+}$ DNA, a 10.7-kb band with IA-$2^{-/-}$ DNA, and both a 6.9- and 10.7-kb band with IA-$2^{+/-}$ DNA.

Further evidence that the homologous recombination was successful and disrupted the IA-2 gene was obtained from Northern blot analysis. As seen in Fig. 2*C*, hybridization of total brain RNA with a probe corresponding to the extracellular domain of IA-2 (nt 485–1,708) resulted in a strong 3.8-kb band with IA-$2^{+/+}$ RNA, a marked reduction in the band with IA-$2^{+/-}$ RNA, and no band with IA-$2^{-/-}$ RNA. A probe corresponding to the intracellular domain of IA-2 (nt 1992–3036) yielded similar results (Fig. 2*D*). In contrast, a probe generated from the 3′ noncoding region (nt 3,040–3,193) of the closely related protein IA-2β (23,24) showed that IA-2β mRNA was not affected by the

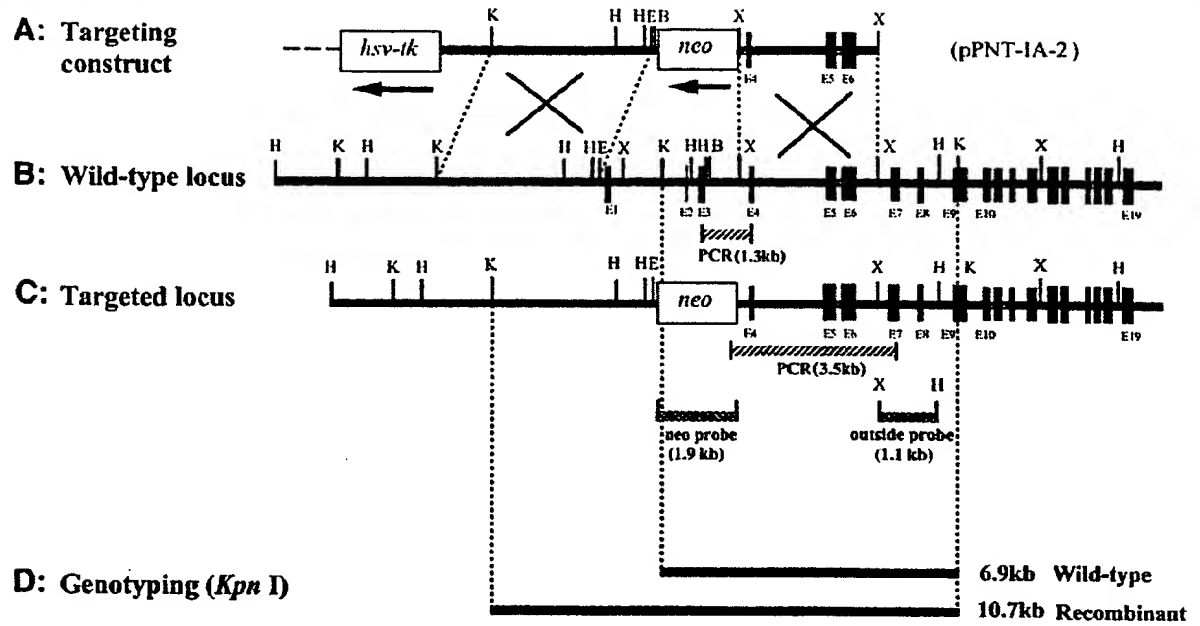

FIG. 1. Targeted disruption of the IA-2 gene. Vertical bars represent exons E1 through E19. Restriction enzyme sites shown are *Kpn*I (K), *Hin*dIII (H), *Eco*RI (E), *Xho*I (X), and *Bam*HI (B). *A*: Targeting construct shows that a portion of the 5′-upstream promoter, exons 1, 2, and 3 and introns 1, 2, and most of 3, are replaced by the neomycin cassette. *B*: Wild-type locus. Dashed lines with large "X" show areas where homologous recombination takes place. *C*: Targeted locus shows integration of targeting construct, containing the neomycin cassette, into the wild-type locus. *D*: Size of restriction fragments when wild-type locus and targeted locus are cleaved with *Kpn*I and hybridized with the 1.1-kb outside probe. Location of PCR products and probes was with PCR (1.3 kb), PCR (3.5 kb), neo probe (1.9 kb), and outside probe (1.1 kb).

IA-2 knockout and was expressed equally in IA-$2^{+/+}$ and IA-$2^{-/-}$ mice (Fig. 2*E*). Western blot analysis, using rabbit anti–IA-2 sera to measure protein expression in mouse brain extract, showed no expression of IA-2 protein in IA-$2^{-/-}$ mice as compared to IA-$2^{+/+}$ mice (Fig. 2*F*).

Physical examination of the IA-$2^{-/-}$ mice revealed no gross abnormalities. Litter size (data not shown) and body weight did not differ from the IA-$2^{+/+}$ mice (Fig. 3*A*). Histological studies failed to reveal any abnormality in the neuroendocrine cells of the IA-$2^{-/-}$ mice, including pancreatic islets (Fig. 4*A*) and brain (Fig. 4*E* and *F*), nor were abnormalities found in any of the other organs or cell types examined. Immunohistochemical studies on the IA-$2^{-/-}$ mice also revealed normal-appearing pancreatic islets, with no difference in the morphology or staining pattern of the insulin-, glucagon-, or somatostatin-producing cells (Fig. 4*B–D*) as compared to the IA-$2^{+/+}$ controls (not shown).

Nonfasting blood glucose levels of the IA-$2^{-/-}$ male mice, measured over a 22-week period, were slightly elevated as compared to IA-$2^{+/+}$ mice, but they did not fall within the diabetic range (Fig. 3*B*). Glucose tolerance tests, however, showed that glucose was significantly elevated at 15 and 30 min in both male and female IA-$2^{-/-}$ mice (Fig. 5*A*). Moreover, after glucose injection, acute insulin release was depressed in both male and female IA-$2^{-/-}$ mice, with statistically significant differences in the female mice and near significance ($P = 0.055$ at 15 min) in the male mice (Fig. 5*B*). In glucose-stimulated insulin secretion assays, pancreatic islets isolated from IA-$2^{-/-}$ mice also responded less vigorously to glucose stimulation. As seen in Fig. 6, male and female IA-$2^{-/-}$ mice released 48 and 42% less insulin, respectively, than IA-$2^{+/+}$ mice when switched from basal (3.3 mmol/l) to high (27.7 mmol/l) glucose.

DISCUSSION

Insulin is located in the dense-core secretory granules of pancreatic β-cells. Dense-core granules are complex structures, but a number of their constituents are now known (25). IA-2, a transmembrane glycoprotein, is an integral component of dense-core granules (16). The intracellular domain of IA-2 is thought to protrude into the cytoplasm of the cell, whereas at least a portion of the extracellular (luminal) domain resides within dense-core granules. There are two potential dibasic (KK) cleavage sites located at amino acid positions 386–387 and 448–449 of the extracellular domain. Transfection and pulse chase experiments have shown that IA-2 is expressed as a 120-kDa glycosylated protein that is then processed into a predominant 64-kDa fragment and several smaller fragments (26). Whether these fragments from the extracellular domain remain within the cytoplasm or are retained within the secretory granules is still not clear, nor is their function known. Similar posttranslational modifications have been observed in bovine pituitary cells (27). Except for these studies and a reported correlation between secretagogue stimulation of β-cells and upregulation of IA-2 mRNA (28,29), very little is known about the cell biology of IA-2.

In the present study, we succeeded in deleting the IA-2 gene by targeted gene disruption. Northern and Western

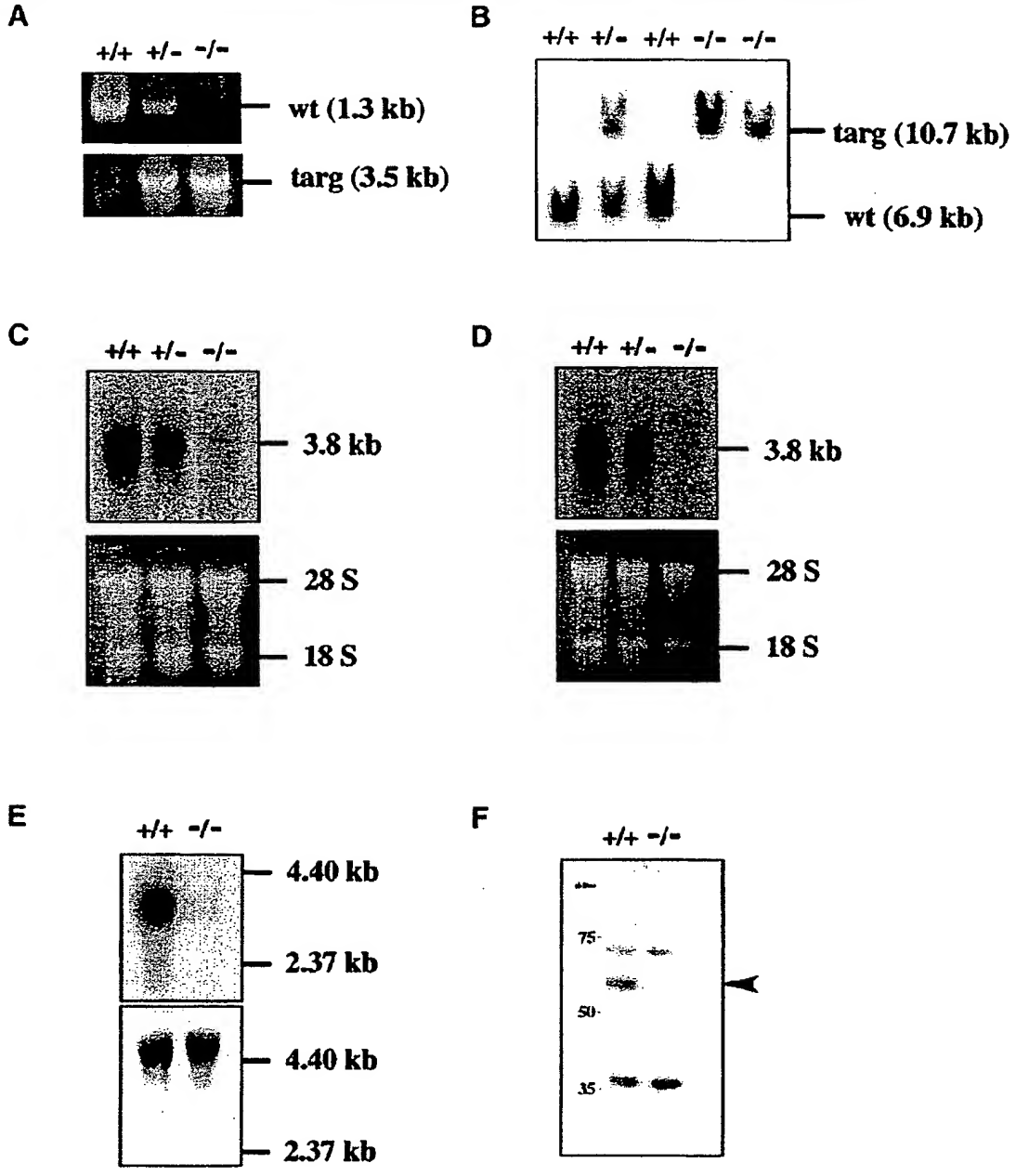

FIG. 2. Evidence for IA-2 gene disruption. *A*: PCR analysis. Primer pairs designed to produce a 1.3-kb product with cDNA from IA-$2^{+/+}$ mice, but a 3.5-kb product from IA-$2^{-/-}$ mice (see Fig. 1), showed that homologous recombination took place and that wild-type IA-2 had been eliminated. *B*: Southern blot analysis. DNA from IA-$2^{+/+}$, IA-$2^{+/-}$, and IA-$2^{-/-}$ mice were digested with *Kpn*I and hybridized with the 1.1-kb outside probe. DNA from the IA-$2^{+/+}$ mice yielded the expected 6.9-kb band, whereas DNA from the IA-$2^{-/-}$ mice gave a 10.7-kb band. IA-$2^{+/-}$ mice showed both bands. *C* and *D*: Northern analysis. Probes generated from either the extracellular (*C*) or intracellular (*D*) domains of IA-2 showed a strong 3.8-kb band with IA-$2^{+/+}$ mice, a weaker band with IA-$2^{+/-}$ mice, and no band with the IA-$2^{-/-}$ mice. *E*: IA-2β mRNA expression in IA-$2^{+/+}$ and IA-$2^{-/-}$ brain tissue. Probe generated from the intracellular domain of IA-2 showed a strong 3.8-kb band with IA-$2^{+/+}$, but no band with IA-$2^{-/-}$ mice (top). In contrast, a probe generated from the 3′ noncoding region of IA-2β showed a strong band (~5.5 kb) with both IA-$2^{+/+}$ and IA-$2^{-/-}$ mice (bottom). *F*: Western blot analysis. Antibody to IA-2 recognizes the IA-2 protein (arrow) in brain tissue from the IA-$2^{+/+}$ mice, but not from the IA-$2^{-/-}$ mice.

blot analysis showed that neither IA-2 mRNA nor protein was expressed. Although nonfasting blood glucose levels remained in the normal range, glucose tolerance tests revealed statistically significant elevated blood glucose levels in both male and female IA-$2^{-/-}$ mice. Glucose-stimulated insulin secretion showed statistically depressed insulin release in female IA-$2^{-/-}$ mice, with a similar trend, just missing statistical significance, in male

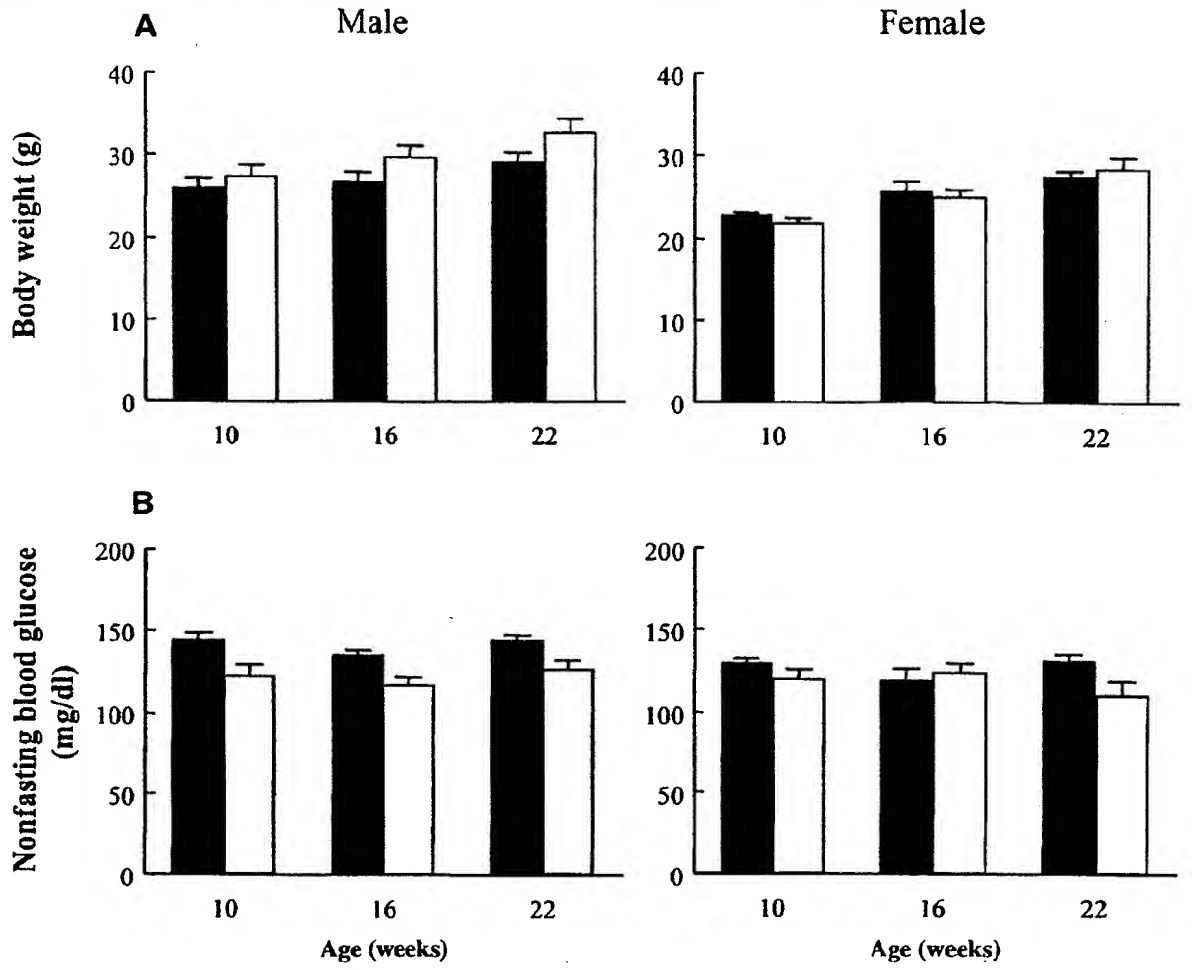

FIG. 3. Body weight and nonfasting blood glucose levels. Body weight (*A*) and nonfasting blood glucose levels (*B*) in male (n = 6) and female (n = 6) IA-$2^{-/-}$ (■) and male (n = 6) and female (n = 6) IA-$2^{+/+}$ (□) mice measured over 22 weeks. Data are means ± SE

IA-$2^{-/-}$ mice. Islets from both male and female IA-$2^{-/-}$ mice also showed significantly lower insulin release than islets from IA-$2^{+/+}$ mice when the cultures were switched from basal (3.3 mmol/l) to high (27.7 mmol/l) glucose levels. These findings, taken together with the known location of IA-2 in dense-core secretory granules, argue that IA-2 plays a role in insulin secretion. Although the alterations in glucose tolerance tests and insulin release are statistically significant, they are mild, and this may explain why IA-$2^{-/-}$ mice do not develop elevated nonfasting blood glucose levels and overt diabetes.

The findings with IA-$2^{-/-}$ mice raise questions about the contribution of IA-2β, also known as phogrin, to the secretory process. IA-2β is structurally similar to IA-2, showing 74% identity within the intracellular domain. This protein also is an integral component of dense-core granules and is phosphorylated in a Ca^{2+}-sensitive manner in response to secretagogue stimulation of β-cells (30). It is therefore possible that IA-2 and IA-2β work together or that one serves in a compensatory capacity for the other. However, at least at the mRNA level, IA-2 knockout does not result in a compensatory increase in IA-2β mRNA (Fig. 2*E*). Recently we succeeded in deleting the IA-2β gene (A.K. and A.L.N., unpublished data), and experiments are now underway to determine whether this protein also is involved in insulin secretion.

In terms of the pathogenesis of type 1 diabetes, it is of interest to ask whether there is any relationship between the autoimmune response to IA-2 and the functional role of IA-2 in secretion. It is known that autoantibodies to IA-2 are directed exclusively to the intracellular domain of the molecule that protrudes into the cytoplasm. Because there is no evidence that these autoantibodies are internalized and act within the cytoplasm, it seems unlikely that the autoimmune response to IA-2 would have any effect on the secretory function of the IA-2 molecule. Depressed insulin secretion, however, is one of the features of type 2 diabetes. Although

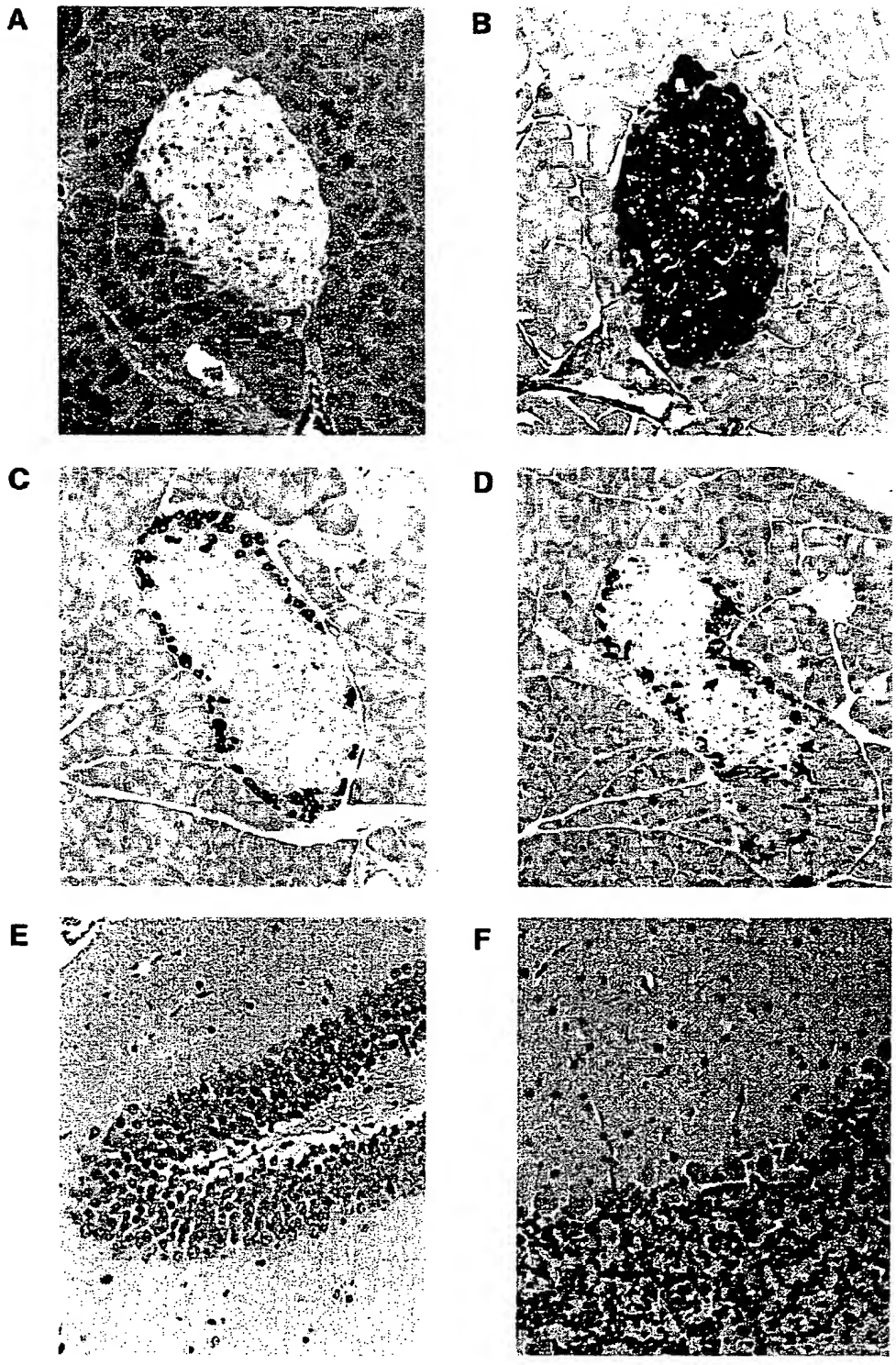

FIG. 4. Histological appearance and immunostaining of pancreases and brain from IA-2$^{-/-}$ mice. Sections of pancreases were fixed and stained with hematoxylin and eosin (*A*) or incubated with anti-insulin antibody (*B*), anti-glucagon antibody (*C*), or anti-somatostatin antibody (*D*) followed by biotin-conjugated second antibody and streptavidin horseradish peroxidase. Sections of brain (hippocampus [*E*] and cerebellum [*F*]) were fixed and stained with hematoxylin and eosin (magnification ×200 [*A*–*E*] and ×300 [*F*]).

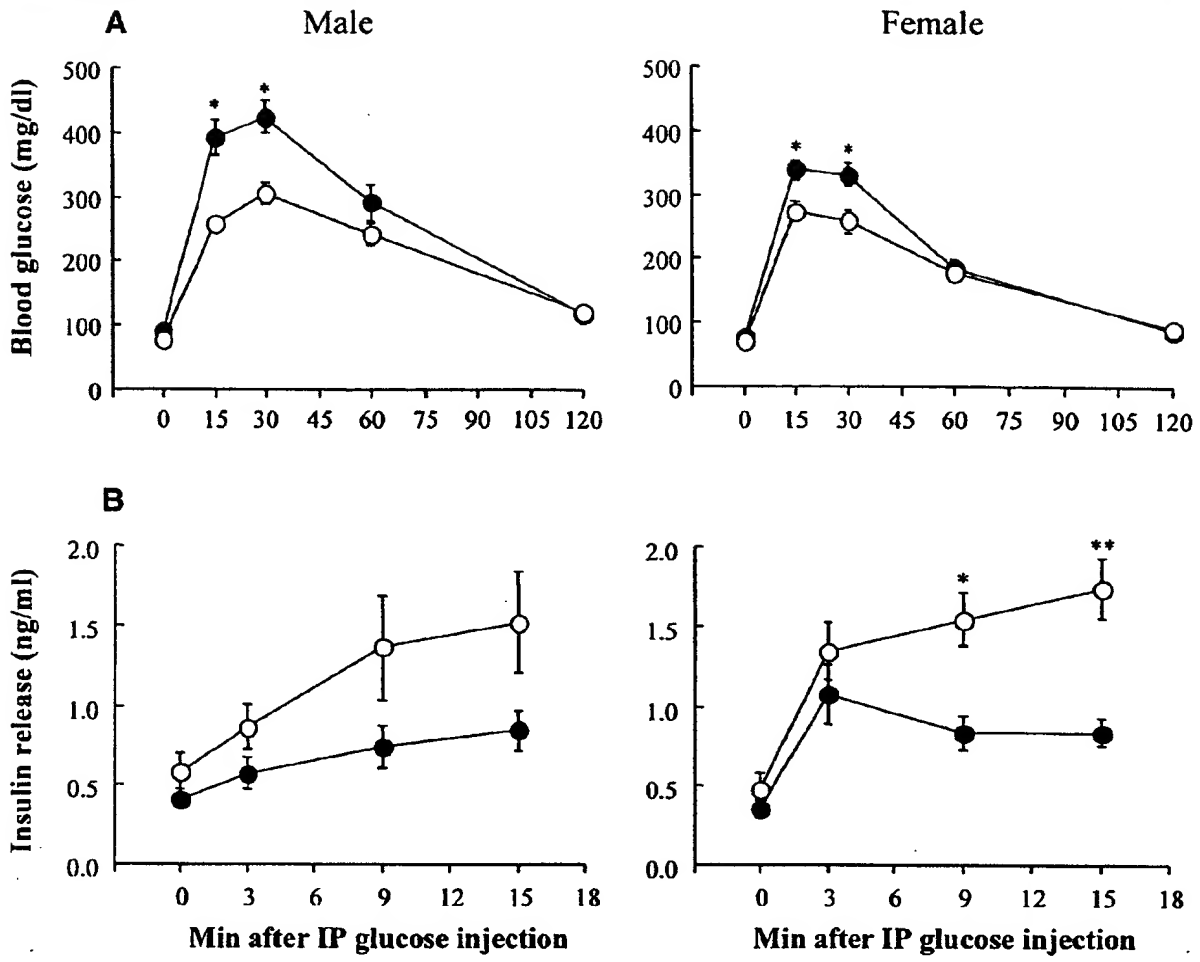

FIG. 5. Glucose tolerance and insulin secretion tests. *A*: Intraperitoneal (IP) glucose tolerance tests in male (n = 20) and female (n = 22) IA-2$^{+/+}$ (○) and male (n = 15) and female (n = 19) IA-2$^{-/-}$ (●) mice. After overnight fasting, D-glucose (2 g/kg body wt) was injected intraperitoneally, and blood glucose levels were measured at different time points. *B*: Acute insulin secretion in response to intraperitoneal glucose in male (n = 17) and female (n = 17) IA-2$^{+/+}$ (○) and male (n = 17) and female (n = 14) IA-2$^{-/-}$ (●) mice. Blood samples were drawn from the tail vein using heparinized capillary tubes before and after glucose injection (3 g/kg body wt). The results represent the average of three independent experiments. Data are means ± SE. *P < 0.01; **P < 0.001.

no association between IA-2 and type 2 diabetes has been recognized thus far, any gene that is involved in insulin secretion becomes a possible candidate gene for type 2 diabetes.

The process of secretion is complex and encompasses a number of different signals and pathways (25). Secretory vesicles are transported from the Golgi to the plasma membrane, where docking, priming, and fusion take place. Insulin is then secreted by exocytosis, a process that involves Ca^{2+} influx through voltage-dependent channels and regulation of exocytosis by a variety of phosphorylation events (31). Where in this multistep process IA-2 plays a role is not known. Recently, by use of the yeast two-hybrid system and co-immunoprecipitation, several proteins have been identified that bind to IA-2. This includes βIV spectrin and the PDZ domains of β2-syntrophin and neuronal nitric oxide synthase. Solimena and colleagues (32,33) have postulated that IA-2 may link the secretory granules with the actin cystoskeleton through its association with βIV spectrin or β2-syntrophin, and that this might affect granule traffic and exocytosis. Alternatively, because nitric oxide regulates the release of certain hormones, it is possible that the association of IA-2 with nitric oxide synthase may modulate insulin secretion.

The demonstration in the present study that deletion of IA-2 affects insulin secretion and the identification in other studies of IA-2 binding proteins (32,33) begin to provide insight into the function and possible mechanism of action of IA-2. The fact that IA-2 is present in the secretory granules of many different neuroendocrine cells raises the possibility that IA-2 may be involved not only in the secretion of insulin from β-cells, but also in the secretion of hormones from a broad range of neuroendocrine cells.

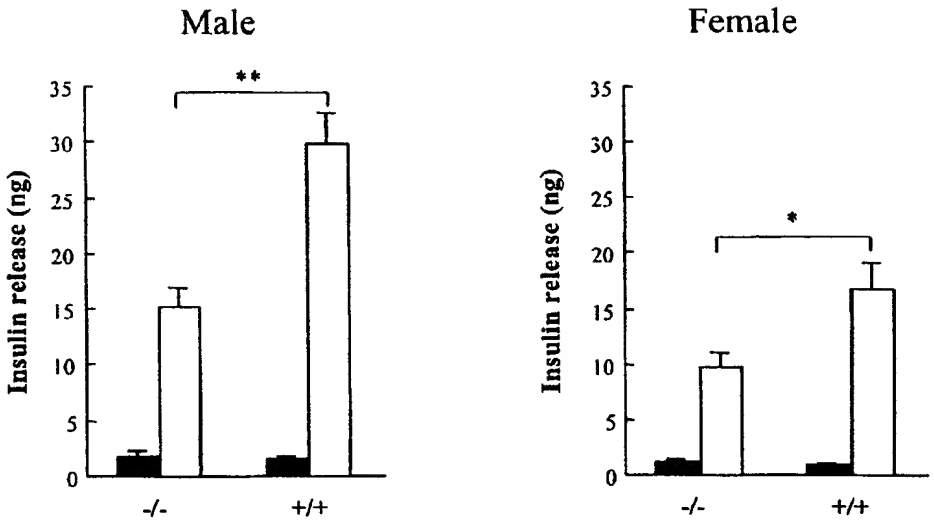

FIG. 6. Glucose-stimulated insulin release in vitro. Pancreatic islets isolated from IA-2$^{+/+}$ and IA-2$^{-/-}$ mice were placed in five wells, each containing 10 islets, in KRBB with 3.3 mmol/l glucose (■). At the end of 1 h, insulin levels in the supernatants were measured. The cells were then transferred to KRBB containing 27.7 mmol/l glucose (□), and at the end of 1 h insulin levels were again measured. The results represent the average of three independent experiments. Data are means ± SE. *$P < 0.01$; **$P < 0.001$.

ACKNOWLEDGMENTS

The authors thank Dr. Ashok Kulkarni for his advice and Glenn Longenecker for his help in preparing the IA-2 knockout mice.

REFERENCES

1. Lan MS, Lu J, Goto Y, Notkins AL: Molecular cloning and identification of a receptor-type protein tyrosine phosphatase, IA-2, from human insulinoma. *DNA Cell Biol* 13:505–514, 1994
2. Lan MS, Wasserfall C, Maclaren NK, Notkins AL: IA-2, a transmembrane protein of the protein tyrosine phosphatase family, is a major autoantigen in insulin-dependent diabetes mellitus. *Proc Natl Acad Sci U S A* 93:6367–6370, 1996
3. Gorus FK: Diabetes registries and early biological markers of insulin-dependent diabetes mellitus: Belgian Diabetes Registry. *Diabetes Metab Rev* 13:247–274, 1997
4. Verge CF, Gianani R, Kawasaki E, Yu L, Pietropaolo M, Jackson RA, Chase HP, Eisenbarth GS: Prediction of type I diabetes in first-degree relatives using a combination of insulin, GAD, and ICA512bdc/IA-2 autoantibodies. *Diabetes* 45:926–933, 1996
5. Hawa M, Rowe R, Lan MS, Notkins AL, Pozzilli P, Christie MR, Leslie RD: Value of antibodies to islet protein tyrosine phosphatase-like molecule in predicting type 1 diabetes. *Diabetes* 46:1270–1275, 1997
6. Bingley PJ, Bonifacio E, Williams AJ, Genovese S, Bottazzo GF, Gale EA: Prediction of IDDM in the general population: strategies based on combinations of autoantibody markers. *Diabetes* 46:1701–1710, 1997
7. Kulmala P, Savola K, Petersen JS, Vahasalo P, Karjalainen J, Lopponen T, Dyrberg T, Akerblom HK, Knip M: Prediction of insulin-dependent diabetes mellitus in siblings of children with diabetes: a population-based study: the Childhood Diabetes in Finland Study Group. *J Clin Invest* 101:327–336, 1998
8. Leslie RD, Atkinson MA, Notkins AL: Autoantigens IA-2 and GAD in type I (insulin-dependent) diabetes. *Diabetologia* 42:3–14, 1999
9. Notkins AL, Lernmark A: Autoimmune type I diabetes: resolved and unresolved issues. *J Clin Invest* 108:1247–1252, 2001
10. Lampasona V, Bearzatto M, Genovese S, Bosi E, Ferrari M, Bonifacio E: Autoantibodies in insulin-dependent diabetes recognize distinct cytoplasmic domains of the protein tyrosine phosphatase-like IA-2 autoantigen. *J Immunol* 157:2707–2711, 1996
11. Zhang B, Lan MS, Notkins AL: Autoantibodies to IA-2 in IDDM: location of major antigenic determinants. *Diabetes* 46:40–43, 1997
12. Xie H, Zhang B, Matsumoto Y, Li Q, Notkins AL, Lan MS: Autoantibodies to IA-2 and IA-2 beta in insulin-dependent diabetes mellitus recognize conformational epitopes: location of the 37- and 40-kDa fragments determined. *J Immunol* 159:3662–3667, 1997
13. Xie J, Zhang B, Lan MS, Notkins AL: Genomic structure and promoter sequence of the insulin-dependent diabetes mellitus autoantigen, IA-2 (PTPRN). *Genomics* 54:338–343, 1998
14. Cai T, Krause MW, Odenwald WF, Toyama R, Notkins AL: The IA-2 gene family: homologs in *Caenorhabditis elegans*, *Drosophila* and zebrafish. *Diabetologia* 44:81–88, 2001
15. Magistrelli G, Toma S, Isacchi A: Substitution of two variant residues in the protein tyrosine phosphatase-like PTP35/IA-2 sequence reconstitutes catalytic activity. *Biochem Biophys Res Commun* 227:581–588, 1996
16. Solimena M, Dirkx R Jr, Hermel JM, Pleasic-Williams S, Shapiro JA, Caron L, Rabin DU: ICA 512, an autoantigen of type I diabetes, is an intrinsic membrane protein of neurosecretory granules. *Embo J* 15: 2102–2114, 1996
17. Saeki K, Xie J, Notkins AL: Genomic structure of mouse IA-2: comparison with its human homologue. *Diabetologia* 43:1429–1434, 2000
18. Tybolewicz VL, Crawford CE, Jackson PK, Bronson RT, Mulligan RC: Neonatal lethality and lymphopenia in mice with a homozygous disruption of the c-abl proto-oncogene. *Cell* 65:1153–1163, 1991
19. Li E, Bestor TH, Jaenisch R: Targeted mutation of the DNA methyltransferase gene results in embryonic lethality. *Cell* 69:915–926, 1992
20. Geiser AG, Letterio JJ, Kulkarni AB, Karlsson S, Roberts AB, Sporn MB: Transforming growth factor beta 1 (TGF-beta 1) controls expression of major histocompatibility genes in the postnatal mouse: aberrant histocompatibility antigen expression in the pathogenesis of the TGF-beta 1 null mouse phenotype. *Proc Natl Acad Sci U S A* 90:9944–9948, 1993
21. Brunstedt J, Nielsen JH, Lernmark A, Hagedorn Study Group: Isolation of islets from mice and rats. In *Methods in Diabetes Research*. New York, John Wiley & Sons, 1985, p. 245–259
22. Latif ZA, Noel J, Alejandro R: A simple method of staining fresh and cultured islets. *Transplantation* 45:827–830, 1988
23. Lu J, Li Q, Xie H, Chen ZJ, Borovitskaya AE, Maclaren NK, Notkins AL, Lan MS: Identification of a second transmembrane protein tyrosine phosphatase, IA-2beta, as an autoantigen in insulin-dependent diabetes mellitus: precursor of the 37-kDa tryptic fragment. *Proc Natl Acad Sci U S A* 93:2307–2311, 1996
24. Wasmeier C, Hutton JC: Molecular cloning of phogrin, a protein-tyrosine phosphatase homologue localized to insulin secretory granule membranes. *J Biol Chem* 271:18161–18170, 1996
25. Lang J: Molecular mechanisms and regulation of insulin exocytosis as a paradigm of endocrine secretion. *Eur J Biochem* 259:3–17, 1999
26. Xie H, Deng YJ, Notkins AL, Lan MS: Expression, characterization,

processing and immunogenicity of an insulin-dependent diabetes mellitus autoantigen, IA-2, in Sf-9 cells. *Clin Exp Immunol* 113:367–372, 1998
27. Hermel JM, Dirkx R Jr, Solimena M: Post-translational modifications of ICA512, a receptor tyrosine phosphatase-like protein of secretory granules. *Eur J Neurosci* 11:2609–2620, 1999
28. Lee MS, Dirkx R Jr, Solimena M, Dannies PS: Stabilization of the receptor protein tyrosine phosphatase-like protein ICA512 in GH4C1 cells upon treatment with estriadol, insulin, and epidermal growth factor. *Endocrinology* 139:2727–2733, 1998
29. Seissler J, Nguyen TB, Aust G, Steinbrenner H, Scherbaum WA: Regulation of the diabetes-associated autoantigen IA-2 in INS-1 pancreatic beta-cells. *Diabetes* 49:1137–1141, 2000
30. Wasmeier C, Hutton JC: Secretatogue-dependent phosphorylation of the insulin granule membrane protein phogrin is mediated by cAMP-dependent protein kinase. *J Biol Chem* 276:31919–31928, 2001
31. Jones PM, Persaud SJ: Protein kinases, protein phosphorylation, and the regulation of insulin secretion from pancreatic beta-cells. *Endocr Rev* 19:429–461, 1998
32. Ort T, Maksimova E, Dirkx R, Kachinsky AM, Berghs S, Froehner SC, Solimena M: The receptor tyrosine phosphatase-like protein ICA512 binds the PDZ domains of beta2-syntrophin and nNOS in pancreatic beta-cells. *Eur J Cell Biol* 79:621–630, 2000
33. Berghs S, Aggujaro D, Dirkx R Jr, Maksimova E, Stabach P, Hermel JM, Zhang JP, Philbrick W, Slepnev V, Ort T, Solimena M: BetaIV spectrin, a new spectrin localized at axon initial segments and nodes of ranvier in the central and peripheral nervous system. *J Cell Biol* 151:985–1002, 2000

BIOCHEMICAL AND BIOPHYSICAL RESEARCH COMMUNICATIONS 229, 891–895 (1996)
ARTICLE NO. 1898

Mice Lacking the 65 kDa Isoform of Glutamic Acid Decarboxylase (GAD65) Maintain Normal Levels of GAD67 and GABA in Their Brains but Are Susceptible to Seizures

Hideo Asada, Yuuki Kawamura, Kei Maruyama, Hideaki Kume, Ri-gao Ding, Feng Yun Ji, Nobuko Kanbara, Hiroko Kuzume, Makoto Sanbo,* Takeshi Yagi,* and Kunihiko Obata[1]

*Laboratory of Neurochemistry and *Laboratory of Neurobiology and Behavioral Genetics, National Institute for Physiological Sciences, Myodaiji, Okazaki, Aichi 444 Japan*

Received November 13, 1996

The gene encoding of the 65 kDa isoform of the γ-aminobutyric acid (GABA)-synthesizing enzyme, glutamic acid decarboxylase (GAD), GAD65, was targeted in mice by homologous recombination. Viable GAD65 −/− mice were obtained with the expected mendelian frequency and displayed no gross morphological defects. Despite the complete loss of GAD65 mRNA and protein in a homozygous mutant, there was no difference in GABA content in the brains of GAD65 +/+, +/−, and −/− mice. As for the other 67 kDa isoform (GAD67), the levels of mRNA and protein were largely unchanged by the GAD65 mutation. General behavior, including locomotor activity and performance in the Morris water maze task, appeared normal, but seizures were more easily induced by picrotoxin and pentylenetetrazol: the latencies to seizures induced by picrotoxin were shorter and the dose of pentylenetetrazol required for induction of seizures was lower. © 1996 Academic Press

γ-Aminobutyric acid (GABA) is a principal inhibitory neurotransmitter in the mammalian central nervous system (1) and is synthesized from glutamic acid by glutamic acid decarboxylase (GAD) in a specific population of nerve cells (GABAergic neurons). GAD has two isoforms, GAD65 and GAD67, named for their molecular mass of 65 and 67 kDa, respectively, which are encoded by two independent genes (2, 3). It has been suggested that GAD65 is rather membrane-associated, whereas GAD67 is a soluble cytosolic protein (3, 4). Although GAD65 and GAD67 appear to be coexpressed in GABAergic neurons, there are some differences in the subcellular distribution in nerve terminals and cell bodies (3-5). Furthermore, GABA and GAD are transiently expressed in embryonic nervous tissue and affect proliferation, migration and neurite extension of neurons, and synapse formation (6-9), indicating that there are some developmental or trophic functions of GABA, in addition to the conventional neurotransmitter role. Several truncated forms of GAD67 are also expressed transiently during development (10). After seizure in the adult rat, GAD67 and GABA appear in the granule cells of the hippocampus, which are non-GABAergic excitatory neurons (11 and K. Obata, unpublished observation). These findings suggest that GABA itself may be present in different intracellular compartments of not only well-differentiated, GABAergic neurons, but also in undifferentiated or non-GABAergic cells, and may serve diverse functions in the nervous system. Gene targeting of GAD in mice will be useful for elucidating the specific roles of GAD65 and GAD67.

In the present investigation GAD65 gene was disrupted by targeted mutation in mice, and chemical and histological analyses on GAD expression and behavioral studies were performed.

[1] Corresponding author. Fax: +81-564-55-7825. E-mail: obata@nips.ac.jp.
Abbreviations: GAD, glutamic acid decarboxylase; GABA, γ-aminobutyric acid.

0006-291X/96 $18.00

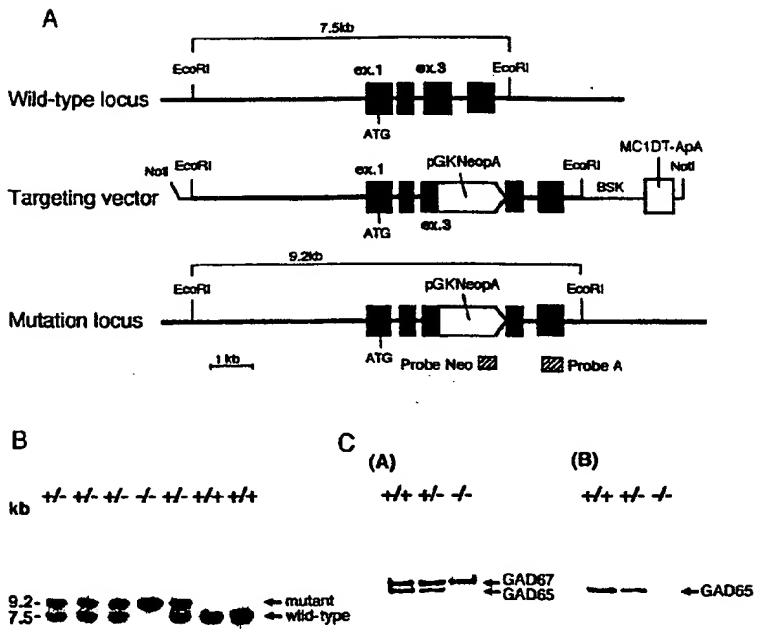

FIG. 1. Targeted disruption of the mouse GAD65 gene. (A) Schematic representation of GAD65 genomic DNA, targeting vector, and the disrupted gene. The targeting vector contains the diphtheria toxin A fragment gene (pMC1DT-ApA) for negative selection. Exon 1 contains the translation initiation codon ATG, and a neomycin-resistant cassette (PGKNeopA, Ref. 15) was inserted into exon 3. Probes Neo and A were used for Southern blot analysis. (B) Southern blot analysis using probe A was performed on EcoRI-digested tail DNA isolated from 21-day-old mice. (C) Western blot analysis of GAD65 and GAD65 expression in wild-type(+/+) and GAD65 mutant (+/− and −/−) brain. The GAD proteins were detected with anti-GAD65/67 (A) and anti-GAD65 (B) antisera.

GAD65 −/− mice maintained normal GAD67 and GABA levels in the brain. General behavior was not impaired but seizure was more easily induced by picrotoxin and pentylenetetrazol.

MATERIALS AND METHODS

Production of the GAD65 mutant mice. A genomic library of TT2 cell (12) was screened using the 5′ portion of GAD65 cDNA. The whole sequence of mouse GAD65 cDNA was registered at accesssion number D42051 in GenBank (13) as a probe (14). The structure of the targeting vector is shown in Fig 1A. The 0.6 kb Xho I-Sal I fragment of pMC1DT-A (15) and the 3.7 kb Sal I-Sma I fragment of pGKPuro (16) were ligate to yield pMC1DT-ApA. TT2 embryonic stem cells (15) were transfected with the targeting vector and then introduced into 8-cell embryos from ICR mice. The mutant mice were obtained by mating chimeric mice with C57BL/6 mice, as reported (15).

Biochemical analysis of the mutant mice. Southern blot analysis was performed according to the general procedure (14, 17). Rabbit antisera, anti-GAD65/67, against C-terminal portion of GAD (DIDFLIEEIERLGQDL) and anti-GAD65, against N-terminal portion of GAD65 (ASPGSGFWSFGSEDGS), were obtained by the injection of synthetic peptides, respectively. Western blot was performed as previously described (17). Anti-GAD65/67 recognized both GAD 65 and GAD67 and anti-GAD65 selectively detected GAD65 in Western blots. Enzymatic activity of GAD was assayed by convertion of ^{14}C-glutamate to $^{14}CO_2$ in the presence and absence of pyridoxal 5′-phosphate (PLP) as in (18), with a slight modification. GABA in the tissue homogenates was measured by high performance liquid chromatography (BAS, Japan).

Behavioral analysis of mutant mice. Locomotor activity and water maze learning were studied with an open field (diameter: 60 cm) and a water maze (diameter: 120 cm) (Neuroscience, Inc.). Motor coordination was observed on a Rota-Rod treadmill (UGO Basile). Passive avoidance learning was tested using a step-through type apparatus (O'Hara).

Induction of convulsion by picrotoxin and pentylenetetrazol. Five mg/kg picrotoxin was injected intraperitoneally and the times of onset of sedation and seizure were recorded. Immediately after a generalized convulsion was induced, diazepam (5 mg/kg) was intraperitoneally administered to suppress the convulsion. Effective doses of pentylenetetrazol were determined by the time of onset of twitch, clonic convulsion and limb extension leading to death after starting intravenous injection with a 1% solution at a constant rate (100 μl/min.) (19).

RESULTS

Southern blot analysis of 21-day-old mice tail DNA (Fig. 1B) showed that wild-type, heterozygous and homozygous mutant mice were obtained from heterozygous GAD65+/− parents with the expected mendelian frequency (+/+, number of mice n=19; +/−, n=33; −/−, n=13). Homozygous GAD65 −/− mice appeared healthy, were of similar size and weight to wild-type and heterozygous GAD65 +/− littermates, and had no gross defects. No morphological abnormalities were observed in brain sections (data not shown).

Northern blot analysis showed that GAD65 mRNA was absent in GAD65 −/− brain and was reduced to one-half of wild-type brain levels in GAD65 +/− brain (data not shown). Levels of GAD67 mRNA in homozygous and heterozygous brain tissue were similar to those in wild-type brain. These results were confirmed by *in situ* hybridization histochemistry of mice brain (not illustrated): homozygous mice had no GAD65 mRNA-positive neurons, and in heterozygous mice the number of GAD65 mRNA-positive neurons was normal, but the intensity of staining was about one-half that of wild-type neurons. No change was found in the number and staining intensity of GAD67 mRNA-positive neurons. Western blot analysis also demonstrated that GAD65 protein was absent in GAD65 −/− brain and was reduced to about one-half the level in GAD65 +/− brain (Fig. 1C). Close examination did not reveal any bands which might be derived from the partial translation of exons 1 and 2 of GAD65 gene remaining after mutation. Levels of GAD67 protein were almost the same. Immunohistochemistry of GAD65 −/− mice brain also demonstrated that no cell was GAD65-positive and the expected population of neurons were GAD67-positive (not illustrated).

GAD activities in the cerebral cortex in the presence of PLP were (cpm/30min/μg protein: mean ± SEM, n=3): 8.22±0.96 for wild-type mice, 5.97±0.35 for GAD65 +/− mutants and 3.63±0.54 for null mutants. The decrease for the null mutants was statistically significant ($p<0.05$) and was largely due to decrease in PLP-dependent activity. It is known that a large part of GAD65 exists as apoenzyme and requires exogenous PLP (2). The similar changes in GAD activities of the mutants were also observed in the striatum, hippocampus and cerebellum. GABA contents were (nmol/mg protein: n=15): 2.39±0.19 for the cerebral cortex, 3.45±0.27 for the striatum, 3.22±0.27 for the hippocampus and 2.61±0.25 for the cerebellum. No significant difference was observed among three groups of mice. Immunohistochemistry of GABA also demonstrated normal number and distribution of GABA-positive neurons in GAD65 −/− brain sections (not illustrated).

Locomotor activity in novel environments and its accommodation with time were studied in an open field. Distances (cm) which mice passed during 2 min. immediately after introduction into the apparatus and after 10 min. of stay in the same apparatus were: 1,423±107 and 894±77 for wild-type litermates (number of mice, n=9), 1,314±60 and 682±62 for GAD65 +/− mice (n=18) and 1,377±193 and 938±119 for GAD65 −/− mice (n=4), respectively. These values did not differ statistically among groups. No ataxic behavior was observed in free movement in an open field and during stay on a rotating rod (Rota-Rod test). No difference was observed in passive avoidance test. For training, electrical shock was delivered to mice from the grids on the floor when they moved from a lighted compartment to a dark compartment. When the mice were introduced to the same dark compartment 24 hours after the training, most mice including all GAD65−/− mice did not step through to the dark room during 3 min. of observation. Spatial learning was evaluated by escape latency to a hidden platform in the Morris water maze and did not reveal any differences among three groups.

TABLE 1
Sensitivity of *GAD65* Mutant Mice to Seizure Induced with Picrotoxin or Pentylenetetrazol

	Latency of picrotoxin effects (sec)		Dose for pentylenetetrazol convulsion (mg/kg)	
Genotype	Sedation	Seizure	Seizure	Tonic extension
+/+	249.1±16.0(7)	849.2±52.3 (7)	62.1±2.1 (4)	86.7±8.8 (4)
+/−	250.3±15.3(12)	831.9±56.9 (12)	52.9±1.5[a](4)	78.5±14.7 (3)
−/−	215.0±32.2(6)	515.7±68.8[a,b](8)	41.1±6.8[a](4)	54.6±7.9[a] (4)

Note. Picrotoxin (5mg/kg) was injected intraperitoneally, and pentylenetetrazol was infused into the tail vein at a constant rate of 0.0167 mg/sec. Values represent mean±SEM (numbers of mice).
[a] Statistically different from wild-type group using Student t-test. ($p<0.05$).
[b] Statistically different from heterozygous group using Student t-test. ($p<0.05$).

Escape latencies (sec) in the first session (mean value of five trials in each session) were: 85.7±2.8 for wild-type mice (n=6), 82.8±4.7 for GAD65 +/− mice (n=8) and 81.2±8.8 for GAD65 −/− mice (n=4). On the 6th day (session 6), escape latencies of the same mice were 12.4±2.7 for wild-type, 12.0±1.5 for GAD65 +/− and 13.0±2.2 for GAD65 −/− animals. On the 7th day, the mice were forced to learn to locate a visible platform with a flag in the same water maze. All mice escaped to the platform within 10 sec after 3-4 trials.

Sensitivity of mutant mice to convulsants was assessed in two ways. Intraperitoneal administration of picrotoxin (5 mg/kg) induced sedation in most mice after 3-5 min.: sedation was characterized by lying motionless on their stomach with lightly extended limbs. After 10-15 min. of sedation the animals again assumed crouching posture and walked around. This was followed by a generalized convulsive fit. Latency to seizure was significantly shorter for GAD65 −/− mice (Table 1). Six GAD65 −/− mice had a similar latency to sedation but in the remaining 2 homozygotes a convulsion developed without sedation, probably representing a higher seizure susceptibility. Continuous infusion of pentylenetetrazol induced twitch, clonic convulsion and tonic extension, sequentially. Doses required for induction of clonic and tonic convulsion were significantly lower for homozygous mutants than for wild-type mice (Table 1). Seizure threshold for heterozygous mutants was between those for wild-type and −/− mice.

DISCUSSION

Targeted disruption of the GAD65 gene at exon 3 might allow expression of a small N-terminal peptide, but will certainly eliminate GAD65 enzyme activity (2). Absence of GAD65 in homozygotes was confirmed by Western blot analysis and immunohistochemistry. Compensatory up-regulation of GAD67 was not the observed. In GAD65 −/− mice, GABA should be synthesized exclusively by GAD67. There were no significant changes in GABA levels in four brain regions in GAD65 −/− and +/− mice, in which GAD65 expression was reduced, indicating the presence of homeostatic regulation of GABA synthesis. Although the PLP dependent GAD activity was reduced in the mutant mice, the remaining GAD67 activity might be enough to keep the level of GABA.

Although locomotor activity and several types of behavior were not affected, GAD65 −/− mice showed an increased susceptibility to picrotoxin and pentylenetetrazol. Picrotoxin blocks the GABA receptor complex (1) and one of the targets of pentylenetetrazol is also the GABA receptor (20). Therefore, higher sensitivity of GAD65 −/− mice to these convulsants may reflect reduced GABAergic transmission. A possible mechanism could be the reduction of

GABA in GABAergic nerve terminals of GAD65 −/− mice, since GAD65 is considered to be concentrated in the nerve terminals (3,5). Electrophysiological investigation of GABAergic synapses will be required to determine if there is any change in GABA release from GABAergic nerve terminals and/or a change in the sensitivity of GABA receptors in postsynaptic neurons. Changes in GABA release will also be evaluated by brain microdialysis.

Gross anatomy and brain histology revealed no marked abnormality in GAD65 −/− mice. It has been suggested that GABA regulates proliferation, migration and process extension of neurons (5-8) and that GABA derived from GAD67 might play the important role in the early neurogenesis.

The present findings on GAD65 −/− mice will provide the basis for further investigation on the diverse functions of GABA and GAD. Multilateral analyses of GAD65 −/−, GAD67 −/− and double knockout mice should allow the elucidation of specific or cooperative roles of GAD65 and GAD67 in histogenesis, synaptic transmission and other trophic/regulatory mechanism of the nervous system.

ACKNOWLEDGMENT

This work was supported by Grants-in-Aid from the Ministry of Education, Science, Sports and Culture (Japan).

REFERENCES

1. Obata, K. (1977) *in* Handbook of Physiology: The Nervous System (Kandel, E. R., Ed.), Vol. 1, Part 1, pp.625–650, American Physiological Society, Bethesda, MD.
2. Erlander, M. G., Tillakaratne, N. J. K., Feldblum, S., Patel, N., and Tobin, A. J. (1991) *Neuron* **7**, 91–100.
3. Erlander, M. G., and Tobin, A. J. (1991). *Neurochem. Res.* **16**, 215–226.
4. Dirkx, R., Jr., Thomas, A., Li, L., Lemmark, Å., Sherwin, R. S., De Camilli, P., and Solimena, M. (1995) *J. Biol. Chem.* **270**, 2241–2246.
5. Esclapez, M., Tillakaratne, N. J. K., Kaufman, D. L., Tobin, A. J., and Houser, C. R. (1994) *J. Neurosci.* **14**, 1834–1855.
6. Barbin, G., Pollard, H., Gaïarsa, J. L., and Ben-Ari, Y. (1993) *Neursci. Lett.* **152**, 150–154.
7. Behar, T. N., Schaffner, A. E., Colton, C. A., Somogyi, R., Olah, Z., Lehel, C., and Barker, J. L. (1994) *J. Neurosci.* **14**, 29–38.
8. LoTurco, J. J., Owens, D. F., Heath, M. J. S., Davis, M. B. E., and Kriegstein, A. R. (1995) *Neuron* **15**, 1287–1298.
9. Schousboe, A., and Redburn, D. A. (1995) *J. Neursci. Res.* **41**, 1–7.
10. Szabo, G., Katarova, Z., and Greenspan, R. (1994) *Mol. Cell. Biol.* **14**, 7535–7545.
11. Schwarzer, C., and Sperk, G. (1995) *Neurascience* **69**, 705–709.
12. Yagi, T., Tokunaga, T., Furuta, Y., Nada, S., Yoshida, M., Tsukada, T., Saga, Y., Takeda, N., Ikawa, Y., and Aizawa, S. (1993) *Anal. Biochem.* **214**, 70–76.
13. Asuda, H., Maruyama, K., Kawamura, Y., and Obata, K. (1995) *Soc. Neurosci. Abstr.* **21**, 2198.
14. Sambrooke, J., Fritsch, E. F., and Maniatis, T. (1989) Molecular Cloning: A Laboratory Mannual, 2nd ed., Cold Spring Harbor Laboratory Press, Cold Spring Harbor, NY.
15. Yagi, T., Aizawa, S., Tokunaga, T., Shigetani, Y., Takeda, N., and Ikawa, Y. (1993) *Nature* **366**, 742–745.
16. Watanabe, S., Kai, N., Yasuda, M., Kohmura, N., Sanbo, M., Mishina, M., and Yagi, T. (1995) *Biochem. Biophys. Res. Commun.* **213**, 130–137.
17. Kume, H., Maruyama, K., Tomita, T., Iwatsubo, T., Saido, T. C., and Obata, K. (1996) *Biochem. Biophys. Res. Commun.* **219**, 526–530.
18. Moskal, J. R., and Basu, S. (1975) *Anal. Biochem.* **65**, 449–457.
19. Tecott, L. H., Sun, L. M., Akana, S. F., Strack, A. M., Lowenstein, D. H., Dallman, M. F., and Julius, D. (1995) *Nature* **374**, 542–546.
20. Stringer, J. L. (1994) *Brain Res.* **636**, 221–226.

Article

Mice lacking desmocollin 1 show epidermal fragility accompanied by barrier defects and abnormal differentiation

Martyn Chidgey,[1,2] Cord Brakebusch,[3] Erika Gustafsson,[3] Alan Cruchley,[4] Chris Hail,[2] Sarah Kirk,[1] Anita Merritt[1], Alison North,[1] Chris Tselepis,[2] Jane Hewitt,[1] Carolyn Byrne,[1] Reinhard Fassler,[5] and David Garrod[1]

[1]School of Biological Sciences, University of Manchester, Manchester M13 9PT, UK
[2]Division of Medical Sciences, University of Birmingham, Birmingham B15 2TH, UK
[3]Department of Experimental Pathology, Lund University, S-221 85 Lund, Sweden
[4]Clinical and Diagnostic Oral Sciences, Barts and The London, Queen Mary's School of Medicine and Dentistry, London E1 2AT, UK
[5]Department of Molecular Medicine, Max Plank Institute for Biochemistry, D-82152 Martinsried, Germany

The desmosomal cadherin desmocollin (Dsc)1 is expressed in upper epidermis where strong adhesion is required. To investigate its role in vivo, we have genetically engineered mice with a targeted disruption in the *Dsc1* gene. Soon after birth, null mice exhibit flaky skin and a striking punctate epidermal barrier defect. The epidermis is fragile, and acantholysis in the granular layer generates localized lesions, compromising skin barrier function. Neutrophils accumulate in the lesions and further degrade the tissue, causing sloughing (flaking) of lesional epidermis, but rapid wound healing prevents the formation of overt lesions. Null epidermis is hyperproliferative and overexpresses keratins 6 and 16, indicating abnormal differentiation. From 6 wk, null mice develop ulcerating lesions resembling chronic dermatitis. We speculate that ulceration occurs after acantholysis in the fragile epidermis because environmental insults are more stringent and wound healing is less rapid than in neonatal mice. This dermatitis is accompanied by localized hair loss associated with formation of utriculi and dermal cysts, denoting hair follicle degeneration. Possible resemblance of the lesions to human blistering diseases is discussed. These results show that Dsc1 is required for strong adhesion and barrier maintenance in epidermis and contributes to epidermal differentiation.

Introduction

The desmosomal cadherins, desmocollin (Dsc)* and desmoglein (Dsg), mediate adhesion in desmosomes, one of the principal types of intercellular junction in epithelia and cardiac muscle (Chitaev and Troyanovsky, 1997; Marcozzi et al., 1998; Tselepis et al., 1998). Each constitutes a cadherin subfamily that comprises three genetic isoforms (Dsc1, 2, and 3 and Dsg1, 2, and 3) (Buxton et al., 1993). Dscs and Dsgs show tissue-specific expression: Dsc2 and Dsg2 are ubiquitous in desmosome-containing tissues, whereas Dscs 1 and 3 and Dsgs 1 and 3 are restricted to stratified epithelia. In stratified epithelia such as epidermis, the desmosomal cadherins also show differential expression with the "1" isoforms expressed in suprabasal differentiated layers and the "2" and "3" isoforms in more basal layers (Garrod et al., 1996). Dsg1 and 3 and Dsc1 and 3 expression in epidermis is graded reciprocally; the "3" isoforms decrease exponentially from the basal layer as the "1" isoforms increase (Shimizu et al., 1995; North et al., 1996). This implies that their expression patterns may be linked, a possibility also

Address correspondence to David R. Garrod, School of Biological Sciences, 3.239 Stopford Bldg., University of Manchester, Oxford Rd., Manchester M13 9PT, UK. Tel.: 44-161-275-5243. Fax: 44-161-275-3915. E-mail: david.garrod@man.ac.uk

J. Hewitt's present address is Queen's Medical Centre, Genetics Division, Nottingham University, Nottingham NG7 2UH, UK.

A. North's present address is The Rockefeller University, 1230 York Ave., New York, NY 10021.

*Abbreviations used in this paper: DP, desmoplakin; Dsc, desmocollin; Dsg, desmoglein; ES, embryonic stem; K, keratin; PF, pemphigus foliaceus; PG, plakoglobin; RT, reverse transcriptase; TEWL, transepidermal water loss.

Key words: desmosome; desmocollin; epidermis; epidermal barrier; null mutation

The Journal of Cell Biology, Volume 155, Number 5, November 26, 2001 821–832
http://www.jcb.org/cgi/doi/10.1083/jcb.200105009

suggested by the adjacent chromosomal locations of desmosomal cadherin genes (Hunt et al., 1999). Where they occur together, Dsc1 and Dsc3 are mixed in the same desmosomes. Thus, the Dsc1:Dsc3 ratio increases with stratification, indicating turnover during epidermal differentiation and showing that adhesion at different levels in the epidermis involves different combinations of desmosomal cadherins (North et al., 1996).

Desmosomal adhesion plays an important role in the maintenance of tissue architecture as indicated by the study of human disease and null mutations in mice (Hashimoto et al., 1997; Amagai, 1999; Mahoney et al., 1999; Green and Gaudry, 2000). The loss of expression of desmosomal components in some human carcinomas and the ability of desmosomal expression to block cellular invasion suggests that desmosomes may also have a tumor suppressor function (Garrod, 1995; Shinohara et al., 1998; Tselepis et al., 1998).

A pressing question is whether the differential expression of desmosomal cadherins indicates specific functions for the distinct isoforms. Their graded expression in stratified epithelia implies a possible role in epithelial differentiation. Stratification itself is clearly not dependent on the presence of multiple desmosomal cadherin isoforms, since cornea possesses only Dsc2 and Dsg2 (Messent et al., 2000). In other epithelia, Dsc3 and Dsg3 are associated positionally with cell proliferation and the early stages of differentiation, whereas Dsc1 and Dsg1 are associated with terminal differentiation and keratinization. Thus, the "1" isoforms may provide strong adhesion to resist abrasion in keratinized epithelia, and the "3" isoforms may provide weaker adhesion required for cell proliferation and motility (Legan et al., 1994). Desmosomal cadherins also may be involved in differentiative signaling. Desmosomes participate in both inside-out and outside-in signal transduction (Osada et al., 1997; Wallis et al., 2000). Furthermore, the Dsc and Dsg cytoplasmic domains bind the armadillo proteins plakoglobin (PG) and plakophilin, and PG signaling in the epidermis has been demonstrated, since overexpression affects hair growth (Charpentier et al., 2000). The nuclear location of plakophilins suggests a possible gene regulation role (Hatzfeld, 1999). Thus, either a structural/morphogenetic role and/or a direct or indirect differentiative signaling role for desmosomal cadherins may be envisaged. Mice expressing dominant negative Dsg3 exhibit abnormalities of epidermal proliferation and differentiation (Allen et al., 1996), although $Dsg3^{-/-}$ mice show no obvious abnormalities of epidermal differentiation (Koch et al., 1997).

To approach the question of the function of Dsc isoforms, we have performed targeted ablation of the mouse *Dsc1* gene. This results in a complex phenotype, showing epidermal fragility together with defects of epidermal barrier and differentiation. The epidermis of neonatal mice shows lesions, which resemble those found in IgA pemphigus, and older mice develop chronic dermatitis. These results demonstrate that Dsc1 contributes substantially to epidermal adhesion and function.

Results

Characterization of the *Dsc1* gene

Two λ clones (λC1 and λC4) and a PAC clone (364c17) containing Dsc1 sequence were obtained from library screens. From these, the mouse *Dsc1* gene was characterized in detail. The gene spans ~32 kb and consists of 17 exons (Fig. 1). Exon 10 is the largest (260 bp) and exon 16, which is alternatively

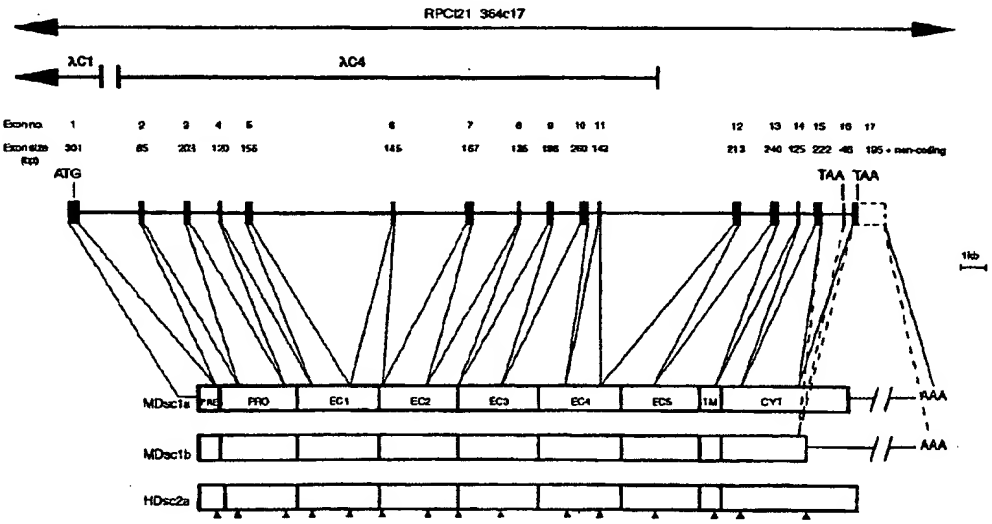

Figure 1. **Exon-intron organization of the murine *Dsc1* gene.** The analysis was conducted using a PAC clone (RPCI21 346c17) and two λ clones (λC1 and λC4). The location of each exon is shown relative to the *Dsc1* gene and a schematic representation of the mouse (M) Dsc1a and Dsc1b proteins. Results from RNase protection assay (unpublished data) suggest that there are no additional 5′ exons. Alternative splicing of RNA can occur; the shorter "b" form of the protein is produced if RNA encoded by exon 16 (which contains an in-frame stop codon) is included in the final message. PRE, signal peptide; PRO, propeptide; EC1-EC5, extracellular homologous repeat domains 1–5; TM, transmembrane domain; CYT, cytoplasmic domain. The locations of introns in human (H) *DSC2* (Greenwood et al., 1997) are shown for comparison and indicated by arrowheads.

Table I. Exon-intron boundaries of the mouse *Dsc1* gene

Exon	Exon size	5′ donor	Intron size	3′ acceptor
	bp		*kb*	
1	NC + 63	TTTCTCCTGgtgagt	2.6	ttgagGTTCTGGTA
2	85	TAGGCAAAGgtgagc	1.7	ctgtagTGAATCTGG
3	203	GAAAAAAAGgtaaag	1.1	atatagGTTTTTAGG
4	120	ATTCAGCAGgtctgt	1.1	ttatagATCCAATCT
5	156	CAATTTTTGgtaaga	5.8	ttccagGTATATGGA
6	145	GCCGATCTGgtgagt	3.0	gaacagGAACTTCAG
7	167	GACAGAGAGgtaatg	1.9	ttacagAAATGTGAC
8	135	CAAACTTCTgtgagt	1.2	cctcagTATACTACA
9	186	AGGCTTAAGgtaatg	1.1	aaacagCCACTGAAC
10	260	AGGCTTAAGgtaatg	0.4	acctagGTATGAGAT
11	143	CAGATACAGgtgagt	5.5	tcctagCTGGCCGAT
12	213	CACAGGATGgtaagt	1.3	cttcagGTAAACGTG
13	240	TGCTACTGTgtaagt	0.8	ctgtagGCATTTTGT
14	125	GAAGTGACGgtaaat	0.7	ctttagGAAGCCAAT
15	222	CTTGGTGAAgtaagt	0.9	atacagAAGGTGTAT
16	46	CTTGGTGAAgtaagt	0.3	atgtagGAATCCATT
17	195 + NC			

Consensus ag/gt splice sequences are shown in bold. Intron sizes were determined by PCR using primers positioned on flanking exons. NC, noncoding.

spliced to generate the "a" and "b" forms of the protein (Collins et al., 1991), is the smallest (46 bp). Single exons do not correspond to known structural elements such as the extracellular domain internal repeats or the transmembrane or cytoplasmic domains (Fig. 1). All intron-exon borders conform to 5′ and 3′ splice site consensus sequences (Table I). The organization of mouse *Dsc1* shows a striking resemblance to that of other Dsc and classical cadherin genes (Greenwood et al., 1997; Whittock et al., 2000) with exon boundaries highly conserved (Fig. 1).

Generation of *Dsc1*-null mice by homologous recombination

The *Dsc1* gene was disrupted in embryonic stem (ES) cells using the targeting vector shown in Fig. 2 A. On homologous recombination, the vector replaces the translation initiation codon (ATG) and the coding sequence from exon 1 with a neo-cassette. 98 bp at the 3′ end of exon 1 (including 63 bp encoding the start of the Dsc1 signal peptide) and 2.2 kb of intron 1 are replaced by vector DNA.

Four ES cell clones containing a disrupted *Dsc1* allele were identified, and one was used to generate chimeric mice that transmitted the mutated allele to their progeny. Mice heterozygous for the targeted mutation were identified by Southern blotting; wild-type and mutant alleles produced fragments of 20- and 6-kb, respectively (Fig. 2 B). Additional Southern blotting with a probe located 3′ to the homologous sequences in the targeting vector confirmed the presence of the mutated allele in heterozygous mice, and a

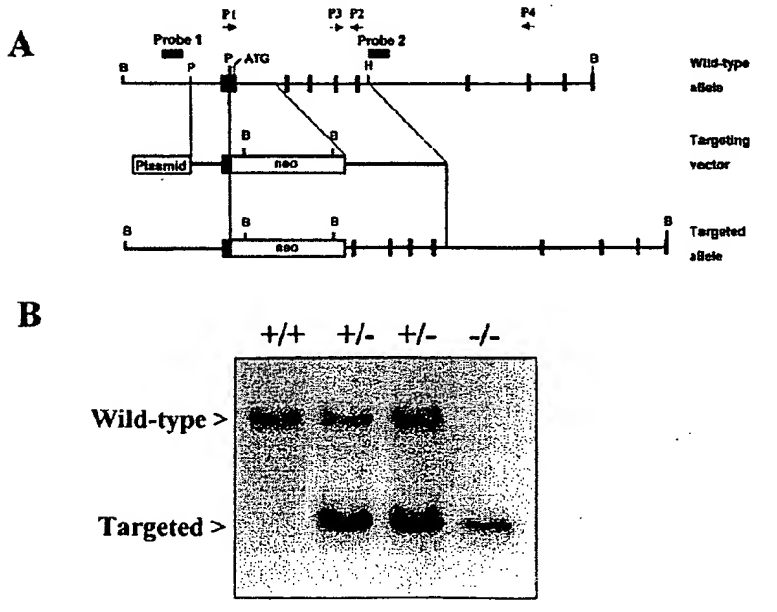

Figure 2. **Targeted disruption of the mouse *Dsc1* gene.** (A) Targeting strategy. The targeting vector consisted of pUC DNA, a neomycin (neo) resistance cassette, and portions of the *Dsc1* gene including 2.1 kb of homology (5′ arm) and 5.2 kb of homology (3′ arm). Filled vertical boxes represent exons. B, BamHI; P, PvuII; H, HindIII. (B) Southern blot analysis of genomic DNA from wild-type (+/+), heterozygous (+/−), and homozygous (−/−) mice. DNA was digested with BamHI, subjected to agarose gel electrophoresis, and transferred to nitocellulose. Wild-type (20 kb) and mutant (6 kb) alleles were detected with probe 1, which hybridized to DNA just outside of the 5′ region of homology. Similarly, probe 2, which hybridized to DNA just outside the 3′ region of homology, detected wild-type (20 kb) and mutant (14 kb) bands (unpublished data).

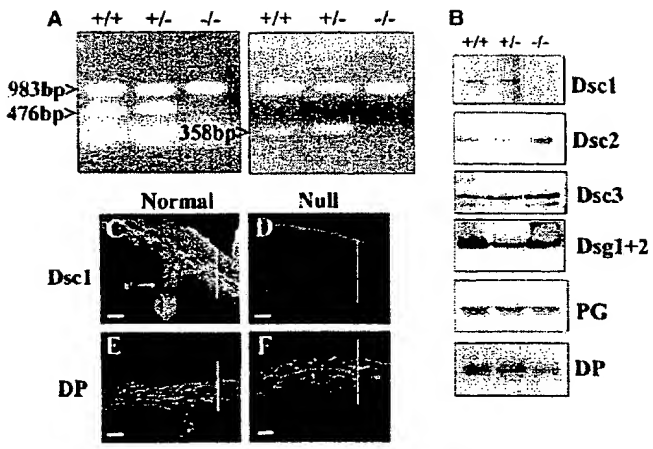

Figure 3. **Expression of desmosomal constituents in Dsc1 mutant mice.** (A) RT-PCR showing absence of Dsc1 message in *Dsc1*$^{-/-}$ mice. Amplification of Dsc1 mRNA was performed using primer pairs P1 and P2 and P3 and P4 (Fig. 2 A) to give 476- and 358-bp products, respectively, in wild-type and heterozygous mice only. Control amplifications using glyceraldehyde-3-phosphate dehydrogenase primers (983-bp product) were performed. (B) Western blot analysis of epidermal extracts using antibodies specific for Dsc1, Dsc2, Dsc3, Dsg1+2, PG, and DP. Equal protein loadings were determined by prior staining with Coomassie brilliant blue. (C–F) Immunofluorescence of epidermis from 2-d-old normal and null mice. Dsc1 is expressed in the epidermis and hair follicles of normal mice (C) but is absent from the skin of null animals (D). DP distribution is unaffected apparently by the absence of Dsc1 and is similar in normal (E) and null mice (F). Vertical bars indicate position of epidermis. Skin samples were taken from the backs of mice. hf, hair follicle. Bars, 25 μm.

neo-derived probe was used to show the presence of only one copy of the neo gene (unpublished data). Heterozygous mice, which could not be distinguished from their wild-type littermates, were crossed and their progeny genotyped. Litter sizes were normal. Of the pups, 26% were wild-type (+/+), 56% were heterozygous (+/−), and 18% were homozygous for the disrupted allele (−/−) (n = 308). Thus, the number of homozygous-null offspring was slightly lower than expected. Dsc1 is first expressed at embryonic day (E)13.5 in the outer layers of epidermis (King et al., 1996; Chidgey et al., 1997). To determine whether absence of Dsc1 results in some embryonic mortality, we genotyped E17 embryos from heterozygous crosses. Of these, 28% were wild-type, 43% were heterozygous, and 29% were −/− (n = 65). This is a normal Mendelian ratio. These data suggest that some of the *Dsc1*$^{-/-}$ neonates are eaten by the mothers at birth, although no direct evidence for this was found. *Dsc1*$^{-/-}$ mice were fertile: pups from *Dsc1*$^{-/-}$ × *Dsc1*$^{-/-}$ crosses were reared and weaned successfully.

Mice lacking Dsc1 show a neonatal phenotype involving skin, hair, eyes, and growth

Using primers P1 and P2 specific for exons 1 and 5, respectively (Fig. 2 A), full-length Dsc1 mRNA was absent from the epidermis of *Dsc1*$^{-/-}$ mice by reverse transcriptase (RT)-PCR (Fig. 3 A). To confirm the absence of a 5′-truncated message, RT-PCR was performed using primers P3 and P4 specific for exons 4 and 7, respectively (Fig. 2 A). No evidence for a truncated message was found (Fig. 3 A). Primer P3 hybridizes to DNA downstream of that encoding the beginning of the mature protein. Hence, it is extremely unlikely that a truncated message smaller than that which would be detected by primer pair P3-P4 would produce a functional protein. Western blotting with a polyclonal antibody raised against a substantial portion of the extracellular domain of Dsc1 (North et al., 1996) showed absence of the protein from *Dsc1*$^{-/-}$ epidermis (Fig. 3 B). No evidence for the production of a truncated protein was found. Western blotting also showed no clear differences in expression of other desmosomal components (Dsc2, Dsc3, Dsg1+2, PG, desmoplakin [DP]) (Fig. 3 B). Immunofluorescence demonstrated absence of Dsc1 from *Dsc1*$^{-/-}$

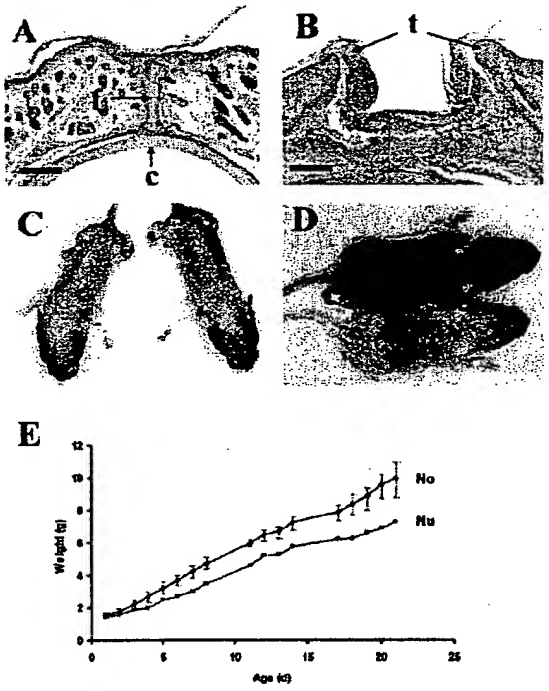

Figure 4. **Eye, skin, and growth abnormalities in Dsc1-null mice.** (A) Eyelids from a 2-d-old normal mouse. f, fused eyelid epidermis; c, cornea. (B) Eyelids from a *Dsc1*$^{-/-}$ littermate showing a failure of eyelid fusion, inflammation, and corneal damage. t, eyelid tips which have failed to fuse. (C) Flaky skin in two null mice at 2-d-old. At this age, null mice were indistinguishable in size from their normal littermates. (D) Flaky skin and characteristic runted appearance in an 8-d-old null mouse (bottom animal) when compared with a normal littermate (top animal). (E) Delayed weight gain in Dsc1-null mice. Results from a typical litter consisting of nine pups in which a null (Nu) mouse and its normal (No) littermates were born with equal weights, but at weaning (21 d) the null mouse weighed 30% less than the average of the others. Bars represent range of weights of normal littermates. 10 litters were examined with similar results. Bars, 150 μm.

epidermis and the inner root sheaths of hair follicles (Fig. 3, C and D). Other desmosomal components were unchanged (DP shown) (Fig. 3, E and F).

At birth, homozygous mice were generally indistinguishable from their littermates, but 10% were born with one or both eyes open (Fig. 4, A and B). Failure of eyelid fusion led to corneal damage and inflammation and corneal opacity or micropthalmia later in life. From day 2, null mice could be distinguished from their normal (i.e., *Dsc1*$^{+/+}$ and *Dsc1*$^{+/-}$) littermates because null skin was covered in white flakes or scales (Fig. 4, C and D).

Although born at the same size, null mice usually grew less rapidly (Fig. 4 D), and by weaning (21 d) they were ~30% smaller than littermates (Fig. 4 E; see Fig. 9 A). Slower growth was not due to an obvious feeding defect. The guts of null mice had milk in their stomachs and a normal appearance throughout their length, indicating that the food was processed normally. Dsc1 is expressed in mouse tongue, hard palate, esophagus, and forestomach (King et al., 1996, 1997), but histological examination of these tissues from null mice revealed no abnormalities of the epithelia. Inspection of the oral cavities of null pups revealed no blistering of epithelia. Thus, *Dsc1*$^{-/-}$ mice did not show the type of oral blistering defects responsible for feeding defects and small size in *Dsg3*$^{-/-}$ mice (Koch et al., 1997). Of null animals, 10% remained runted, but others caught up after weaning so that by 3 mo there was no significant difference in weight between them and normal mice. Thus, although growth was slower adult size was not generally affected.

Dsc1 is expressed in the Hassal bodies of human thymus (Nuber et al., 1996). To test for an effect on thymus, we examined it histologically and counted numbers of peripheral blood T cells labeled with antibodies to CD4 and CD8 by flow cytometry. No differences were found.

Mice lacking Dsc1 show abnormal epidermal proliferation and differentiation

Histology showed that the epidermis of *Dsc1*$^{-/-}$ mice was considerably thicker than that of littermates. Normal epidermis consisted of two to three cell layers below the cornified layer, but that of null mice had one, two, or three additional layers, and thickening was found at all body sites. At 2 d, thickening was principally in the spinous layer (Fig. 3, E and F, and Fig. 5, A and B), although localized hyperkeratosis and parakeratosis were also seen (Fig. 5 C). The epidermal cells often but not always appeared larger in the thickened null epidermis (Fig. 5, A and B, compared with Fig. 3, E and F). To determine whether epidermal thickening was due to increased cell proliferation, we examined the skin from null and normal mice using an antibody against Ki67. Proliferating cells were infrequent (3% of all epidermal nuclei) in normal mouse skin and found exclusively in the basal cell layer (Fig. 5 D). By contrast, in null mouse epidermis keratinocytes with nuclear Ki67 were extremely abundant (33% of all epidermal nuclei) and observed frequently in suprabasal layers (Fig. 5 E).

To investigate the effects of the null mutation on epidermal differentiation, we examined the expression of differentiation markers by immunofluorescence. No differences between normal and null epidermis from 2-d-old animals were observed in the distributions of the basal markers P-cadherin (Fig. 6, A and B), β_4-integrin (Fig. 6, D and E), and keratin 5 (unpublished data). Early markers of terminal differentiation (keratin [K]1, involucrin) and a marker for late epidermal differentiation (filaggrin) were normal in 2-d-old null mice (unpublished data). However, a striking difference in the hyperproliferation markers keratins 6 and 16 was found. In normal 2-d epidermis, expression of K6 was restricted mostly to hair follicles (Fig. 6 G), although localized interfollicular epidermal staining was found occasionally. In null epidermis, K6 was present in both hair follicles and interfollicular epidermis (Fig. 6 H). Such K6 expression was observed at all body sites but was patchy locally: in some places expression was present throughout interfollicular epidermis but was absent from others. In normal epidermis, K16 was expressed in hair follicles, and superficial staining was present in suprabasal interfollicular epidermis (Fig. 6 J). In null animals, expression of the protein was upregulated and detected in all cell layers of interfollicular epidermis (Fig. 6 K).

In later life, null mice were susceptible to skin ulceration (see below). In lesioned epidermis from adult null mice,

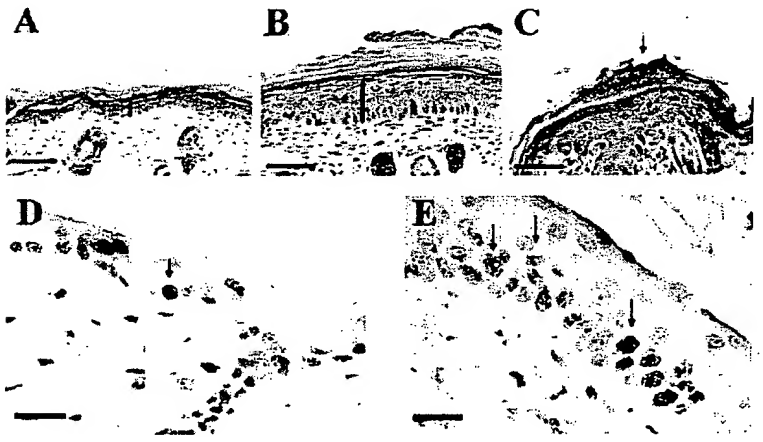

Figure 5. **Hyperplasia and increased cell proliferation in Dsc1-deficient epidermis.** (A) Epidermis from a 2-d-old normal mouse. (B) Epidermis from a *Dsc1*$^{-/-}$ littermate showing hyperplasia. Bars (e) indicate thickness of living layers of epidermis. (C) Epidermis from a Dsc1-null mouse showing localized hyperkeratosis and parakeratosis (retention of nuclei in the cornified layer) (arrow). (D) Expression of Ki67 in the epidermis in a normal mouse. (E) Ki67 staining in the epidermis of a *Dsc1*$^{-/-}$ mouse. Only one proliferating cell located in the basal layer is present in D (arrow), whereas in E almost all of the cells in the basal layer and numerous suprabasal cells (arrows) are undergoing cell division. A–C show head skin; D and E show back skin. Bars: (A–C) 100 μm; (D and E) 50 μm.

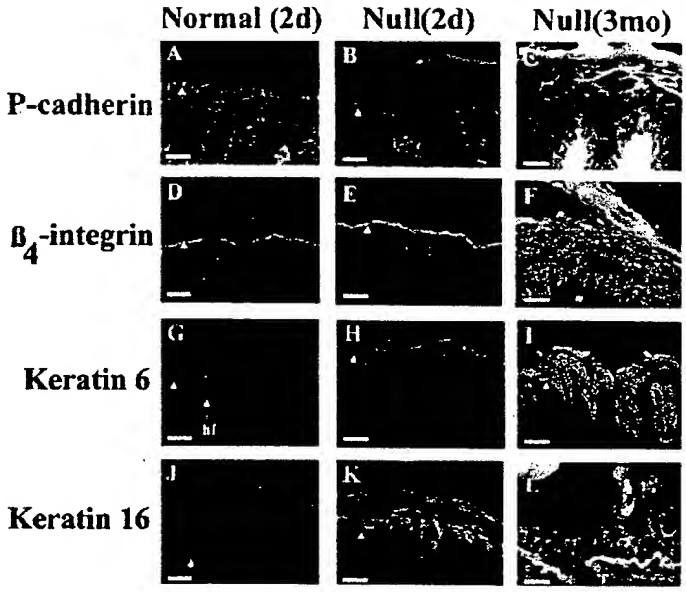

Figure 6. **Immunofluorescence of differentiation markers in Dsc1-null mice.** Distribution of P-cadherin in normal (A) and null (B) 2-d-old animals. In both cases, expression is confined to the basal cell layer and hair follicles. However, dramatic upregulation of P-cadherin is found in lesioned epidermis from adult (~3-mo-old) null animals (C). Similarly, distribution of β_4-integrin expression is similar in normal (D) and null (E) 2-d epidermis but is increased dramatically in all cell layers of lesioned epidermis from older null mice (F). Keratin 6 is expressed in hair follicles of normal mice (G), whereas in unlesioned epidermis from 2-d-old null animals it is found both in hair follicles and interfollicular epidermis (H). Dramatic upregulation of keratin 6 is found in lesioned epidermis from adult null animals (I). In normal animals, superficial keratin 16 staining is detected in suprabasal layers (J), whereas in null mice it is expressed strongly throughout the epidermis including the basal cell layer in both nonlesioned (K) and lesioned epidermis (L). Arrowheads indicate the basement membrane. All micrographs show back skin. Bars: (A–F and J–L) 25 μm; (G–I) 150 μm.

basal layer markers were expressed in all cell layers (Fig. 6, C and F). There were no differences in the distributions of K1 and filaggrin. Both K6 (Fig. 6 I) and K16 (Fig. 6 L) were found throughout lesioned epidermis.

Cornified envelope formation is an important aspect of epidermal terminal differentiation. Because a Dsc, Dsc3, has been reported as a component of cornified envelopes (Robinson et al., 1997) and because *Dsc1*$^{-/-}$ mice showed abnormal epidermal differentiation, we compared cornified envelopes from the epidermis of null and wild-type mice. No difference in appearance was detectable.

Dsc1 deficiency produces epidermal fragility with localized loss of barrier activity

Two observations from neonatal mice suggested that the epidermis of *Dsc1*$^{-/-}$ mice is more fragile than that of littermates. First, histology revealed splits in the epidermis. Such acantholysis, which was absent from normal epidermis, occurred within the granular layer between the granular and spinous layers (Fig. 7 A) or between the cornified and granular layers. Second, when we attempted to isolate the epidermis from 2-d-old mice we found that null epidermis could only be removed in small pieces, whereas normal epidermis remained in sheets (Fig. 7, B and C).

We determined the effects of eliminating Dsc1 on desmosome ultrastructure in the epidermis. No abnormalities in the structure or number of desmosomes were found, including those at the level of the upper spinous and granular layers where Dsc1 expression is strongest (Fig. 7, D and E). Similarly no changes in desmosomes in the inner root sheaths of hair follicles were apparent (unpublished data). By EM, epidermal splits showed an absence of cell lysis and desmosomes, indicating that splitting occurred because of weakened adhesion (Fig. 7 F).

We speculated that flaky skin and epidermal fragility could lead to defects in the skin barrier. To examine this, barrier activity was tested by dye penetration assays (Hardman et al., 1998; Marshall et al., 2000). E17 embryos showed no staining so the barrier was complete before birth. Also, 2-d-old normal mice stayed uniformly white, indicating complete barrier formation (unpublished data; Hardman et al., 1998). However, 2-d-old null mice showed numerous dark spots, indicating localized loss of barrier function (Fig. 8 A). These lesions were not left-right symmetric, indicating that environmental factors contributed to their formation.

Histology of stained spots showed that formation and repair of the lesions could be viewed as sequential events. Early lesions appear in the subcorneal region of epidermis as localized accumulations of neutrophils (Fig. 8, B and C). Such lesions bear a striking resemblance to those found in the subcorneal pustular dermatosis form of IgA pemphigus (Fig. 8 B compared with Fig. 1 c in Hashimoto et al., 1997). Next, the epidermis is degraded by inflammatory cells and partially detaches from the underlying matrix (Fig. 8, D and E), allowing penetration of dye (Fig. 8 A). Concurrently, epithelial cell migration into the wound site is initiated (Fig. 8 E). Finally, when wound healing is complete the damaged epidermis detaches from the underlying tissue, leaving behind an intact newly formed barrier (Fig. 8 F).

To quantify loss of barrier function, body skin from 2-d-old animals was used for determination of permeability constants (Kp) to water and mannitol, a marker for paracellular permeability (Fig. 8 G). Values for Kp were significantly higher ($p < 0.05$) for null animals. The null skin Kp for mannitol was twice that for normal skin, and permeability to water was increased 1.6-fold (Fig. 8 G). These results indicate that absence of Dsc1 causes a defect in the skin barrier.

To examine transepidermal water loss (TEWL), measurements were performed on 25 wild-type and 29 null pups. These gave values of 5.2 mg/h and 6.3 mg/h, respectively.

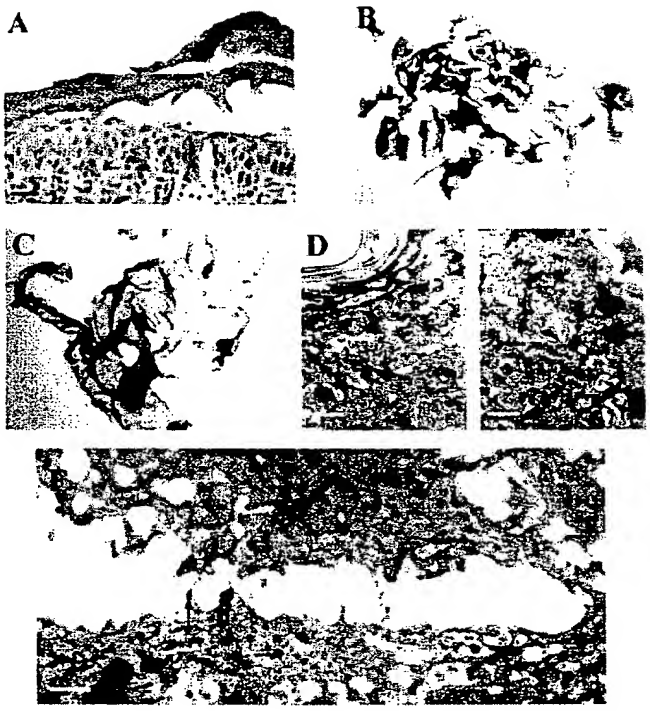

Figure 7. **Absence of Dsc1 weakens adhesion in upper epidermis despite the presence of ultrastructurally normal desmosomes.** (A) Epidermis from a 2-d-old null mouse showing hyperplasia and acantholysis. The granular layer appears to be separating from the upper spinous layer. (B) Epidermis isolated from a 2-d-old $Dsc1^{-/-}$-null mouse after treatment with EDTA showing that the tissue fragments allow only small pieces of epidermis to be separated from the dermis. (C) Epidermis isolated using the same technique from a normal littermate. (D) Ultrastructure of outer layers of epidermis from a normal mouse showing desmosomes (arrows). (E) Ultrastructure of outer layers of epidermis from a Dsc1-null mouse with desmosomes (arrows) of a normal appearance. (F) Ultrastructure of lesional epithelium in a Dsc1-null mouse showing splitting between cells and an absence of cell lysis. Arrows indicate possible remains of split desmosomes. All samples were from back skin. Bars: (A) 20 μm; (D and E) 1 μm; (F) 2 μm.

Thus, TEWL for null mice was ~1.2-fold greater than for wild-type controls ($p = 0.02$).

Dsc1-null mice develop alopecia and chronic dermatitis

The coats of adult null mice had a slightly untidy ruffled appearance (Fig. 9 A). Their pelage hairs were indistinguishable from those of normal littermates with similar distributions of awls, auchenes, zig-zags, and guard hairs, and whiskers appeared normal. In later life (usually manifesting at between 1 and 2 mo), >90% of null mice suffered hair loss and skin ulceration (Fig. 9, B and C). Hair loss was most common ventrally (Fig. 9 B), but some individuals had bald patches on the back, and two mice showed more general hair loss. Ulceration was most common around the muzzle (Fig. 9 C) but was also found elsewhere on the head, ventrally, or on the back. Muzzle lesions appeared between 6 wk and 6 mo, and affected mice were killed. Mice that were caged alone developed the same phenotype.

To investigate the mechanism of hair loss, we examined hair follicles at various stages of the hair cycle. No striking abnormalities were found at 5 (first anagen), 18 (catagen), 21 (telogen), and 28 d (second anagen). Tape stripping of the coats detached no more hairs from null than from normal mice, indicating that hairs were firmly anchored in null follicles.

In older animals, severe epidermal and follicular hyperplasia was observed in ulcerated areas of skin (Fig. 9 C) and occasionally in uninvolved skin. In hyperplastic epidermis, substantial thickening of the stratum corneum (hyperkeratosis) was observed (Fig. 9, D and E). Normally differentiated hair follicles were absent and replaced by large comedo-like malformations (utriculi) and cysts (Fig. 9, D and F). Such structures characteristically result from disintegration of hair follicles, suggesting that the observed alopecia is a result of hyperplasia and loss of normal hair follicle morphology. In some ulcerated regions, the epidermis was lost completely (Fig. 9 E). Severe inflammation and tissue necrosis were also observed. The most striking examples of focal overgrowth of keratinocytes were found in both apparently normal and ulcerated whisker pads, which showed a marked papillomatous nature (Fig. 9, G compared with H) with hyperkeratosis and parakeratosis. No evidence of malignant conversion was found. *Dsc1*-null mice were diagnosed as suffering from chronic dermatitis.

Discussion

Deletion of *Dsc1* has two consequences for epidermis. First, weakened adhesion gives rise to epidermal fragility and acantholysis. In early life, this produces a striking localized loss of barrier function and skin flaking. In older mice, substantial ulceration occurs. Second, epidermal differentiation is abnormal, manifested as epidermal hyperproliferation and thickening, an upregulation of keratin 6 and 16 expression, and localized hyperkeratosis and parakeratosis.

Absence of Dsc1 did not result in any alteration in the structure of desmosomes in the upper epidermis, but acantholysis indicates that they are more weakly adhesive than in normal mice, presumably relying on other Dscs for their structure and adhesion. However, there was also no apparent alteration in the expression of other desmosomal components, a result similar to that found in $Dsg3^{-/-}$ mice (Koch et al., 1997). Thus, although the expression of the glycopro-

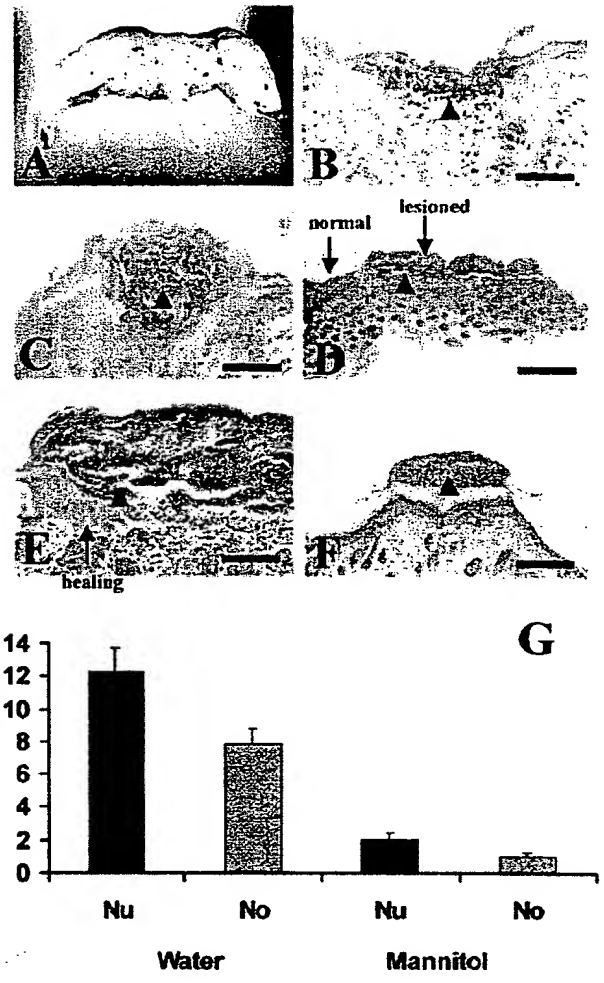

Figure 8. **Dsc1-null mice have skin barrier defects.** (A) Localized breaches in the skin barrier allow penetration of dye into the epidermis of a null mouse but not its normal littermate, which was completely white, that is, unstained (unpublished data). (B and C) Early lesions in the skin of 2-d-old null mice showing infiltration of epidermis with polymorphonuclear cells (neutrophils). (D) More developed lesion in 2-d epidermis showing epidermal degradation and detachment from the underlying dermis. (E) Higher magnification showing epithelial cell migration from intact tissue into wound site. (F) Healed lesion in the epidermis of a 2-d-old null mouse. The damaged epidermis has completely detached from the underlying healed tissue. Arrowheads indicate polymorphonuclear cells. (G) Measurement of permeability coefficients (Kp) for water and mannitol under passive conditions show that skin from 2-d-old null mice is more permeable to both water and solutes ($p < 0.05$ in both cases) than that of a normal littermate. Nu, null; No, normal. Bars: (B, C, and E) 25 μm; (D and F) 100 μm.

tein genes has been postulated to be linked (North et al., 1996; King et al., 1997) two examples of gene deletion have not resulted in compensatory upregulation of other family members.

The acantholysis in the upper epidermis in *Dsc1*$^{-/-}$ resembles that seen in the human autoimmune blistering disease pemphigus foliceus (PF) (Mahoney et al., 1999), reflecting the similar epidermal expression patterns of Dsc1 and the PF antigen Dsg1. In PF, acantholysis results from binding of IgG autoantibody to the extracellular domain of Dsg1. There is no evidence for the involvement of antibodies to Dsc1 in PF. Subsequently, the localized acantholytic lesions in *Dsc1*$^{-/-}$ mice become infiltrated with polymorphonuclear cells (neutrophils). The lesions are reminiscent of those seen in the human subcorneal form of IgA pemphigus in which IgA autoantibodies to Dsc1 bind to the peripheries of epidermal keratinocytes (Hashimoto et al., 1997). No evidence for the pathogenicity of these antibodies has yet emerged. Whether the resemblance between the lesions is coincidental or has significance for the etiology of IgA pemphigus awaits clarification.

Although the acantholytic lesions appear similar, those in young *Dsc1*$^{-/-}$ mice do not progress. In the human diseases, red encrusted lesions are characteristic of PF and red pustular blisters are characteristic of IgA pemphigus, yet the epidermis of the mice remain unblemished apart from the appearance of white flakes. We suggest that skin lesions in young mice are triggered by local acantholysis but do not progress because wound healing is rapid. Reepithelialization of wounds takes ~50% longer in 6–8-wk-old mice than in neonatal mice (Whitby and Ferguson, 1991). This difference in the rate of wound healing can account for the difference in severity between the lesions of neonatal mice and older mice. The environmental insults experienced by older animals are more severe than in young mice during suckling. Repeated insults, especially scratching, give rise to lesions in the epidermis that cannot be healed as rapidly as in neonatal animals. Exacerbation of lesions leads to ulceration and chronic dermatitis, which in this case is a proliferative response of the epidermis to damage. Similar lesions have been found in *Dsg3*$^{-/-}$ mice (Amagai et al., 2000).

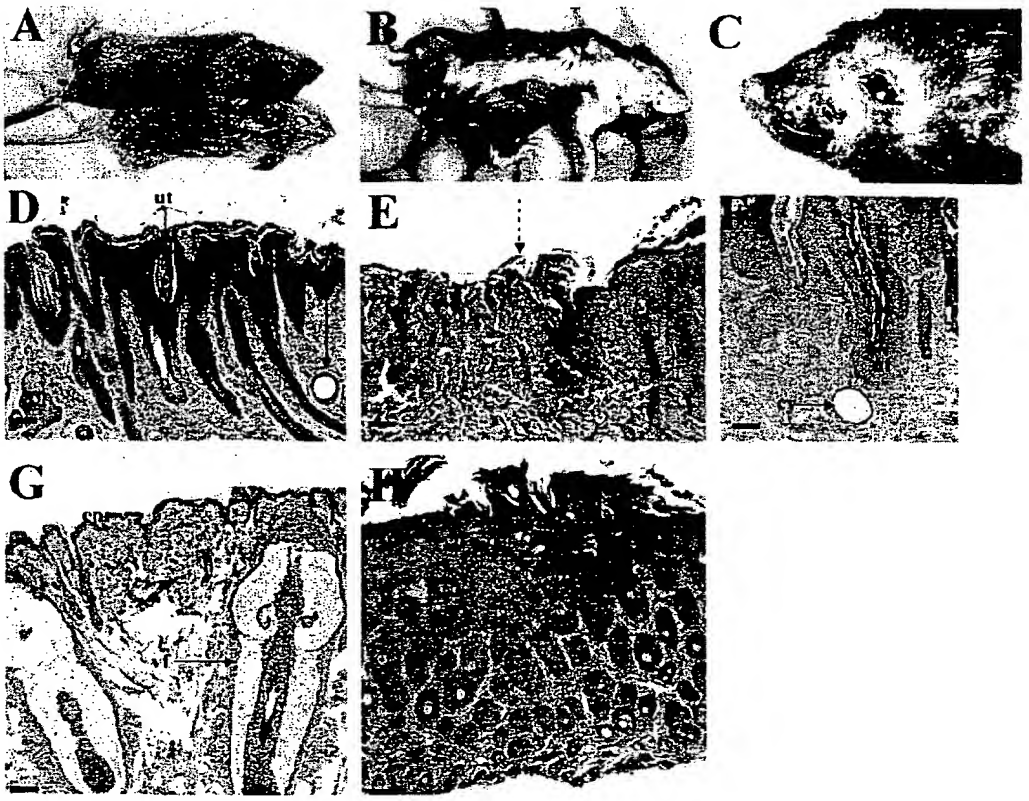

Figure 9. **Phenotype of Dsc1-null mice increases in severity with age.** (A) Scruffy and untidy coat appearance in an adult null mouse (bottom) compared with a normal littermate (top). Mice shown are 21-d-old (day of weaning). Note that the null mouse is smaller. (B) Alopecia in an adult null mouse showing the most typical pattern observed. Some ulceration on the ventral surface of the head and neck is visible also. (C) Snout ulceration in an adult null mouse showing a moderately severe example of the pattern found in all null animals and commencing after 1 mo of age. (D) Hyperplastic epidermis from the ventral surface of an adult null mouse showing acanthosis, hyperkeratosis with utriculi (ut), and cysts (cy). (E) Ulcerated skin from the abdomen of an adult Dsc1$^{-/-}$ mouse showing complete loss of epidermis from the site of the ulcer and severe inflammation. The right hand margin of the ulcer is indicated by an arrow. At this low magnification, the presence of inflammatory cells is indicated by the dermal basophilia of this region. (F) Higher magnification of a utricule (ut) and a cyst (cy). (G) Whisker pad of an adult normal mouse. vf, vibrissa follicle. (H) Whisker pad of an adult null mouse. Severe hyperplasia is present in the null as indicated by the increased number of epidermal cell layers. Approximate thickness of epidermis indicated by bars (ep) in G and H. Bars: (D, E, and G) 150 μm; (F) 25 μm.

Epidermal barrier function is compromised in neonatal *Dsc1*$^{-/-}$ mice. The defect appears to arise as a consequence of localized acantholysis and thus does not imply a direct role for Dsc1 in barrier formation, although we cannot completely exclude the possibility of a slight, more generalized defect. The effect is clearly mild and not life threatening. However, the slight reduction in epidermal barrier function and increase in water loss may cause stress to null mice and result in growth retardation. Area measurements of water and mannitol permeability and TEWL indicate a decrease in barrier function of less than twofold. A fourfold increase in TEWL is not lethal in mice transgenic for COOH-terminally truncated loricrin (Suga et al., 2000). By contrast, a targeted mutation in the keratin 10 gene results in an eightfold increase in TEWL and neonatal death (Jensen et al., 2000). Mice deficient in the cornified envelope proteins involucrin and loricrin exhibit no neonatal barrier defect, although the latter show delayed barrier formation before birth (Dijan et al., 2000; Koch et al., 2000). Therefore, these mice are affected less severely than *Dsc1*$^{-/-}$ mice.

Clear evidence for hyperproliferation and epidermal thickening was found in *Dsc1*$^{-/-}$ mice. Hyperproliferation may be a response to damage to the skin barrier. Underlying cells can sense defects in cells above and respond by proliferating in several experimental situations. Disruption of the barrier elicits DNA synthesis and epidermal hyperplasia (Proksch et al., 1991; Denda et al., 1998), and expression of the *whn* gene and NH_2-terminally truncated Dsg3 in suprabasal layers of transgenic mouse epidermis leads to both hyperproliferation and an immune response (Allen et al., 1996; Prowse et al., 1999). However, the major barrier defect in *Dsc1*$^{-/-}$ mice is localized, whereas the hyperproliferation and epidermal thickening is not. Thus, it seems likely that alterations in the program of keratinocyte terminal differentiation occur in the absence of Dsc1. Two pieces of evidence support this view. First, proliferating keratinocytes were

found in suprabasal layers of null epidermis, and second, parakeratosis was found, suggesting that the later stages of differentiation are delayed. Furthermore, there is evidence to suggest that expression of K6 and K16 in interfollicular epidermis is associated with alterations in differentiation rather than hyperproliferation (Scherner et al., 1989; Sellhayer et al., 1993; Porter et al., 1998b). However, the whole question of whether the effects we observe are a primary consequence of loss of Dsc1 or a secondary consequence of acantholysis and wound healing is a complex one that will form the subject of further investigation.

Epidermal hyperproliferation may suggest a resemblance to the common human skin disease psoriasis. However, the changes in differentiation and skin inflammation are less severe than in psoriasis, and other features, such as loss of the granular layer, formation of deep rete pegs, and dilation of dermal blood vessels, are absent.

Hair loss in *Dsc1*$^{-/-}$ mice differs from that in Dsg3-null animals. In the latter, hair loss occurs in wave-like patterns as the result of defective cell adhesion in the telogen phase of the hair cycle (Koch et al., 1998). Dsc1 is expressed in inner cell layers of the hair follicle (Chidgey et al., 1997; King et al., 1997), but despite extensive examination we found no abnormalities in timing of the hair cycle or in structure of hair follicles in *Dsc1*$^{-/-}$ mice of up to 4 wk of age. Hair loss occurred generally in older animals and was often associated with loss of normal hair follicle morphology and the presence of comedo-like structures (utriculi) and dermal cysts. Such structures characteristically result from hair follicle degeneration (Montagna et al., 1952; Mann, 1971; Panteleyev et al., 1998). Further work will be required to determine whether hair follicle degeneration is an indirect consequence of the hyperproliferative and inflammatory environment or whether Dsc1 has a role in the maintenance of normal follicle morphology.

In conclusion, the phenotype of *Dsc1*$^{-/-}$ mice demonstrates a role for this desmosomal glycoprotein in keratinocyte adhesion in the upper epidermis and in the normal function of the skin. Furthermore, our data suggest that Dsc1 contributes to the regulation of epidermal differentiation, and *Dsc1*$^{-/-}$ mice may prove useful in determining the role of desmosomes in skin disease.

Materials and methods

Isolation and characterization of the mouse *Dsc1* gene

Mouse 129SVJ λFixII (Stratagene) and PAC (RPCI21; UK HGMP Resource Centre) genomic libraries were screened with overlapping fragments of the mouse Dsc1 cDNA. Two unique nonoverlapping λ clones (λC1 and λC4) and one PAC clone (364c17) were characterized in detail. Intron sizes were determined by generating PCR products using synthetic oligonucleotide primers based on flanking exon sequences derived from the Dsc1 cDNA sequence (King et al., 1996). Exon-intron boundaries were determined by DNA sequencing and comparison with cDNA sequence.

Construction of a targeting vector and generation of Dsc1-null mice

To construct a targeting vector, a PvuII fragment from λC1, comprising 2.1 kb of DNA 5′ of the *Dsc1* initiation codon, was cloned upstream of a neomycin resistance gene under the control of a phosphoglycerate kinase promoter (Fig. 2 A). A 5.2-kb NotI (from the λFixII vector) to HindIII fragment from λC4, containing exons 2–5 of *Dsc1*, was cloned downstream of the neo gene. Vector DNA was linearized and electroporated into ES cells. Neomycin-resistant clones were isolated and screened by Southern blot analysis using BamHI-digested genomic DNA and a probe (1 kb), which hybridized to DNA 5′ to the homologous sequences used in the targeting vector (Fig. 2 A). One recombinant ES cell clone was injected into C57Bl/6J blastocysts, and the resulting chimeric male offspring were mated with female C57Bl/6J mice. Tail DNA from agouti offspring was tested for the presence of the mutated allele by Southern blot hybridization. Heterozygous mice were intercrossed to obtain mice, which were homozygous for the *Dsc1*-null allele.

RT-PCR

Newborn (2-d-old) mice were killed, and their skin was removed and immersed in 5 mM EDTA in PBS for 3 min at 50°C. The epidermis was peeled from the dermis, homogenized in Trizol reagent, and total RNA was prepared according to the manufacturer's instructions (Life Technologies). First strand cDNA synthesis was performed from RNA using a kit (Roche) and random primers. An aliquot (1 μl) of the first strand cDNA reaction was amplified using primers P1 (AGGGAGCACCTTCTCTAAGCAG) and P2 (AAGGCTCTTTGTCTACTCCTGG), specific for exons 1 and 5, respectively, and P3 (GGTCCATTTCCACAACACATT) and P4 (TGTACTTCAGACGAGTGTGTA), specific for exons 4 and 7, respectively. Glyceraldehyde-3-phosphate dehydrogenase primers (CLONTECH Laboratories, Inc.) were added to PCR reactions as a positive control.

Western blotting

Epidermis was isolated from 2-d-old mice as above and dissolved in sample buffer. Proteins were separated by SDS-polyacrylamide gel electrophoresis and transferred to polyvinylidene difluoride membrane (Amersham Pharmacia Biotech). Primary antibodies were JCMC (1:10,000) against Dsc1 (North et al., 1996), JB1 (1:500) against Dsc2 (Hyam, J.L.M., personal communication), rabbit anti–mouse Dsc3 (1:100; unpublished data; Liu, K., and D. Marshall, personal communication), DG3.10 (1:100) against Dsg1+2 (Progen), mouse anti–human PG (1:5,000; Transduction Laboratories), and 11–5F (1:40) against DP (Parrish et al., 1987). Primary antibodies were detected using appropriate peroxidase-conjugated secondary antibodies and the ECL detection system (Amersham Pharmacia Biotech).

Histological and immunochemical analysis

For histological analysis, tissues were fixed routinely in formol saline, embedded in paraffin, and stained with hematoxylin and eosin. Cell proliferation was examined in paraffin sections by staining for Ki67 (Gerdes et al., 1984). Expression of desmosomal constituents and differentiation markers were examined in frozen sections. Tissue was embedded in cryoprotectant (OCT; Miles), frozen in liquid nitrogen, and cryosections fixed in ice-cold methanol (5 min). Primary antibodies were JCMC (1:500), PAT-C (1:10) against Dsc2 (Messent et al., 2000), DG3.10 (1:50), PG-11E4 (1:100) against PG (Zymed Laboratories), 11–5F (1:25), MK1 (1:2,500) against keratin 1 (Covance), MK6 (1:2,500) against keratin 6 (Covance), MK14 (1:20,000) against keratin 14 (Covance), RPmK16 (1:500) against keratin 16 (Porter et al., 1998a), rat anti–mouse β_4 integrin (10 μg/ml; Pharmingen), PCD-1 (10 μg/ml) against P-cadherin (R & D Systems), rabbit antiinvolucrin (1:100; Covance), and rabbit antifilaggrin (1:1,000; Covance). Primary antibodies were detected with the appropriate FITC-conjugated secondary antibodies. Sections were examined using an Olympus BX49 microscope.

EM

Fresh skin was dissected into small pieces (~1 × 1 × 0.5 mm) and fixed by immersion in 2% formaldehyde (freshly made from paraformaldehyde powder) plus 2% glutaraldehyde in 0.1 M sodium cacodylate buffer (pH 7.3). Tissues were fixed for 2 h at room temperature and then washed four times with cacodylate buffer. They were then post-fixed with 1% osmium tetroxide for 2 h, dehydrated through an ethanol series, and embedded in Spurr's resin. Ultrathin sections were contrasted with uranyl acetate and lead citrate and examined on a Philips 400 electron microscope.

Analysis of skin barrier function

Dye penetration assays. These were performed as described by Hardman et al. (1998) and Marshall et al. (2000).

Passive diffusion of solutes. Samples of mouse back skin were clamped in continuous flow-through perfusion chambers. ^3H_2O (5 μCi/ml) and [^{14}C]mannitol (0.1 μCi/ml) were added to the donor compartment, and PBS (4 ml/h) was passed across the connective tissue side and collected hourly for up to 18 h. Samples were counted in a Beckman LS 6000 liquid scintillation counter, and a steady-state permeability constant (Kp) was determined in units of cm/min (Healy et al., 2000; Selvaratnam et al., 2001). Experiments were performed at 32°C.

TEWL. This was determined using a Tewameter (Courage and Khazaka). After decapitation or halothane anesthesia, a probe (1 cm diameter) was applied to the back of 2-d-old animals, and measurements of 1-min duration were taken.

Cornified envelope preparation

Epidermis from 2-d-old mice (see above) was heated to 95°C for 10 min in extraction buffer (0.1 M Tris-HCl, pH 8.5, 2% SDS, 20 mM dithiothreitol, and 5 mM EDTA), and the cornified envelopes were collected by centrifugation at 5,000 *g* for 15 min. The extraction was repeated once, and the envelopes were resuspended and stored in extraction buffer.

We are grateful to Dr. S. Andrew, Dr. E. Bell, Professor C.M. Griffiths, Dr. M. Hardman, Professor T. Hashimoto, Mr. D. Marshall, Mr. G. Morrissey, Mrs. J. Morrissey, and Miss Anjana Patel for help and advice.

The work was supported by the Wellcome Trust, Medical Research Council, and Royal Society.

Submitted: 1 May 2001
Revised: 22 August 2001
Accepted: 15 October 2001

References

Allen, E., Q.-C. Yu, and E. Fuchs. 1996. Mice expressing a mutant desmosomal cadherin exhibit abnormalities in desmosomes, proliferation, and epidermal differentiation. *J. Cell Biol.* 133:1367–1382.

Amagai, M. 1999. Autoimmunity against desmosomal cadherins in pemphigus. *J. Dermatol. Sci.* 20:92–102.

Amagai, M., K. Tsunoda, H. Suzuki, K. Nishifuji, S. Koyasu, and T. Nishikawa. 2000. Use of autoantigen-knockout mice in developing an active autoimmune disease model for pemphigus. *J. Clin. Invest.* 105:625–631.

Buxton, R.S., P. Cowin, W.W. Franke, D.R. Garrod, K.J. Green, I.A. King, P.J. Koch, A.I. Magee, D.A. Rees, J.R. Stanley, et al. 1993. Nomenclature of the desmosomal cadherins. *J. Cell Biol.* 121:481–483.

Charpentier, E., R.M. Lavker, E. Acquista, and P. Cowin. 2000. Plakoglobin suppresses epithelial proliferation and hair growth in vivo. *J. Cell Biol.* 149:503–519.

Chidgey, M.A.J., K.K.M. Yue, S. Gould, C. Byrne, and D.R. Garrod. 1997. Changing pattern of desmocollin 3 expression accompanies epidermal organisation during skin development. *Dev. Dyn.* 210:315–327.

Chitaev, N.A., and S.M. Troyanovsky. 1997. Direct Ca^{2+}-dependent heterophilic interaction between desmosomal cadherins, desmoglein and desmocollin, contributes to cell–cell adhesion. *J. Cell Biol.* 138:193–201.

Collins, J.E., P.K. Legan, T.P. Kenny, J. MacGarvie, J.L. Holton, and D.R. Garrod. 1991. Cloning and sequence analysis of desmosomal glycoproteins 2 and 3 (desmocollins): cadherin-like desmosomal adhesion molecules with heterogeneous cytoplasmic domains. *J. Cell Biol.* 113:381–391.

Denda, M., J. Sato, T. Tsuchiya, P.M. Elias, and K.R. Feingold. 1998. Low humidity stimulates epidermal DNA synthesis and amplifies the hyperproliferative response to barrier disruption: implication for seasonal exacerbations of inflammatory dermatoses. *J. Invest. Dermatol.* 111:873–878.

Dijan, P., K. Easley, and H. Green. 2000. Targeted ablation of the murine involucrin gene. *J. Cell Biol.* 151:381–387.

Garrod, D.R. 1995. Desmosomes and cancer. *In* Cancer Surveys. Vol. 24. Cell adhesion and cancer. I. Hart and N. Hogg, editors. Cold Spring Harbor Laboratory Press, New York. 97–111.

Garrod, D., M. Chidgey, and A. North. 1996. Desmosomes: differentiation, development, dynamics and disease. *Curr. Opin. Cell Biol.* 8:670–678.

Gerdes, J., H. Lemke, H. Baisch, H.H. Wacker, U. Schwab, and H. Stein. 1984. Cell cycle analysis of a cell proliferation-associated human nuclear antigen defined by the monoclonal antibody Ki-67. *J. Immunol.* 133:1710–1715.

Green, K.J., and C.A. Gaudry. 2000. Are desmosomes more than tethers for intermediate filaments? *Nat. Rev. Mol. Cell Biol.* 1:208–216.

Greenwood, M.D., M.D. Marsden, C.M.E. Cowley, V.K. Sahota, and R.S. Buxton. 1997. Exon-intron organisation of the human type 2 desmocollin gene (DSC2): desmocollin gene structure is closer to "classical" cadherins than to desmogleins. *Genomics.* 44:330–335.

Hardman, M.J., P. Sisi, D.N. Banbury, and C. Byrne. 1998. Patterned acquisition of skin barrier function during development. *Development.* 125:1541–1552.

Hashimoto, T., C. Kiyokawa, O. Mori, M. Miyasato, M.A.J. Chidgey, D.R. Garrod, Y. Kobayashi, K. Komori, K. Ishii, M. Amagai, et al. 1997. Human desmocollin 1 (Dsc1) is an autoantigen for the subcorneal pustular dermatosis type of IgA pemphigus. *J. Invest. Dermatol.* 109:127–131.

Hartfeld, M. 1999. The armadillo family of structural proteins. *Int. Rev. Cytol.* 186:179–224.

Healy, C.M., A.T. Cruchley, M.H. Thornhill, and D.M. Williams. 2000. The effect of sodium lauryl sulphate, triclosan and zinc on the permeability of normal oral mucosa. *Oral Diseases.* 6:118–123.

Hunt, D.M., V.K. Sahota, K. Taylor, D. Simrak, N. Hornigold, J. Arnemann, J. Wolfe, and R.S. Buxton. 1999. Clustered cadherin genes: a sequence-ready contig for the desmosomal cadherin locus on human chromosome 18. *Genomics.* 62:445–455.

Jensen, J.-M., S. Schütze, C. Neumann, and E. Proksch. 2000. Impaired cutaneous permeability barrier function, skin hydration, and sphingomyelinase activity in keratin 10 deficient mice. *J. Invest. Dermatol.* 115:708–713.

King, I.A., T.J. O'Brien, and R.S. Buxton. 1996. Expression of the "skin-type" desmosomal cadherin DSC1 is closely linked to the keratinization of epithelial tissues during mouse development. *J. Invest. Dermatol.* 107:531–538.

King, I.A., B.D. Angst, D.M. Hunt, M. Kruger, J. Arnemann, and R.S. Buxton. 1997. Hierarchical expression of desmosomal cadherins during stratified epithelial morphogenesis in the mouse. *Differentiation.* 62:83–96.

Koch, P.J., M.G. Mahoney, H. Ishikawa, L. Pulkkinen, J. Uitto, L. Shultz, G.F. Murphy, D. Whitaker-Menezes, and J.R. Stanley. 1997. Targeted disruption of the pemphigus vulgaris antigen (desmoglein 3) gene in mice causes loss of keratinocyte cell adhesion with a phenotype similar to pemphigus vulgaris. *J. Cell Biol.* 137:1091–1102.

Koch, P.J., M.G. Mahoney, G. Cotsarelis, K. Rothenberger, R.M. Lavker, and J.R. Stanley. 1998. Desmoglein 3 anchors telogen hair in the follicle. *J. Cell Sci.* 111:2529–2537.

Koch, P.J., P.A. de Viragh, E. Scharer, D. Bundman, M.A. Longley, J. Bickenbach, Y. Kawachi, Y. Suga, Z. Zhou, M. Huber, et al. 2000. Lessons from loricrin-deficient mice: compensatory mechanisms maintaining skin barrier function in the absence of a major cornified envelope protein. *J. Cell Biol.* 151:389–400.

Legan, P.K., K.K.M. Yue, M.A.J. Chidgey, J.L. Holton, R.W. Wilkinson, and D.R. Garrod. 1994. The bovine desmocollin family: a new gene and expression patterns reflecting epithelial cell proliferation and differentiation. *J. Cell Biol.* 126:507–518.

Mahoney, M.G., Z. Wang, K. Rothenberger, P.J. Koch, M. Amagai, and J.R. Stanley. 1999. Explanation for the clinical and microscopic localization of lesions in pemphigus foliaceus and vulgaris. *J. Clin. Invest.* 103:461–468.

Mann, S.J. 1971. Hair loss and cyst formation in hairless and rhino mutant mice. *Anat. Rec.* 170:485–500.

Marcozzi, C., I.D.J. Burdett, R.S. Buxton, and A.I. Magee. 1998. Coexpression of both types of desmosomal cadherin and plakoglobin confers strong intercellular adhesion. *J. Cell Sci.* 111:495–509.

Marshall, D., M.J. Hardman, and C. Byrne. 2000. SPRR1 gene induction and barrier formation occur as coordinated moving fronts in terminally differentiating epithelia. *J. Invest. Dermatol.* 114:967–975.

Messent, A.J., M.J. Blisset, G.L. Smith, A.J. North, A. Magee, D. Foreman, D.R. Garrod, and M. Boulton. 2000. Expression of a single pair of desmosomal glycoproteins renders the corneal epithelium unique amongst stratified epithelia. *Invest. Ophthalmol. Vis. Sci.* 41:8–15.

Montagna, W., H.B. Chase, and H.P. Melarango. 1952. The skin of hairless mice. The formation of cysts and the distribution of lipids. *J. Invest. Dermatol.* 19: 83–94.

North, A.J., M.A.J. Chidgey, J.P. Clarke, W.G. Bardsley, and D.R. Garrod. 1996. Distinct desmocollin isoforms occur in the same desmosomes and show reciprocally graded distributions in bovine nasal epidermis. *Proc. Natl. Acad. Sci. USA.* 93:7701–7705.

Nuber, U.A., S. Schafer, S. Stehr, H.-R. Rackwitz, and W.W. Franke. 1996. Patterns of desmocollin synthesis in human epithelia: immunolocalization of desmocollins 1 and 3 in special epithelia and in cultured cells. *Eur. J. Cell Biol.* 71:1–13.

Osada, K., M. Seishima, and Y. Kitajima. 1997. Pemphigus IgG activates and translocates protein kinase C from the cytosol to the particulate/cytoskeleton fractions in human keratinocytes. *J. Invest. Dermatol.* 108:482–487.

Panteleyev, A.A., C. van der Veen, T. Rosenbach, S. Müller-Röver, V. Sokolov, and R. Paus. 1998. Towards defining the pathogenesis of the *hairless* phenotype. *J. Invest. Dermatol.* 110:902–907.

Parrish, E.P., P.V. Steart, D.R. Garrod, and R.O. Weller. 1987. Antidesmosomal monoclonal antibody in the diagnosis of intracranial tumors. *J. Pathol.* 153: 265–273.

Porter, R.M., A.M. Hutcheson, E.L. Rugg, R.A. Quinlan, and E.B. Lane. 1998a. cDNA cloning, expression, and assembly characteristics of mouse keratin 16.

J. Biol. Chem. 275:32265–32272.

Porter, R.M., J. Reichelt, D.P. Lunny, T.M. Magin, and E.B. Lane. 1998b. The relationship between hyperproliferation and epidermal thickening in a mouse model for BCIE. *J. Invest. Dermatol.* 110:951–957.

Proksch, E., K.R. Feingold, M. Mao-Qiang, and P.M. Elias. 1991. Barrier function regulates epidermal DNA synthesis. *J. Clin. Invest.* 87:1668–1673.

Prowse, D.M., D. Lee, L. Weiner, N. Jiang, C.M. Magro, H.P. Baden, and J.L. Brissette. 1999. Ectopic expression of the *nude* gene induces hyperproliferation and defects in differentiation: implications for the self-renewal of cutaneous epithelia. *Devl. Biol.* 212:54–67.

Robinson, N.A., S. Lapic, J.F. Welter, and R.L. Eckert. 1997. S100A11, S100A10, annexin1, desmosomal proteins, small proline-rich proteins, plasminogen activator inhibitor-2, and involucrin are components of the cornified envelope of cultured human epidermal keratinocytes. *J. Biol. Chem.* 272:12035–12046.

Schermer, A., J.V. Jester, C. Hardy, D. Milano, and T.-T. Sun. 1989. Transient synthesis of K6 and K16 keratins in regenerating rabbit corneal epithelium: keratin markers for an alternative pathway of keratinocyte differentiation. *Differentiation.* 42:103–110.

Sellheyer, K., J.B. Bickenbach, J.A. Rothnagel, D. Bundman, M.A. Longley, T. Krieg, N.S. Roche, A.B. Roberts, and D.R. Roop. 1993. Inhibition of skin development by overexpression of transforming growth factor β_1 in the epidermis of transgenic mice. *Proc. Natl. Acad. Sci. USA.* 90:5237–5241.

Selvaratnam, L., A.T. Cruchley, H. Navsaria, P. Wertz, E. Hagi-Pavli, I.M. Leigh, C.A. Squier, and D.M. Williams. 2001. Oral keratinocytes develop a functional and biochemical permeability barrier similar to intact oral mucosa. *Oral Diseases.* 7:252–258.

Shimizu, H., T. Masunaga, A. Ishiko, A. Kikuchi, T. Hashimoto, and T. Nishikawa. 1995. Pemphigus vulgaris and pemphigus foliaceus sera show an inversely graded binding pattern to extracellular regions of desmosomes in different layers of human epidermis. *J. Invest. Dermatol.* 105:153–159.

Shinohara, M., A. Hiraki, T. Ikebe, S. Nakamura, S.-I. Kurahara, K. Shirasuna, and D.R. Garrod. 1998. Immunohistochemical study of desmosomes in oral squamous cell carcinoma: correlation with cytokeratin and E-cadherin staining, and with tumour behaviour. *J. Pathol.* 184:369–381.

Suga, Y., M. Jarmick, P.S. Attar, M.A. Longley, D. Bundman, A.C. Steven, P.J. Koch, and D.R. Roop. 2000. Transgenic mice expressing a mutatant form of loricrin reveal the molecular basis of the skin diseases, Vohwinkel syndrome and progressive symmetric erythrokeratoderma. *J. Cell Biol.* 151: 401–412.

Tselepis, C., M. Chidgey, A. North, and D. Garrod. 1998. Desmosomal adhesion inhibits invasive behavior. *Proc. Natl. Acad. Sci. USA.* 95:8064–8069.

Wallis, S., S. Lloyd, I. Wise, G. Ireland, T.P. Fleming, and D. Garrod. 2000. The α isoform of protein kinase C is involved in signaling the response of desmosomes to wounding in cultured epithelial cells. *Mol. Biol. Cell.* 11:1077–1092.

Whitby, D.J., and M.W.J. Ferguson. 1991. The extracellular matrix of lip wounds in fetal, neonatal and adult mice. *Development.* 112:651–668.

Whittock, N.V., D.M. Hunt, L. Rickman, S. Malhi, A.P. Vogazianou, L.F Dawson, R.A.J. Eady, R.S Buxton, and J.A. McGrath. 2000. Genomic organisation and amplification of the human desmosomal cadherin genes *DSC1* and *DSC3*, encoding desmocollin types 1 and 3. *Biochem. Biophys Res. Comm.* 276:455–460.

Neuron, Vol. 33, 789–804, February 28, 2002, Copyright ©2002 by Cell Press

Decreased Synaptic Vesicle Recycling Efficiency and Cognitive Deficits in Amphiphysin 1 Knockout Mice

Gilbert Di Paolo,[1,2]
Sethuraman Sankaranarayanan,[5]
Markus R. Wenk,[1,2] Laurie Daniell,[1,2] Ezio Perucco,[6]
Barbara J. Caldarone,[4] Richard Flavell,[1,3]
Marina R. Picciotto,[4] Timothy A. Ryan,[5]
Ottavio Cremona,[6,7] and Pietro De Camilli[1,2,8]
[1]Howard Hughes Medical Institute
[2]Department of Cell Biology
[3]Sections of Immunology
[4]Department of Psychiatry
Yale University School of Medicine
New Haven, Connecticut 06510
[5]Department of Biochemistry
The Weill Medical College of Cornell University
New York, New York 10021
[6]Dipartimento di Scienze Mediche
Università del Piemonte Orientale "A. Avogadro"
28100 Novara
[7]Università Vita-Salute San Raffaele
Milano, San Raffaele Scientific Institute
20132 Milano
Italy

Summary

The function of the clathrin coat in synaptic vesicle endocytosis is assisted by a variety of accessory factors, among which amphiphysin (amphiphysin 1 and 2) is one of the best characterized. A putative endocytic function of amphiphysin was supported by dominant-negative interference studies. We have now generated amphiphysin 1 knockout mice and found that lack of amphiphysin 1 causes a parallel dramatic reduction of amphiphysin 2 selectively in brain. Cell-free assembly of endocytic protein scaffolds is defective in mutant brain extracts. Knockout mice exhibit defects in synaptic vesicle recycling that are unmasked by stimulation and suggest impairments at multiple stages of the cycle. These defects correlate with increased mortality due to rare irreversible seizures and with major learning deficits, suggesting a critical role of amphiphysin for higher brain functions.

Introduction

Neurotransmission relies on a tightly regulated balance between synaptic vesicle exocytosis and endocytosis to maintain a pool of functional synaptic vesicles. A major pathway through which synaptic vesicle membranes can be recycled is clathrin-mediated endocytosis (Cremona and De Camilli, 1997; Brodin et al., 2000). Following depolarization-mediated synaptic vesicle fusion at active zones, membrane retrieval occurs either by the formation of individual clathrin-coated vesicles or by bulk invagination of the plasmalemma to generate endosome-like structures from which clathrin-coated vesicles originate. Once clathrin-coated vesicles have pinched off, they rapidly shed their coat and are directed back to the cluster of synaptic vesicles, from where they can be mobilized for subsequent rounds of release. Recently, a variety of accessory factors thought to assist the clathrin coat in its function have been identified. These include proteins that affect membrane dynamics by direct physical interaction, lipid metabolizing enzymes, regulatory components of the actin cytoskeleton, signaling proteins, and adaptor proteins that link these factors to each other and to the clathrin coat (reviewed in Marsh and McMahon, 1999; Owen and Luzio, 2000; Slepnev and De Camilli, 2000).

In nerve terminals, clathrin-mediated endocytosis occurs at sites that are spatially segregated from sites of exocytosis (Heuser and Reese, 1973; Gad et al., 1998; Teng and Wilkinson, 2000). These endocytic zones form a belt around the active zones of secretion and are regions where components of the endocytic machinery are concentrated (Roos and Kelly, 1999). They are also enriched in actin (Gad et al., 2000; Dunaevsky and Connor, 2000), consistent with evidence that several clathrin accessory factors may be components of protein scaffolds that regulate the actin cytoskeleton (reviewed in Geli and Riezman, 1998; Qualmann et al., 2000; Slepnev and De Camilli, 2000). For instance, the GTPase dynamin, which plays a critical role in fission, also interacts with actin binding proteins and may affect actin dynamics at the synapse through these interactions (Witke et al., 1998; Qualmann et al., 1999; McNiven et al., 2000; Ochoa et al., 2000). The polyphosphoinositide phosphatase synaptojanin 1 hydrolyzes a pool of phosphatidylinositol-4,5-bisphosphate [PI(4,5)P_2] that participates both in clathrin coat recruitment and in actin polymerization at endocytic zones in nerve terminals (Cremona et al., 1999; Gad et al., 2000; Harris et al., 2000). Syndapin/pacsin and DAP160/intersectin, which bind dynamin 1 and synaptojanin 1, are also involved in actin function via an interaction with regulatory components (WASP and Cdc42, respectively) of the Arp2/3 actin nucleating complex (Roos and Kelly, 1998; Qualmann et al., 1999; Modregger et al., 2000; Hussain et al., 2001; Wasiak et al., 2001).

One of the best characterized clathrin accessory factors is amphiphysin (reviewed in Wigge and McMahon, 1998). The amphiphysin protein family is conserved from yeast to man and has a three domain structure (see Figure 3A): an NH_2-terminal BAR (Bin-Amphiphysin-Rvs) domain (Elliott et al., 1999), which mediates binding to acidic phospholipids (Takei et al., 1999; Farsad et al., 2001) and homo/heterodimerization (Wigge et al., 1997a; Slepnev et al., 1998; Ramjaun et al., 1999), a central variable domain, and a COOH-terminal Src homology 3 (SH3) domain that interacts with dynamin 1 and synaptojanin 1 (David et al., 1996; McPherson et al., 1996). Two isoforms of amphiphysin, amphiphysin 1 and 2, are expressed in mammals. Amphiphysin 1 is primarily expressed in brain and is the dominant target of autoimmunity in human paraneoplastic Stiff-man syndrome (De Camilli et al., 1993). Amphiphysin 2 is more widely ex-

*Correspondence: pietro.decamilli@yale.edu

pressed as alternatively spliced isoforms, with the highest levels found in brain and striated muscle (Butler et al., 1997; Leprince et al., 1997; Ramjaun et al., 1997; Wechsler-Reya et al., 1997; Wigge et al., 1997a). The predominant neuronal isoforms of amphiphysin 2 form heterodimers with amphiphysin 1 and the heterodimer is concentrated in nerve terminals (Wigge et al., 1997a; Ramjaun et al., 1997), where it is localized in the presynaptic cytomatrix and is further enriched on coated endocytic intermediates (Bauerfeind et al., 1997). Both components of this heterodimer contain in their central region binding sites for clathrin and AP-2 (McMahon et al., 1997; Ramjaun and McPherson, 1998; Slepnev et al., 2000), while the muscle isoform of amphiphysin 2 lacks the clathrin and AP-2 binding sites, suggesting functions for these isoforms independent of the clathrin coat. Similarly, *Drosophila* amphiphysin lacks clathrin coat binding sites (Razzaq et al., 2000; Leventis et al., 2001). Additional proteins that contain a BAR domain, but are otherwise different from amphiphysin in their domain structure, are expressed in mammals and other organisms (Crouzet et al., 1991; Ge and Prendergast, 2000; Routhier et al., 2001).

A function for amphiphysin in synaptic vesicle endocytosis is supported by several lines of evidence in addition to its localization and biochemical interaction with other endocytic proteins. Expression or microinjection of amphiphysin fragments that compete for the binding of this protein to any of its major partners, such as dynamin, AP-2, and clathrin, strongly inhibits clathrin-mediated endocytosis, possibly by titrating out these factors, thus demonstrating that these interactions can occur in vivo (Shupliakov et al., 1997; Wigge et al., 1997b; Slepnev et al., 2000). More importantly, presynaptic microinjection of peptides that bind the SH3 domain of amphiphysin, and therefore compete its SH3-dependent interactions, also severely impair synaptic vesicle endocytosis (Shupliakov et al., 1997). The interaction of amphiphysin with dynamin affects dynamin's enzymatic activity and oligomeric state (Wigge et al., 1997a; Owen et al., 1998; Takei et al., 1999). Furthermore, the interaction of amphiphysin with dynamin and other endocytic partners in enhanced by nerve terminal depolarization via Ca^{2+}-dependent dephosphorylation, when a burst of endocytic activity is needed (Bauerfeind et al., 1997; Slepnev et al., 1998). Finally, amphiphysin binds and deforms lipid bilayers and may, therefore, facilitate membrane deformations that accompany vesicle budding (Takei et al., 1999; Farsad et al., 2001).

Additional evidence for a role of amphiphysin in endocytosis comes from studies in *Saccaromyces cerevisiae*. In this organism, the homolog of amphiphysin, Rvs167, forms a heterodimer with Rvs161—a protein that comprises a BAR domain only (Crouzet et al., 1991; Lombardi and Riezman, 2001). Although neither gene is essential, mutations in either one of them produce endocytic defects that correlate with a disruption of the actin cytoskeleton (Sivadon et al., 1995). Collectively, these observations suggest that amphiphysin may have an important role in the physiology of endocytic zones of synapses. It may act as a multifunctional adaptor that links cytosolic proteins to the membranes and coordinates the function of clathrin coat proteins, other accessory factors, and the actin cytoskeleton.

In this study, we have used a genetic approach to investigate the role of amphiphysin in synaptic physiology. We have generated mice that lack the expression of amphiphysin 1 and, as an unexpected consequence, also lack brain amphiphysin 2. These mice exhibit synaptic vesicle recycling defects that are compatible with the basic function of the nervous system. However, the mice are prone to seizures, which dramatically decrease their viability, and exhibit severe learning deficits.

Results

Inactivation of the Amphiphysin 1 Gene and Resulting Loss of Both Amphiphysin 1 and 2 in Brain

The amphiphysin 1 gene was disrupted by insertion of a gene encoding a selection marker (neo cassette) in the first coding exon (Figure 1A). The occurrence of correct recombination events was confirmed by Southern blot analysis of ES cells and F2 mice (Figure 1B). Homozygous mutant animals were born, and their genotypes had normal mendelian distribution, revealing lack of embryonic lethality. They did not exhibit any obvious anatomical or histological changes and appeared to develop and reproduce normally, although they displayed an increased mortality rate after reaching adulthood (see below). The expression of the amphiphysin 1 protein was completely abolished in homozygous mutant animals, as shown by Western blotting analysis of brain extracts using a panel of poly- and monoclonal antibodies directed against either the COOH- or the NH_2-terminal region of amphiphysin 1 (Figure 1C and data not shown; see also Figure 2B).

Interestingly, Western blot analysis revealed that expression of amphiphysin 2 was also nearly abolished in the brain of amphiphysin 1-deficient animals (Figure 1C), regardless of the developmental stage of mutant animals (data not shown). No change in the expression level of a variety of other synaptic proteins was observed, including the major interacting partners of amphiphysin such as dynamin 1, synaptojanin 1, clathrin, and the clathrin adaptor AP-2. Levels of intrinsic membrane proteins of synaptic vesicles were also unchanged (Figure 1C and data not shown). The parallel disappearance of amphiphysin 1 and 2 was confirmed by immunofluorescence staining of brain frozen sections (data not shown) and of cortical neurons in culture (Figure 1D). While amphiphysin 1 and 2 colocalize with the synaptic marker synaptophysin in wild-type neurons, the immunoreactivity for both proteins, but not for synaptophysin, is absent in knockout neurons (Figure 1D and data not shown). By Northern blot analysis expression levels of the 2.2 kb transcript encoding amphiphysin 2 were comparable in wild-type and knockout brain (Figure 2A), suggesting that transcriptional mechanisms do not account for the downregulation of amphiphysin 2 in mutant brain. In skeletal muscle, where a shorter isoform of amphiphysin 2 is expressed and where amphiphysin 1 is undetectable (Figure 2B and see also Butler et al., 1997; Wigge et al., 1997a), amphiphysin 2 protein levels were not affected (Figure 2B). These data suggest that amphiphysin 1 is required for the stability of amphiphysin 2 only in neurons, where the two isoforms are primarily found as heterodimers and colocalize accordingly (Figure 2C; see also Ramjaun et al., 1997; Wigge et al., 1997a; Slepnev et al., 1998).

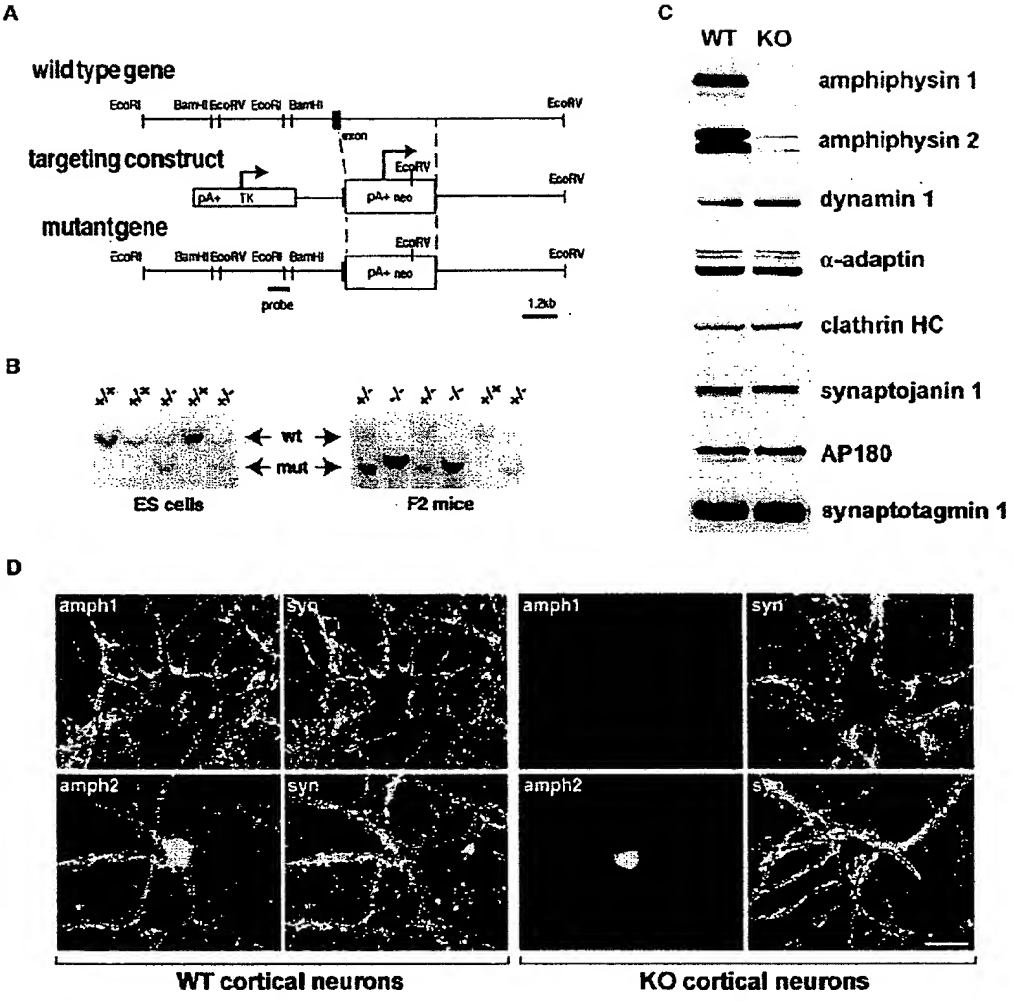

Figure 1. Generation of Amphiphysin 1 Knockout Mice and Downregulation of Amphiphysin 2 Expression

(A) Schematic diagram showing the amphiphysin 1 gene locus, the targeting vector, and the mutant allele following homologous recombination. The neo cassette substitutes part of the first coding exon and part of the following intron. The EcoRV restriction sites and the probe used for the Southern blot analysis are indicated.

(B) Southern blot of EcoRV-digested genomic DNA from wild-type (+/+) and heterozygous (+/−) ES cell clones and from wild-type (+/+), heterozygous (+/−), and homozygous mutant mice (−/−) of the F2 generation.

(C) Western blot of brain extracts from wild-type and knockout mice with antibodies directed against either amphiphysin 1 or 2 or several other synaptic proteins, including major interacting partners of amphiphysin 1 (HC, heavy chain). The knockout extract contains no amphiphysin 1 and drastically reduced levels of amphiphysin 2.

(D) Double immunofluorescence of primary cultures of cortical neurons prepared from the brain of wild-type and knockout mice. Sections were stained for either amphiphysin 1 or 2 (amph) and counterstained for the presynaptic marker synaptophysin (syn). Lack of amphiphysin 1 expression correlates with loss of amphiphysin 2 immunoreactivity in knockout neurons. Residual immunoreactivity found in the nucleus may represent a nuclear pool of amphiphysin 2 (Wechsler-Reya et al., 1997). Scale bar = 15 μm.

Defective Cell-Free Assembly of Endocytic Protein Complexes in Brain Extracts of Amphiphysin 1 Knockout Mice

The properties of the amphiphysin 1/2 heterodimer to bind and deform lipid bilayers (Takei et al., 1999) and to interact with several endocytic proteins (Figure 3A; see also Wigge and McMahon, 1998) suggest that it functions as a multifunctional adaptor at the membrane. We tested this putative function of amphiphysin by determining in cell-free reactions whether the formation of complexes among these proteins, or between these proteins and lipid bilayers, was affected by the lack of the amphiphysin 1/2 heterodimers from brain cytosol. Liposomes composed of total brain lipids were incubated with cytosol from wild-type and mutant brain in the presence of nucleotides (Cremona et al., 1999; Gad et al., 2000). Proteins bound to membranes were then isolated by ultracentrifugation and analyzed by quantita-

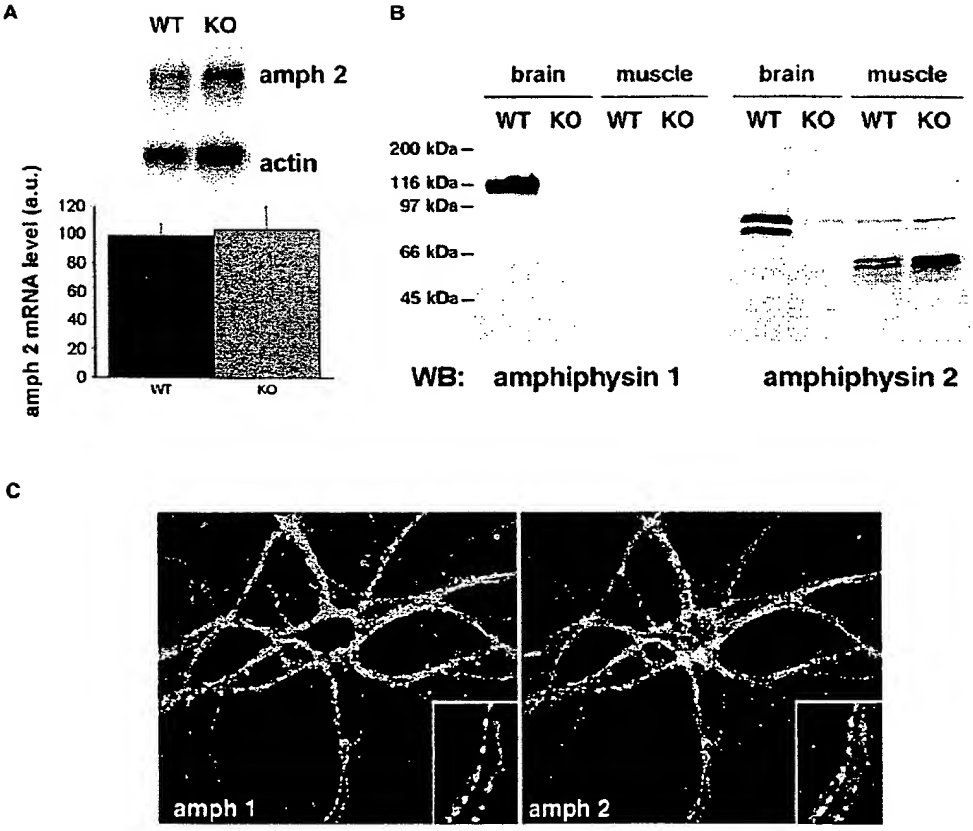

Figure 2. Selective Loss of Amphiphysin 2 in Brain where Amphiphysin 1 and 2 Form Heterodimers and Colocalize

(A) Northern blot analysis showing normal levels of amphiphysin 2 mRNA in knockout brain. Actin mRNA was used as a control for loading. mRNA levels were quantified by phosphoimaging, and amphiphysin 2 mRNA levels were normalized to those of actin mRNA ($n = 2$).

(B) Western blot analysis of brain and skeletal muscle extracts from wild-type and knockout mice using anti-amphiphysin 1 and anti-amphiphysin 2 antibodies. While amphiphysin 1 is only detected in brain, amphiphysin 2 is expressed at high levels in both brain and skeletal muscle, but as isoforms of different molecular weight. In mutant mice, the downregulation of amphiphysin 2 expression levels occurs selectively in brain.

(C) Double immunofluorescence of cultured cortical neurons from wild-type mice showing precise colocalization of amphiphysin 1 with amphiphysin 2 at synaptic sites. Inset: higher magnification.

tive immunoblotting along with proteins in the starting cytosols. While levels of all proteins examined were the same in the starting cytosol (data not shown), the recovery of clathrin (heavy chain) and AP-2 (α-adaptin) in the "bound" fraction was reduced by 40% and 25%, respectively, in mutant extract relative to wild-type extract (Figures 3B and 3C). A 40% decrease in the recovery of the polyphosphoinositide phosphatase synaptojanin 1 was also observed. Accordingly, incubation of the pelleted liposomes in the presence of ^{32}P-labeled ATP after the binding reaction resulted in an increased level of [^{32}P]-PI(4,5)P_2, most likely reflecting altered PI(4,5)P_2 turnover due to decreased synaptojanin 1-mediated PI(4,5)P_2 hydrolysis (Figure 3D). The recovery of dynamin 1 in the "bound" fraction of liposomes was not affected by the lack of amphiphysin 1 (Figure 3B and 3C). This observation most likely reflects, at least in part, the direct binding of dynamin to lipid membranes via both its pleckstrin homology (PH) domain and the recently identified additional lipid binding site (Burger et al., 2000). As it was shown previously, although amphiphysin does not enhance dynamin recruitment to liposomes, it affects the morphology and the properties of dynamin oligomers at the surface of liposomes (Takei et al., 1999).

We further investigated the potential adaptor function of amphiphysin in the assembly of endocytic proteins in brain, by performing affinity chromatography of a detergent brain extract from wild-type and knockout mice on the COOH-terminal proline-rich tail of dynamin 1 (GST-PRD)—i.e., the amphiphysin binding domain of dynamin. The use of wild-type extracts for these experiments leads to the affinity purification not only of amphiphysin 1 and 2 and other direct interactors of dynamin's tail, such as endophilin and intersectin, but also of clathrin and AP-2 (Figure 3A; see also Slepnev et al., 1998). Immunoblotting of the affinity-purified material revealed a reduction in AP-2 (α-adaptin) and clathrin

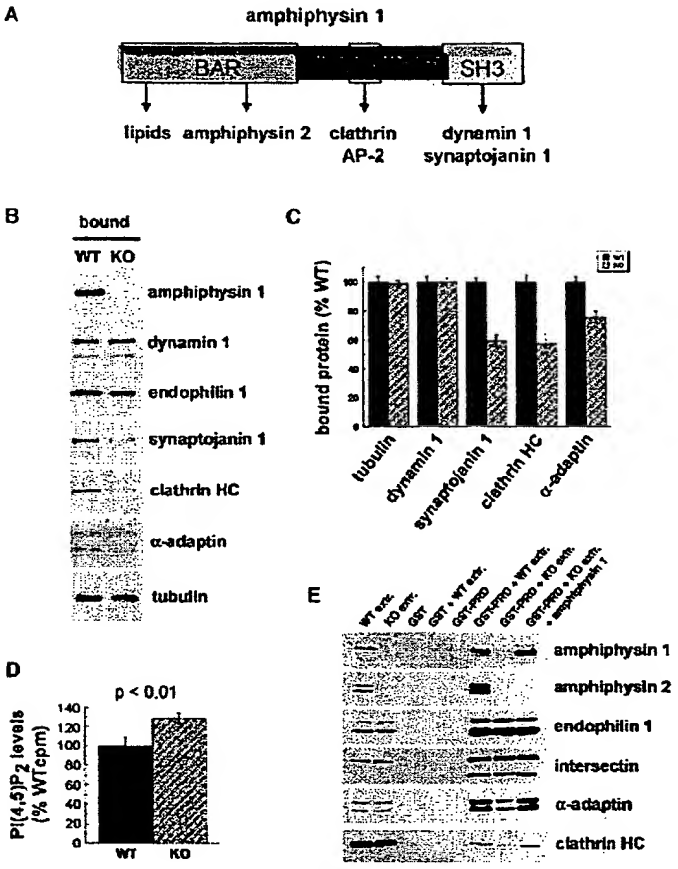

Figure 3. Evidence for a Role of Amphiphysin as an Adaptor Protein in the Recruitment of Cytosolic Endocytic Complexes

(A) Schematic drawing depicting the structure of amphiphysin 1 and its interactors.

(B and C) Recovery of endocytic proteins on liposomes following their incubation with brain cytosol from wild-type and knockout mice in the presence of ATP and GTP. Representative Western blots are shown in (B), and a quantification by phosphoimaging of results from three experiments is shown in (C). Note the absence of amphiphysin 1 and the selective decrease of clathrin, AP-2 (α-adaptin subunit), and synaptojanin 1 in the "bound" material from knockout animals.

(D) Quantification of ^{32}P incorporation into $PI(4,5)P_2$ in liposomes that were first incubated with brain cytosol in the presence of GTP and cold ATP, washed, and subsequently incubated with [$\gamma^{32}P$]ATP. Decreased recovery of synaptojanin 1 in membranes shown in (B) and (C) correlates with increased labeling of $PI(4,5)P_2$.

(E) Western blot analysis of a representative affinity chromatography experiment from wild-type and mutant brain extracts on GST alone, or GST fused to the proline-rich domain (PRD) of dynamin 1. The first two lanes show starting material from both genotypes. Mock affinity purifications (lack of extract) are included as indicated. The knockout brain extract used for the last lane was supplemented with recombinant amphiphysin 1 at physiological concentration. The PRD of dynamin affinity purifies less clathrin and AP-2 from knockout cytosol and exogenous amphiphysin 1 rescues the effect.

Values in (C) and (D) denote means ± SD. The p value from a Student's t test analysis is indicated.

binding, but not in that of endophilin and intersectin, when brain extracts from knockout animals were used (Figure 3E), consistent with a bridging function of amphiphysin. This decrease was rescued by the addition to the knockout extract of recombinant amphiphysin 1 at physiological concentration prior to affinity purification. Collectively, these results provide strong evidence for a role of amphiphysin in the assembly of endocytic complexes at the membrane.

Decreased Stimulus-Dependent Labeling of Synaptic Vesicles Following a "Pulse" Incubation with an Endocytic Tracer

In spite of the biochemical results described above, no obvious ultrastructural differences were observed by electron microscopy in synapses of wild-type and mutant neurons both in brain tissue or in cultures. No accumulation of endocytic intermediates was observed in mutant synapses and the number of synaptic vesicles per synapse was the same in the two genotypes (data not shown). To assess the possible occurrence of synaptic vesicle recycling defects that could be unmasked by stimulation, we used two distinct and complementary approaches.

First, we performed experiments on cerebral cortex synaptosomes. This preparation allows for the analysis of exo- and endocytosis on a global synaptic population, thus avoiding possible bias due to uneven neuronal sampling. Furthermore, synaptosomes, in contrast to neuronal cultures (see below), reflect the properties of synapses in the adult brain. Using a well established fluorimetry-based glutamate release assay (Nicholls and Sihra, 1986), we found no difference in the kinetics or amount of glutamate release between wild-type and knockout synaptosomes upon high K^+ stimulation, which points to a normal exocytic function in knockout synapses (Figures 4A and 4B). Fluorescent amphipathic styryl dyes were then used to study synaptic vesicle recycling. We employed FM2-10 for these experiments, because it has the fastest "off rate" among commonly used styryl dyes and was shown to give a good signal-to-noise ratio in synaptosomes (Cousin and Robinson, 1998; Marks and McMahon, 1998; Cousin and Robinson, 2000). We started by determining the ability of synaptosomes to internalize the dye into vesicular compartments in a stimulation-dependent fashion. Briefly, synaptosomes were preincubated with FM2-10 and depolarized for 90 s by the addition of high K^+ in the continued presence of dye. Then, after a brief wash, synaptosomes were hypotonically lysed, subjected to low-speed centrifugation, and the fluorescence trapped

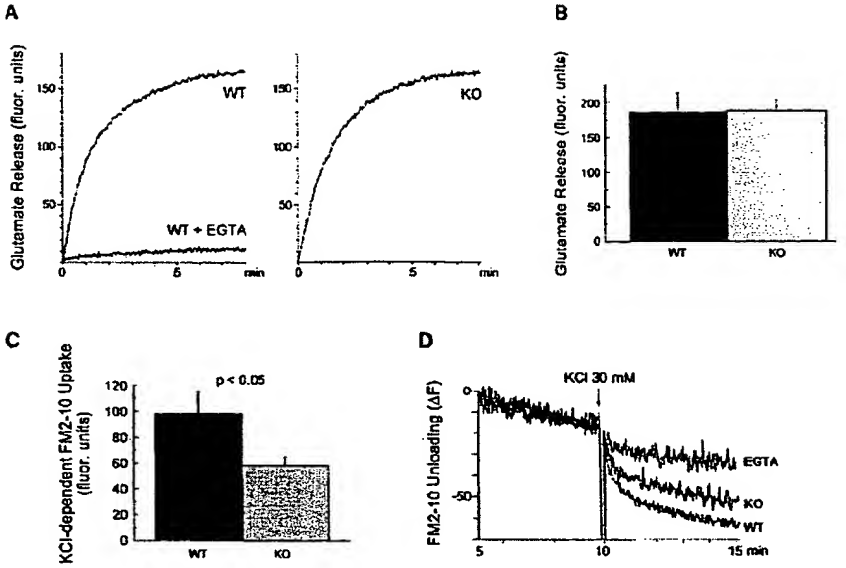

Figure 4. Normal Glutamate Release but Defective Recycling of FM2-10 in Knockout Mice

(A) Fluorimetric tracings of wild-type and knockout synaptosomes showing comparable Ca^{2+}-dependent glutamate release for both genotypes after stimulation with 30 mM KCl.

(B) Quantification of total glutamate release after stimulation with 30 mM KCl for 8 min.

(C) Recovery of FM2-10 in a low speed supernatant of lysed synaptosomes after a first round of stimulation with 30 mM KCl in the presence of dye. The amount of dye trapped in this fraction (endosomes and small vesicles) was smaller in mutant synaptosomes.

Values in (B) and (C) denote means ± SEM (n = 3). The p value from a Student's t test analysis is indicated.

(D) Fluorimetric tracing of wild-type and knockout synaptosomes showing high K^+-dependent unloading of FM2-10 following a first round of stimulation in the presence of dye and a 10 min incubation in dye-free low K^+ to allow for recycling of the dye into the releasable vesicle pool. A tracing showing dye unloading of wild-type synaptosomes in the presence of 2 mM EGTA is also shown.

within membranous organelles of the supernatant, which include primarily endosomes and small vesicles, was measured by fluorimetry. This assay revealed a 40% decrease in the depolarization-dependent internalization of dye in knockout synaptosomes, compared to wild-type synaptosomes (Figure 4C). In the next series of experiments, synaptosomes were stimulated for 90 s in the presence of dye, further incubated for 10 min in dye-free medium to allow for chasing of the dye into releasable synaptic vesicles, and finally exposed to a second high K^+ incubation to induce exocytotic release of the dye. Under these assay conditions, knockout synaptosomes released significantly less FM2-10 than wild-type synaptosomes (Figure 4D), suggesting that synaptic vesicle recycling efficiency is also reduced in amphiphysin 1-deficient nerve terminals.

Second, we used electron microscopy in combination with the fluid-phase uptake of the endocytic marker horseradish peroxidase (HRP) to monitor formation of endocytic intermediates in cultured cortical neurons (Heuser and Reese, 1973). Neurons were grown in culture for at least 2 weeks to allow for the formation of numerous synaptic contacts (see Figure 1D). They were then preincubated with HRP for 3 min, stimulated with high K^+ for 90 s (or mock-incubated in low K^+) in the continued presence of the tracer, fixed, and processed for electron microscopy analysis. High K^+ stimulation produced a significant increase in the HRP labeling of synaptic vesicles and endosomal structures as expected (Figure 5A). However, morphometric analysis indicated that the fraction of HRP-labeled synaptic vesicles and endosome-like structures was significantly reduced in knockout synapses relative to wild-type after stimulation, demonstrating the occurrence of a recycling defect in knockout animals (Figures 5B and 5C). No statistical difference in the number of labeled organelles was found under resting conditions (Figures 5B and 5C).

Smaller Recycling Vesicle Pool Size, Slower Destaining Kinetics, and Delayed Vesicle Repriming in Mutant Nerve Terminals

The reduced stimulus-dependent dye uptake into vesicular compartments described above could be explained by a delayed endocytic uptake of the tracers but also by a smaller size of the recycling pool of synaptic vesicles. Although the number of vesicles per synapse appears to be normal, the functional recycling pool could be smaller. To determine the possible contribution of a smaller functional recycling vesicle pool and to validate the results described above with a more physiological stimulus, we performed styryl dye uptake and release studies in paired cortical cultures from wild-type and mutant animals using action potential trains of variable duration at 20 Hz. Cultures were first exposed to an initial dye-staining step with FM1-43 using a variable number (x) of action potentials (where x ranges from 20

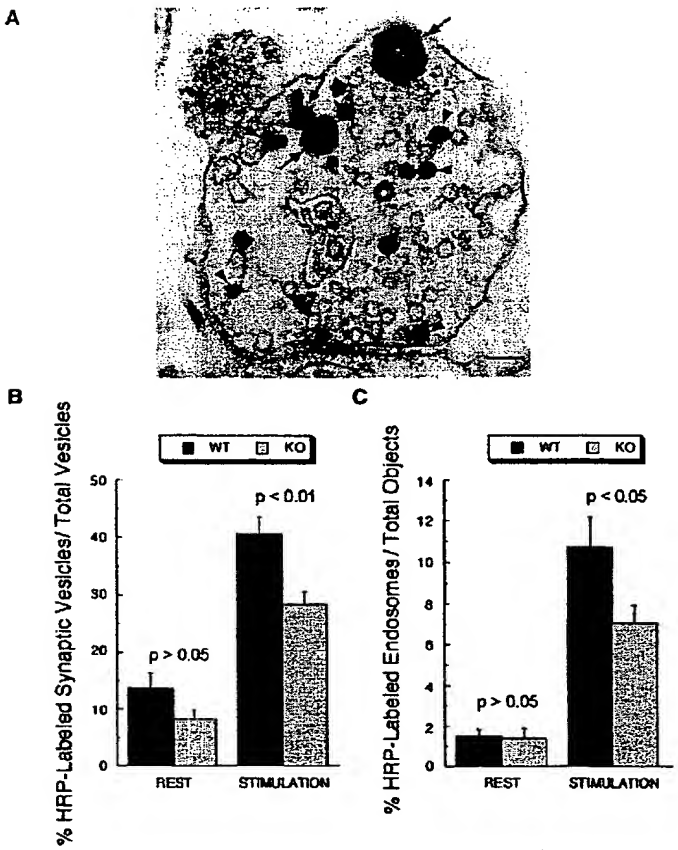

Figure 5. Decreased Labeling of Synaptic Vesicles and Endosome-like Structures after a "Pulse" Incubation with the Fluid Phase Tracer HRP in Synapses of Mutant Cortical Neurons in Culture

(A) Electron micrograph of wild-type synapse stimulated with 90 mM KCl for 90 s in the presence of tracer. A fraction of synaptic vesicles is labeled by HRP (arrowsheads). HRP-labeled objects defined as endosome-like structures are indicated by arrows. Scale bar = 100 nm.

(B) Morphometric analysis indicating the percentage of total small vesicles that are labeled by HRP. The stimulation-dependent increase in the labeling of synaptic vesicles is greater for wild-type synapses than for knockout synapses.

(C) Percentage of HRP-labeled endosomal structures over total number of objects (small vesicles plus labeled endosomal structures). Even in this case, the stimulation-dependent increase in the labeling of endosomes is less pronounced in the case of mutant synapses. Values denote means ± SEM, and p values according to ANOVA are indicated.

to 800) followed by an additional 90 s incubation in the continued presence of the dye in order to label endocytic vesicles whose formation lags behind the interruption of the stimulus. Then, after a 10 min washing period to allow for the chasing of the dye into the releasable pool vesicles, internalized dye was released by a stimulus protocol previously shown to result in maximal destaining (Ryan, 1999). The amount of released dye gives an estimate of the dye taken up in the staining period and thus an estimate of the fraction of synaptic vesicles that underwent exocytosis during a particular action potential stimulus in the dye-loading step.

The total amount of dye uptake with different number of action potentials was normalized to the uptake at 600 action potentials in wild-type terminals and plotted as a function of action potential numbers (Figure 6A). As expected, there was clearly an increase in the size of the vesicle pool that is mobilized with a longer stimulus train in both wild-type and knockout cultures. However, the recycling vesicle pool was 25%–30% smaller in the knockout cultures compared to the wild-type cultures over the entire range of action potential stimuli.

The experiments described in Figure 6A, which showed a smaller total recycling vesicle pool size in knockout cultures, also allowed us to determine whether there was a difference in the fraction of the recycling pool that is engaged by a given duration of action potential train in knockout cultures. To this aim, each of the FM1-43 uptake values from Figure 6A was normalized to the uptake at 600 action potentials for both wild-type and knockout cultures. Comparison of the two sets of values revealed a statistically significant defect in the fractional pool of vesicles mobilized at intermediate AP stimuli in knockout synapses. The fractional pool mobilized at 200 and 300 AP was 0.61 ± 0.02 and 0.74 ± 0.02 for wild-type cultures (n = 265 boutons, three experiments) and 0.54 ± 0.01 and 0.61 ± 0.02 for knockout cultures (n = 288 boutons, three experiments).

We also measured the destaining kinetics of synaptic terminals loaded with FM1-43 during a 600 action potential stimulus. A delay in the delivery of newly internalized vesicles to the releasable vesicle pool would be reflected in a greater time constant for dye release. Onset of the stimulus was associated with a decline in fluorescence in both wild-type and knockout synaptic terminals (Figure 6B). The decline in fluorescence was identical until 100 action potentials, the fifth time point measured. However, at later time points (>200 action potentials), there was a statistically significant delay in the destaining kinetics of knockout terminals relative to wild-type terminals. The time constant of destaining was 17.6 ± 0.6 s in wild-type compared to 21.1 ± 0.5 s in knockout terminals ($p < 0.02$, n = 3).

The slower destaining kinetics of FM1-43-loaded syn-

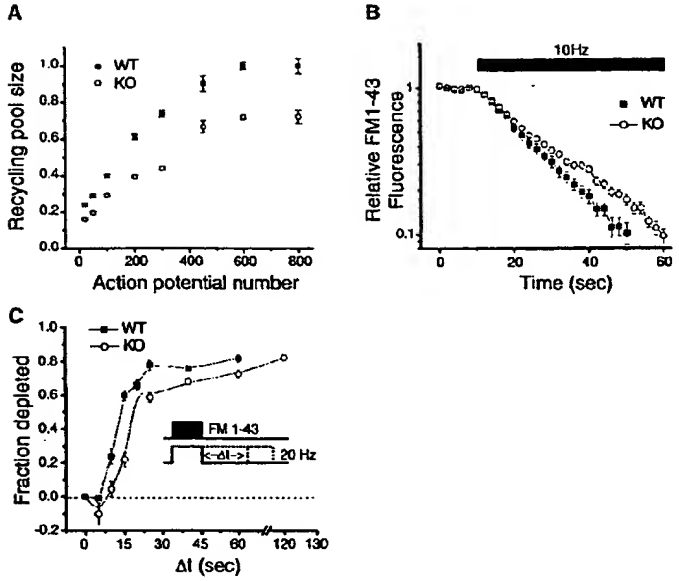

Figure 6. Defects in Synaptic Vesicle Dynamics Revealed by FM1-43 Studies in Synapses of Knockout Mice

(A) Measurement of synaptic vesicle functional pool size in response to action potential (AP) trains of variable duration at 20 Hz. Cortical cultures were first loaded with FM1-43 during a train of APs (abscissa), then, after a 10 min wash-out period, they were subjected to two rounds of AP trains at 20 Hz (separated by a 2 min rest period) to ensure complete dye release. The total amount of dye released during the destaining period gives an estimate of dye uptake into synaptic vesicles during the staining period, and, indirectly, of the vesicle pool size engaged in exo-endocytosis during the same period. Values of FM1-43 uptake at different AP stimuli for both wild-type and mutant synapses were normalized to the uptake at 600 APs in wild-type synapses. Mutant cultures have a smaller vesicle pool size. The total FM1-43 uptake at 600 AP stimuli was 3969 ± 73 (a.u.) in wild-type cultures (n = 635 boutons, five experiments) compared to 2867 ± 45 (a.u.) in knockout cultures (n = 725 boutons, six experiments), statistically significant at $p < 0.001$, Student's t test.

(B) Following FM1-43 loading with 600 APs at 10 Hz, the time course of destaining differs between wild-type and mutant nerve terminals. Destaining of knockout synapses lags behind wild-type. Comparable results were obtained in six other experiments.

(C) Time course of vesicle repriming. The inset shows the experimental protocol. Nerve terminals were stimulated, during a 5 s exposure to FM1-43, by a train of action potentials at 20 Hz that exceeded the period of dye exposure by an amount of time Δt. The resulting dye uptake was measured during a subsequent destaining stimulus at 20 Hz after a 10 min rest. The dye uptake at $\Delta t = 0s$ (F_0) represents the total number of releasable vesicles engaged by the stimulus. The dye uptake measured in runs where $\Delta t > 0s$ ($F_{\Delta t}$) provides an estimate of vesicle depletion, due to fusion of reprimed vesicles, during the additional action potential stimulation after dye washout. The data points represents the fraction depleted ($F_0 - F_{\Delta t}/F_0$) as a function of Δt. The data are from a total of 80–165 boutons for each time point in both wild-type and knockout cultures. Error bars are ± SEM.

aptic terminals could be due to a delay in repriming time, defined as the time that elapses before newly endocytosed vesicles become available for a new round of release (Ryan and Smith, 1995). We tested this hypothesis by directly measuring the repriming time course in cultured cortical neurons (Figure 6C). Nerve terminals were loaded with FM1-43 for a fixed period of 5 s, during a train of action potentials at 20 Hz that exceeded the period of dye exposure by an amount of time Δt (inset in Figure 6C). The total fluorescence incorporated into vesicles was measured 10 min later using a maximal destaining stimulus ($F_{\Delta t}$). These data were normalized to the average fluorescence in bracketed control and recovery runs, when the stimulation was terminated at exactly the same time as the washout of dye ($\Delta t = 0$, F_0). The ratio ($F_0 - F_{\Delta t}/F_0$) represents the fraction of the fluorescence that was depleted during the additional period of stimulation and reflects the time course of gain in rerelease-competence of recently endocytosed vesicles. Any delay in the endocytic journey of the vesicle will prolong this time. Results of such analyses show that both wild-type and amphiphysin 1-deficient nerve terminals released about 80% of the endocytosed vesicles in the next 120 s of continuous stimulation. However, mutant nerve terminals showed a significant delay in dye depletion compared to wild-type terminals (at $\Delta t = 15$ s, wild-type was 60% depleted compared to 20% in knockout cultures, $p < 0.001$). The time to deplete 40% of dye taken up was 12 s in the wild-type terminals compared to 17 s in the knockout cultures. Thus, a delay in repriming of vesicles may at least partially account for the slower destaining kinetics observed in knockout cultures (Figure 6B).

Collectively, these results demonstrate the occurrence of complex recycling defects in amphiphysin knockout terminals, which range from a decreased functional recycling pool size to delayed recycling and repriming rates.

Reduced Viability and Increased Susceptibility to Seizures in Amphiphysin 1 Knockout Mice

Given the cell biological defects described above at synapses of knockout animals, we further investigated changes at the organismal level. A significant decrease in survival rate was observed in the amphiphysin 1 knockout colony, such that only 50% of the animals survived to 10 months of age, as compared with 95% for wild-type mice (Figure 7A). Animals were found dead, mainly between 2 and 5 months of age, with no previous decrease in body weight or other noticeable health problems. To document what appeared to be sudden death, continuous digital camera monitoring of a small group of animals was performed. This approach revealed the occurrence of rare spontaneous seizures. Death resulted from seizures that reached a tonic extension and failed to resolve. Such an observation suggested that amphiphysin 1 knockout mice may exhibit a lower threshold to seizures compared to wild-type animals.

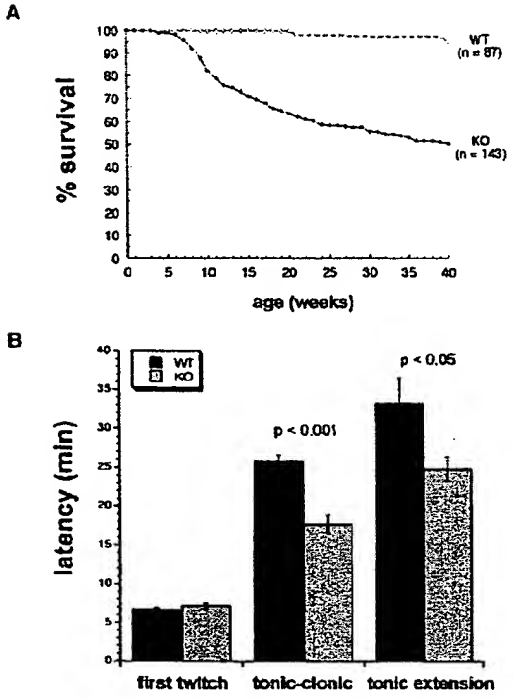

Figure 7. Amphiphysin 1 Knockout Mice Exhibit Increased Mortality and a Higher Propensity to Seizures

(A) Survival curves showing reduced viability of knockout mouse colonies at adult age. Animals die from rare irreversible seizures.

(B) Time (latency) required for wild-type and knockout mice to develop three phases of epilepsy after repeated intraperitoneal injections of pentamethylenetetrazole (metrazol), an epileptogenic $GABA_A$ receptor antagonist. No difference is observed for the first phase (first twitch), but amphiphysin 1 knockout mice progress significantly faster to the hyperkinetic tonic-clonic phase and finally to tonic extension and death. Values denote means ± SEM (n = 7 for wild-type; n = 10 for knockout). P values from a Student's t test analysis are indicated.

To test this hypothesis, we investigated the response of the animals to intraperitoneal injections of pentamethylenetetrazole (metrazol), an epileptogenic $GABA_A$ receptor antagonist (Tecott et al., 1995). Increasing blood levels of the drug results in a series of well-defined responses that start with intermittent body twitches, leading to hyperkinetic tonic-clonic seizures and finally to a tonic extension and death. Whereas the time lag to the first neurological symptoms (first twitch) was comparable in both genotypes, knockout mice progressed significantly faster to the next two phases (tonic-clonic and tonic extension, respectively), demonstrating an increased propensity to seizures (Figure 7B).

Amphiphysin 1 Knockout Mice Exhibit Cognitive Defects

Considering the synaptic vesicle recycling defects revealed by our studies, the lack of impairment in nervous tissue function, besides occasional seizures, was puzzling. Behavioral tests were therefore performed to assess higher brain function. We first examined the spatial learning ability of amphiphysin 1 knockout mice using the Morris water maze task (Morris, 1989). Mice were trained on a task in which they searched for a hidden submerged platform in order to escape from water, using visual cues from the environment. The escape latency, recorded over several sessions, revealed a progressive improvement of the performance in all animals. However, a striking learning deficit in the mutant animals was detected (Figure 8A). After training in the hidden platform test, the transfer test in which mice were allowed to swim freely for 60 s following removal of the platform, was performed. A measurement of quadrant occupancy revealed that wild-type mice spent significantly more time in the quadrant where the platform had been originally located, whereas mutant mice did not (Figure 8C). Moreover, crossings of amphiphysin 1 knockout mice over the original platform location were significantly lower compared to wild-type animals (Figure 8D). No difference in path length was observed between the two genotypes (Figure 8E), indicating that swimming ability is not impaired in knockout mice. To rule out any differences in visual acuity, locomotor activity, or motivation, mice were trained on a visible platform test, in which the platform was placed above the surface of the water with a prominent "flag" attached to it. The escape latency was recorded over the course of 4 days. During this time, the performance of mice from both genotypes improved, although less dramatically in the case of mutant mice (Figure 8B). These results strongly suggest that amphiphysin 1 knockout mice exhibit deficits in learning that may not be only restricted to spatial learning.

To assess whether other forms of learning are impaired in mutant mice, we performed a fear-conditioning test (Paylor et al., 1994), which measures an amygdala-dependent form of associative emotional learning (reviewed in LeDoux, 2000). In this paradigm, an innocuous conditioned stimulus (tone) elicits fear response after being associatively paired with an aversive unconditioned stimulus (footshock). The fear response is measured by the frequency of freezing behaviors, which is defined as a stereotyped motionless crouching posture. Amphiphysin 1 knockout mice exhibited very mild fear responses in both the context test and the auditory cue test compared to their wild-type littermates. In contrast, the fear response generated by a novel context was comparable for both genotypes (Figure 8F). As a control, nociceptive reactions to footshocks were also investigated for both genotypes and were found to be comparable (data not shown). Altogether, our data indicate that amphiphysin 1 knockout mice exhibit major learning deficits, which are not restricted to spatial learning deficits.

Discussion

The results of this study show that in mammals amphiphysin function is required for efficient synaptic vesicle recycling. The data further demonstrate that a partial impairment of this process, and possibly of other membrane recycling pathways at the synapse, is compatible with the basic operation of the nervous system, although

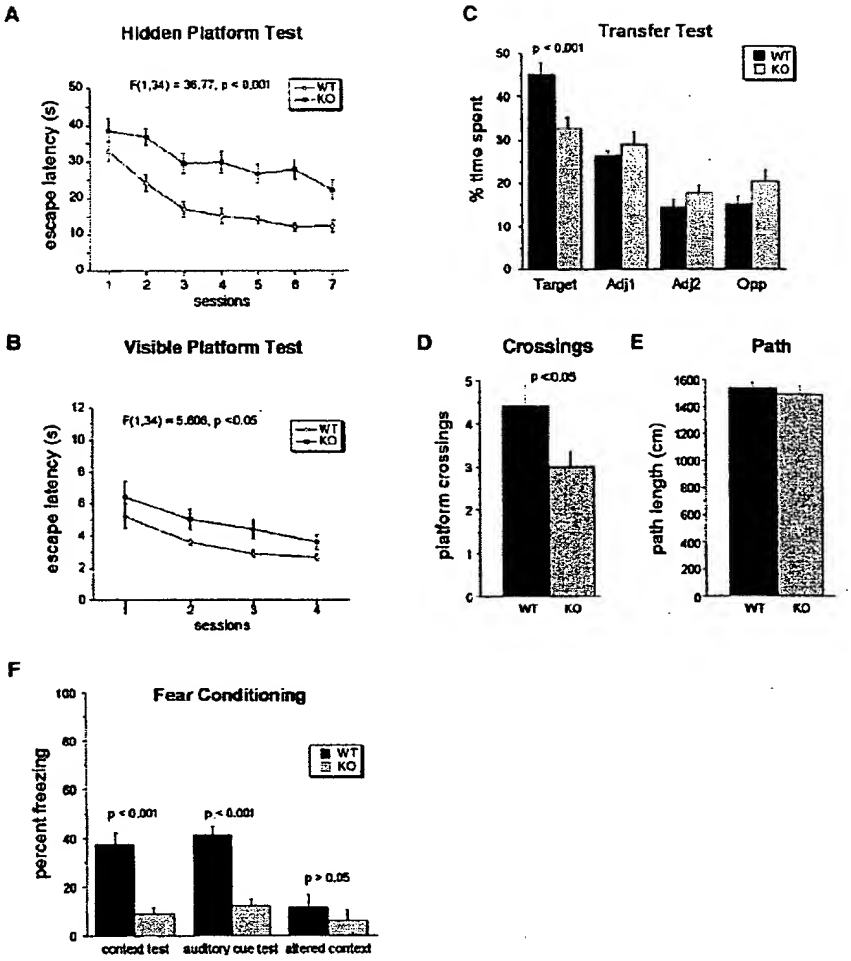

Figure 8. Amphiphysin 1 Knockout Mice Exhibit Learning Deficits in the Morris Water Maze Task (A–E) and in the Fear Conditioning Task (F)

5- to 7-month-old wild-type or knockout animals were used. All values denote means ± SEM.

(A) Learning curve indicating the time required to reach the hidden platform over seven days (n = 18 for each genotype). Statistical analysis was performed by two-way ANOVA for repeated measures.

(B) Latency to find the visible platform over the course of four sessions.

(C–E) Transfer test performance after the acquisition trials of the hidden platform task.

(C) Bars represent the time spent in the four quadrants (target, adjacent 1, adjacent 2, and opposite). Wild-type animals spent significantly more time in the quadrant that originally contained the platform than in each of the other quadrants. This was not the case for knockout animals.

(D) Number of crosses over the area that originally contained the platform during the transfer test were significantly lower for knockout animals relative to wild-type. P values from Mann-Whitney *U*-test are indicated.

(E) Path length (cm) during the transfer test. No statistical difference was observed between the two genotypes.

(F) Freezing responses in the fear conditioning test (n = 9 for each genotype). Amphiphysin 1 knockout mice exhibited significantly less freezing behavior than wild-type mice in both the context test and the auditory cue test. Comparable responses to altered context were observed for both genotypes. Statistical analysis was performed according to Student's t test, and p values are indicated.

it is associated with decreased viability and with defects in higher brain function.

At the molecular level, a striking consequence of the lack of amphiphysin 1 expression in brain was the nearly complete disappearance of amphiphysin 2. Since levels of amphiphysin 2 mRNA are unchanged in the brain of mutant mice, this phenomenon is likely to result from decreased stability of amphiphysin 2 and is consistent with the reported occurrence of amphiphysin 1 and 2 primarily as stable heterodimers in brain (Wigge et al., 1997a; Ramjaun et al., 1997; Slepnev et al., 1998). No downregulation of amphiphysin 2 occurs in skeletal muscle where this protein is normally expressed at very high levels without amphiphysin 1 (Butler et al., 1997). It remains to be determined whether the stability of this skeletal muscle isoform, which differs from the major

brain amphiphysin 2 isoform (Butler et al., 1997), is accounted for by its greater intrinsic resistance to proteolytic degradation or different proteolytic machinery in muscle, by heterodimerization with another BAR domain-containing protein, or by its localization in a subcellular compartment which protects it from high turnover.

The property to form dimers, which resides in the BAR domain, is a conserved feature in the amphiphysin family of proteins, since it also applies to yeast Rvs167, which heterodimerizes with Rvs161 (Navarro et al., 1997; Lombardi and Riezman, 2001). Furthermore, deletion of either the *RVS167* or the *RVS161* gene leads to a significant decrease in the half-life of the protein encoded by the other gene. Interestingly, overexpression of the Rvs161 protein in the *RVS167* knockout strain aggravates, rather than rescues the abnormal phenotype, indicating that the stoichiometry of interaction between related amphiphysin isoforms is a critical parameter for their function (Wigge et al., 1997a; Lombardi and Riezman, 2001).

Our biochemical results strongly support the hypothesis that one of the functions of brain amphiphysin is to act as a multifunctional adaptor connecting various cytosolic components of the endocytic machinery to each other and to the lipid bilayer (Takei et al., 1999). They suggest that amphiphysin may contribute to the recruitment of clathrin, AP-2, and synaptojanin 1 to the membrane. Moreover, although binding of dynamin to lipid bilayers was not dependent upon amphiphysin under our in vitro conditions, affinity purification experiments on the proline-rich tail of dynamin demonstrated that amphiphysin can indeed act as a bridge between clathrin coat components and dynamin. Thus, amphiphysin may help to coordinate the function of all these proteins at the membrane. Furthermore, the direct binding of dynamin to membrane in situ may undergo regulation, and a contribution of amphiphysin to dynamin recruitment in vivo cannot be ruled out.

The defects revealed by our cell-free approaches did not correlate with obvious morphological changes in mutant synapses. However, changes in the efficiency of synaptic vesicle recycling were demonstrated by a variety of physiological approaches after synapse stimulation. These include decreased uptake of extracellular tracers into small vesicles after an endocytic labeling pulse and a slower recycling time as demonstrated by a delay in styryl dye unloading, both during a prolonged stimulus (minimum repriming time) and after recovery from a stimulus (destaining kinetics). Consistent changes were observed both in synaptosomes and in synapses of cultured cortical neurons. Based on FM1-43 experiments in cultured neurons, the pool size of recycling synaptic vesicles also appeared to be smaller. This finding cannot merely be accounted for by a difference in the number of synaptic vesicles per synapse, based on both biochemical (comparable levels of synaptic proteins in brain homogenates) and morphometric results. Thus, the lack of amphiphysin seems to affect several stages of recycling. It seems likely, that although the kinetics of endocytosis is not perturbed (data not shown), the fate of vesicles endocytosed in the absence of amphiphysin is altered such that capacity for subsequent reuse of synaptic vesicles is diminished. This could arise for example if amphiphysin plays a role in mediating the correct sorting of components necessary for efficient postendocytic trafficking to the budding membrane. Although some data could also be explained by the occurrence of a partial defect in exocytosis (for example, the delay in dye unloading after stimulation), the normal glutamate release observed in synaptosomes argues against a significant impairment of this process. It remains possible that the upregulation of a putative "kiss-and-run" recycling pathway partially compensates for recycling defects in knockout animals and contributes to glutamate release stability during prolonged stimulation.

The complex recycling defects may be the results of adaptive changes triggered by an endocytic defect. They may also depend on actions of amphiphysin that are linked to its proposed, albeit not yet understood, function in actin cytoskeleton dynamics. Such a function is suggested by the severe disruption of actin cytoskeleton that is observed in *rvs167* and *rvs161* yeast mutants, in addition to endocytic defects (Sivadon et al., 1995; Lombardi and Riezman, 2001). So far, evidence for a role for amphiphysin in actin dynamics in mammalian cells is only indirect (Mundigl et al., 1998), but the putative role in actin function of some of its partners, dynamin and synaptojanin, support this possibility (Sakisaka et al., 1997; Gad et al., 2000; McNiven et al., 2000). Furthermore, the occurrence of amphiphysin 2 isoforms that lack clathrin and AP-2 binding sites points to functions of amphiphysin that are unrelated to the clathrin coat.

Interestingly, acute disruption of amphiphysin function at synapses of stimulated giant lamprey axons by microinjection either of peptides that bind specifically the SH3 domain of amphiphysin (Shupliakov et al., 1997) or of anti-lamprey amphiphysin antibodies (N. Tomilin, M. Marcucci, H. Gad, P. Löw, V. Slepnev, L. Brodin, P.D.C., and O. Shupliakov, unpublished data) produce more severe vesicle recycling defects than those reported here. Compensatory changes dependent upon the presence of proteins whose function is partially redundant with that of amphiphysin may explain the lack of a dramatic cellular phenotype in neurons of mice that develop in the absence of amphiphysin. It is of note that an acute antisense-mediated inhibition of amphiphysin 1 expression in cultured neurons results in major defects of neurite outgrowth (Mundigl et al., 1998), whereas this process occurs normally in mutant neurons. A puzzling observation is the lack of biochemical evidence for an interaction between amphiphysin and dynamin in *Drosophila* (Razzaq et al., 2001), where the synaptic dynamin interacting network seems to be at least partially different from the corresponding mammalian one (Roos and Kelly, 1998). In *Drosophila*, the single amphiphysin gene lacks clathrin and AP-2 binding sites and is abundantly expressed in skeletal muscle (Razzaq et al., 2001). Accordingly, amphiphysin-deficient flies predominantly show a muscle phenotype (Razzaq et al., 2001; Zelhof et al., 2001). In mammals, the presence of two neuronal isoforms of amphiphysin (amphiphysin 1 and the neuronal form of amphiphysin 2) in brain underlines their importance for nervous system function.

A striking observation is that the subtle vesicle recycling defects observed in amphiphysin 1 knockout mice produce important defects at the organismal levels.

While amphiphysin 1 knockout mice develop and reproduce normally, suggesting a basic normal functioning of the nervous system, some important neurological and behavioral defects were also observed. The death rate of mutant animals is significantly increased compared to normal littermates, in particular during the first few months of adulthood. Death was caused by rare irreversible seizures and, accordingly, mutant mice have a lower threshold to seizures. It was shown that synaptic depression during high-frequency stimulation occurs much faster at excitatory synapses than at inhibitory synapses, and this difference may be a critical mechanism protecting the nervous system from seizures (Galarreta and Hestrin, 1998; Varela et al., 1999; Kraushaar and Jonas, 2000). In turn, the remarkable stability of inhibitory synapses during ongoing stimulation is critically dependent upon the vesicle cycle, as shown by the loss of this stability in synaptojanin 1 knockout mice (Cremona et al., 1999; Lüthi et al., 2001). Thus, an increased susceptibility to seizures is consistent with the occurrence of a recycling defect in amphiphysin 1 knockout mice.

Another consequence of the lack of amphiphysin is a cognitive deficit, as defined by a significant impairment in learning tasks. Mutant animals exhibited severe learning disabilities in the Morris water maze test as well as in the fear-conditioning task, which rely on distinct neuronal circuitries. Although we cannot rule out that subthreshold seizures interfered with these experiments, it appears unlikely that seizure activity accounted for the defects observed. First, other knockout mouse models which experience severe seizures, such as synapsin 1 knockout mice, do not show impaired learning (Silva et al., 1996). Second, we used 5- to 7-month-old animals for our behavioral experiments, and we found that in this age category as well as in older animals, the death rate drops dramatically compared to younger adult animals. Since knockout animals die from seizures, we may have selected for our experiments a category of animals that is less prone to epilepsy.

Many mouse models with abnormal function of signaling pathways show learning deficits (Mayford and Kandel, 1999). A role of amphiphysin in signaling pathways cannot be excluded given the strong interconnections between endocytosis and signaling (Di Fiore and De Camilli, 2001; McPherson et al., 2001). Indeed some interactions of amphiphysin with signaling proteins have been reported (Kadlec and Pendergast, 1997; Leprince et al., 1997). Furthermore, in view of growing evidence for a critical role of clathrin-mediated endocytosis in the internalization of postsynaptic receptors (Turrigiano, 2000; Carroll et al., 2001; Kittler et al., 2000), it is possible that postsynaptic vesicle recycling changes may contribute to the cognitive defects of amphiphysin 1 knockout animals. However, we can at least conclude from our study that amphiphysin is indeed an effector in synaptic vesicle recycling and in the physiology of endocytic zones of mammalian synapses and that a perturbation of this function is likely to play a role in the cognitive deficits observed in mutant animals.

Several human conditions involve substantial cognitive defects that are not associated with major neurological impairments. In most cases, responsible genes have not yet been identified. An inherited mental retardation syndrome was mapped to the gene encoding a Rab GDP-dissociation inhibitor (GDI), a protein that controls the Rab cycle, and therefore the vesicle cycle, in nerve terminals and possibly also postsynaptically (D'Adamo et al., 1998). The learning defects observed in amphiphysin 1 knockout mice provide another example of a gene which functions in vesicle recycling and whose mutation underlies learning defects in a mammalian organism. Other human psychiatric conditions may be due to defects in membrane trafficking at the synapse.

Experimental Procedures

Generation of Amphiphysin 1 Knockout Mice

A λFIXII genomic library from 129SV/J mice was screened with a 250 bps DNA fragment corresponding to the 5′ end of the rat amphiphysin 1 cDNA. Phage clones containing the first coding exon of amphiphysin 1 gene were isolated and identified. A replacement targeting vector was constructed as shown in Figure 1A. In the targeting vector, most of the 3′ end of the first coding exon and a fragment of the following intron were replaced by the selection cassette (neomycin resistance gene under the PGK promoter [neo cassette]). The herpes simplex virus-1 thymidine kinase gene under the PGK promoter (TK cassette) was added at the end of the short arm of the construct. Both the neo and the TK cassette have a transcription direction that is the same as the amphiphysin 1 gene. The vector was linearized and electroporated into embryonic stem (ES) cells (129/Sv agouti ES cells) that were then selected according to standard procedures (Yang et al., 1997). Recombination events were identified by Southern blot screening using a PCR-generated probe corresponding to a fragment outside the recombination site but inside the restriction fragment generated by EcoRV digestion (Figure 1A). Chromosomal counting on recombinant ES cell clones was performed before blastocyst microinjection, in order to increase the chances of germline transmission. Positive clones were independently microinjected into blastocysts, which were then reimplanted into pseudopregnant foster mothers. Several chimeras were generated and independently bred with C57BL/6 mice. Germline transmission was achieved, and heterozygous animals were produced. Knockout mice were generated by successive breedings and identified by Southern blot analysis using the same screening strategy as for the identification of recombinant ES cell clones (Figure 1B). For Northern blot analysis, probes consisting of full length amphiphysin 2 and actin sequences, respectively, were obtained by PCR amplification from a mouse brain cDNA library and were labeled by random priming.

Antibodies, Immunoblotting, and Immunofluorescence

Brains from wild-type and knockout mice were homogenized in a lysis buffer containing 25 mM HEPES (pH 7.4), 150 mM KCl, 2 mM EGTA supplemented with a cocktail of proteinase inhibitors. Postnuclear supernatants (50 μg) were processed for SDS-PAGE and immunoblotting using ECL procedures (Amersham Pharmacia Biotech, Inc., Piscataway, NJ). The following antibodies were generated in our lab: rabbit antisera to synaptojanin 1, amphiphysin 1 and 2, endophilin 1, synaptophysin, as well as mouse mAb to amphiphysin 1 and AP180. Other antibodies are from commercial sources: Bin 1 (Upstate Biotechnology, Lake Placid, NY), dynamin 1 (Transduction Laboratories, Lexington, KT), α-adaptin (Affinity BioReagents, Golden, CO), a mouse hybridoma producing antibodies to clathrin heavy chain (ATCC, Rockville, MD), and α-tubulin (Sigma, St. Louis, MO). The mAb to synaptotagmin was a kind gift from Dr. R. Jahn (University of Göttingen, Germany). Immunofluorescence was performed on 2- to 3-week-old cultures of cortical neurons as previously described (Mundigl et al., 1998).

Biochemical Procedures

The experiment using liposomes was performed as previously described (Cremona et al., 1999; Gad et al., 2000). Quantification was performed using a phosphoimaging. For the lipid experiment, liposomes (0.25 mg/ml) were incubated with brain cytosol (0.5 mg/ml) for 15 min at 37°C in the presence of 2 mM ATP and 0.2 mM GTP.

Liposomes were then isolated by ultracentrifugation, washed three times, and incubated in the presence of 20 μCi [γ^{32}P]ATP for 10 min at 37°C. Lipids were extracted and processed for analysis by thin layer chromatography, and the identity of lipids was confirmed by high performance liquid chromatography as described previously (Cremona et al., 1999). Using phosphoimaging, counts for PI(4,5)P2 were normalized to total counts, which mainly included those of phosphatidic acid. The affinity chromatography using GST fused to the proline-rich region of dynamin was performed as in Slepnev et al. (1998), with slight modifications. 15 mg detergent extracts from wild-type and knockout brains were incubated for 4 hr at 4°C in the presence of 0.8 mg GST or GST fused to the proline-rich region of human dynamin 1 prebound to 150 μl Sepharose 4B beads (Amersham Pharmacia Biotech, Inc., Piscataway, NJ) in a buffer containing 25 mM HEPES (pH 7.4), 150 mM KCl, 1 mM EGTA, 1% Triton X-100, and a cocktail of protease inhibitors. In one experimental condition, 15 mg knockout extract were supplemented with 30 μg purified recombinant amphiphysin 1 prior to affinity chromatography. Following five washes with the same buffer, proteins were eluted in sample buffer and processed for immunoblotting.

FM2-10 Uptake in Synaptosomes

Synaptosomes were prepared from four mouse cortices as previously described (Marks and McMahon, 1998). For each experiment, 500 μg synaptosomes were used. In the "unloading" experiment, synaptosomes were incubated for 5 min at 37°C in low K^+ saline solution prior to transfer to the 1 ml cuvette preheated at 37°C in a Hitachi F-3010 fluorimeter. Synaptosomes were preincubated for 3 min with FM2-10 (Molecular Probes, Inc., Eugene, OR) at 100 μM final concentration and stimulated with 30 mM KCl for 90 s. Synaptosomes were washed twice with 1 ml low K^+ saline solution containing 1 mg/ml BSA, resuspended in low K^+ buffer, and transferred back to the cuvette. Following a 10 min incubation, a second stimulation with 30 mM KCl was applied, and fluorescence was measured at 467/550 nm as a function of time. In the FM2-10 internalization experiment, a similar protocol was used except that, following the first stimulation with 30 mM KCl and the washes, synaptosomes were lysed in a hypotonic solution containing 20 mM HEPES (pH 7.4), vortexed for 10 s, supplemented with KCl to 150 mM final concentration, and centrifuged for 2 min in a microfuge at maximal speed. Fluorescence associated with the supernatant, containing FM2-10 labeled internal membranes, was subsequently measured with the fluorimeter. The glutamate release was performed as previously described (Nicholls and Sihra, 1986).

Electron Microscopy and Morphometry of HRP-Labeled Cortical Neurons in Culture

Primary cultures of cortical neurons were prepared according to procedures previously described (Banker and Goslin, 1991; Cremona et al., 1999). Cells were maintained up to 3 weeks in Neurobasal/B27 medium (Life Technologies/Gibco-BRL, Gaithersburg, MD) at 37°C in a 5% CO_2 humidified incubator. Neurons were labeled with the fluid-phase marker HRP (Sigma, St Louis, MO) at 10 mg/ml for 3 min at 37°C before stimulation in a low K^+ saline solution containing 130 mM NaCl, 5 mM KCl, 2 mM $CaCl_2$, 2 mM $MgCl_2$, 25 mM HEPES (pH 7.33), 30 mM glucose, 10 μM CNQX, and 50 μM AP-V (Research Biochemicals, Inc., Natick, MA). Neurons were then either kept in low K^+ for another 90 s ("rest") or stimulated for 90 s with a solution containing 90 mM KCl and 45 mM NaCl in the presence of HRP ("stimulation"). Cells were fixed in 2% glutaraldehyde/2% sucrose in 0.1M sodium phosphate buffer (pH 7.4) for 2 hr at 4°C and processed for electron microscopy as described (Cremona et al., 1999). For morphometry, 37–54 synapses were analyzed at a final magnification of 63,000×. For each condition, 2000–4000 objects were scored. They included labeled or unlabeled synaptic vesicles and clathrin-coated vesicles as well as labeled endosome-like structures. Endosome-like structures were defined as HRP-labeled compartment larger than synaptic vesicles. Statistics were performed using ANOVA. Results of two independent experiments were pooled.

FM1-43 Uptake and Release in Cultured Cortical Neurons

Cortical cultures were generated from 1- to 2-day-old amphiphysin 1 knockout and wild-type mice. Brains were dissected; cerebral cortices were separated from the hippocampus and basal ganglia and dissociated using protocols similar to those used for hippocampal cultures (Ryan, 1999). Confocal laser scanning microscopy, electrical field stimulation, FM1-43 uptake, and release experiments were performed as described (Ryan, 1999) in 2- to 3-week-old cultures. FM1-43 (Molecular Probes, Eugene, OR) was stored at 4°C as 3 mM aliquots and used at a final concentration of 15 μM.

Metrazol Injection

12-week-old mice were injected intraperitoneally with a solution of pentamethylenetetrazole at 15 mg/kg every 5 min until observation of the last phase of seizure. The time required to reach the various phases of seizure was recorded. The first twitch was generally detectable in the ear; the tonic-clonic phase was defined as repeated hyperkinetic movements of forelimbs followed by a loss of postural control and falling, after which both the forelimbs and hindlimbs were characterized by clonic movements; the tonic extension phase began when animals arched their body and their limbs, after which, in most cases, they stopped breathing and died. Seven wild-type and ten knockout mice were used for the experiment. Statistics were performed using ANOVA.

Behavioral Paradigms

The Morris water maze test was performed as described previously (Morris, 1989; Wickman et al., 2000). In total, 18 mice (nine males, nine females) of 5–7 months of age were used for the experiments for both wild-type and knockout genotypes. A circular white plastic tub 1 min in diameter was filled with water (21°–22°C) and divided into four quadrants of equal surface. Swim times, path length, and all other measurements were made using the Poly-track Video Tracking System (San Diego Instruments). For the hidden platform test, a 10 cm^2 transparent Plexiglas platform was submerged 0.5 cm beneath the surface and positioned consistently over the course of the test. Mice were allowed to swim until they encountered the platform or for a maximal duration of 60 s, after which they were placed on the platform for 15 s. Mice began each of the four daily trials from a different quadrant, and the time required to find the platform was recorded and averaged. The intertrial interval was 3.5 min. The test was performed for 7 consecutive days, always in the afternoon. On day 8, the transfer test was performed. Briefly, the platform was removed, and mice were allowed to swim for 60 s, starting from the center of the pool. The time spent in every quadrant, the number of entries into the area where the platform had been originally located, and the swimming distance were measured. On days 9–12, in the visible platform test, trials were performed like in the hidden platform test, except that the platform was flagged.

The fear-conditioning test was performed as described (Paylor et al., 1994; Caldarone et al., 2000). In total, nine mice (five males, four females) of 5–7 months of age were used for the experiments for both wild-type and knockout genotypes. On the first day of training, each mouse was placed in a training chamber and freezing behavior was assessed every 10 s. After 2 min, the conditioned stimulus, a tone, was applied for 30 s and terminated by a 2 s unconditioned stimulus, a footshock of 0.5 mA. This sequence was repeated a second time, after which animals were kept for 30 s in the chamber and returned to their original cages. On the second day, animals were first tested for contextual fear. Each mouse was placed in the training chamber, and freezing behavior was assessed for 5 min in the absence of tone. One hour later, animals were tested for their fear response to the auditory stimulus. Each mouse was placed in a different training chamber and exposed to a smell of orange extract. During the first 3 min, freezing to altered context was measured, after which the tone was continuously presented for another 3 min, and freezing behavior to the auditory stimulus was scored.

Acknowledgments

We would like to thank David A. McCormick, Anita Lüthi, and Fabio Benfenati for helpful discussions and preliminary work; Lijuan Liu and Wayne Yan for excellent technical assistance; Khashayar Farsad, Sergei Voronov, Raani Punglia, and Sarah L. King for help at various stages of the study; and Reinhard Jahn (Gottingen, Germany) for the kind gift of antibodies. This work was supported in

part by National Institutes of Health grants (NS36251 and CA46128) and a grant from the United States Army Medical Research and Development Command to P.D.C., by NIH grants to T.A.R. (NS24692 and GM61925) and to M.R.P. (DA00436 and MH25642), by Telethon (project D.11) and COFIN2000 grants to O.C. T.A.R. is an Alfred P. Sloan Research Fellow.

Received August 6, 2001; revised January 9, 2002.

References

Banker, G.A., and Goslin, K. (1991). Culturing Nerve Cells (Cambridge, MA: MIT Press).

Bauerfeind, R., Takei, K., and De Camilli, P. (1997). Amphiphysin I is associated with coated endocytic intermediates and undergoes stimulation-dependent dephosphorylation in nerve terminals. J. Biol. Chem. *272*, 30984–30992.

Brodin, L., Low, P., and Shupliakov, O. (2000). Sequential steps in clathrin-mediated synaptic vesicle endocytosis. Curr. Opin. Neurobiol. *10*, 312–320.

Burger, K.N., Demel, R.A., Schmid, S.L., and de Kruijff, B. (2000). Dynamin is membrane-active: lipid insertion is induced by phosphoinositides and phosphatidic acid. Biochemistry *39*, 12485–12493.

Butler, M.H., David, C., Ochoa, G.C., Freyberg, Z., Daniell, L., Grabs, D., Cremona, O., and De Camilli, P. (1997). Amphiphysin II (SH3P9; BIN1), a member of the amphiphysin/Rvs family, is concentrated in the cortical cytomatrix of axon initial segments and nodes of ranvier in brain and around T tubules in skeletal muscle. J. Cell Biol. *137*, 1355–1367.

Caldarone, B.J., Duman, C.H., and Picciotto, M.R. (2000). Fear conditioning and latent inhibition in mice lacking the high affinity subclass of nicotinic acetylcholine receptors in the brain. Neuropharmacology *39*, 2779–2784.

Carroll, R.C., Beattie, E.C., von Zastrow, M., and Malenka, R.C. (2001). Role of AMPA receptor endocytosis in synaptic plasticity. Nat. Rev. Neurosci. *2*, 315–324.

Cousin, M.A., and Robinson, P.J. (1998). Ba^{2+} does not support synaptic vesicle retrieval in rat cerebrocortical synaptosomes. Neurosci. Lett. *253*, 1–4.

Cousin, M.A., and Robinson, P.J. (2000). Two mechanisms of synaptic vesicle recycling in rat brain nerve terminals. J. Neurochem. *75*, 1645–1653.

Cremona, O., and De Camilli, P. (1997). Synaptic vesicle endocytosis. Curr. Opin. Neurobiol. *7*, 323–330.

Cremona, O., Di Paolo, G., Wenk, M.R., Luthi, A., Kim, W.T., Takei, K., Daniell, L., Nemoto, Y., Shears, S.B., Flavell, R.A., et al. (1999). Essential role of phosphoinositide metabolism in synaptic vesicle recycling. Cell *99*, 179–188.

Crouzet, M., Urdaci, M., Dulau, L., and Aigle, M. (1991). Yeast mutant affected for viability upon nutrient starvation: characterization and cloning of the RVS161 gene. Yeast *7*, 727–743.

D'Adamo, P., Menegon, A., Lo Nigro, C., Grasso, M., Gulisano, M., Tamanini, F., Bienvenu, T., Gedeon, A.K., Oostra, B., Wu, S.K., et al. (1998). Mutations in GDI1 are responsible for X-linked non-specific mental retardation. Nat. Genet. *19*, 134–139.

David, C., McPherson, P.S., Mundigl, O., and De Camilli, P. (1996). A role of amphiphysin in synaptic vesicle endocytosis suggested by its binding to dynamin in nerve terminals. Proc. Natl. Acad. Sci. USA *93*, 331–335.

De Camilli, P., Thomas, A., Cofiell, R., Folli, F., Lichte, B., Piccolo, G., Meinck, H.M., Austoni, M., Fassetta, G., Bottazzo, G., et al. (1993). The synaptic vesicle-associated protein amphiphysin is the 128-kD autoantigen of Stiff-Man syndrome with breast cancer. J. Exp. Med. *178*, 2219–2223.

Di Fiore, P.P., and De Camilli, P. (2001). Endocytosis and signaling. Cell *106*, 1–4.

Dunaevsky, A., and Connor, E.A. (2000). F-actin is concentrated in nonrelease domains at frog neuromuscular junctions. J. Neurosci. *20*, 6007–6012.

Elliott, K., Sakamuro, D., Basu, A., Du, W., Wunner, W., Staller, P., Gaubatz, S., Zhang, H., Prochownik, E., Eilers, M., and Prendergast, G.C. (1999). Bin1 functionally interacts with Myc and inhibits cell proliferation via multiple mechanisms. Oncogene *18*, 3564–3573.

Farsad, K., Ringstad, N., Takei, K., Floyd, S.R., Rose, K., and De Camilli, P. (2001). Generation of high curvature membranes mediated by direct endophilin bilayer interactions. J. Cell Biol. *155*, 193–200.

Gad, H., Low, P., Zotova, E., Brodin, L., and Shupliakov, O. (1998). Dissociation between Ca^{2+}-triggered synaptic vesicle exocytosis and clathrin-mediated endocytosis at a central synapse. Neuron *21*, 607–616.

Gad, H., Ringstad, N., Low, P., Kjaerulff, O., Gustafsson, J., Wenk, M., Di Paolo, G., Nemoto, Y., Crun, J., Ellisman, M.H., et al. (2000). Fission and uncoating of synaptic clathrin-coated vesicles are perturbed by disruption of interactions with the SH3 domain of endophilin. Neuron *27*, 301–312.

Galarreta, M., and Hestrin, S. (1998). Frequency-dependent synaptic depression and the balance of excitation and inhibition in the neocortex. Nat. Neurosci. *1*, 587–594.

Ge, K., and Prendergast, G.C. (2000). Bin2, a functionally nonredundant member of the BAR adaptor gene family. Genomics *67*, 210–220.

Geli, M.I., and Riezman, H. (1998). Endocytic internalization in yeast and animal cells: similar and different. J. Cell Sci. *111*, 1031–1037.

Harris, T.W., Hartwieg, E., Horvitz, H.R., and Jorgensen, E.M. (2000). Mutations in synaptojanin disrupt synaptic vesicle recycling. J. Cell Biol. *150*, 589–600.

Heuser, J.E., and Reese, T.S. (1973). Evidence for recycling of synaptic vesicle membrane during transmitter release at the frog neuromuscular junction. J. Cell Biol. *57*, 315–344.

Hussain, N.K., Jenna, S., Glogauer, M., Quinn, C.C., Wasiak, S., Guipponi, M., Antonarakis, S.E., Kay, B.K., Stossel, T.P., Lamarche-Vane, N., and McPherson, P.S. (2001). Endocytic protein intersectin-l regulates actin assembly via Cdc42 and N-WASP. Nat. Cell Biol. *3*, 927–932.

Kadlec, L., and Pendergast, A.M. (1997). The amphiphysin-like protein 1 (ALP1) interacts functionally with the cABL tyrosine kinase and may play a role in cytoskeletal regulation. Proc. Natl. Acad. Sci. USA *94*, 12390–12395.

Kittler, J.T., Delmas, P., Jovanovic, J.N., Brown, D.A., Smart, T.G., and Moss, S.J. (2000). Constitutive endocytosis of GABAA receptors by an association with the adaptin AP2 complex modulates inhibitory synaptic currents in hippocampal neurons. J. Neurosci. *20*, 7972–7977.

Kraushaar, U., and Jonas, P. (2000). Efficacy and stability of quantal GABA release at a hippocampal interneuron-principal neuron synapse. J. Neurosci. *20*, 5594–5607.

LeDoux, J.E. (2000). Emotion circuits in the brain. Annu. Rev. Neurosci. *23*, 155–184.

Leprince, C., Romero, F., Cussac, D., Vayssiere, B., Berger, R., Tavitian, A., and Camonis, J.H. (1997). A new member of the amphiphysin family connecting endocytosis and signal transduction pathways. J. Biol. Chem. *272*, 15101–15105.

Leventis, P.A., Chow, B.M., Stewart, B.A., Iyengar, B., Campos, A.R., and Boulianne, G.L. (2001). Drosophila amphiphysin is a post-synaptic protein required for normal locomotion but not endocytosis. Traffic *2*, 839–850.

Lombardi, R., and Riezman, H. (2001). Rvs161p and Rvs167p, the two yeast amphiphysin homologs, function together in vivo. J. Biol. Chem. *276*, 6016–6022.

Lüthi, A., Di Paolo, G., Cremona, O., Daniell, L., De Camilli, P., and McCormick, D.A. (2001). Synaptojanin 1 contributes to maintaining the stability of GABAergic transmission in primary cultures of cortical neurons. J. Neurosci. *21*, 9101–9111.

Marks, B., and McMahon, H.T. (1998). Calcium triggers calcineurin-dependent synaptic vesicle recycling in mammalian nerve terminals. Curr. Biol. *8*, 740–749.

Marsh, M., and McMahon, H.T. (1999). The structural era of endocytosis. Science *285*, 215–220.

Mayford, M., and Kandel, E.R. (1999). Genetic approaches to memory storage. Trends Genet. *15*, 463–470.

McMahon, H.T., Wigge, P., and Smith, C. (1997). Clathrin interacts specifically with amphiphysin and is displaced by dynamin. FEBS Lett. *413*, 319–322.

McNiven, M.A., Kim, L., Krueger, E.W., Orth, J.D., Cao, H., and Wong, T.W. (2000). Regulated interactions between dynamin and the actin-binding protein cortactin modulate cell shape. J. Cell Biol. *151*, 187–198.

McPherson, P.S., Garcia, E.P., Slepnev, V.I., David, C., Zhang, X., Grabs, D., Sossin, W.S., Bauerfeind, R., Nemoto, Y., and De Camilli, P. (1996). A presynaptic inositol-5-phosphatase. Nature *379*, 353–357.

McPherson, P.S., Kay, B.K., and Hussain, N.K. (2001). Signaling on the endocytic pathway. Traffic *2*, 375–384.

Modregger, J., Ritter, B., Witter, B., Paulsson, M., and Plomann, M. (2000). All three PACSIN isoforms bind to endocytic proteins and inhibit endocytosis. J. Cell Sci. *113*, 4511–4521.

Morris, R.G. (1989). Synaptic plasticity and learning: selective impairment of learning rats and blockade of long-term potentiation in vivo by the N-methyl-D-aspartate receptor antagonist AP5. J. Neurosci. *9*, 3040–3057.

Mundigl, O., Ochoa, G.C., David, C., Slepnev, V.I., Kabanov, A., and De Camilli, P. (1998). Amphiphysin I antisense oligonucleotides inhibit neurite outgrowth in cultured hippocampal neurons. J. Neurosci. *18*, 93–103.

Navarro, P., Durrens, P., and Aigle, M. (1997). Protein-protein interaction between the RVS161 and RVS167 gene products of Saccharomyces cerevisiae. Biochim. Biophys. Acta *1343*, 187–192.

Nicholls, D.G., and Sihra, T.S. (1986). Synaptosomes possess an exocytotic pool of glutamate. Nature *321*, 772–773.

Ochoa, G.C., Slepnev, V.I., Neff, L., Ringstad, N., Takei, K., Daniell, L., Kim, W., Cao, H., McNiven, M., Baron, R., and De Camilli, P. (2000). A functional link between dynamin and the actin cytoskeleton at podosomes. J. Cell Biol. *150*, 377–389.

Owen, D.J., and Luzio, J.P. (2000). Structural insights into clathrin-mediated endocytosis. Curr. Opin. Cell Biol. *12*, 467–474.

Owen, D.J., Wigge, P., Vallis, Y., Moore, J.D., Evans, P.R., and McMahon, H.T. (1998). Crystal structure of the amphiphysin-2 SH3 domain and its role in the prevention of dynamin ring formation. EMBO J. *17*, 5273–5285.

Paylor, R., Tracy, R., Wehner, J., and Rudy, J.W. (1994). DBA/2 and C57BL/6 mice differ in contextual fear but not auditory fear conditioning. Behav. Neurosci. *108*, 810–817.

Qualmann, B., Roos, J., DiGregorio, P.J., and Kelly, R.B. (1999). Syndapin I, a synaptic dynamin-binding protein that associates with the neural Wiskott-Aldrich syndrome protein. Mol. Biol. Cell *10*, 501–513.

Qualmann, B., Kessels, M.M., and Kelly, R.B. (2000). Molecular links between endocytosis and the actin cytoskeleton. J. Cell Biol. *150*, F111–F116.

Ramjaun, A.R., and McPherson, P.S. (1998). Multiple amphiphysin II splice variants display differential clathrin binding: identification of two distinct clathrin-binding sites. J. Neurochem. *70*, 2369–2376.

Ramjaun, A.R., Micheva, K.D., Bouchelet, I., and McPherson, P.S. (1997). Identification and characterization of a nerve terminal-enriched amphiphysin isoform. J. Biol. Chem. *272*, 16700–16706.

Ramjaun, A.R., Philie, J., de Heuvel, E., and McPherson, P.S. (1999). The N terminus of amphiphysin II mediates dimerization and plasma membrane targeting. J. Biol. Chem. *274*, 19785–19791.

Razzaq, A., Su, Y., Mehren, J.E., Mizuguchi, K., Jackson, A.P., Gay, N.J., and O'Kane, C.J. (2000). Characterisation of the gene for Drosophila amphiphysin. Gene *241*, 167–174.

Razzaq, A., Robinson, I.M., McMahon, H.T., Skepper, J.N., Su, Y., Zelhof, A.C., Jackson, A.P., Gay, N.J., and O'Kane, C.J. (2001). Amphiphysin is necessary for organization of the excitation-contraction coupling machinery of muscles, but not for synaptic vesicle endocytosis in Drosophila. Genes Dev. *15*, 2967–2979.

Roos, J., and Kelly, R.B. (1998). Dap160, a neural-specific Eps15 homology and multiple SH3 domain- containing protein that interacts with Drosophila dynamin. J. Biol. Chem. *273*, 19108–19119.

Roos, J., and Kelly, R.B. (1999). The endocytic machinery in nerve terminals surrounds sites of exocytosis. Curr. Biol. *9*, 1411–1414.

Routhier, E.L., Burn, T.C., Abbaszade, I., Summers, M., Albright, C.F., and Prendergast, G.C. (2001). Human BIN3 complements the F-actin localization defects caused by loss of Hob3p, the fission yeast homolog of Rvs161p. J. Biol. Chem. *276*, 21670–21677.

Ryan, T.A. (1999). Inhibitors of myosin light chain kinase block synaptic vesicle pool mobilization during action potential firing. J. Neurosci. *19*, 1317–1323.

Ryan, T.A., and Smith, S.J. (1995). Vesicle pool mobilization during action potential firing at hippocampal synapses. Neuron *14*, 983–989.

Sakisaka, T., Itoh, T., Miura, K., and Takenawa, T. (1997). Phosphatidylinositol 4,5-bisphosphate phosphatase regulates the rearrangement of actin filaments. Mol. Cell. Biol. *17*, 3841–3849.

Shupliakov, O., Low, P., Grabs, D., Gad, H., Chen, H., David, C., Takei, K., De Camilli, P., and Brodin, L. (1997). Synaptic vesicle endocytosis impaired by disruption of dynamin-SH3 domain interactions. Science *276*, 259–263.

Silva, A.J., Rosahl, T.W., Chapman, P.F., Marowitz, Z., Friedman, E., Frankland, P.W., Cestari, V., Cioffi, D., Sudhof, T.C., and Bourtchuladze, R. (1996). Impaired learning in mice with abnormal short-lived plasticity. Curr. Biol. *6*, 1509–1518.

Sivadon, P., Bauer, F., Aigle, M., and Crouzet, M. (1995). Actin cytoskeleton and budding pattern are altered in the yeast rvs161 mutant: The Rvs161 protein shares common domains with the brain protein amphiphysin. Mol. Gen. Genet. *246*, 485–495.

Slepnev, V.I., and De Camilli, P. (2000). Accessory factors in clathrin-dependent synaptic vesicle endocytosis. Nat. Rev. Neurosci. *1*, 161–172.

Slepnev, V.I., Ochoa, G.C., Butler, M.H., Grabs, D., and De Camilli, P. (1998). Role of phosphorylation in regulation of the assembly of endocytic coat complexes. Science *281*, 821–824.

Slepnev, V.I., Ochoa, G.C., Butler, M.H., and De Camilli, P. (2000). Tandem arrangement of the clathrin and AP-2 binding domains in amphiphysin 1 and disruption of clathrin coat function by amphiphysin fragments comprising these sites. J. Biol. Chem. *275*, 17583–17589.

Takei, K., Slepnev, V.I., Haucke, V., and De Camilli, P. (1999). Functional partnership between amphiphysin and dynamin in clathrin-mediated endocytosis. Nat. Cell Biol. *1*, 33–39.

Tecott, L.H., Sun, L.M., Akana, S.F., Strack, A.M., Lowenstein, D.H., Dallman, M.F., and Julius, D. (1995). Eating disorder and epilepsy in mice lacking 5-HT2c serotonin receptors. Nature *374*, 542–546.

Teng, H., and Wilkinson, R.S. (2000). Clathrin-mediated endocytosis near active zones in snake motor boutons. J. Neurosci. *20*, 7986–7993.

Turrigiano, G.G. (2000). AMPA receptors unbound: membrane cycling and synaptic plasticity. Neuron *26*, 5–8.

Varela, J.A., Song, S., Turrigiano, G.G., and Nelson, S.B. (1999). Differential depression at excitatory and inhibitory synapses in visual cortex. J. Neurosci. *19*, 4293–4304.

Wasiak, S., Quinn, C.C., Ritter, B., de Heuvel, E., Baranes, D., Plomann, M., and McPherson, P.S. (2001). The Ras/Rac guanine nucleotide exchange factor mammalian Son-of-sevenless interacts with PACSIN 1/syndapin I, a regulator of endocytosis and the actin cytoskeleton. J. Biol. Chem. *276*, 26622–26628.

Wechsler-Reya, R., Sakamuro, D., Zhang, J., Duhadaway, J., and Prendergast, G.C. (1997). Structural analysis of the human BIN1 gene. Evidence for tissue- specific transcriptional regulation and alternate RNA splicing. J. Biol. Chem. *272*, 31453–31458.

Wickman, K., Karschin, C., Karschin, A., Picciotto, M.R., and Clapham, D.E. (2000). Brain localization and behavioral impact of the

G-protein-gated K+ channel subunit GIRK4. J. Neurosci. *20*, 5608–5615.

Wigge, P., and McMahon, H.T. (1998). The amphiphysin family of proteins and their role in endocytosis at the synapse. Trends Neurosci. *21*, 339–344.

Wigge, P., Kohler, K., Vallis, Y., Doyle, C.A., Owen, D., Hunt, S.P., and McMahon, H.T. (1997a). Amphiphysin heterodimers: potential role in clathrin-mediated endocytosis. Mol. Biol. Cell *8*, 2003–2015.

Wigge, P., Vallis, Y., and McMahon, H.T. (1997b). Inhibition of receptor-mediated endocytosis by the amphiphysin SH3 domain. Curr. Biol. *7*, 554–560.

Witke, W., Podtelejnikov, A.V., Di Nardo, A., Sutherland, J.D., Gurniak, C.B., Dotti, C., and Mann, M. (1998). In mouse brain profilin I and profilin II associate with regulators of the endocytic pathway and actin assembly. EMBO J. *17*, 967–976.

Yang, D., Tournier, C., Wysk, M., Lu, H.T., Xu, J., Davis, R.J., and Flavell, R.A. (1997). Targeted disruption of the MKK4 gene causes embryonic death, inhibition of c-Jun NH2-terminal kinase activation, and defects in AP-1 transcriptional activity. Proc. Natl. Acad. Sci. USA *94*, 3004–3009.

Zelhof, A.C., Bao, H., Hardy, R.W., Razzaq, A., Zhang, B., and Doe, C.Q. (2001). Drosophila Amphiphysin is implicated in protein localization and membrane morphogenesis but not in synaptic vesicle endocytosis. Development *128*, 5005–5015.

Neuron, Vol. 39, 163–176, July 3, 2003, Copyright ©2003 by Cell Press

Synaptic Transmission and Plasticity in the Absence of AMPA Glutamate Receptor GluR2 and GluR3

Yanghong Meng,[1,2,3] Yu Zhang,[1,3] and Zhengping Jia[1,2,*]
[1]Program in Brain and Behavior
The Hospital for Sick Children
555 University Avenue
Toronto, Ontario M5G 1X8
[2]Department of Physiology
University of Toronto
Toronto, Ontario M5S 1A8
Canada

Summary

The AMPA glutamate receptor (AMPAR) subunits GluR2 and GluR3 are thought to be important for synaptic targeting/stabilization of AMPARs and the expression of hippocampal long-term depression (LTD). In order to address this hypothesis genetically, we generated and analyzed knockout mice deficient in the expression of both GluR2 and GluR3. We show here that the double knockout mice are severely impaired in basal synaptic transmission, demonstrating that GluR2/3 are essential to maintain adequate synaptic transmission in vivo. However, these mutant mice are competent in establishing several forms of long-lasting synaptic changes in the CA1 region of the hippocampus, including LTD, long-term potentiation (LTP), depotentiation, and dedepression, indicating the presence of GluR2/3-independent mechanisms of LTD expression and suggesting that AMPA receptor GluR1 alone is capable of various forms of synaptic plasticity.

Introduction

AMPA glutamate receptors (AMPARs) are the principle mediators of the fast excitatory synaptic transmission in the mammalian central nervous system (CNS), and they are important for the expression of several forms of long-lasting synaptic plasticity, including LTP and LTD, extensively studied forms of synaptic plasticity thought to be critical to learning and memory (Bliss and Collingridge, 1993; Malenka and Nicoll, 1999; Bear and Abraham, 1996). In the CA1 region of the hippocampus, while the induction of LTP and LTD requires activation of NMDA receptors (NMDARs) and the subsequent calcium influx, the expression mechanisms appear much more complex, possibly involving both presynaptic and postsynaptic modifications. However, recent studies indicate that activity-dependent AMPAR insertion and internalization at the postsynaptic membrane play a critical role in the expression of LTP and LTD, respectively (Shi et al., 1999; 2001; Hayashi et al., 2000; Carroll et al., 1999; 2001; Beattie et al., 2000; Lin et al., 2000; Man et al., 2000; Wang and Linden, 2000). Thus, regulation of AMPAR trafficking may represent a key mechanism for the modification of synaptic efficacy (Luscher et al., 2000; Malinow and Malenka, 2002)

AMPARs are heteromeric complexes assembled from four distinct subunits GluR1–GluR4 (also referred to as GluRA–GluRD) encoded by four separate genes (Hollmann and Heinemann, 1994). Several studies suggest that these receptor subunits may play distinct roles in the regulation of AMPAR trafficking and synaptic plasticity. For example, the GluR1 subunit is required for NMDAR-dependent synaptic delivery of AMPARs, a process thought to be responsible for adding new receptors to increase synaptic transmission during LTP (Shi et al., 1999; 2001; Hayashi et al., 2000; Passafaro et al., 2001). In contrast, the GluR2/3 subunits are thought to be important for activity-independent movements of AMPARs, a constitutive process thought to be essential for stable basal synaptic responses (Shi et al., 2001; Passafaro et al., 2001). Although the molecular mechanisms underlying these subunit-specific functions are unknown, the protein-protein interactions between the AMPAR subunits and adjacent postsynaptic proteins may play an important role (see reviews by Barry and Ziff, 2002; Song and Huganir, 2002; Sheng and Kim, 2002).

Ample biochemical studies indicate that the C-terminal tails of the GluR2/3 subunits can selectively interact with a number of intracellular proteins (e.g., GRIP1, ABP, NSF, and PICK1) and that these interactions are important for targeting and accumulating GluR2-containing AMPARs at specific subcellular sites, either at the postsynaptic membrane or inside the cell (Dong et al., 1997; 1999; Nishimune et al., 1998; Osten et al., 1998, 2000; Srivastava et al., 1998; Song et al., 1998; Dev et al., 1999; Xia et al., 1999; Perez et al., 2001). Consistent with these biochemical data, postsynaptic injection of synthetic peptides designed to disrupt protein interactions between GluR2 and AMPAR-interacting proteins causes a rapid and selective change in AMPAR-mediated synaptic responses (Nishimune et al., 1998; Noel et al., 1999; Luscher et al., 1999; Luthi et al., 1999; Daw et al., 2000; Lee et al., 2002). Furthermore, some of these peptides or deletions of the C-terminal tail of GluR2 also interfere with activity-dependent AMPAR internalization and the expression of LTD both in the hippocampus and cerebellum (Luscher et al., 1999; Luthi et al., 1999; Daw et al., 2000; Xia et al., 2000; Lin et al., 2000; Lee et al., 2002). Therefore, it has been hypothesized that the expression of hippocampal LTD and AMPAR internalization from the postsynaptic surface involve interactions between GluR2/3 and AMPAR-interacting proteins (Kullmann, 1999; Luthi et al., 1999; Daw et al., 2000; Xia et al., 2000).

In this study, we took genetic approaches to address the in vivo function of GluR2/3 in synaptic regulation by conducting hippocampal slice recordings in three genetically manipulated mouse strains. First, as an extension to our previous studies (Jia et al., 1996), we analyzed LTD and depotentiation in knockout mice lacking GluR2 and found that both LTD and depotentiation could be established in these mice. Since GluR3 is closely related to GluR2 in the protein sequence and in

*Correspondence: jia@sickkids.ca
[3]These authors contributed equally to this work.

fact GluR3 can interact with a number of GluR2-interacting proteins (Braithwaite et al., 2000), we then explored the possibility that GluR3 may play a similar role in synaptic plasticity by generating and analyzing knockout mice lacking GluR3. We showed that the GluR3 knockout mice exhibited normal basal synaptic transmission and LTD but enhanced LTP, indicating that GluR3 was not critical for the expression of LTD. Finally, to address the possibility that GluR2/3 may have redundant functions, we analyzed double knockout mice lacking both GluR2 and GluR3. We demonstrated that the double knockout mice exhibited a dramatic reduction in the mean amplitude of basal synaptic transmission, indicating that GluR2/3 are essential to maintain high levels of synaptic transmission in vivo. However, in spite of a severe reduction in basal synaptic function, the double knockout mice were capable of establishing and maintaining several forms of long-lasting synaptic changes, including LTP, LTD, depotentiation, and dedepression. These results provide genetic evidence for the existence of GluR2/3-independent mechanisms for the expression of hippocampal LTD and depotentiation and suggest that the GluR1 subunit is sufficient for expressing hippocampal synaptic plasticity.

Results

Hippocampal LTD and Depotentiation in GluR2 Knockout Mice

If GluR2 is important for the expression of hippocampal LTD by regulating AMPAR trafficking, one would expect that LTD or depotentiation is affected in GluR2 knockout mice (Jia et al., 1996). To test this possibility, we carried out electrophysiological recordings in the CA1 region of the hippocampus. Previously, we found no significant differences in the degree of LTD of field excitatory postsynaptic potential (fEPSPs) between the wild-type and the knockout mice in an 129XCD1 genetic background (Jia et al., 1996). Since the present study focused on GluR3 and GluR2/3 double knockout mice which were generated in an 129XC57/BL6 genetic background, we therefore backcrossed the GluR2 null mutation into a C57/BL6 genetic background and further verified that both LTD and depotentiation were present in the absence of GluR2. As shown in Figure 1A, no significant differences were found in the degree of LTD induced by low-frequency stimulation (LFS; 1 Hz lasting 15 min) between the two groups of mice (79.2 ± 2.3% for $GluR2^{+/+}$ versus 77.2 ± 4.2% for $GluR2^{-/-}$, $p = 0.66$; Figure 1A). Although LTP induced by high-frequency stimulation (HFS; 100 Hz lasting 1 s) was enhanced in GluR2 knockout mice (155.3% ± 3.2% for $GluR2^{+/+}$ versus 181.6% ± 3.9% for $GluR2^{-/-}$, $p = 0.006$), depotentiation induced by LFS was not significantly altered (87.9% ± 2.2% for $GluR2^{+/+}$ versus 76.3% ± 13.5% for $GluR2^{-/-}$, $p = 0.18$; Figure 1B). In adult hippocampal slices, depotentiation could not be induced by LFS in either wild-type or GluR2 knockout mice (Figure 1C). These results indicate that GluR2 is not essential for the expression of hippocampal LTD or depotentiation. However, because GluR3 is closely related to GluR2 in the structure and biochemical properties (Hollmann and Heinemann, 1994; Braithwaite et al., 2000, Shi et al., 2001) and is expressed in the hippocampus, it is possible that the GluR3 subunit is involved in the expression of hippocampal LTD. Alternatively, GluR3 may have a redundant function sufficient to compensate for the loss of GluR2 so that LTD and depotentiation can be established in the GluR2 knockout mice. It is also important to note that despite the fact that GluR3 is abundantly expressed in many regions of the CNS and that it can form functional heteromeric receptors with other AMPA receptor subunits, there have been very few studies directly focusing on the GluR3 subunit. Therefore, we set out to investigate the in vivo function of GluR3 by generating and analyzing knockout mice deficient in the expression of GluR3.

Normal CNS Anatomy and Synaptic Structures in GluR3 Knockout Mice

The GluR3 knockout mice were generated by standard homologous recombination techniques using R1 ES line (Figures 2A and 2B) (Jia et al., 1996; Nagy et al., 1993). The *GluR3* gene is X chromosome linked; therefore, only one copy is present in the male mice. Since the male knockout animals (X^-Y, $GluR3^-$) bred poorly, all experiments were performed using male offspring (X^-Y as GluR3 knockout and X^+Y littermate as wild-type control) generated from F1 X^+Y ($GluR3^+$) and X^+X^- ($GluR3^{+/-}$) breeding. The GluR3 knockout mice were viable and showed no apparent behavioral deficits, including normal locomotor activities. The whole-brain lysate from the GluR3 knockout mice showed no detectable expression of GluR3 mRNA, but normal levels of mRNA for GluR1 and GluR2 (data not shown). Since there are no commercially available antibodies specific to the GluR3 subunit, we generated GluR2/3 double knockout mice by crossing the GluR3 knockout mice to GluR2 knockout mice. Using antibodies that recognize both GluR2 and GluR3, we showed that the double knockout mice had no expression of GluR2 or GluR3 protein, confirming the absence of GluR3 protein in the GluR3 knockout mice (Figure 2C). The protein levels for other glutamate receptors and postsynaptic proteins, including GluR1, GluR2, GluR4, NR1, NR2A/B, and CaMKIIα(CKIIα) were not altered in GluR3 knockout mice (Figure 2C). The GluR3 knockout mice showed no detectable abnormalities in the gross anatomy or synaptic structures of the CNS (Figures 2Db and 2Df).

Normal Basal Synaptic Transmission in GluR3 Knockout Mice

To further investigate the effect of GluR3 deletion on the properties of synaptic transmission and plasticity, we conducted field and whole-cell recordings in the CA1 region of the hippocampus in the GluR3 knockout mice. Analysis of evoked fEPSPs revealed no differences in the stimulus intensity/response curve, maximal response, and fEPSP waveform (Figure 3A). The passive membrane properties of CA1 pyramidal neurons, including resting membrane potential, input resistance, threshold to fire action potential, and its amplitude were not altered in GluR3 knockout mice (data not shown). Analysis of spontaneous miniature excitatory postsynaptic currents (mEPSCs) of CA1 pyramidal neurons also showed no differences in the frequency (Figure 3B), amplitude (Figure 3C), and kinetics between the wild-type and GluR3 knockout mice. Similarly, evoked EPSCs of

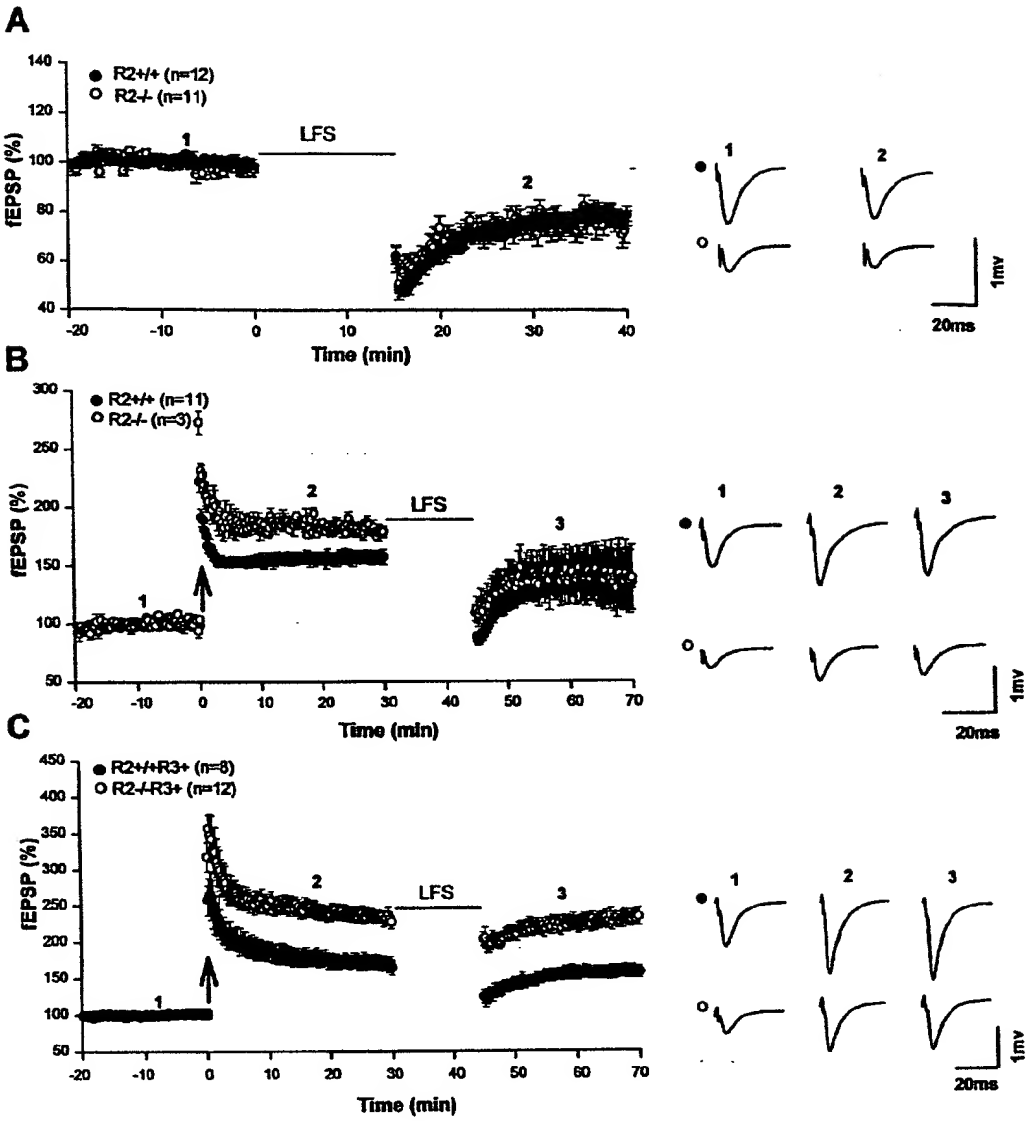

Figure 1. Normal Hippocampal LTD and Depotentiation in GluR2 Knockout Mice

(A) LTD induced by LFS (1 Hz stimulation, 15 min) was indistinguishable between the wild-type and GluR2 knockout mice (12–16 days).

(B) Depotentiation induced by LFS (1 Hz stimulation, 15 min) after establishment of LTP induced by HFS (100 Hz, 1s, upward arrow) showed no differences between the wild-type and GluR2 knockout mice (2–3 weeks).

(C) Depotentiation could not be induced by LFS in hippocampal slices from adult animals (2–3 months) of either the wild-type or GluR2 knockout mice. LTP was enhanced in the knockout mice.

CA1 pyramidal neurons showed no differences in the amplitude, current/voltage relation, and reversal potential between these two groups of mice (Figure 3D). These results indicate that synaptic targeting and function of AMPARs were not significantly disrupted by genetic deletion of GluR3 alone.

Enhanced LTP but Normal LTD in GluR3 Knockout Mice

To examine the role of GluR3 in the regulation of synaptic plasticity, we analyzed LTP and LTD in the CA1 region of the hipp campus. While LTD induced by LFS was indistinguishable between the wild-type and knockout mice (79.1% ± 3.8% for GluR3$^+$ versus 83.7% ± 2.5% for GluR3$^-$, p = 0.33; Figure 4B), the magnitude of LTP induced by HFS was significantly enhanced in the GluR3 knockout mice (128.2% ± 4.5% for GluR3$^+$ versus 152.5% ± 5.0% for GluR3$^-$, p = 0.0039; Figure 4C). The saturated level of LTP induced by multiple HFS trains was also enhanced in the knockout mice (162.8% ± 6.5% for GluR3$^+$ versus 205.2% ± 10.0% for GluR3$^-$, p = 0.0073; Figure 4D). While LTP was enhanced, depotentiation after establishment of LTP was not significantly altered in GluR3 knockout mice (85.0% ± 1.4%

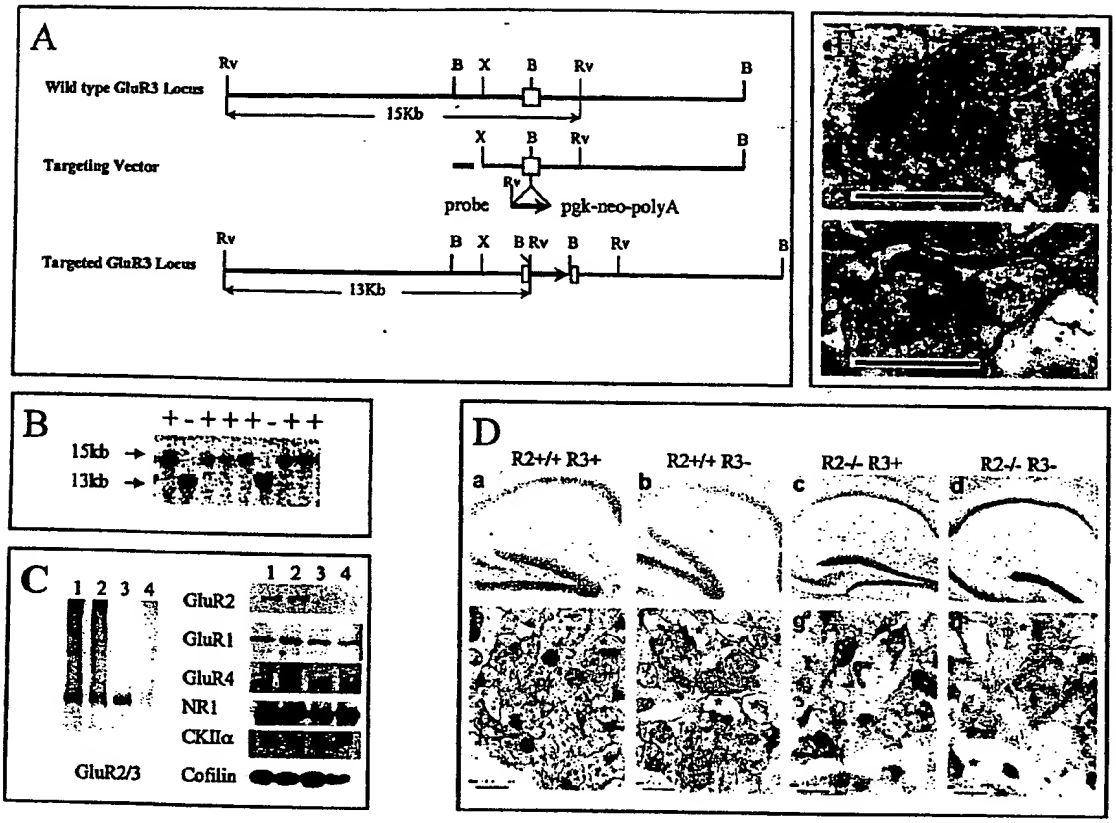

Figure 2. Creation of GluR3 and GluR2/3 Double Knockout Mice

(A) Schematic representation of the wild-type *GluR3* genomic locus, the targeting vector, and the targeted *GluR3* locus. The open box indicates the position of the exon containing the second TM where the insertion of pgk-neo-polyA cassette was made in the targeted *GluR3* locus. Upstream and downstream exons were not mapped.

(B) Representative Southern blot analysis of tail DNA of GluR3 knockout mice. Genomic DNA was isolated from male mice, digested by EcoRV (Rv), and hybridized with the external probe shown in (A). As expected, the probe detected a 15 kb fragment in the wild-type (X^+Y) and a 13 kb fragment in the knockout (X^-Y) mice.

(C) Absence of GluR2 and GluR3 proteins in the GluR2/3 double knockout mice. The GluR2/3 double knockout mice were obtained by intercrossing between mice heterozygous for both GluR2 and GluR3 ($GluR2^{+/-}$ $GluR3^{+/-}$). Total brain lysates were isolated from 12- to 16-day-old male animals of various genotypes (lane 1, $GluR2^{+/+}$ $GluR3^+$; lane 2, $GluR2^{+/+}$ $GluR3^-$; lane 3, $GluR2^{-/-}$ $GluR3^+$; lane 4, $GluR2^{-/-}$ $GluR3^-$), immunoblotted, and detected by indicated antibodies. The GluR2/3 antibodies detected no signals in the GluR2/3 double knockout mice, confirming the absence of both GluR2 and GluR3 in the double knockout mice (left panel). The level of GluR1 and GluR4 was quantified (see Experimental Procedures) and showed no differences between the wild-type and the double knockout mice.

(D) Normal hippocampal formation and synaptic structure in GluR2, GluR3, and GluR2/3 double knockout mice. Nissl staining (a–d) and EM (e–h) micrographs of fixed brain sections showed normal anatomy of hippocampus (a–d) and the density of asymmetric synapses (e–h) identified by the presence of postsynaptic density (asterisks) and presynaptic vesicles in CA1 area.

(E) High magnifications of EM micrographs showed apparently normal distribution of presynaptic vesicles and postsynaptic density. Scale bar in (D) and (E), 500 nm.

for $GluR3^+$ versus 82.5% ± 9.2% for $GluR3^-$; Figure 4E). NMDA receptor antagonist DL-APV (100 μM) completely blocked LTP in both the wild-type and knockout mice (data not shown). Therefore, the enhanced LTP in the GluR3 knockout mice does not involve NMDAR-independent mechanisms. To test whether GluR3 plays a role in presynaptic functions, we compared paired-pulse facilitation and found no differences between the wild-type and knockout mice (Figure 4A). Therefore, hippocampal synaptic plasticity can occur in the absence of GluR3.

Normal Gross CNS and Synaptic Structures in GluR2/3 Double Knockout Mice

To address the possibility that GluR2 and GluR3 are functionally redundant and that only one of them is required for the expression of synaptic plasticity, we generated and analyzed knockout mice lacking both GluR2 and GluR3. The double knockout mice ($GluR2^{-/-}$ $GluR3^-$, males) were born indistinguishable from the wild-type littermates, but during postnatal weeks 2–4 displayed an increased mortality (approximately 20%–30%) and gradual appearance of global abnormalities, including smaller body sizes, reduced locomotor activities, and severe tremors upon movements. Surprisingly, the double knockout mice showed no detectable abnormalities in the gross anatomy of the CNS, including hippocampus (Figure 2D). In addition, the synaptic structures in the CA1 region of the hippocampus appeared unchanged in the double knockout mice (Figures 2Dd, 2Dh, and 2E). There were no significant differences in

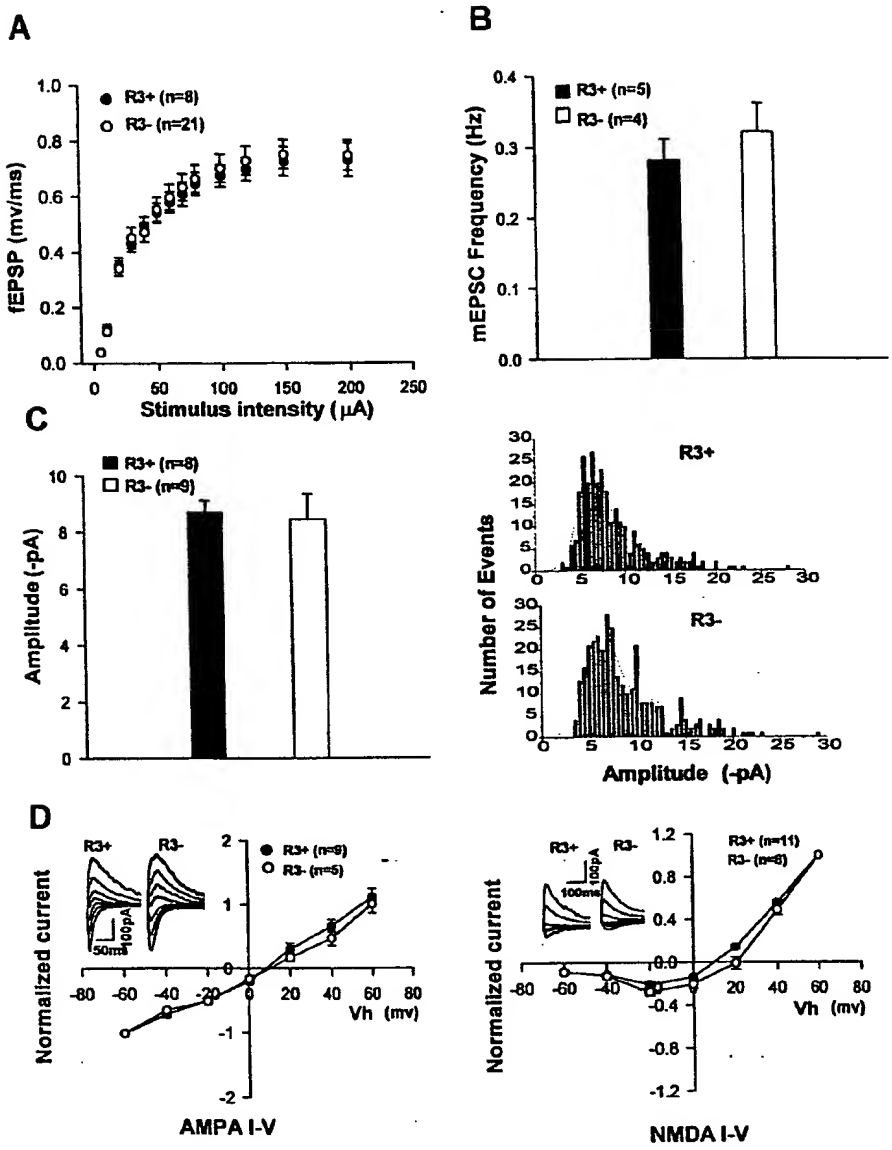

Figure 3. Normal Basal Synaptic Transmission in GluR3 Knockout Mice

(A) fEPSP slopes plotted as a function of stimulus intensity. The distance between the stimulating and recording electrodes was kept constant between slices.

(B) Summary histogram showing the frequency of mEPSCs of CA1 pyramidal neurons recorded under whole-cell voltage clamp mode in the presence of TTX (1 μM) and picrotoxin (100 μM). mEPSCs were blocked by AMPA receptor antagonist CNQX (5 μM).

(C) Summary histogram showing averaged (left) and distribution of mEPSC amplitudes of one representative neuron from each genotype (right).

(D) Averaged amplitudes of evoked AMPA receptor- (left) and NMDA receptor- (right) mediated EPSCs recorded from CA1 pyramidal neurons showing no differences between the wild-type ($R3^+$) and GluR3 knockout ($R3^-$) mice. The AMPAR-mediated EPSCs were estimated at indicated holding potentials in the presence of 100 μM picrotoxin 5 ms after the stimulus and normalized to the EPSC at −60mV. The NMDAR-mediated EPSCs were measured with peak amplitudes in the presence of 100 μM picrotoxin and 10 μM CNQX and normalized to the EPSC at 60mV. The representative EPSC traces at various holding potentials were averages of four successive sweeps.

the numbers of asymmetric synapses and the lengths of postsynaptic density between the wild-type and the double knockout mice (see Experimental Procedures). These results indicate that the excitatory synapses are formed and maintained in the absence of GluR2/3.

Reduced Basal Synaptic Transmission in GluR2/3 D uble Knockout Mice

To investigate the properties of basal synaptic function in GluR2/3 double knockout mice, we analyzed fEPSPs evoked by various stimulus intensities. In these experi-

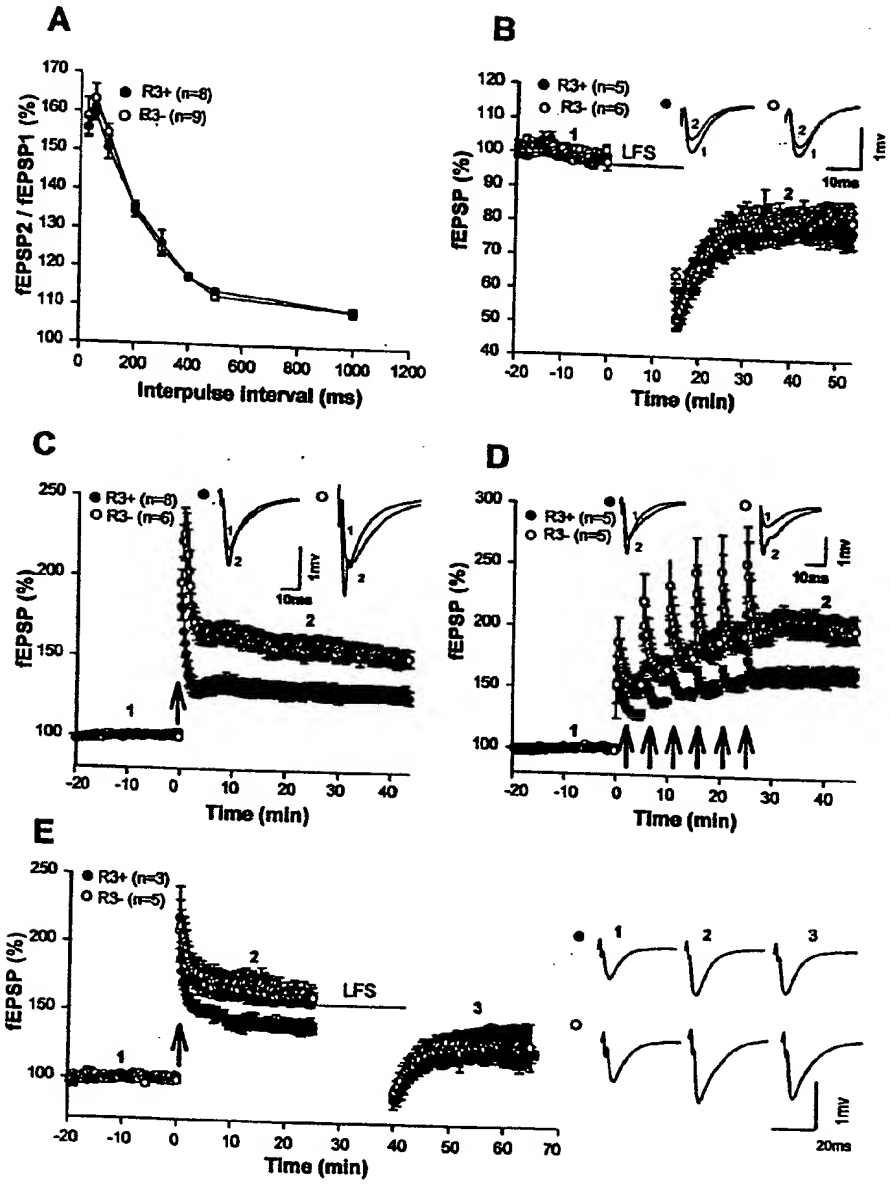

Figure 4. Normal Presynaptic Function and LTD but Enhanced LTP in GluR3 Knockout Mice

(A) Normal paired-pulse facilitation. The plot summarizes facilitation of the second fEPSP slope compared to the first one as a function of the interpulse interval.

(B) Normal hippocampal LTD. LTD induced by LFS showed no differences between the wild-type ($R3^+$) and GluR3 knockout ($R3^-$) mice (12–16 days).

(C) Enhanced hippocampal LTP. LTP induced by single HFS train was higher in GluR3 knockout than the wild-type mice (2–3 months).

(D) Enhanced level of saturated LTP. LTP induced by six trains of HFS (5 min intertrain intervals, upward arrows) was significantly enhanced in GluR3 knockout mice (2–3 months).

(E) Normal depotentiation. Depotentiation induced by LFS following establishment of LTP showed no differences between the wild-type ($R3^+$) and GluR3 knockout ($R3^-$) mice (2–3 weeks).

ments, we used adult mice to minimize the effect of GluR4 on synaptic transmission. As shown in Figure 5A, the mean amplitudes of fEPSPs in the double knockout mice were significantly smaller over a wide range of stimulus intensities (data not shown) or presynaptic fiber volley compared to those of the wild-type or GluR2 knockout mice. The maximal amplitude of fEPSPs in the double knockout slices was only 10%–20% of that in the wild-type control. To investigate the mechanisms underlying this reduced synaptic response, we recorded

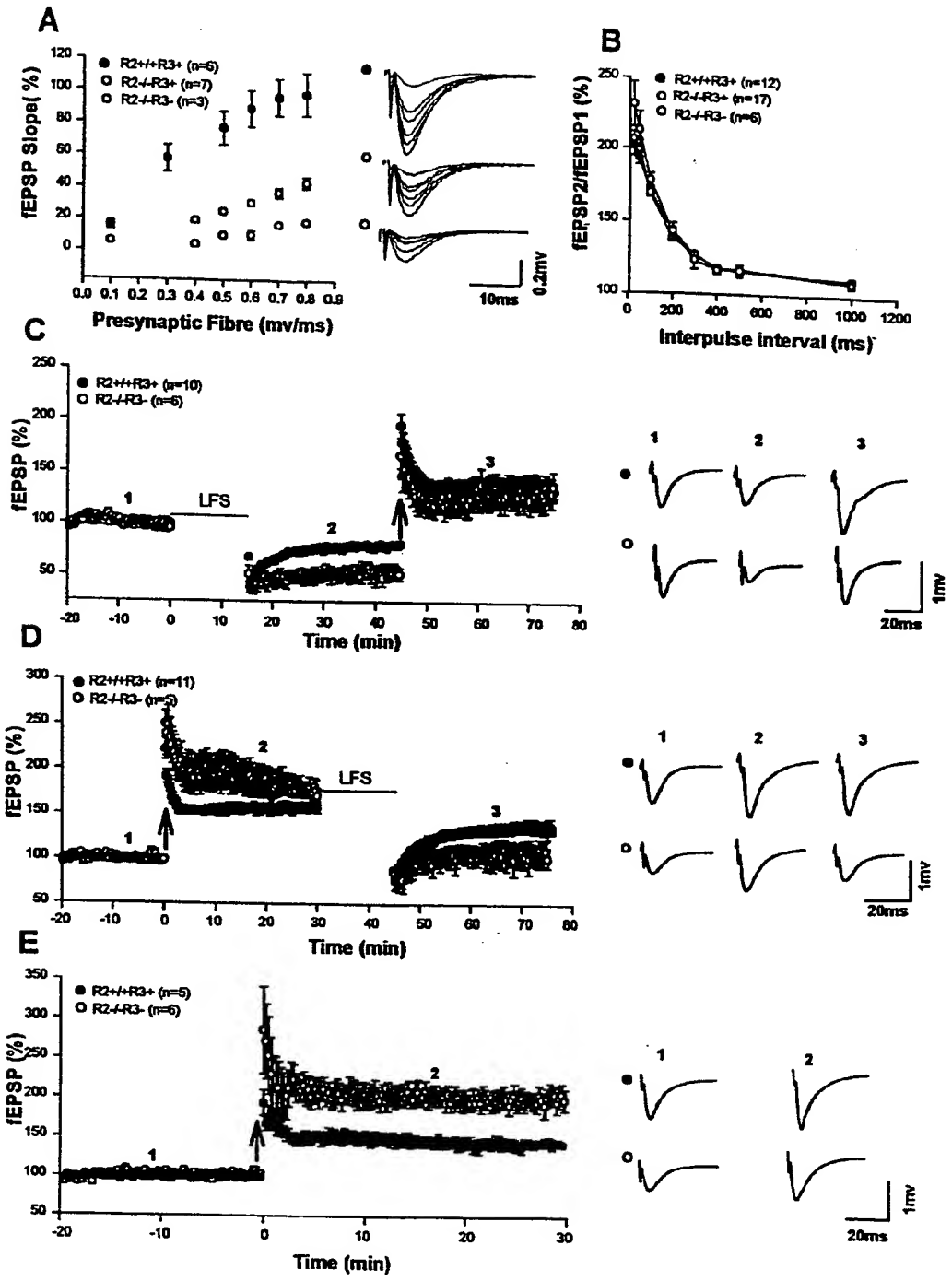

Figure 5. Enhanced Synaptic Plasticity in GluR2/3 Double Knockout Mice

(A) Reduced synaptic response. fEPSP slopes were plotted as function of presynaptic fiber volley. The maximal fEPSP slopes were significantly smaller in the double knockout mice (GluR2$^{-/-}$ GluR3^{-}) than those in the wild-type (GluR2$^{+/+}$ GluR3^{+}) and GluR2 knockout (GluR2$^{-/-}$ GluR3^{+}) mice (2–3 months). The traces show typical fEPSPs evoked with various stimulus intensities.

(B) Normal paired-pulse facilitation. The plot summarizes the facilitation of the second fEPSPs compared with the first one as a function of interpulse interval. No differences were found between these three groups of mice (2–3 months).

(C) Enhanced LTD and dedepression. Both LTD induced by LFS and dedepression induced by HFS (upward arrow) after establishment of LTD were significantly higher in the double knockout (GluR2$^{-/-}$ GluR3^{-}) than the wild-type (GluR2$^{+/+}$ GluR3^{+}) mice (12–16 days).

(D) Enhanced LTP and depotentiation. Both LTP induced by HFS (upward arrow) and depotentiation induced by LFS after the establishment of LTP were significantly enhanced in the GluR2/3 double knockout mice (2–3 weeks).

(E) Sufficiency of GluR1 for LTP. LTP induced by HFS (upward arrow) in hippocampal slices prepared from adult mice (3–6 months) was also significantly higher in the GluR2/3 double knockout than the wild-type mice. The traces on the right are averages of four successive sweeps at indicated time points.

mEPSCs from CA1 pyramidal neurons and found no significant differences in either the frequency (0.23% ± 0.01% Hz for GluR2$^{+/+}$ GluR3^{+} versus 0.25% ± 0.02% Hz for GluR2$^{-/-}$ GluR3^{-}, n = 9 neurons, p = 0.5) or amplitude (10.61% ± 0.58% pA for GluR2$^{+/+}$ GluR3^{+} versus 10.92% ± 0.19% pA for GluR2$^{-/-}$ GluR3^{-}, n = 9 neurons, p = 0.63) between the wild-type and double knockout mice. To test whether presynaptic function was altered, we analyzed paired-pulse facilitation and found no differences in the degree of facilitation between the wild-type and the double knockout mice (Figure 5B). Therefore, the reduction in basal synaptic responses in the double knockout mice was not likely caused by presynaptic changes.

Synaptic Plasticity in GluR2/3 Double Knockout Mice

To address the role of GluR2/3 in the regulation of hippocampal synaptic plasticity, we compared several forms of long-lasting synaptic changes between the wild-type and the double knockout mice. First, we induced LTD with LFS and after LTD was stabilized, delivered HFS to induce LTP or dedepression. As shown in Figure 5C, both LTD (79.2% ± 3% for GluR2$^{+/+}$ GluR3^{+} versus 51.4% ± 8.0% for GluR2$^{-/-}$ GluR3^{-}, p = 0.0026) and dedepression (189.3% ± 8.3% for GluR2$^{+/+}$ GluR3^{+} versus 237.3% ± 16.5% for GluR2$^{-/-}$ GluR3^{-}, p = 0.014) were present and clearly enhanced in the double knockout mice. Second, we induced LTP by HFS and then depotentiation by LFS following establishment of LTP (Figure 5D). Again, both LTP (155.3% ± 4.0% for GluR2$^{+/+}$ GluR3^{+} versus 181.0% ± 10.4% for GluR2$^{-/-}$ GluR3^{-}, p = 0.013), and depotentiation (88.0% ± 8.3% for GluR2$^{+/+}$ GluR3^{+} versus 60.6% ± 5.7% for GluR2$^{-/-}$ GluR3^{-}, p = 0.00015) could be elicited and significantly enhanced in the double knockout mice. Since GluR4 is only expressed in developing hippocampus, we then tested whether LTP could be established in adult hippocampal slices (2–3 months) of the double knockout mice (which should have GluR1 only AMPARs). As shown in Figure 5E, LTP was present and significantly higher in the double knockout mice (141.9% ± 5.5% for GluR2$^{+/+}$ GluR3^{+} versus 198.6% ± 11.5% for GluR2$^{-/-}$ GluR3^{-}, p = 0.0025).

To address the possibility that hippocampal LTP and LTD in the double knockout mice may differ from those of the wild-type animals, we conducted following experiments. First, we induced LTD in the presence of 100 μM DL-APV and showed that LTD was largely abolished by APV in both genotypes (102.3% ± 2.6% for GluR2$^{+/+}$ GluR3^{+} versus 92.1% ± 3.7% for GluR2$^{-/-}$ GluR3^{-}; Figures 6A and 6B). Therefore, the induction of hippocampal LTD in the double knockout mice was mainly through NMDAR-dependent mechanisms. This conclusion was consistent with the finding that LTD in the double knockout mice was insensitive to the application of MCPG (0.5 mM) or bicuculline (20 μM) (Figure 6C). Both of these drugs have been shown to block metabotropic glutamate receptor (mGluR)-dependent LTD, which is known to coexist with NMDAR-dependent LTD in CA1 pyramidal neurons under certain conditions (Oliet et al., 1997). Second, we recorded fEPSPs from two independent pathways and induced LTP or LTD in one pathway. As shown in Figures 7A–7C, synapse-specific LTP (Figure 7B) or LTD (Figure 7C) of the conditioned pathway was obtained in the double knockout mice. After stabilization of LTP or LTD, we applied AMPAR antagonist CNQX (10 μM) and found that fEPSPs were completely abolished, indicating that all synaptic responses during LTP or LTD were mediated by AMPARs. Then the extracellular solution was changed to low Mg^{2+} (0.1 mM) plus CNQX to isolate NMDAR-mediated synaptic responses in both pathways (Mainen et al., 1998; Kullmann et al., 1996). In these experiments, we found little changes in NMDAR-mediated transmission associated with LTP (111.4% ± 2.99% for GluR2$^{+/+}$ GluR3^{+} versus 120.6% ± 5.5% for GluR2$^{-/-}$ GLuR3^{-}) or LTD (99.1% ± 3.25% for GluR2$^{-/-}$ GluR3^{-}) (Figures 7B and 7C), indicating predominant changes in AMPAR-mediated synaptic transmission during LTP or LTD both in the wild-type and the double knockout mice. Finally, we examined the effect of a 15 amino acid peptide (D15) corresponding the PRD domain of the dynamin (dynamin 828–842) on synaptic transmission and LTD in the double knockout mice. This peptide is known to interfere with the binding of amphiphysin with dynamin, an interaction that is important for endocytosis and has been shown to block the expression of LTD (Luscher et al., 1999). Postsynaptic injections of D15 blocked LTD in 8 out of 12 neurons recorded, whereas LTD was obtained in all 10 recorded neurons filled with control peptide S15. The averaged LTD was 82.9% ± 5.9% for neurons filled with D15 and 69.8% ± 4.5% filled with control peptide S15 (p < 0.05). These peptides had similar effects on LTD of the wild-type neurons (data not shown). Collectively, these results indicate that hippocampal LTD in the double knockout mice requires NMDAR activation and postsynaptic endocytosis.

Discussion

Previous studies using cultured hippocampal neurons and inhibitory peptides indicate that the GluR2/3 subunits are important for synaptic trafficking of AMPARs and the expression of LTD. In this study, we demonstrate that knockout mice deficient in the expression of both GluR2 and GluR3 are severely affected in basal synaptic function. However, in spite of a dramatic reduction in the mean amplitude of basal synaptic responses, the double knockout mice are capable of undergoing several forms of long-lasting synaptic plasticity, including LTD and depotentiation in the CA1 region of the hippocampus. These results demonstrate that GluR2/3 are critically involved in maintaining basal synaptic transmission and suggest that GluR1 is sufficient for the expression of synaptic plasticity in vivo.

Importance of GluR2/3 for Basal Synaptic Transmission

In GluR2/3 double knockout mice, the mean amplitude of evoked fEPSP with a wide range of stimulation intensities is much smaller compared to the wild-type animals, indicating that GluR2/3 are critical for maintaining high levels of basal synaptic responses. This difference is most significant in adult hippocampus where the expression of GluR4 is absent, suggesting that GluR4 may

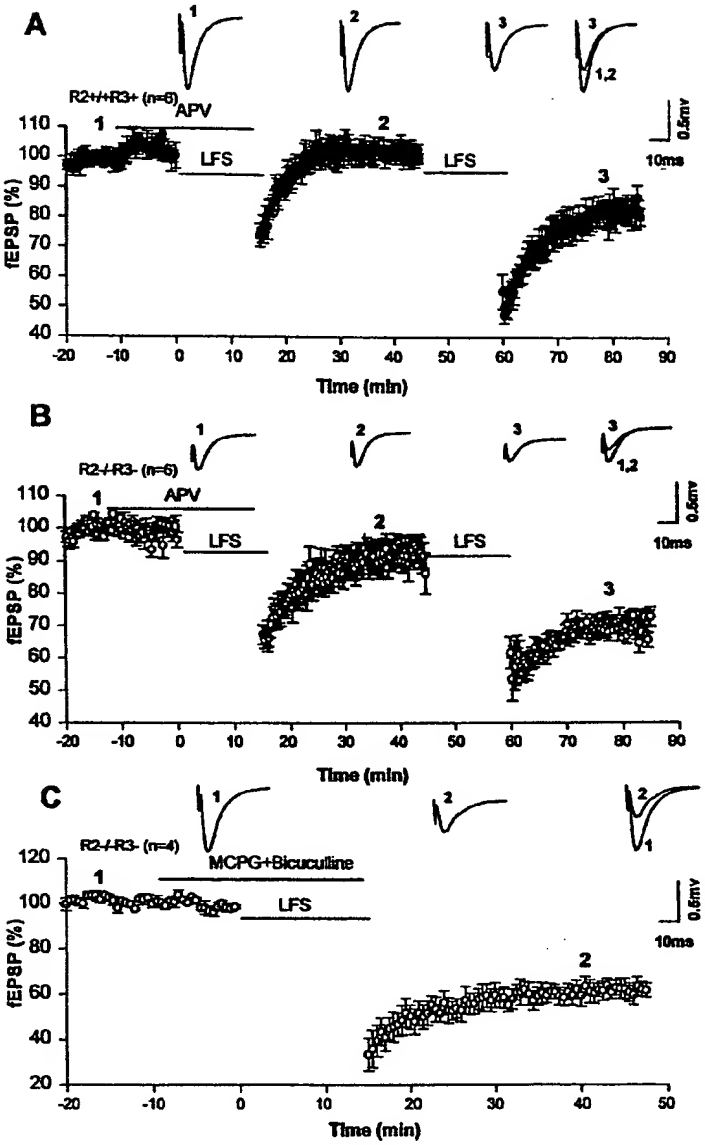

Figure 6. Dependence of LTD on NMDA Receptors in GluR2/3 Double Knockout Mice

(A) LTD was blocked by DL-APV in the wild-type mice (12–16 days). Bath application of DL-APV (100 μM) blocked the induction of LTD. Subsequent LFS after washout of DL-APV produced LTD in the same slices.

(B) LTD was also largely blocked by DL-APV (100 μM) in the GluR2/3 double knockout mice (12–16 days). The experiments were performed as described in (A).

(C) LTD was not affected by MCPG and bicuculline. Bath application of mGluR antagonist MCPG (1 mM) and $GABA_A$ inhibitor bicuculline (20 μM) had no significant effect on LTD in the double knockout mice (12–16 days). Traces are averages of four successive sweeps at indicated time points.

partially compensate for the loss of GluR2/3 in developing brain. It is unlikely that a reduction in the size of fEPSPs is caused by structural perturbations, as there is no evidence that the number of neurons, the density of excitatory synapses, the length of PSD, or the number of presynaptic vesicles is altered in the double knockout mice. The simplest explanation is that GluR2/3 are required for synaptic targeting and stabilization of AMPARs in vivo. Thus, in the absence of GluR2/3, AMPARs would not be sufficiently targeted or stabilized, resulting in a smaller number of synaptic AMPARs and reduced synaptic transmission. This possibility is consistent with the results obtained from in vitro biochemical studies and cultured hippocampal neurons demonstrating that the C-terminal tails of GluR2/3 are capable of interacting with several postsynaptic proteins and that disruption of the interaction causes a selective reduction in AMPAR-mediated basal synaptic transmission and surface expression of AMPARs (see reviews by Braithwaite et al., 2000; Barry and Ziff, 2002; Song and Huganir, 2002). The smaller fEPSPs in the double knockout mice are also consistent with the idea that GluR2/3-containing AMPARs may undergo constitutive recycling, a process considered to be important for preserving stability of basal synaptic transmission (Shi et al., 2001; Passafaro et al., 2001). However, even in adult hippocampus where GluR1 is likely the only remaining AMPAR subunit in the double knockout mice, synaptic transmission occurs and sufficiently high for the establishment of various forms of long-lasting synaptic changes, indicating that GluR1 alone AMPARs are capable of synaptic targeting and dynamic changes.

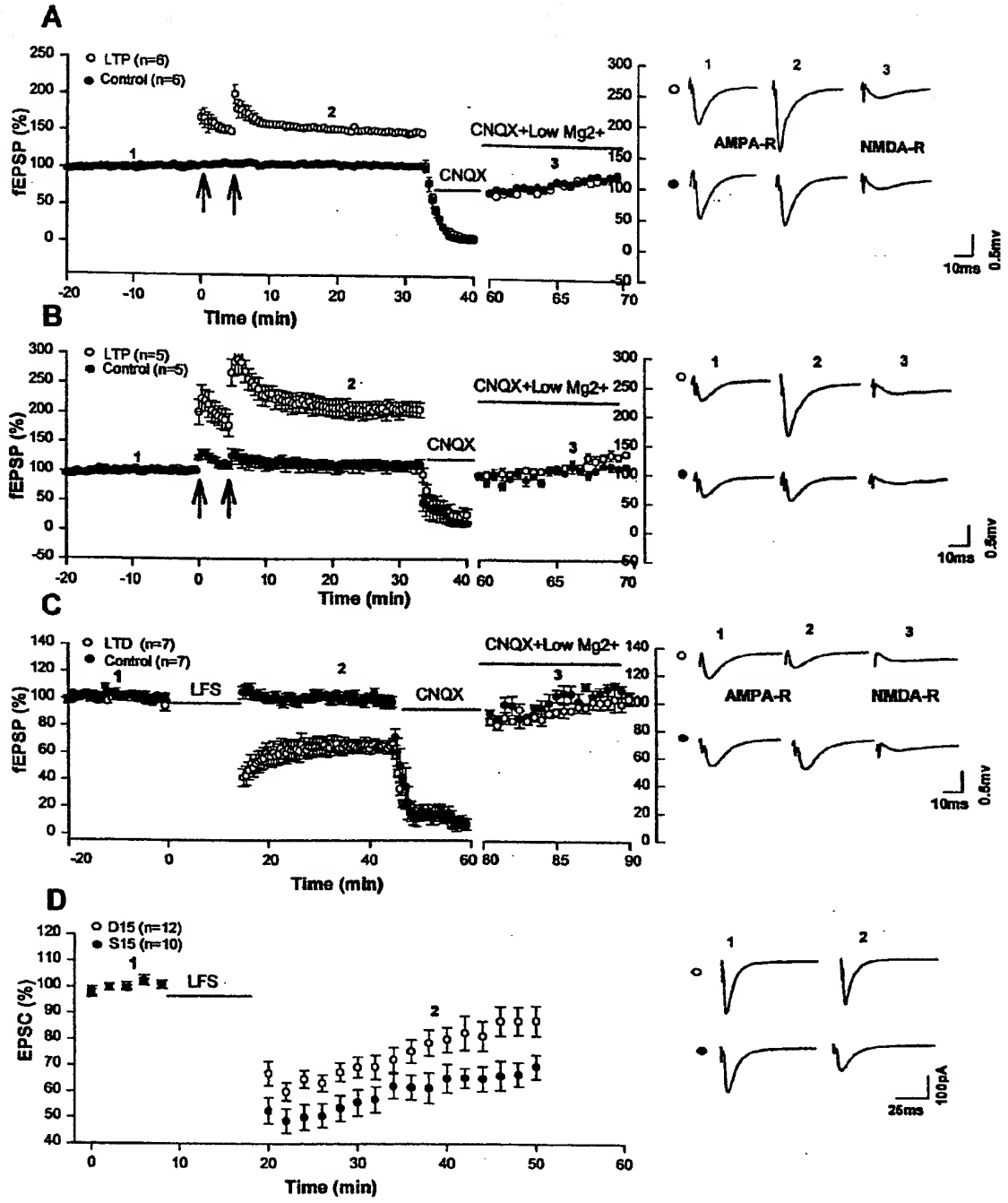

Figure 7. Expression Mechanisms of LTP and LTD in GluR2/3 Double Knockout Mice

(A) Field recordings from two independent pathways (LTP or tetanized pathway and control pathway) showed predominant changes in AMPAR-mediated synaptic transmission during LTP in the wild-type animals (2 months).

(B) Field experiments showed predominant changes in AMPAR-mediated synaptic transmission in LTP pathway in GluR2/3 double knockout mice (2 months).

(C) Field experiments showed predominant changes in AMPAR-mediated synaptic responses in LTD pathway in GluR2/3 double knockout mice (12–16 days). Traces on the right in (A)–(C) are sample fEPSPs from the LTP or LTD and control pathways evoked before HFS or LFS (1), 30 min after first HFS or LFS (2), and after bath application of an extracellular solution containing CNQX (10 μM) and low Mg^{2+} (0.1 mM) to isolate NMDAR-mediated synaptic responses (3). NMDAR responses were normalized to AMPAR-mediated responses before LTP or LTD (Kullmann et al., 1996). The absolute mean fEPSP slope of NMDAR responses is 0.046% ± 0.01% mV/ms for GluR2$^{+/+}$ GluR3^{+} (n = 6) and 0.037% ± 0.004% mV/ms for GluR2$^{-/-}$ GluR3^{-} (n = 5). The ratio of NMDAR- versus AMPAR-mediated fEPSPs is 0.13 ± 0.02 for GluR2$^{+/+}$ GluR3^{+} (n = 6) and 0.15 ± 0.02 for GluR2$^{-/-}$ GluR3^{-} (n = 5).

(D) Whole-cell recordings showed inhibition of LTD by postsynaptic injection of D15 but not by S15 in the double knockout mice (13–16 days). Active peptide D15 or its control peptide S15 was included in the intracellular solution and LTD was induced by LFS (1 Hz lasting 10 min at −40mV) after 15 min of baseline recording. Traces on the right were averages of four successive EPSCs at indicated time points.

Synaptic Plasticity in the Absence of GluR2/3

An intriguing and rather surprising finding of the present study is that various forms of hippocampal synaptic plasticity can be established in the double knockout mice. In particular, the presence of hippocampal LTD and depotentiation in the absence of GluR2/3 is not predicted by the hypothesis that GluR2/3 are necessary for AMPAR endocytosis and LTD (Luthi et al., 1999; Daw et al., 2000; Xia et al., 2000). One possible interpretation for this discrepancy is that the mechanisms of synaptic plasticity in our genetically altered mice may differ from those of the wild-type animals. This appears unlikely because hippocampal LTD in the double knockout mice is (1) largely blocked by NMDAR antagonist APV; (2) insensitive to MCPG or bicuculiin, therefore mGluR-independent; (3) expressed predominantly via changes in AMPAR-mediated synaptic transmission; and (4) still inhibited by perturbations of endocytosis, although to a less degree compared to the wild-type animals. These results indicate that GluR2/3-independent AMPAR endocytosis contributes significantly to hippocampal LTD in the double knockout mice. However, we cannot rule out the possibility that some aspects of synaptic plasticity are distinct in the double knockout mice. Indeed, LTD was only partially blocked by D15 peptide, the same peptide that has been shown to completely abolish LTD in other preparations from the wild-type animals (e.g., Luscher et al., 1999), suggesting that a component of LTD is endocytosis independent in these knockout mice. Further experiments are needed to determine exactly what proportion of LTD is contributed by endocytosis-dependent or endocytosis-independent processes. Since most AMPARs exist as heteromeric assemblies of GluR1/2 or GluR2/3, not as GluR1 homomeric receptors present in the double knockout mice, it also remains to be investigated whether (or under what conditions) GluR2/3-independent AMPAR endocytosis operates and how much it contributes to synaptic changes in the wild-type animals.

In the absence of GluR2/3, the relative amount (as compared to basal synaptic response) of synaptic plasticity is significantly greater (Figures 5–7). This enhancement, in particular of LTD and depotentiation (Figures 5C and 5D), cannot be accounted for simply by an increased Ca^{2+} influx during the induction phase because (1) LTD is blocked by APV and (2) the relative amount of NMDAR- versus AMPAR-mediated fEPSPs is not much greater in the double knockout than in the wild-type mice (Figures 7A–7C). These results suggest that one of the in vivo functions of the GluR2/3 subunits may be to inhibit synaptic changes. It is reasonable to hypothesize that the interaction between GluR2/3- and AMPAR-interacting proteins also function to retain and/or stabilize the receptors either at synaptic surface (Noel et al., 1999; Osten et al., 2000; Lee et al., 2002) or inside the cell (Daw et al., 2000; Perez et al., 2001; Greger et al., 2002) during synaptic changes as proposed for basal synaptic transmission. Thus, disruption of the interaction, for example, by protein phosphorylation/dephosphorylation (Matsuda et al., 1999; 2000; Xia et al., 2000; Kim et al., 2001; Daw et al., 2000; Chung et al., 2000) may facilitate receptor trafficking and synaptic changes.

However, it should be emphasized that because basal synaptic transmission is so drastically reduced in the absence of GluR2/3, the absolute amount of changes in synaptic transmission during LTP/LTD in most experiments is actually smaller in the double knockout mice. Therefore, one interpretation of the results is that GluR2/3 may normally participate in facilitating and/or stabilizing synaptic changes by interacting with AMPAR-interacting proteins as mentioned above. Thus, disruption of these interactions or deletion of GluR2/3 would lead to reduced synaptic plasticity. As indicated earlier, this possibility is supported by results from many previous studies using cultured hippocampal neurons (Nishimune et al., 1998; Luthi et al., 1999; Daw et al., 2000; Xia et al., 2000; Kim et al., 2001; Lee et al., 2002). Given the complexity of protein interactions that occur at the GluR2/3 C termini (e.g., Braithwaite et al., 2002; Hanley et al., 2002; see reviews by Barry and Ziff, 2002; Malinow and Malenka, 2002), it is likely that these interactions have differential and potentially opposing effects on AMPAR trafficking and synaptic plasticity. Targeted deletions or mutations of individual protein binding sites in GluR2/3 C-terminal tails in mice would be important to address the specific function of each interaction.

GluR1 Sufficiency for Hippocampal LTP

In the adult hippocampus where most AMPARs are made of GluR1/2 or GluR2/3 (Wenthold et al., 1996), LTP could be established and also dramatically enhanced in the absence of GluR2/3, indicating that GluR1 is sufficient for the expression of hippocampal LTP. These results are consistent with the observations that LTP is impaired in GluR1 knockout mice (Zamanillo et al., 1999) and that GluR1 is necessary for NMDAR-dependent synaptic targeting of AMPARs in cultured hippocampal slices (Shi et al., 1999, 2001). The C-terminal tail of GluR1 can also interact with a number of proteins, including SAP97 (Leonard et al., 1998), actin binding protein 4.1N (Shen et al., 2000), and AP2 (Lee et al., 2002). Disruption of the interaction between GluR1 and these proteins blocks the activity-dependent synaptic delivery of GluR1 and LTP (Shi et al., 2001). Since LTD experiments were performed using mice at postnatal days 12–15 when GluR4 is also expressed in the hippocampus, it is not clear whether GluR1 is sufficient for the expression of LTD. However, since depotentiation could be established and enhanced in the double knockout animals at postnatal week 3 when the expression of GluR4 is diminishing in the hippocampus (Zhu et al., 2000), our results also suggest that GluR1 may be sufficient for the expression of synaptic depression.

In conclusion, by employing genetic approaches in mice, we provide evidence that the primary function of GluR2/3 is to stabilize synaptic transmission. Thus, in the absence of GluR2/3, both basal synaptic transmission and synaptic plasticity are affected. The complex interactions between GluR2/3 and various cytosolic proteins may provide multiple mechanisms to ensure the stability of synaptic transmission. We suggest that GluR1 contains all the necessary molecular determinants to allow long-lasting synaptic plasticity to occur. Important issues remain to be investigated, including the analysis of the synaptic properties such as AMPAR trafficking in the double knockout mice and to define the in vivo function of specific protein binding sites of GluR2/3 C-terminal tails.

Experimental Procedures

Creation of GluR3 and GluR2/3 Double Knockout Mice

A genomic clone containing the TM1 and TM2 domains of the *GluR3* gene was isolated from a genomic 129/sv library. The targeting vector for generating GluR3 knockout mice was constructed by inserting a 1.8 kb PGK-neo cassette into the BamHI site of exon 12 in a sense direction with creation of an additional EcoRV site for the purpose of diagnostic restriction digestion of the genomic DNA. The G418 resistant ES clones were tested for a targeted event by Southern blot analysis. The procedures for culturing and screening ES cells and for generation of chimeric mice were described previously (Nagy et al., 1993; Jia et al., 1996). The chimeric mice were backcrossed to C57/BL6 to generate the F1 population. The *GluR3* gene is X chromosome linked; therefore, only one copy is present in male mice. Since the male GluR3 knockout animals (X^-Y, $GluR3^-$) bred poorly, most experiments for GluR3 knockout mice were performed using male offsprings (X^-Y as knockout and X^+Y littermate as wild-type control) generated from F1 X^+Y (wild-type male, $GluR3^+$) and X^+X^- (heterozygous female, $GluR3^{+/-}$) breeding. The GluR2/3 double knockout mice ($GluR2^{-/-}$ $GluR3^-$, male) were generated by intercrossing between $GluR2^{+/-}$ $GluR3^+$ males and $GluR2^{+/-}$ $GluR3^{+/-}$ females. All the mice used in the present study had a genetic background of 129XC57/BL6. The genotype of the double knockout mice was determined by Southern blot analysis using three independent DNA probes: an external probe for GluR2 (Jia et al., 1996), an external probe for GluR3 (Figure 2), and an internal neo-probe. The absence of GluR2 and GluR3 proteins in the double knockout mice was confirmed by Western blot analysis using anti-GluR2/3 antibodies. The observed number for GluR2/3 double knockout mice was consistent with the expected Mendelian ratio (1/16), suggesting no embryonic lethality for the double knockout mice.

Immunoblotting, Histochemistry, and Electron Microscopy

The procedures for Western blot analysis of total brain or hippocampal lysates and for Nissl staining of fixed brain sections were described previously (Jia et al., 1996; Meng et al., 2002). The primary antibodies used were: anti-NMDAR1 (Chemicon, Temeculo, CA), anti-NMDAR2A/B (Upstate, Charlottesville, VA), anti-GluR1 (Chemicon), anti-GluR2 (Chemicon), anti-GluR2/3 (Upstate and Chemicon), anti-GluR4 (Upstate and Chemicon), anti-CaMKIIα (gift of Dr. Bill Trimble), and anti-cofilin (Santa Cruz, Santa Cruz, CA). The levels of GluR1 and GluR4 were estimated and normalized against the amount of cofilin using the enhanced chemiluminescence (Amersham) method in more than ten separate experiments from three animals of each genotype and showed no significant differences (GluR1: 94% ± 17% arbitrary unit for wild-type and 153% ± 21% for double knockout, $p = 0.1$; GluR4: 104% ± 10% for wild-type and 80% ± 15% for double knockout, $p = 0.3$). For electron microscopy, the transcardially fixed brain samples were sliced (500 μm) on a vibratome and 1 × 1 mm CA1 areas isolated from comparable sections of each genotype. The blocks were then postfixed for an additional 3 hr and processed according to standard methods. For each block, 1 μm thick sections were cut and stained with 1% toluidine blue to guide further trimming to isolate equivalent CA1 subfields. Thin sections (60 nm) were then cut and stained with uranyl acetate and Reynolds lead citrate. The numbers of the synapses (wild-type: 0.324 ± 0.016%/μm², $n = 33$ images; GluR2/3 double knockout: 0.359 ± 0.014%/μm², $n = 55$ images, $p = 0.11$) and the lengths of postsynaptic density (wild-type: 171.3% ± 3.9% [nm], $n = 208$ synapses; GluR2/3 double knockout: 175.7% ± 0.34% [nm], $n = 227$ synapses, $p = 0.33$) were estimated on thin-section images covering neuropil regions totaling 4000–7000 μm² from two animals for each genotype (Meng et al., 2002).

Electrophysiology

The procedures for electrophysiological recordings were described previously (Jia et al., 1996; Meng et al., 2002). Briefly, hippocampal slices (400 μm) were prepared from 10 days to 6-month-old mice (the age of the mice was indicated in each experiment) and allowed to recover in a holding chamber for at least 1 hr. A single slice was then transferred to the recording chamber and submerged and superfused with 95% O_2-5% CO_2 saturated artificial CSF (ACSF, 2 ml/min). The ACSF contained 120 mM NaCl, 2.5 mM KCl, 1.3 mM $MgSO_4$, 1.0 mM NaH_2PO_4, 26 mM $NaHCO_3$, 2.5 mM $CaCl_2$, and 11 mM D-glucose. For field EPSPs, the recording pipette (3 MΩ) was filled with ACSF solution. For whole-cell voltage-clamp recordings, the patch pipette (3–5 MΩ) contained the following: 132 mM Cs gluconate, 17.5 mM CsCl, 0.05 mM EGTA, 10 mM HEPES, 2 mM Mg-ATP, 0.2 mM Na-GTP, QX-314, pH7.4 (292 mOsm); for current clamp, it contained 150mM K_2MeSO_4, 0.1 mM EDTA, 10 mM HEPES, and 2 mM Mg-ATP, pH 7.4 (290 mOsm). Synaptic responses were evoked by bipolar tungsten electrodes placed 200–400 μm from the cell body layer in the CA1 area. fEPSPs were measured by taking the slope of the rising phase between 5% and 60% of the peak response. Unless otherwise indicated, LTP and dedepression were induced with two trains (intertrain interval of 10 s) of 100 Hz stimulation each lasting 1 s. LTD and depotentiation were induced by low-frequency stimulation (LFS) at 1 Hz lasting 15 min for field experiments and lasting 10 min at a holding potential of −40mV for whole-cell experiments. Peptides were synthesized and purified by the Advanced Protein Technology Center at the University of Toronto, Toronto, Ontario, CAN. The amino acid sequence for D15 was PPPQVPSRPNRAPPG and the corresponding scrambled peptide (S15) was ANVRRGPPPPPQPPS. Peptides (1.0 mM) were added to the intracellular solution immediately before experiments. All data acquisition and analysis were done using pCLAMP 7 software (Axon Instruments). When average data were plotted, data were normalized to the average of the baseline responses unless indicated otherwise. All data were statistically evaluated by Student's t test.

Acknowledgments

We are indebted to J. Hwang and Y.M. Heng for electron microscopy assistance and to Dr. S. Heinemann for providing the GluR3 cDNA. This work was supported by grants to Z.P.J. from Heart and Stroke Foundation of Canada, Canadian Institutes of Health Research (CIHR), and The Hospital For Sick Children Foundation. Y.H.M is supported by an HSC Trainee Fellowship, and Z.P.J. is a New Investigator of CIHR.

Received: November 11, 2002
Revised: April 17, 2003
Accepted: May 23, 2003
Published: July 2, 2003

References

Barry, M.F., and Ziff, E.B. (2002). Receptor trafficking and the plasticity at excitatory synapses. Curr. Opin. Neurobiol. *12*, 279–286.

Bear, M.F., and Abraham, W.C. (1996). Long-term depression in the hippocampus. Annu. Rev. Neurosci. *19*, 437–462.

Beattie, E.C., Carroll, R.C., Yu, X., Morishita, W., Yashuda, H., von Zastrow, M., and Malenka, R.C. (2000). Regulation of AMPA receptor endocytosis by a signaling mechanism shared with LTD. Nat. Neurosci. *3*, 1291–1300.

Bliss, T.V.P., and Collingridge, G.L. (1993). A synaptic model of memory: long-term potentiation in the hippocampus. Nature *361*, 31–39.

Braithwaite, S.P., Meyer, G., and Henley, J.M. (2000). Interactions between AMPA receptors and intracellular proteins. Neuropharmacology *39*, 919–930.

Braithwaite, S.P., Xia, H., and Malenka, R.C. (2002). Differential roles for NSF and GRIP/ABP in AMPA receptor cycling. Proc. Natl. Acad. Sci. USA *99*, 7096–7101.

Carroll, R.C., Lissin, D.V., von Zastrow, M., Nicoll, R.A., Malenka, R.C., and Zastrow, M. (1999). Dynamin-dependent endocytosis of ionotropic glutamate receptors. Proc. Natl. Acad. Sci. USA *96*, 14112–14117.

Carroll, R.C., Beattie, E.C., von Zastrow, M., and Malenka, R.C. (2001). Role of AMPA receptor endocytosis in synaptic plasticity. Nat. Rev. Neurosci. *2*, 315–324.

Chung, H.J., Xia, J., Scannevin, R.H., Zhang, X., and Huganir, R.L.

(2000). Phosphorylation of the AMPA receptor subunit GluR2 differentially regulates its interaction with the PDZ domain-containing proteins. J. Neurosci. *20*, 7258–7267.

Daw, M., Chittajalu, R., Bortolotto, Z.A., Dev, K.K., Duprat, F., Henley, J.M., Collingridge, G.L., and Isaac, J.T.R. (2000). PDZ proteins interacting with C-terminal GluR2/3 are involved in a PKC-dependent regulation of AMPA receptors at hippocampal synapses. Neuron *28*, 873–886.

Dev, K.K., Nishimune, A., Henley, J.M., and Nakanishi, S. (1999). The protein kinase C binding protein PICK1 interacts with short but not long form alternative splice variants of AMPA receptor subunits. Neuropharmacology *38*, 635–644.

Dong, H., O'Brien, R.J., Fung, E.T., Lanahan, A.A., Worley, P.F., and Huganir, R.L. (1997). GRIP: a synaptic PDZ-containing protein that interacts with AMPA receptors. Nature *386*, 279–284.

Dong, H., Zhang, P., Song, I., Petralia, R.S., Liao, D., and Huganir, R.L. (1999). Characterisation of the glutamate receptor-interacting proteins GRIP1 and GRIP2. J. Neurosci. *19*, 6930–6941.

Greger, I.H., Khatri, L., and Ziff, E.B. (2002). RNA editing at Arg607 controls AMPA receptor exit from the endoplasmic reticulum. Neuron *34*, 759–772.

Hanley, J.G., Khatri, L., Hanson, P.I., and Ziff, E.B. (2002). NSF ATPase and alpha/beta-SNAPs disassemble the AMPA receptor-PICK1 complex. Neuron *34*, 53–67.

Hayashi, Y., Shi, S.H., Esteban, J.A., Poncer, J.C., and Malinow, R. (2000). Driving AMPA receptors into synapses by LTP and CaMKII: requirement for GluR1 and PDZ domain interaction. Science *287*, 2262–2267.

Hollmann, M., and Heinemann, S. (1994). Cloned glutamate receptors. Annu. Rev. Neurosci. *17*, 31–108.

Jia, Z., Agopyan, N., Miu, P., Xiong, Z., Henderson, J., Gerlai, R., Taverna, F.A., Velumian, A., MacDonald, J., Carlen, P., et al. (1996). Enhanced LTP in mice deficient in the AMPA receptor GluR2. Neuron *17*, 945–956.

Kim, C.H., Chung, H.J., Lee, H.K., and Huganir, R.L. (2001). Interaction of the AMPA receptor subunit GluR2/3 with PDZ domains regulates long-term depression. Proc. Natl. Acad. Sci. USA *98*, 11725–11730.

Kullmann, D.M. (1999). AMPA receptor attrition in long-term depression. Neuron *24*, 288–290.

Kullmann, D.M., Erdemli, G., and Asztely, F. (1996). LTP of AMPA and NMDA receptor-mediated signals: evidence for presynaptic expression and extrasynaptic glutamate spill-over. Neuron *17*, 461–474.

Lee, S.H., Liu, L., Wang, Y.T., and Sheng, M. (2002). Clathrin adaptor AP2 and NSF interact with overlapping sites of GluR2 and play distinct roles in AMPA receptor trafficking and hippocampal LTD. Neuron *36*, 661–674.

Leonard, A.S., Davare, M.A., Horne, M.C., Garner, C.C., and Hell, J.W. (1998). SAP97 is associated with the alpha-amino-3-hydroxy-5-methylisoxazole-4-propionic acid receptor GluR1 subunit. J. Biol. Chem. *273*, 19518–19524.

Lin, J.W., Ju, W., Foster, K., Lee, S.H., Ahmadian, G., Wyszynski, M., Wang, Y.T., and Sheng, M. (2000). Distinct molecular mechanisms and divergent endocytic pathways of AMPA receptor internalization. Nat. Neurosci. *3*, 1282–1290.

Luscher, C., Xia, H., Beattie, E.C., Carroll, R.C., von Zastrow, M., Malenka, R.C., and Nicoll, R.A. (1999). Role of AMPA receptor cycling in synaptic transmission and plasticity. Neuron *24*, 649–658.

Luscher, C., Nicoll, R.A., Malenka, R.C., and Muller, D. (2000). Synaptic plasticity and dynamic regulation of the postsynaptic membrane. Nat. Neurosci. *3*, 545–550.

Luthi, A., Chittajallu, R., Duprat, F., Palmer, M.J., Benke, T.A., Kidd, F.L., Henley, J.M., Isaac, J.T.R., and Collingridge, G.L. (1999). Hippocampal LTD expression involves a pool of AMPARs regulated by the NSF-GluR2 interaction. Neuron *24*, 389–399.

Mainen, Z.F., Jia, Z.P., Roder, J., and Malinow, R. (1998). Use-dependent AMPA receptor block in mice lacking GluR2 suggests postsynaptic site for LTP expression. Nat. Neurosci. *1*, 579–586.

Malenka, R.C., and Nicoll, R.A. (1999). Long-term potentiation—a decade of progress? Science *285*, 1870–1874.

Malinow, R., and Malenka, R.C. (2002). AMPA receptor trafficking and synaptic plasticity. Annu. Rev. Neurosci. *25*, 103–126.

Man, Y.H., Lin, J.W., Ju, W.H., Ahmadian, G., Liu, L., Becker, L.E., Sheng, M., and Wang, Y.T. (2000). Regulation of AMPA receptor-mediated synaptic transmission by clathrin-dependent receptor internalization. Neuron *25*, 649–662.

Matsuda, S., Mikawa, S., and Hirai, H. (1999). Phosphorylation of serine-880 in GluR2 by protein kinase C prevents its C terminus from binding with glutamate receptor-interacting protein. J. Neurochem. *73*, 1765–1768.

Matsuda, S., Launey, T., Mikawa, S., and Hirai, H. (2000). Disruption of AMPA receptor GluR2 clusters following long-term depression induction in cerebellar Purkinje neurons. EMBO J. *9*, 2765–2774.

Meng, Y.H., Zhang, Y., Tregoubov, V., Janus, C., Cruz, L., Jackson, M., Lu, W.Y., MacDonald, J.F., Wang, J., Falls, D.L., et al. (2002). Abnormal spine morphology and enhanced LTP in LIMK-1 knockout mice. Neuron *35*, 121–133.

Nagy, A., Rossant, J., Nagy, R., Abramow-Newerly, W., and Roder, J.C. (1993). Derivation of completely cell culture-derived mice from early passage embryonic stem cells. Proc. Natl. Acad. Sci. USA *90*, 8424–8428.

Nishimune, A., Isaac, J.T.R., Molnar, E., Noel, J., Nash, S.R., Tagaya, M., Collingridge, G.L., Nakanishi, S., and Henley, J.M. (1998). NSF binding to GluR2 regulates synaptic transmission. Neuron *21*, 87–97.

Noel, J., Ralph, G.S., Pickard, L., Williams, J., Molnar, E., Uney, J.B., Collingridge, G.L., and Henley, J.M. (1999). Surface expression of AMPA receptors in hippocampal neurons is regulated by an NSF-dependent mechanism. Neuron *23*, 365–376.

Oliet, S.H.R., Malenka, R.C., and Nicoll, R.A. (1997). Two distinct forms of long-term depression coexist in CA1 hippocampal pyramidal cells. Neuron *18*, 969–982.

Osten, P., Srivastava, S., Inman, G.J., Vilim, F.S., Khatri, L., Lee, L.M., States, B.A., Einheber, S., Milner, T.A., Hanson, P.I., et al. (1998). The AMPA receptor GluR2 C terminus can mediate a reversible, ATP-dependent interaction with NSF and alpha- and beta-SNAPs. Neuron *21*, 99–110.

Osten, P., Khatri, L., Kohr, G., Giese, G., Daly, C., Schulz, T.W., Wensky, A., Lee, L.M., and Ziff, E.B. (2000). Mutagenesis reveals a role for ABP/GRIP binding to GluR2 in synaptic surface accumulation of the AMPA receptor. Neuron *27*, 313–325.

Passafaro, M., Piech, V., and Sheng, M. (2001). Subunit-specific temporal and spatial patterns of AMPA receptor exocytosis in hippocampal neurons. Nat. Neurosci. *4*, 917–926.

Perez, J.L., Khatri, L., Chang, C., Srivastava, S., Osten, P., and Ziff, E.B. (2001). PICK1 targets activated protein kinase C alpha to AMPA receptor clusters in spines of hippocampal neurons and reduces surface levels of the AMPA-type glutamate receptor subunit 2. J. Neurosci. *21*, 5417–5428.

Shen, L., Liang, F., Walensky, L.D., and Huganir, R.L. (2000). Regulation of AMPA receptor GluR1 subunit surface expression by a 4.1N-linked actin cytoskeletal association. J. Neurosci. *20*, 7932–7940.

Sheng, M., and Kim, M.J. (2002). Postsynaptic signaling and plasticity mechanisms. Science *298*, 776–780.

Shi, S.-H., Hayashi, Y., Petralia, R.S., Zaman, S.H., Wenthold, R.J., Svoboda, K., and Malinow, R. (1999). Rapid spine delivery and redistribution of AMPA receptors after synaptic NMDA receptor activation. Science *284*, 1811–1816.

Shi, S.-H., Hayashi, Y., Esteban, J.A., and Malinow, R. (2001). Subunit-specific rules governing AMPA receptor trafficking to synapses in hippocampal pyramidal neurons. Cell *105*, 331–343.

Song, I., and Huganir, R.L. (2002). Regulation of AMPA receptors during synaptic plasticity. Trends Neurosci. *25*, 578–588.

Song, I., Kamboj, S., Xia, J., Dong, H., Liao, D., and Huganir, R.L. (1998). Interaction of the N-ethylmaleimide-sensitive factor with AMPA receptors. Neuron *21*, 393–400.

Srivastava, S., Osten, P., Vilim, F.S., Khatri, L., Inman, G., States,

B., Daly, C., DeSouza, S., Abagyan, R., Valtschanoff, J.G., et al. (1998). Novel anchorage of GluR2/3 to the postsynaptic density by AMPA receptor-binding protein ABP. Neuron *21*, 581–591.

Wang, Y.T., and Linden, D.J. (2000). Expression of cerebellar long-term depression requires postsynaptic clathrin-mediated endocytosis. Neuron *25*, 635–647.

Wenthold, R.J., Petralia, R.S., Blahos, J., and Niedzielski, A.S. (1996). Evidence for multiple AMPA receptor complexes in hippocampal CA1/CA2 neurons. J. Neurosci. *16*, 1982–1989.

Xia, J., Zhang, X., Staudinger, J., and Huganir, R.L. (1999). Clustering of AMPA receptors by the synaptic PDZ domain-containing protein PICK1. Neuron *22*, 179–187.

Xia, J., Chung, H.J., Wihler, C., Huganir, R., and Linden, D.J. (2000). Cerebellar long-term depression requires PKC-regulated interactions between GluR2/3 and PDZ domain-containing proteins. Neuron *28*, 499–510.

Zamanillo, D., Sprengel, R., Hvalby, O., Jensen, V., Burnashev, N., Rozov, A., Kaiser, K.M., Koster, H.J., Borchardt, T., Worley, P., et al. (1999). Importance of AMPA receptors for hippocampal synaptic plasticity but not for spatial learning. Science *284*, 1805–1811.

Zhu, J.J., Esteban, J.A., Hayashi, Y., and Malinow, R. (2000). Synaptic potentiation during early development:delivery of GluR4-containing AMPA receptors by spontaneous activity. Nat. Neurosci. *3*, 1098–1106.